UNIVERSITAT DE BARCELONA

New insights into RANK signaling pathway in the mammary gland

Sandra Benítez

UNIVERSITY OF BARCELONA

FACULTY OF PHARMACY AND FOOD SCIENCE

Programme of Biomedicine

New insights into RANK signaling pathway in the mammary gland.

Memory presented by Sandra Benítez to obtain the title of doctor by the University of Barcelona

Thesis director: Eva González Suárez

Thesis tutor: Albert Tauler Girona

PhD student: Sandra Benítez Sorribas

Sandra Benítez Sorribas, 2020

UNIVERSITY OF BARCELONA

FACULTY OF PHARMACY AND FOOD SCIENCE

PROGRAMME OF BIOMEDICINE

New insights into RANK signaling pathway in the mammary gland.

Memory presented by Sandra Benítez to obtain the title of doctor by the University of Barcelona.

2020

Affiliation:
Bellvitge Biomedical Research Institute (IDIBELL)

Research Group:
Transformation and Metastasis Group

Author:
Sandra Benítez Sorribas

Tutor:
Albert Tauler Girona

Director:
Eva González Suárez

Firmado por BENITEZ SORRIBAS, SANDRA (FIRMA)
Día 14/09/2020
con el certificado AC DNIE 005

UNIVERSITAT DE BARCELONA

IDIBELL
Bellvitge Biomedical Research Institute

AGRAÏMENTS

AGRAÏMENTS

Semblava que no arribaria mai aquest dia… s'acosta el final d'una gran etapa de la meva vida i escriure els agraïments de la tesi i mostrar la meva admiració a la gent que m'envolta és sens dubte una de les coses més importants, ja que sense vosaltres no hagués sigut possible.

Mirar enrere i recordar tota la gent que m'ha ajudat a arribar fins aquí és molt especial... i la gent que hem coneix sap que aquestes línies de la tesi estan escrites amb melancolia, emoció i una barreja de tristesa i felicitat... No voldria oblidar-me de tots el que ho heu fet possible, demano disculpes a qui no mencioni en aquest apartat (no serà intencionat).

El meu primer i més càlid agraïment és per la meva família... en especial, gràcies als meus pares i al meu monstruito de germà ;) per tantes coses, converses, experiències... que no es poden explicar. Heu sigut i sempre sereu un dels pilars de la meva vida! Vosaltres m'heu fet com sóc i us estic súper agraïda. Des de petits tot i que com a totes les famílies sempre hi ha discussions, rabietes, plors i algun dia de morros, m'heu transmès la importància d'aprendre coses noves, tenir curiositat per estudiar... que m'han portat a estudiar biomedicina i a fer una tesi doctoral. Encara recordo el dia que li vam dir a la iaia que volia estudiar biomedicina, on ella pel que fos va entendre que volia ser detectiu privat! Tenia a tota la meva família pendent...jajaja Moltes gràcies als meus avis tant materns com paterns per donar-me suport, tot i no acabar d'entendre que estudiava, però os sentíeu orgullosos de mi. Gràcies a tota la meva família, aquesta tesi va dedicada a vosaltres.

Fent un viatge per recordar com i per què hem vaig endinsar en el món científic ens hem de situar a l'escola on entre altres professors d'ESO i Batxillerat, m'agradaria destacar a la Maite, la Laura i en Ferran on a les vostres classes ens transmetíeu curiositat i ganes d'aprendre de la ciència. Gràcies per la paciència i pels bons consells! Destacar també durant els 5 anys de carrera i màster, l'ajut i predisposició dels professors de la facultat de medicina de Lleida i el grup d'investigació oncològica per ajudar-me en tot el que necessités i poder establir el meu primer contacte en la realització d`un projecte científic que hem donaria les capacitats necessàries per realitzar el doctorat. Gràcies per tot!

Ja situada a Barcelona..., me gustaría agradecer a Eva el darme la oportunidad de poder realizar la tesis doctoral en su laboratorio, dónde he aprendido mucho y, creo, he mejorado como científica. A mi tutor, Albert Tauler, por su paciencia y estar dispuesto a ayudarme en los momentos más difíciles de esta última etapa. Durante mi estancia en el laboratorio, sin duda lo mejor que me llevo es la amistad entre todos los miembros del PEBC6 o recientemente divididos en el 6 y en el 3. La parte humana de

los grupos de Eva y Puri es uno de los pilares de esos grupos de investigación. Os voy a echar mucho de menos.

Cuando entré en el laboratorio, desde el primer día tuve la oportunidad de conocer a un chico segoviano con muchas cualidades, dónde aparte de ser una de las personas más generosas, amables, dispuesto a ayudarte en todo y un gran mentor, tuve el privilegio de poder ser una de las principales protagonistas de unos maravillosos cantos gregorianos que amenizaban los días. MISS OVICHON ♫♫. Guille millones de gracias por todo lo que hemos pasado juntos dentro del laboratorio, pero también cuando *miss ovichon* se iba a *playing in the garden with some friends*, también hemos vivido muchas experiencias juntos, dónde espero que sigamos compartiendo esos buenos momentos. Y con Albita, una chica siempre dispuesta a ayudarte en todo y mi pilar en esas excursiones interminables, dónde se han dado casos que teníamos más cansada la lengua de hablar que las piernas de andar… XD. También has sido mi fiel compañera en el gym, dónde esas clases de suspensión ya no serán lo mismo sin ti. ¡Sin embargo, todavía nos quedan muchas experiencias juntos!

Por supuesto, también quiero dar las gracias a mis *Chungis* favoritas: Laura *la mojitera* y Marta *la diabolilla*. Marta, una chica con un gran corazón, que entre maldad y maldad siempre está dispuesta a ayudarte, y como no a trasmitir la norma de San Agustín! Laura, hemos compartido muchas experiencias juntas, te has convertido en una persona muy importante para mí... Siempre escuchándome, ayudándome… como una hermana que nunca he tenido. Gracias a las dos por nuestras risas y aventuras todo este tiempo, os voy a echar mucho de menos, pero sin duda nuestros momentos juntas van a seguir sumando. Gracias también por poder conocer a Rubén, un pucelano que nos debe un viaje :P y siempre ha sido mi compañero de equipo. A lo poco de entrar en el laboratorio, llegó *estaba*, Laura, una chica extremeña, que rápidamente fue querida por todos nosotros y conocida por su peto y la risa más contagiosa que te puedas encontrar.

També haig de donar les gràcies al solet de Juneda. Adrià ha sigut un plaer compartir laboratori amb un noi com tu, disposat a donar-t'ho tot, tot i no tenir temps per acabar les seves coses tant al laboratori com fora buscant pedres per construir un camí quan estàvem desorientats per la muntanya. Ets una gran persona!

Quiero agradecer también a Alex, Héctor, Ela y Fran, dónde todo y compartir poco tiempo en el laboratorio demostrasteis ser unas maravillosas personas. Jorge, un chico trabajador que alegraba las mañanas con su música y sus chistes de electricidad. Adrián, un maestro dispuesto a enseñarte todo lo que sabía. Pili y Eva, unas madrazas capaces de apoyarte en todo lo que necesites, siempre escuchando y ni los malos momentos os hacen perder esa bondad y alegría que os hace tan especial.
Poco después de entrar en el laboratorio, llegaron Clara, Marina y María, tres chicas que aportaron una gran alegría y dulzura al laboratorio. Clara una gran imitadora y una

de las chicas más fuertes que conozco, gracias a ella tuve el placer de conocer a Marcos, un genio. Marina, una chica dulce y mi melón en todo este tiempo. Y Maria, una compañera estupenda que siempre hacia sacar lo mejor de cada persona.
Gracias también a las maravillosas estudiantes de máster que he podido tutorizar; María, Elba e Ilaria. El laboratorio tuvo mucha suerte de poder contar con vosotras, cada día nos enseñabais cosas nuevas. Destacar también Bea y Elisa del grupo de Puri, convirtiéndose en unas gran compañeras.
Agradecer también a Ana, sobretodo en mi última etapa en el laboratorio por su consejo y ayuda siempre y que lo he necesitado. Kim y Juliana, demostrasteis ser unos grandes científicos. Enrique, nuestro *marketing boy,* muchas gracias por tus consejos y por darnos otra visión de la ciencia, estoy segura de que te irá todo muy bien. Joan y Adrià, aire fresco en el laboratorio de Puri, trabajadores y luchadores, una pena haber coincidido tan poquito tiempo. También como base del trabajo en estos dos últimos años, quiero agradecer a nuestro técnico Manu por su ayuda en esas millones de horas de genotipar.
Finalmente, compartiendo grupo pero no espacio ni ciudad, me queda agradecer a la gente de Madrid dónde han contribuido a que pueda terminar esta tesis. Destacar, Alex *macho* y Alex *hembra*, tuve el placer de compartir laboratorio con vosotros con lo que sé lo estupendos que sois y que tenéis un gran corazón, os deseo mucha suerte y energía con esta nueva aventura, lo haréis genial! Patricia, muchas gracias por el esfuerzo final que has hecho! Maria, gracias a ti también, porque tomas las riendas de este proyecto y estoy segura de que lo llevaras muy bien.

Gracias a todos los integrantes de este maravilloso PEBC o bien ex-PEBC/ IJC por todo vuestro apoyo, colaboración y por todos los buenos momentos que hemos pasado juntos. Entre muchos momentos juntos, no se pueden olvidar esas horas en cultivos dónde nos evadíamos con la radio a tope dónde nos contábamos nuestras preocupaciones o planes y hacían más amenos los días, los anti-retreats… Todos y cada uno de ellos han hecho que más que compañeros, pudiéramos formar esta gran familia que han hecho de estos poco más de 4 años fueran una de las etapas más importantes de mi vida. Gracias a todo el personal de limpieza y estabulario que nos regalaban cada día una sonrisa. ¡Gracias a todos por todo! Mención especial a Fer, un solete de persona, pilar del departamento, dispuesto a ayudarte y a contarte sus anécdotas más que divertidas con toda su dulzura y amabilidad. Chiqui!... No cambies nunca Fer, eres un grande!

Gracias a mis amigas desde la infancia por los buenos momentos que a pesar que pasen los años y nos veamos poquito (espero que esto cambie a partir de ahora…) seguimos disfrutando como el primer día. Blanca, gracias por tu sinceridad, apoyo condicional y dulzura. Raquel, la más valiente del grupo, siempre estás ahí cuando se necesita. Anahí, la que nos mantiene informadas de todo cotilleo, gracias a todas por estar ahí en todo momento y hacer nuestra amistad cada vez más fuerte.

Y, finalmente, gracias a ti Jordi. Le estoy muy agradecida en primer lugar a mi madre por empujarme a invitarte al básquet como a ti por colarte en mi cumpleaños… Gracias por estar ahí siempre, ayudarme a levantarme… Te adentraste en esta aventura por amor sin saber cómo acabaría. Los dos hemos pasado por una tesis… pero gracias por creer siempre en mí, por tus consejos y ayudarme a tomar decisiones. ¡Has tenido una paciencia infinita! Esta tesis no hubiera sido posible sin ti.TQM

MIL GRÀCIES A TOTS!

INDEX

INDEX

ABBREVIATIONS

ABBREVIATIONS

-/-, +/+: Homozygous

-/+: Heterozygous

-a647: Alexa 647

ADAMs: Metalloprotease-disintegrins

ANOVA: Analysis of Variance

AP: Alkaline Phosphatase

APC: Allophycocyanin

ARF: Alternative-Reading Frame

BCSC: Breast Cancer Stem Cell

BrdU: 5-bromodeoxyuridine

cDNA: Complementary Deoxyribonucleic Acid

CD: Cluster of Differentiation

CDKs: Cyclin-Dependent Kinases

CSC: Cancer Stem Cells

c-Myc: c-Myelocytomatosis viral oncogene

DAB: 3, 3'-diaminobenzidine

DAPI: 4 ', 6-diamidino-2-fenilindol

DCIS: Ductal Carcinoma *in situ*

DDR: DNA damage Response

DMBA: 7-12-dimethylbenz[α]anthrance

DMEM: Dulbecco's Modified Eagle's medium

DMSO: Dimethyl Sulfoxide

Doxy: Doxycycline

EGF: Epidermal Growth Factor

EPCAM: Epithelial Cell Adhesion Molecule

ERK: Extracellular Regulated Kinase

FACS: Fluorescence-Activated Cell Sorting

FBS: Fetal Bovine Serum

-FITC: Fluorescein Isothiocyanate

Fvb: FVB/NJ mouse strain

GEMM: Genetically Engineered Mouse Model

GSEA: Gene Set Enrichment Analyses

γH2AX: Histone variant H2AX phosphorylated on serine 139

HEK: Human Embryonic Kidney 293 cells

H&E: Hematoxylin and Eosin

HEPES: 4-(2-hydroxyethyl)-1-piperazineethanesulfonic acid)

HP: Hyplerplasia

HR: Hormone Receptor

IL6: InterLeukin-6

ILC: Invasive Lobular Carcinoma

iPSCs: induced Pluripotent Stem Cells

JNK: c-Jun N-Terminal Kinase

K8, K4: Keratin 8, 14

Kg: Kilograms

Klf4: Kruppel-like factor 4

KSR: Knockout Serum Replacement

LGR: Leucine-rich repeat-containing G-protein coupled Receptor

LIF: Leukemia Inhibitory Factor

LTR: Long Terminal Repeat

MAPK: Mitogen-Activated Protein Kinase

MaSCs: Mammary Stem Cells

MEC: Mammary Epithelial Cell

MEFs: Mouse Embryonic Fibroblasts

MIN: Mammary Intraepithelial Neoplasia

µg: micrograms

mg: milligrams

µl: microlitres

ml: millilitres

µm: micrometres

mM: millimolar

MMPs: Metalloproteinases

MMTV: Mouse Mammary Tumor Virus

MPA: Medroxyprogesterone

NaCl: Sodium chloride

NF-κB: Nuclear Factor κappa-light-chain-enhancer of activated B cells

Oct4: Octamer-binding transcription factor 4

OIS: Oncogene-Induced Senescence

OPG: Osteoprotegerin

OPGL: Osteoprotegerin Ligand

OSKM: Oct4-Sox2-Klf4-cMyc

p.o: oral gavage

p16INK4A: Cycline-dependent kinase inhibitor 2a

p19ARF: Cycline-dependent kinase inhibitor 2a

p53: Tumor protein p53

PBS: Phosphate Buffered Saline

-PE: Phycoerythrin

-PECy7: Phycoerythrin Cyanine 7

PEG400: Polyethylene Glycol 4000

PI3K: Phosphoinositide 3-kinase

PIP2: Phosphatidylinositol 4,5-bisphosphate

PIP3: Phosphatidylinositol 3, 4, 5-triphosphate

PR: Progesterone Receptor

P/S: Penicillin-Streptomycin

PTEN: Phosphatase and Tensin homologue deleted on chromosome ten

PTHrP: Parathyroid Hormone-related Peptide

PyMT: Polyome Middle T

qRT-PCR: quantitative Reverse Transcription PCR

RANK: Receptor Activator of Nuclear factor κβ

RANKL: Receptor Activator of Nuclear factor κβ ligand

RNA: Ribonucleic Acid

RNAseq: RNA sequencing

ROS: Reactive Oxygen Species

RSPO: R-spondin

RTKs: Receptor Tyrosine Kinases

SA-βGal: Senescence-Associated β-Gal Activity

SASP: Senescence- Associated Secretory Phenotype

Sca1: Stem Cells Antigen 1

SIPS: Stress-induced premature senescence

SMA: Smooth Muscle Actin

Sox2: SRY (Sex determining Region Y)-box2

TEBs: Terminal End buds

TIS: Therapy-induced senescence

TLX: Orphan nuclear receptor subfamily 2 group E member1 (NR2E1)

TNBC: Triple-Negative Breast Cancer

TNF: Tumor Necrosis Factor

U: Units

Wnt: Wingless-type MMTV integration site family

WT: Wild-Type

INTRODUCTION

INTRODUCTION

1 Mammary gland

1.1 Biology and anatomy of the mammary gland

The mammary gland is a quite unique organ developed in mammals with the specific function of synthesizing and secreting milk to sustain the newborns[1]. Both males and females have glandular tissue within the breasts; however, in females, the glandular tissue further develops after puberty in response to estrogen. The mammary gland is comprised by a branched duct epithelial tree immersed in a specialized structure- the fat pad. This structure dramatically changes during pregnancy and lactation, with the development of the alveoli, the milk producing structures of the mammary gland [1].

Multiple cell types can be found in the mammary gland, including epithelial, fibroblasts, adipose, immune, lymphatic and vascular cells[2]. Within the epithelial compartment, two main layers can be found: an inner (luminal) and an outer (basal) layer. Luminal cells are organized with the apical cytoplasm toward the lumen, in which they secrete milk during pregnancy, whereas the basal layer is composed by myoepithelial cells that surround the luminal cells and have properties of smooth muscle cells, being responsible for the contraction of the alveoli and milk secretion[3]. The specific expression of cell surface cytoskeletal keratins allow to classify the basal and luminal layers: in mouse, luminal cells express cytokeratin 8 and 18 (K8,K18), whereas basal cells express cytokeratin 5 and 14 (K5,k14)[3]. Mammary stem cells (MaSCs) are found within the basal compartment[4]. The ducts and alveoli are embedded in the stroma or connective tissue, where the main components are adipocytes, but also fibroblasts, hematopoietic cells and blood vessels (**Figure 1**).

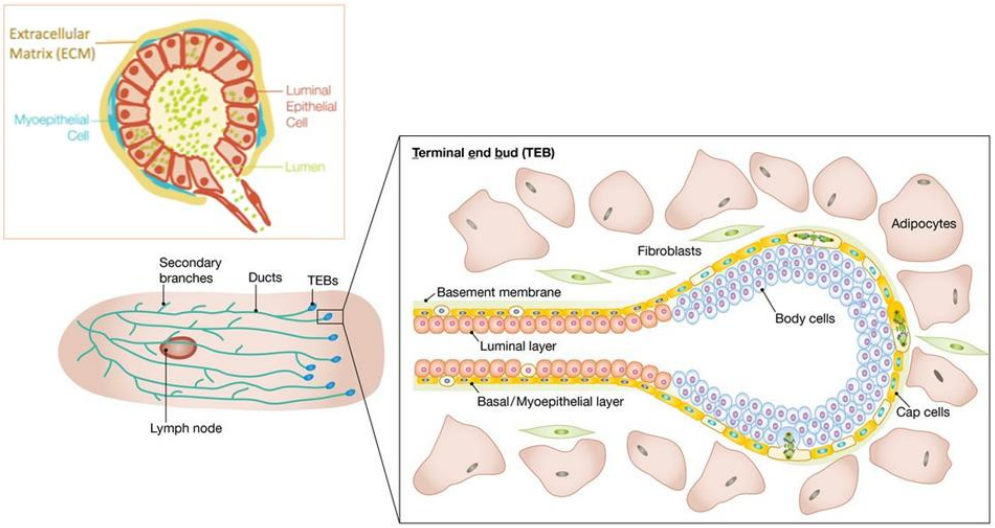

Figure 1*:* Cellular structures of the mammary gland. The ductal epithelium is composed by a basal/myoepithelial layer, which is in contact with the basement membrane, and a luminal layer with secretory function. Adapted from Santoro et al. EMBO Rep. 2016.

1.2 Mammary gland development

Unlike most organs of the body, which develop to a relatively mature state during embryonic life, the mammary gland reaches a mature functional state only during the pregnancy-lactation cycle in the adult female. Breast development during life follows a time course cycle of distinct phases which includes fetal growth, puberty, pregnancy, lactation and involution[5,6]. During these stages, the cells of the mammary gland proliferate, differentiate or die in response to specific stimuli, hormones and growth factors, promoting significant remodeling of the glandular tissue architecture[2].

Mammary gland development starts during embryogenesis with the formation of a small primordial epithelial tree initiated in the nipple[7]. From birth to puberty, the mammary epithelium originated at the nipple will remain quiescent (**Figure 2*A***). After a complex, hormone-dependent process during embryonenesis[7,8], the ductal epithelium of the mammary buds invade into the mammary fat pad, and subsequently the sex hormones initiate the development and differentiation of a small primordial epithelial tree in the nipple (**Figure 2*B***)[9,10]. At this moment, elongation of the ductal tree during pubertal mammary gland development is possible due to the existence of high proliferative terminal end buds (TEBs). TEBs are formed at the front of the ducts and penetrate deep into the fat pad allowing fat pad elongation. Regular bifurcation and branching during ductal elongation produces the main ductal system of the mammary tree[11]. Once the TEBs reach the edges of the fat pad they regress. Further side branching occurs off of the previously formed ducts during subsequent estrous cycles in response to progesterone signaling in the adult mammal but the growth of these side-branches in not driven by TEBs. The final arboreal, bilayered ductal structure is composed of apically oriented luminal epithelial cells that are surrounded on the basal side by contractile myoepithelial cells. Estrogenis responsible for these epithelial ductal tree elongations and side branching into the mammary fat pad or stroma in order to form an adult gland (**Figure 2*C***)[8]. In the virgin mammary gland, the epithelium proliferates and involutes though apoptosis during each estrus cycle[12]. Also, this growth is influenced by growth hormone, which is secreted from the pituitary gland and is an important regulator of mammary gland development. Growth hormone effects are mediated through its downstream insulin-like growth factor-1 (IGF1) effector[13].

During pregnancy, the alveolar epithelium proliferates in response to circulating hormones. Progesterone induces a massive proliferation of ductal branches and the formation of alveolar buds. Furthermore, prolactin/JAK-2/Stat5, RANKL, c/EBP and the cell cycle proteins CyclinD1 and D2 are critical for these differentiation and proliferation events[14]. During the second half of pregnancy, the alveolar buds progressively split and differentiate into single alveoli that will turn into milk-secreting lobules during lactation, therefore, at the end of pregnancy, the alveoli fill almost completely the mammary gland. At the same time, myoepithelial cells that surround

epithelial layers acquire contractility in order to mechanically stimulate milk secretion after the lactogenic switch[15] (**Figure 2*D***). This lactogenic switch is orchestrated by prolactin and consists in the differentiation of the alveolar buds into milk-secreting structures[15]. As a result, the epithelial cells secrete milk proteins and lipids into the lumen[2]. Myoepithelial cells facilitate the mechanic stimulation of milk ejection when being stimulated by oxytocin[15]. After lactation, the lack of milk demand at weaning causes milk to lie dormant in the mammary epithelium. The mammary gland reverts to its initial stage before pregnancy, a process called involution, which is characterized by a high grade of apoptosis, re-development of the mammary adipose tissue, remodeling and restoring the quiescent stage of the mammary gland before pregnancy (**Figure 2*E***)[16]. The metalloproteinase 3 (Mmp3) is the key protease involved in the remodeling of the gland during involution[17].

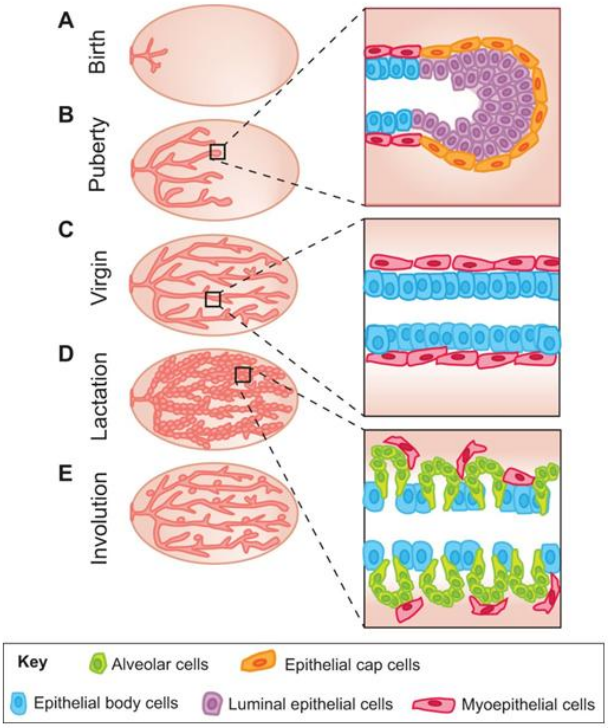

Figure 2: Mammary gland development. **A**) A small ductal tree is visible in the pre-pubertal mammary gland and remains quiescent until puberty. **B**) During puberty, the ductal tree invades the fat pad upon hormonal stimuli. **C**) The virgin mammary gland is filled with epithelial branching structures. The ducts contain an outer layer of myoepithelial cells and an inner layer of luminal epithelial cells. **D**) During pregnancy and lactation, the alveoli differentiate into milk-secreting structures filling the majority of the fat pad. **E**) After lactation, involution restores the "original-like" stage of the adult mammary gland. Scheme reproduced from L.Inman et al., Development 2015.

Several cellular pathways and key proteins are involved in mammary gland development; some of them have been directed related to mammary gland biology such as JAK/STAT hormones, Cyclin D1 and D2 or RANK pathway (as will be explained in next chapters). Moreover, other signaling pathways such as Wnt, Notch, Rspo and Tfap2 are crucial in the formation of the mammary gland[18–23].

1.3 Mammary epithelial cell hierarchy

Mammary gland homeostasis has been long believed to be maintained by bipotent stem or progenitor cells that are are able to give rise to both basal and luminal populations[24,25]. However, in past years this dogma has been challenged and several lines of evidence demonstrate that the lineage hierarchy of the mammary gland is not completely understood and established.

The existence of multipotent mammary stem cells (MaSCs) was demonstrated in mice via cleared fat pad transplantation assays[26]. Deome and colleagues developed a technique that is considered as the "gold-standard" for characterization of the MaSC[26]. Briefly, the gland of 3 week-old recipient mouse is cleared by cutting out the endogenous epithelium, which at that point, has not yet reached the lymph node. The remaining fat pad serves as a receptive environment for portions of normal mammary epithelium from the donor mouse. Successful engraftment of the mammary epithelium was observed in the recipient mouse, evidencing the auto-renewal ability of MaSCs. Subsequent studies demonstrated that successful engraftment could be obtained with any segment of the mammary epithelial tree[27–29], thereby indicating that the repopulating cells, MaSCs, are widely distributed. Moreover, MaSCs can be isolated by flow activated cell sorting (FACS) based on cell-surface markers[24,30]. The MaSCs were characterized by exclusion from well-characterized endothelial (CD31) and hematopoietic (CD45) antigens and enrichment of basal markers. These cells located in the basal layer, are proposed to be bipotent cells able to differentiate in two different lineages of progenitors/stem cells (SCs),and competent to give rise to either luminal or basal cells[31]. In the case of the luminal progenitors, which are hormone receptor negative (HR^-) cells, they would differentiate into both alveolar and ductal cells, whereas the basal progenitors would give rise mainly to myoepithelial cells[32](**Figure 3**).

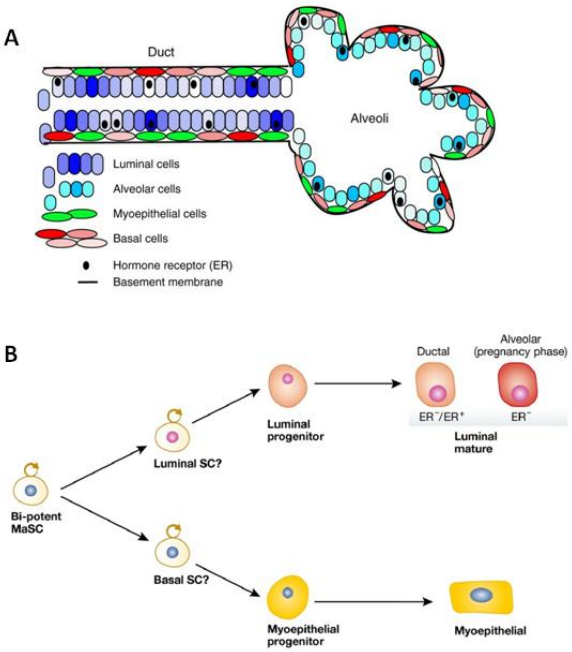

Figure 3: Model of the hierarchy proposed for mammary epithelial cell differentation. **A**) Schematic outline of a ductal alveolar unit (alveoli) in which the location of the various cell types is indicated. Adapted from Cristea S. et al. Nature Communications, 2018. **B**) Graphic summary of the mammary cells at different differentiation stages. Adapted from Santoro A. et al. Embo Reports, 2016.

Heat stable antigen CD24, a membrane glycoprotein, is heterogeneously expressed in the mammary gland. Three mammary epithelial cell (MEC) populations, classified by their CD24 expression levels, were identified: negative ($CD24^-$), CD24low ($CD24^{lo}$) and CD24high ($CD24^{hi}$)[33]. Their cytokeratin expression pattern showed that they represent the non-epithelial, myoepithelial/basal and luminal epithelial cell population, respectively. Mammary fat pad repopulation assays revealed that the basal $CD24^{lo}$ population is enriched in MaSCs[33]. Further characterization of cell-surface markers such as CD29 (β-1 integrin) and CD49f (α-6 integrin) allowed to better identify mammary epithelial cell populations. Indeed, $CD24^{lo}$, $CD29^{hi}$ and $CD49f^{hi}$ cell populations are considered enriched in MaSCs since they show increased mammary repopulating ability *in vivo*[24,30]. These markers were defined as the specific markers used to identify MaSCs. However, other markers such as Lrp5/6[34], Axin2[35], CD1d[32], Lgr5[36], Procr[37], α-smooth muscle actin (αSMAor SMA)$^+$ and $Myh11^+$[38] have also been reported to identify MaSCs.
Further differentiation among cell types is done based on keratin expression: K8 and K18 for luminal cells and K14 for myoepithelial cells, which are also positive for SMA and K5[39,40]. Different pathways regulate mammary cell differentiation and mammary stem cell pool preservation such as Notch, Hedgehog and Polycomb signaling[41,42]. High levels of progesterone in the estrous cycle have also been described to expand the MaSC pool[43].

The luminar layer is classified in two different groups based in their expression of hormone receptors[44]. The hormone responsive cells (HR^+) are considered mature luminal cells with low proliferation rate and are characterized as $CD24^{hi}$, $CD49f^{lo}$ and $Sca1^+$ cells, that express estrogen and progesterone receptors (ER and PR). The other group is HR^- and is characterized as being $CD24^{hi}$, $CD49f^{lo}$ and $Sca1^-$ [45]. They are considered luminal progenitors with higher proliferating rate and contain the CD61+ progenitros with higher proliferating rate and cotain the $CD61^+$ progenitors that establish the alveolar lineage during pregnancy[46] and is encompassed by the $Elf5^+$, common marker for all the luminal progenitors[47]. The discrepancy between hormone receptor expression and proliferation rate suggest that the hormones act by paracrine signaling[48]. The basal layer is characterized as being $CD24^{lo}$, $CD49f^{hi}$, $Sca1^-$ and $CD61^+$ and is mainly composed of contractile myoepithelial cells that surround the ducts and alveoli[33].

Lineage-tracing studies tracking mammary stem/progenitor cells have re-opened the debate denying the existence of bipotent MaSCs in the adult mammary gland and favoring the existence of unipotent stem cells that are able to give rise just to luminal or basal cells that maintain adult tissue homeostasis[49]. Reporter genes such as GFP, RFP, YFP and mCherry are commonly used in these experiments[50]. In order to study the unipotency of MaSCs, lineage-tracing experiments in embryonic, pubertal, adult, pregnant, and involuted mammary glands have been performed[49,51]. The tools most commonly used are: K14-rtTA/TetO-Cre/Rosa-YFP and K5-CreER/Rosa-YFP transgenic mice for tracking basal cells and K8-CreER/Rosa-YFP and K18-CreER/Rosa-YFP transgenic mice for tracking luminal cells. When YFP expression is driven by K14 or K5 promoters in embryos, both luminal and basal cells are labeled at puberty, meaning that embryonic $K14^+$ and $K5^+$ cells are bipotent. However, when K14 or K5 regulated YFP is conditionally induced after birth, exclusive labeling of basal cells is detected, indicating that postnatal $K14^+/K5^+$ cells are unipotent and do not give rise to the luminal cell progeny in adults. Similarly, YFP driven by K8/K18 luminal promoters, labels only luminal cells[49]. In contrast, another report claimed the existence of bipotent MaSCs in adult mice using clonal cell-fate mapping studies with a stochastic multicolour *Cre* reporter (confetti) combined with a new three-dimensional imaging strategy. Besides restricted luminal and basal progenitors, the authors demonstrated the existence of a subset of basal cells with bi-potent ability that were able to give rise to luminal and basal cells[47]. Thus, it is still unclear whether postnatal MaSCs are multipotent or there are two different unipotent stem cells populations in charge of replenishing the adult mammary gland.

Further complicating the already complex image of mammary cell hierarchy, three independent groups have shown that the luminal layer itself is maintained by restricted progenitors, rather than by a common luminal progenitor. Lineage-tracing of ER^+ cells[52] and Notch1[53,54] demonstrated that the luminal hormone receptor positive lineage is independent of the hormone receptor negative thereby challenging the dogma of progenitor and differentiated lineages in the luminal compartment.

2 Breast cancer

2.1 Cancer and tumor nomenclature

Cancer is a broad term that describes diseases resulting from cellular changes favoring the uncontrolled proliferation and transformation of cells. Some types of cancer cause faster cell growth, while others cause cells to grow and divide at a slower rate. Cell fate is tightly regulated by extra and intracellular signaling and abnormal or aged cells are instructed to disappear being replaced with fitter cells. Cancer cells lack the ability to decode the controlling signals and manage to proliferate unrestrained, invade surrounding tissues and metastasize to distant organs[55–57]. Cancer type is generally termed based on the tissue from the body and the type of cell where it originates.

A tumor is an abnormal mass of cells that can either be benign (non-cancerous) or malignant (cancerous). If a tumor remains localized to the area in which it originated and does not spread, it is usually considered benign. Although benign tumors constitute an abnormal mass of cells, they have not entirely escaped from the restrictions imposed by cell growth controls and are not able to invade surrounding tissues or spread to secondary organs, being less dangerous than malignant tumors. In fact, the most aggressive tumors are those capable of invading and destroying healthy tissues; known as malignant tumors. The process by which tumor cells spread and seed in distant areas is known as metastasis. Hanahan and Weinberg have established the ten distinct biological characteristics acquired by tumors during malignant transformation: sustained proliferative signaling, evasion from growth suppressors, activation of invasion and metastasis, acquisition of replicative immortality, induction of angiogenesis, resistance to cell death, deregulation of cellular energetic, genome instability and mutation, tumor-promoting inflammation and escape from immune destruction (**Figure 4**)[58,59].

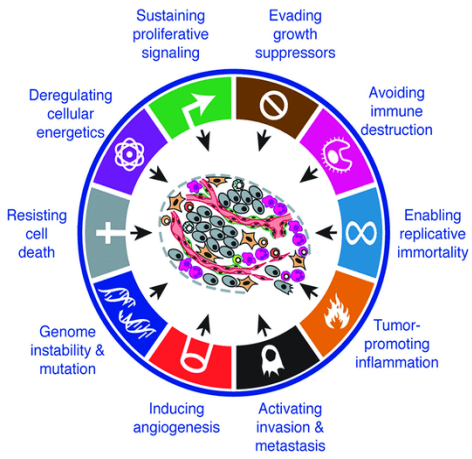

Figure 4: Hallmarks of cancer. Adapted from Hanahan and Weinberg, Cell 2011.

2.2 Incidence and subtypes of breast cancer

Breast cancer is the second most common cancer in women after skin cancer[60]. The risk associated with breast cancer can be divided into two groups, genetic or lifestyle factors[61]. The first group includes factors such as age, sex, race, inherited genetic traits promoting familial occurrence of the neoplastic disease or the occurrence of benign proliferative lesions of the mammary gland. They all constitute independent parameters. The second group would include extrinsic factors conditioned by lifestyle, including diets or long-term medical interventions such as oral hormone replacement therapy, and their influence on the neoplastic process may be modified to a certain degree[62].

Breast cancer can be classified following different criteria: histopathology, clinical stage, histological grade, receptor status and molecular profile. Besides, there are different ways of staging breast cancer, usually its status ranges from stage 0 to 4, which may be broken down into additional stages. Briefly, the main characteristics of breast cancer stages are the following ones:

Stage 0: the cells are limited within a duct and have not invaded surrounding tissues, it is known as ductal carcinoma *in situ* (DCIS). Stage 1: the tumor is small and has not spread to the lymph nodes. Stage 2: the tumor is small, but it has started to spread to nearby lymph nodes. Stage 3: the tumor is up to 5 cm and has spread to axillary lymph nodes or internal mammary lymph nodes. However, it has not spread to other parts of the body. Stage 4: the tumor can have any size and has spread to other organs, especially to the bones, lungs, liver or brain. These are known as metastatic breast cancers.

About 5 to 10% of breast cancer cases are hereditary[63,64]. The main genes whose mutations are associated with higher breast cancer risk are *BRCA1* and *BRCA2*. They are tumor suppressor genes that, when mutated, prevent cell death and favor uncontrolled cell growth,subsequently leading to cancer[65,66]. Mutations in other genes are also associated with breast cancer, such as those in *TP53*, *PTEN*, *RAD50*, *PALB2*, *BRIP1*, *ATM*, among others. These genetic mutations are less common and do not increase breast cancer risk as much as *BRCA1* and *BRCA2* mutations do[67,68].

There are several types of breast cancer, which can be classified according to different parameters, such as the cells of origin, the location in the breast, the degree of invasors, the histologic grade, or gene expression patterns[69]. Histologically, breast cancer can be classified in *in situ* carcinoma and invasive or infiltrating carcinoma[70]. The most common type is originated by epithelial cells within the ducts and lobules, known as DCIS, where abnormal cells have been contained in the lining of the duct, and invasive lobular carcinoma (ILC), in which the abnormal cells have begun to invade surrounding tissue. Further characterization of the type of breast cancer is essential, taking into account the status of HR and other molecular markers such as ER,

progesterone receptor (PR), human epidermal growth factor receptor 2 (HER2/Neu) and p53[71]. Microarray-based gene expression analysis and unbiased hierarchical clustering allowed to identify five molecular subtypes of breast cancer (**Figure 5**)[72]: luminal A ($HR^+/HER2^-$) with low proliferation and better prognosis than other subtypes due to slower growth rates and less aggressive, responding favorably to anti-hormone therapies; luminal B ($HR^+/HER2^-$) and luminal B-like ($HR^+/HER2^+$), both of them are more proliferative (high staining levels of ki67[73]) and with worse prognosis than luminal A subtype; HER2-enriched ($HR^-/HER2^+$), more aggressive than the luminal subtypes and thus associated with worse outcome, although specific antibodies and inhibitors targeting HER2 have been developed for its treatment; and basal-like ($HR^-/HER2^-$) characterized by worst short-term prognosis and lack of targeted therapies, being chemotherapy the only available treatment up until the recent development of immune-based therapies[73]. The basal-like subtype is sometimes called triple-negative breast cancer (TNBC), since these tumors do not express ER, PR, nor HER2. Another TNBC subtype is the claudin-low, described as being $HR^-/HER2^-$ but displaying an enrichment in the expression of epithelial-to-mesenchymal transition (EMT) and immune-response genes as well as in cancer stem cell-like features, and a slower proliferation rate than basal- tumors[74,75]. Recently, a 50-gene signature, PAM50, has been demonstrated to efficiently identify the different breast cancer molecular subtypes and can be characterized by qRTPCR faster and cheaper than microarray analyses or genome sequencing[76].

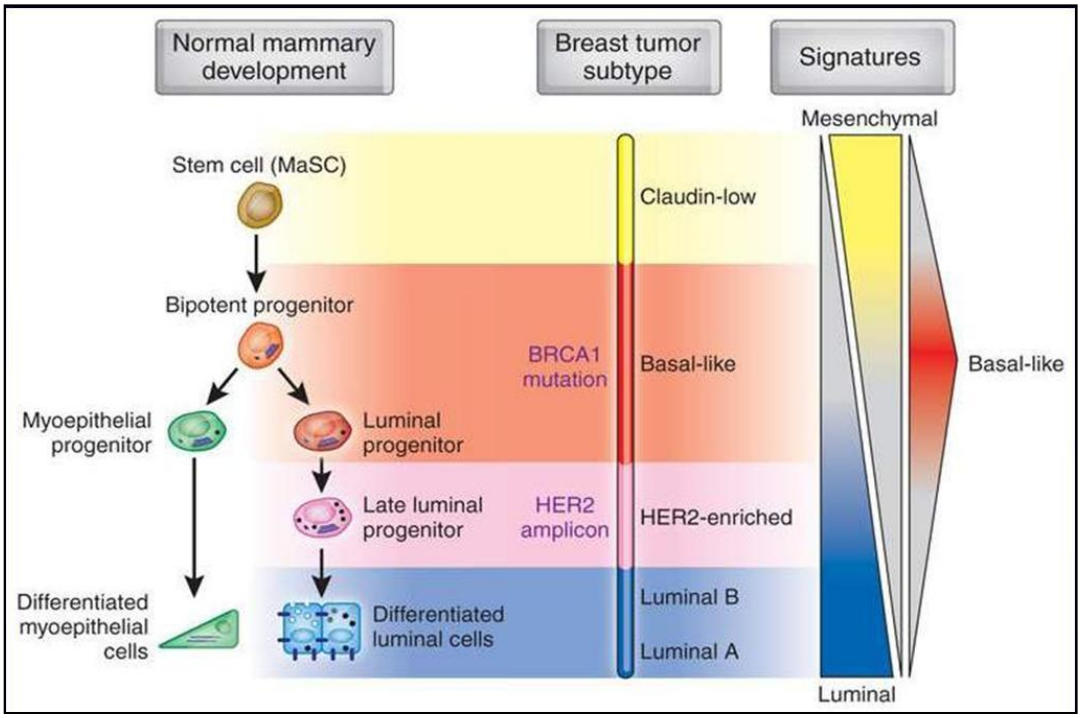

Figure 5: Models of the human mammary epithelial hierarchy linked to breast cancer subtypes. Scheme reproduced from Prat and Perou Nature Medicine 2009.

Regarding the treatment options for breast cancer, they are associated with the molecular subtype defined by ER, PR and HER2 status. In the case of patients diagnosed with luminal A and luminal B breast cancer subtypes, they respond poorly to chemotherapy and their treatment is based on endocrine therapy (targeting estrogen) such as tamoxifen or aromatase inhibitors[75]. For the HER2-enriched tumors, the treatment is based on HER2 pathway inhibitors usually combined with chemotherapy. In the case of basal-like and claudin-low subtypes, they lack clear targets, and thus the current treatment is (neo)adjuvant combinations of chemotherapeutic agents[75].

Even though important improvements in breast cancer molecular classification and treatment have been maded, it is still necessary to find targets to develop novel therapies based on biomarkers specific for each subtype to accurately treat breast cancer patients and improve their prognosis.

2.3 Cancer stem cells

Cancer stem cells (CSCs) are subpopulations of cancer cells sharing characteristics with normal stem or progenitor cells, such as self-renewal ability and multi-lineage differentiation, that are able to drive tumor growth as well as tumor heterogeneity (**Figure 6**). Since these cells have been found in various types of human tumors, they are currently regarded as attractive targets for cancer treatment[77]. CSCs are mainly characterized by the expression of surface markers associated with stem cells, such as CD133, CD24, CD44, CD90, CD29, CD49f and, ALDH1. Althought no single marker can be used to define the CSC population[78], expression of cell surface markers has been used to isolate and enrich CSCs from different tumors by FACS[79–81].

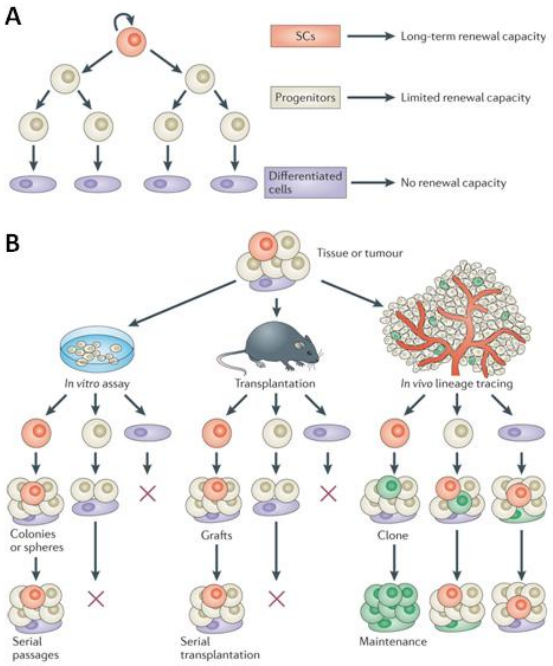

Figure 6: **A**) Cellular hierarchy in normal tissues or tumors implies that not all cells are equivalent and that only stem cells (SCs) present long-term self-renewal and differentiation potential. **B**) Functional assays, such as *in vitro* clonogenic assays, transplantation and lineage-tracing experiments (marked cells are shown in green), can be used to assess the renewal and differentiation potential of SCs, committed progenitors and differentiated cells. Adapted from Beck & Blanpain Nature Reviews in Cancer 2013.

CSCs tumorigenic potential is characterized by their enhanced ability to regenerate the original tumor when transplanted into immunodeficient mice even at low clonal density (limiting dilution assays). Moreover, an sphere-forming assay was also used as an *in vitro* assay for the identification and enrichment of CSCs, whereby only fractions of cells from solids tumors have the ability to form spheres[82](**Figure 6**). In breast cancer, these cells are the so-called breast cancer stem cells (BCSCs).

The expression of CSC surface markers is tissue type-specific. Human BCSCs were characterized to have $CD44^{+}$ and $CD24^{-/low}$ expression[83]. Several pathways with key roles during embryonic development and adult tissue homeostasis have been implicated in the regulation of BCSCs self-renewal, including, among others, Notch, Hedgehog and Wnt/β-catenin[84,85]. CSCs are also believe to be responsible for the metastatic dissemination of tumors. In line with this, it has been described that BCSCs play a crucial role in metastasis,since they show increased motility and invasion ability[86–88]. Therefore, novel therapies targeting CSCs will benefit patient survival and outcome.

2.4 Genetically engineered mouse models of breast cancer

The intensified research based on genetically engineered mouse models (GEMMs) has allowed a deeper understanding of the mechanisms responsible for breast cancer development. Recently developed complex GEMMs have allowed to further investigate underlying processes such as cancer initiation, invasion and metastasis. Moreover, GEMMs have contributed to understand mammary gland biology due to mouse evolutional proximity to humans, their short life-span and easy handling. In GEMMs, specific genes can be overexpressed (knock-in KI) or deleted (knock-out KO) during cancer progression and dissemination. However, experiments with GEMMs are time-consuming, expensive, strain background-dependent and, in some cases, the results obtained are difficult to interpret[89,90]. Besides these limitations, GEMMs have provided new insights into the characterization of tumor evolution and metastasis, representing nowadays an essential tool for preclinical cancer studies.

Regarding breast cancer, the main drawback is that not a single GEMM by itself covers the full spectrum of human breast cancer, whereas individual models address distinct aspects. Each GEMM targets particular signaling pathways outside and inside the mammary cell, and the disruption of these pathways can be performed at different

time points[91]. Apart from GEMMs, another common model is the human tumor xenografts, where human cells are transplanted into immunocompromised mice, either under the skin (subcutaneous) or into the organ in which the tumor was originated (orthoxenografts)[92].

More than 50 GEMMs of breast cancer have been generated up to date. The Mouse Mammary Tumor Virus (MMTV)-long terminal repeat (LTR) is one of the most common promoters used to create transgenic mouse models of breast cancer. MMTV is a RNA virus with oncogenic potential that belongs to the *Retroviridae* family. MMTV promoter is hormonally regulated by glucocorticoids, progesterone and dihydrotestosterone, hormones involved in mammary development, therefore the activation of the promoter is increased during mammary gland development and lactation[93–95]. A large number of oncogenes have been expressed under the control of the MMTV promoter in mice, such as Neu (a rat orthologue of the human ErbB2 gene that is associated with 15-20% of human breast cancer cases), cyclin-D1, Ras, c-myc, the Polyoma virus Middle T oncoprotein of SV40 virus (PyMT) and many others [89,96].

Transgenic mice with mammary gland-specific expression of Neu under the control of the MMTV promoter (MMTV-Neu) develop multifocal adenocarcinomas at the median age of 5-10 months with lung metastasis in FVB background[97–99]. ErbB2 (Neu) belongs to the EGFR family and encodes a receptor tyrosine kinase. ErbB2 signals downstream through the Ras/MAPK cascade, activating c-myc, c-jun and c-fos, and activated protein-1 (AP-1). ErbB2 drives cell proliferation, migration, transformation and survival through the inhibition of apoptosis[100]. As previously mentiond, HER2 (ErbB2) expression is used to allow clinical stratification of breast cancer and it is associated with prognosis[101]. Analyses of the tumors from MMTV-Neu mice revealed sporadic in-frame deletions, point mutations, or cysteine residue insertions within the Neu extracellular domain. These cysteine insertions lead to receptor dimerization, causing receptor activation[102,103]. These data suggest that activating mutations in Neu are essential for mammary tumor initiation in these MMTV-Neu transgenic mice.

Mammary gland-specific expression of PyMT under the control of the MMTV promoter (MMTV-PyMT) results in the transformation of the mouse mammary epithelium and the development of multifocal mammary adenocarcinomas and metastatic lesions in the lymph nodes and lungs[104]. Based on the histopathological changes in these mice, four different stages leading to malignant carcinoma can be distinguished: hyperplasia, adenoma/mammary intraepithelial neoplasia (MIN), and early and late carcinoma[105]. These stages are comparable to human breast disease classified as benign or *in situ* proliferative lesions to invasive carcinomas. MMTV-PyMT mice develop tumors with short latency, 100% incidence and secondary lung metastasis at 3 months of age. Virgin female mice from the FVB background develop multifocal mammary tumors indicating that tumor initiation is independent of pregnancy. A distinct characteristic of

this model is that a primary focus of tumor formation occurs early in the epithelium next to the nipple, and after some weeks, multiple tumor lesions appear all over the mammary gland, showing heterogeneous stages of progression. Tumors derived from MMTV-PyMT mice are ER^- and express high levels of HER2/Neu and CyclinD1[98,106]. Therefore, the MMTV-PyMT model reasonably recapitulates human breat cancer.

Besides, PyMT and Neu mice models form luminal-like tumors that are highly similar to human luminal tumors in terms of cytokeratin expression ($K8^+$, $K18^+$) and molecular subtype[107], although the tumors lack the expression of hormone receptors in the last stages($K8^+$,ER^-,PR^-).

3 RANK/RANKL signaling pathway

3.1 Members of the pathway

Receptor activator of NF-κB or RANK, the ligand of receptor activator of NF-κB or RANKL, and the soluble decoy receptor osteoprotegerin (OPG) are the main members of the RANK/RANKL signaling pathway. They belong to the tumor necrosis factor (TNF) superfamily. The RANK/RANKL/OPG axis was first identified in the late-1990s as a pivotal regulator of bone metabolism and the immune system[108,109]. Subsequently, the RANK/RANKL pathway has been found critical for the regulation of epithelial differentiation of the mammary gland[20,21], hair follicle, thymus and small intestine, as well as the thermoregulation of the central nervous system, among others[110–113].

RANK (*TNFRSF11A*), also known as TNF-related activation-induced cytokine receptor (TRANCE-R) or osteoclast differentiation and activation receptor (ODAR), is a type I transmembrane protein that does not possess intrinsic kinase activity and relies on the recruitment of factors to activate downstream signaling pathways. The full-length human *RANK* cDNA encodes a protein of 616 amino acids (aa) with a cytoplasmic domain of 383 aa and a predicted extracellular domain of 184 aa [114]. In addition to a signal peptide of 28 aa and a transmembrane domain of 21 aa, the extracellular domain contains two N-glycosylation sites and four cysteine-rich pseudo repeats[115]. RANK assembles into functional trimers and recruits adaptor molecules to transduce the signaling upon RANKL binding[116]. These adaptor molecules are called TNFR-associated factors or TRAF's, able to bind to different regions in the cytoplasmic tail of the TNF family receptors and transduce the signal downstream. TRAF6 is the main adaptor molecule that activates the NF-κB pathway downstream of RANKL signaling, required for osteoclastogenesis and osteoclast activation[117,118]. RANK is widely expressed in many organs such as thymus, mammary gland, prostate, bone marrow, brain, skeletal muscle, pancreas, liver, colon, kidney, lung and skin[20,114,117,119].

RANKL (*TNFSF11*), also known as TRANCE, osteoclast differentiation factor (ODF) or osteoprotegerin ligand (OPGL), is a type II transmembrane protein with close homology to other TNFSF members such as TRAIL, FasL and TNFα. The full-length murine *Rankl* cDNA encodes a protein of 316 aa (mRankl) with a predicted cytoplasmic domain of 48 aa and an extracellular domain of 247 aa, which shares 83% sequence homology with human RANKL. RANKL is found as a transmembrane protein or a soluble ligand (sRANKL), generated from a splice variant lacking the transmembrane and cytoplasmic domains, or cleaved from the cell surface membrane by proteases[120]. Indeed, three distinct RANKL isoforms have been identified so far, resulting from the shedding of the transmembrane protein or alternative splicing[120,121]. RANKL1 is the longest isoforms and contains the extra and intracellular as well as transmembrane domains; RANKL2 that has a shorter intracellular domain; and RANKL3, a soluble intracellular protein, lacking the intracellular and transmembrane domains[120]. These

three isoforms are differentially expressed and regulated in several cell lines. sRANKL arise from either proteolytic cleavage or alternative splicing[122]. Both the membrane bound and sRANKL are assembled into functional homotrimers like other members of the TNFSF[123]. So far, RANKL is the only known ligand for RANK, but RANKL has been shown to bind to Leucine Rich Repeat containing G Protein-coupled Receptor 4 (LGR4), which competes with RANK for RANKL binding and negatively regulates the pathway[124] and also to OPG, a negative regulator of the pathway (described below). RANKL is highly expressed in thymus, lymph node and lung, and, at lower levels, in a variety of other tissues, including spleen, bone marrow and by several immune cells[114,117,119].

OPG (*TNFRSF11B*), alternatively named osteoclastogenesis inhibitory factor (OCIF), is a soluble decoy receptor for RANKL that modulates the interaction between RANK and RANKL. OPG binds RANKL with a 500-fold higher affinity than RANK[125], thus competing with RANK for its binding[126]. Full-length OPG protein has 401 aa and shows features of a secreted glycoprotein, such as a hydrophobic leader peptide and four potential sites of N-glycosylation. Besides, OPG contains four cysteine rich pseudo repeats located in the N-terminus and two death domains[127]. The mouse and human proteins are around 85% and 94% identical to the predicted rat protein, respectively, indicating that OPG has been highly conserved throughout evolution[128]. OPG is highly expressed in different tissues, including lung, liver, spleen, thymus, ovary, lymph node and bone marrow[129].

3.2 RANK/RANKL in bone remodeling and bone metastasis

RANK pathway is essential for bone-remodeling and it is deregulated in pathological processes such as postmenopausal osteoporosis or bone metastasis. RANKL, expressed and secreted by osteoblasts, binds to its receptor RANK, expressed on osteoclasts precursors that will, in turn, differentiate into activated osteoclasts (bone-resorbing cells). OPG is secreted by osteoblasts and can bind to RANKL competing for RANKL-RANK binding, thus blocking osteoclast activation[130,131]. The genetic ablation of RANK or RANKL in mice (RANK or RANKL KO) leads to defective tooth eruption and severe osteopetrosis due to defects in the activation of osteoclasts [130], whereas ablation of OPG in mice results in osteoporosis[130].

During menopause, a decrease in OPG and an increase in RANKL expression levels are observed[130]. The resulting enhanced osteoclast activity encourage bone resorption and reduces bone mass[117]. Over time, this process leads to osteoporosis, characterized by compromised bone strength and an increased risk of bone fractures. In terms of metastasis, bone is greatly irrigated by blood vessels making it accessible for circulating cancer cells and therefore a preferential organ for colonization. The cooperation among tumor cells and the bone stroma is known as the vicious cycle and is essential for bone metastatic seeding and colonization[117].

Based on the critical role of RANK pathway in bone-remodeling and bone metastasis, a monoclonal antibody that inhibits bone resorption by binding to and blocking the activity of RANKL, called denosumab, has been developed and already approved for clinical use to reduce the risk of osteoporosis in postmenopausal women and for treatment of skeletal related events, including bone metastasis and several tumor types, including breast cancer[132–134].

3.3 RANK/RANKL in the mammary gland development and stemness

In addition to the crucial role in bone metabolism, RANK signaling is required for mammary gland development[20]. RANK and RANKL expression are relatively low in virgin mammary glands, becaming upregulated upon gestation. Both RANK and RANKL show a tighly regulated expression profile both spatially and temporally during pregnancy and involution[20,21]. RANK is constitutively expressed in HR^- luminal cells and myoepithelial cells[135], whereas RANKL expression is induced upon progesterone stimuli in mature luminal HR^+ cells[20,135,136] (**Figure 7**). Moreover, RANK protein expression significantly increases during gestation, reaching a peak at mid-gestation (days 14.5-15.5), and then decreases until day 1 of lactation[21], whereas RANKL expression is absent in virgin glands, then gradually increases during pregnancy, and decreases again to an undetectable levels at the end of gestation (day 18.5)[137].

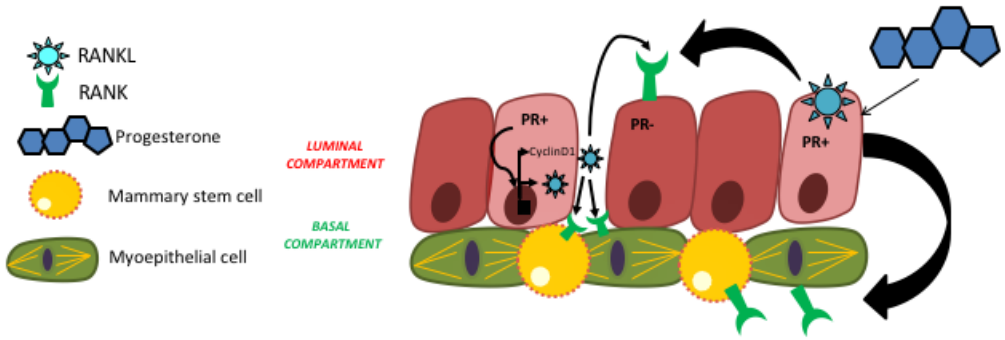

Figure 7*:* Shematic model illustrating paracrine signaling of RANKL under progesterone stimuli. Progesterone binds to its receptor (PR) in the cytoplasm of luminal hormone-sensing cells. PR translocates into the nucleus and activates the expression of target genes, such as *Cyclin D1* and *RANKL*. Cyclin D1 induces the proliferation of luminal hormone-sensing cells, while RANKL binds to RANK and activates Cyclin D1-mediated proliferation by paracrine signaling in mammary stem cells and luminal cells. RANK is constitutively expressed on the surface of basal and luminal MECs, whereas RANKL in a subset of luminal HR^+ cells.

Mice deficient in RANK or RANKL show a drastic defect in MEC differentiation and survival during gestation, although their mammary glands develop normally until puberty. Genetic loss of RANK reduces proliferation and survival of MECs and impairs alveoli development and milk production[20].

Mice overexpressing RANK under the MMTV-promoter (MMTV-RANK) show hyper-proliferative mammary glands and a complete blockade in the differentiation of lobulo-alveolar structures and impaired lactogenesis, eventually leading to

tumorigenesis after multiple pregnancies[21,138]. Thus, disrupted mammary gland development during pregnancy and impaired lactation are observed not only as a loss but also as a consequence of RANK overexpression.

On the other hand, MMTV-RANKL mice show precocious ductal side-branching and alveologenesis in the pubescent mammary gland, with a persistent hyperproliferative phenotype in adult virgin and pregnant mammary glands[139]. These data uncover the essential role of RANK/RANKL signaling pathway in the regulation of mammary gland development and differentation.

RANKL is in fact the main mediator of progesterone signaling in the mammary epithelium[20,21,136] (**Figure 7**). Progesterone has mitogenic effects on MECs through two distinct waves of proliferation. The first wave, faster and weaker than the second, affects PR^+ luminal epithelial cells and requires Cyclin D1, while the second wave affects, indirectly, the HR^- luminal progenitors and myoepithelial cells. The second wave is more prolonged and intense (around 15% of the MECs proliferate during that wave), and takes place around 72h after the progesterone stimuli[48]. Mechanistically, this process is paracrine and RANKL-mediated. Briefly, RANKL is upregulated in the HR^+ cells as a response to the progesterone stimuli. Then, in a paracrine manner, RANKL activates RANK pathway in the RANK expressing HR^- luminal progenitors and myoepithelial cells, leading to their proliferation[136,139]. The second wave of expansion is Cyclin D1 independent, being the HR^- cells are able to proliferate after progesterone stimuli relying on the Wnt pathway[48,135].

Regarding the role of RANK in alveoli differentiation and milk production,a key point was the identification of the cell populations essential for RANK actions. Previous work from our laboratory demonstrated that RANK overexpression led to a decrease in $Sca1^+$ luminal mature and PR^+cells, and an expansion of the basal ($CD24^{lo}$, $CD49f^{hi}$) and luminal progenitor enriched ($CD24^{hi}$, $CD49f^{lo}$, $Sca1^-$ and PR^-) compartments[138]. Importantly, $CD61^+$ luminal cells, considered to be precursors of mature secretory alveolar cells, were dramatically decreased in the luminal fraction of MMTV-RANK mammary glands, whereas the $CD49b^+$ luminal progenitors were expanded[138]. These results suggest that RANK pathway controls mammary epithelial cell fate and its deregulation alters the distribution of the luminal subpopulations, leading to a failure in alveoli differentiation. The lack of normal milk-secreting mammary gland described in RANK and RANKL KO mice is also observed in the PR and prolactin KO models[140,141], indicating that RANK together with progesterone and prolactic signaling are critical for MEC differentiation during gestation. Interestingly, the lack of mammary ductal side branching and alveologenesis in PR KO mice is rescued by RANKL[142], demonstrating its crucial role in progesterone-induced mammary proliferation and differentiation. RANKL dependence for the progesterone-induced MEC proliferation has also been demonstrated in human mammary glands[143].

Besides, it was postulated that RANK pathway could inhibit the terminal differentiation of MECs[21]. In 3D acinar cultures of MECs derived from midgestant (G16.5) WT and MMTV-RANK mice, RANKL treatment led to an impaired secretory differentiation and a downregulation in the expression of genes involved in differentiation and lactation was observed[144]. Conversely, *in vivo* inhibition of RANKL with a recombinant RANKL antagonist, RANK-Fc, in midgestant WT females, led to precocious and exacerbated lactogenesis[144]. Using gain and loss of function strategies we demonstrated that RANKL inhibits lactogenesis and terminal differentiation by interfering with prolactin-driven Stat5 phosphorylation and consequent activation[144].

RANK pathway not only mediates the mitogenic effect of progesterone in the normal mammary gland, but it is also involved in mammary stem cell biology[43,145]. Although MaSCs do not express hormone receptors, they are highly responsive to hormones and the MaSC population significantly decreases in mice after the removal of ovaries (ovarectomization)[145]. RANK deletion in the mammary gland results in a deficinecy in basal and luminal cell expansion driven by progesterone stimuli[146]. In addition, basal cells derived from midgestant mice show decreased colony-forming ability when RANKL is pharmacologically inhibited[145], indicating that RANK pathway controls mammary stem cell function.

Our group has previously shown that RANK overexpression in the mammary gland (MMTV-RANK) leads to the accumulation of progenitor-like $K8^+K14^+$ bipotent cells in the mammary gland[138], as observed in 3D acini of MECs derived from midgestant females, where $K8^+K14^+$ bipotent cells are accumulated after RANKL treatment[147]. Also, RANK overexpressing MECs have increased amount of MaSCs compared to WT MECs as demonstrated by functional assays (mammary repopulating ability), whereas RANKL treatment of 3D acini derived from basal MECs increases the frequency of colony formation (as happen in MMTV-RANK acini compared to WT acini)[138].

Additionally, the expansion of luminal progenitors and basal cells mediated by RANK pathway has been described to involve Wnt signaling, which is related to the self-renewal ability of stem cells in several tissues[84,135]. Finally, in humans, data from our laboratory demonstrated that RANK overexpression in non-transformed MCF10A cells promotes stemness and transformation, as well as EMT[148].

Altogether, these results confirm that RANK pathway expands the pool of MaSCs and progenitors in the normal mammary gland, and RANK overexpression increases the stemness properties also in human non-transformed mammary cells.

3.4 RANK/RANKL in mouse mammary tumorigenesis

Progesterone is essential for the development of the mammary gland during gestation since it favors the expansion of the luminal and basal epithelial cell population and alveoli formation. Besides, progesterone-driven proliferation also promotes

tumorigenesis and PR deficient mice have less breast tumor incidence since they do not respond to the mitogenic signals of progesterone[149,150].

To study the role of RANK/RANKL pathway in hormone-induced tumorigenesis, WT and MMTV-RANK virgin mice were subjected to a carcinogenic protocol that involved the use of an analogous of progesterone, medroxyprogesterone (MPA) and the carcinogen 7,12- dimethylbenz[α]anthrance (DMBA)[151]. MPA treatment induced RANKL expression in the HR^{+}cells both in the normal mammary gland and in preneoplasic lesions and hyperplasias[146,152]. MMTV-RANK mice under MPA-DMBA treatment showed a clear decrease in tumor latency and higher incidence of hyperplasias, MIN and adenocarcinomas as compared to WT mice under the same carcinogenic protocol (***Figure 8A***). Furthermore, inhibition of RANKL signaling (by RANK-Fc treatment) not only prevented tumor formation in WT mice, but also decreased tumor incidence and increased tumor latency in MMTV-RANK mice (**Figure *8B***)[152]. RANKL inhibition in mammary glands from tumor-bearing WT and MMTV-RANK mice significantly reduced the proliferation of the mammary epithelium and preneoplastic hyperplasias, and increased apoptosis in MINs and adenocarcinomas. Similarly, genetic deletion of RANK in the mammary gland resulted in increased mammary tumor latency and enhanced survival after MPA-DMBA treatment[146].

The role of RANK signaling pathway in mammary tumor formation has also been investigated in oncogene-driven mammary tumorigenesis using MMTV-Neu mice. This model spontaneously develops tumors in the absence of exogenous hormone stimuli. RANK expression increases during MMTV-NEU tumor progression, suggesting that RANK pathway may also promote tumorigenesis in this model[152]. In accordance with the loss of PR, RANKL expression is undetectable in MMTV-Neu tumor cells being confined to the surrounding non-transformed mammary gland and stroma[153]. The blockage of RANK signaling pathway by RANK-Fc treatment before tumor onset does not significantly affect tumor latency (***Figure 8C***); however, it decreases the number of pre-neoplastic lesions, tumors and lung metastasis[152](***Figure 8D***). Conversely, RANKL treatment increases the incidence of lung metastasis in MMTV-Neu mice[153].

Similarly, genetic deletion of RANK in MMTV-PyMT mice shows that RANK loss increases the tumor latency, decreases tumor incidence and impairs lung metastasis (**Figure 8*E,F***).

Thus, RANK/RANKL signaling has a crucial role in tumor initiation and promotes mammary tumorigenesis driven by progesterone.

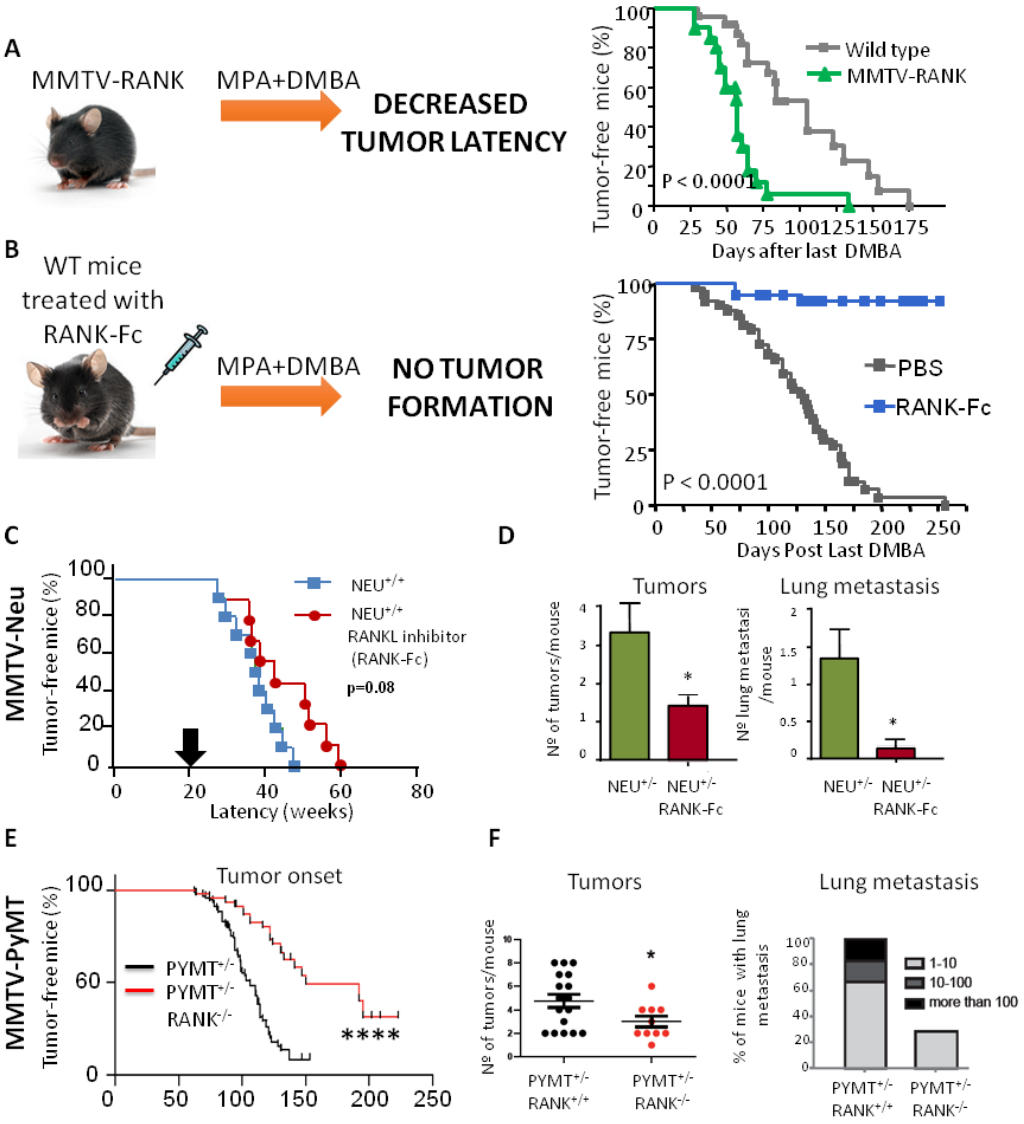

Figure 8: RANKL is the main mediator of the pro-tumorigenic role of progesterone in the mammary gland. **A**) Tumor latency after MPA-DMBA treatment in WT and MMTV-RANK mice. **B**) Tumor latency after MPA-DMBA treatment in WT mice treated with RANK-Fc or PBS. Data are expressed as percentage of mice free of palpable tumors after DMBA treatment. **C and D**) Blocking RANK signaling by injecting RANK-Fc before tumor onset leads to a slightly delay in tumor latency in MMTV-Neu mice (C), and decreased the number of pre-neoplastic lesions, tumors and lung metastasis (D). **E**) Kinetics of palpable tumor onset with age from the RANK deletion in PYMT mice. All palpable lesions were considered. **F**) Number of palpable tumor in 18 PyMT;RANK+/+ and 10 PyMT;RANK-/- mice, and percentage of PyMT;RANK+/+ (n=6) and PyMT;RANK-/- (n=7) mice with lung metastasis. Statistical differences between groups was evaluated by Log-rank test. Adapted from Gonzalez-Suarez et al., Nature 2010 and Yoldi G et al., Cancer Research, 2016.

3.5 RANK signaling and human breast cancer

Breast cancer represents the most common cancer among women worldwide[154] and progesterone and progestins are considered key factors for increased breast cancer risk in women. On the other hand, the expression of RANK and RANKL proteins in human breast cancer are controversial and different studies expose dissimilar results. Whereas some reports have shown high levels of RANK expression in primary breast tumors, metastasic lymph nodes and bone metastasis[155–157], others have reported high levels of RANK just in 14.5%[158] or 6% of primary breast tumors[152]. In the case of RANKL most of the studies agree with its lower expression in primary breast tumors compared to RANK, but still the range is wide, from 6 to 67% of cases[152,155,158], being RANKL also detected in sporadic infiltrating mononuclear cells and in fibroblast-like cells (in 67% of tumor stromal samples). Nonetheless, all reports agree that RANKL expression in tumor cells is higher in HR^+ tumors, mainly in the luminal A subtype, with a clear connection with progesterone signaling, whereas RANK expression is more frequent in TNBC subtype[159–161]. A study based on genomic databases and tissue microarrays of 87 primary tumor samples showed that dual RANK and RANKL expression is particulary related to poorer relapse-free survival and overall survival in TNBC compared to other RANK or RANKL expressing tumors[162], but most studies have reported that RANK and RANKL are not co-expressed in the same tumors. In the case of OPG, some studies indicate that a higher level of OPG is related to increased overall survival in breast cancer patients[163].

In breast tumors, mutations of RANK/RANKL have not been identified so far; however, a genetic variant of RANK gene (SNP (rs34945627)) has been associated with breast cancer risk in women carrying a mutation on *BRCA2*[164] or *BRCA1*[165]. Indeed, RANK has been described to control progenitor cell expansion and tumorigenesis in *BRCA1* mutation carriers[123].

Screenings of RANK, RANKL and OPG expression have been performed in immortalized breast cancer cell lines. In humans, low levels of RANK expression have been described in some human breast cancer cell lines. RANK overexpression in immortalized, non-transformed breast cell lines and breast cancer cell lines causes constitutive activation of the pathway, independently of RANKL[148]. In non-transformed breast cell lines, RANK expression induces a stem cell phenotype and favours transformation, EMT, increase in migration ability and mammosphere formation, anchorage-independent growth as well a endorsing the cells with the ability to reconstitute a murine mammary gland[148]. Several studies have analysed the RANK, RANKL and OPG expression of breast cancer cell lines (HCC70, MCF-7, MCF-7 3.1, MDA-MB-231, MDA-MB-435, MDA-MB-453, T47D and ZR 75-1) using RT-PCR analyses. MCF-7, MDA-MB-231 and T47D express RANK at low levels, and all of them, except for MDA-MB-435, express OPG, whereas RANKL was only detected in HCC70[166–168]. These cell lines, as happens with carcinoma cells that express RANK, have increased invasive and migrating abilities in the presence of RANKL

in vitro[156]. Besides, RANK overexpression in human tumor cells with non-functional BRCA1 enhances invasiveness in *in vitro* acinar cultures and increases tumorigenesis and metastasis in *in vivo* assays in immunodeficient mice, which is accompanied by an increase in the $CD44^{+}/CD24^{-}$ cancer stem cell population[148].

3.6 RANK/RANKL signaling in other tissues

In terms of immune-related tissues, RANK signaling is also relevant for the skin, where it has been demonstrated to regulate the homeostasis and proliferation of Langerhans cells (LC), a subset of dendritic cells of the epidermis[169]. In fact, RANKL expression in skin keratinocytes is strongly upregulated following UV irradiation[170]. Consequently, RANKL activates epidermal Langerhans cells (LCs), which also express RANK. RANKL-activated LCs trigger an expansion of regulatory T cells (Tregs), responsible for maintaining immunological self-tolerance and suppressing excessive immune responses to self-antigens, such as in autoimmune diseases or allergies[169,171]. Also, RANK regulates hair renewal and epidermal homeostasis as it is expressed by the hair follicle germ and bulge stem cells and the epidermal basal cells, realted to the renewal of the epidermopilosebaceos unit[172].

RANK is also determinant for the development and maintenance of the microfold (M) cells of the intestine[170] and contributes to the survival and maturation of medullary thymic epithelial cells, which are mediators of the self-tolerance[111].

3.7 RANK/RANKL downstream signaling pathways

RANK signaling pathway is the regulator of several downstream signaling pathways including PI3K-AKT, MAPK and NF-κB pathways[117,129]. Transmembrane RANKL is cleaved by metalloproteases such as matrix metalloproteinases (MMPs) and metalloprotease-disintegrins (ADAMs). Binding of transmembrane or sRANKL to RANK induces receptor trimerization, recruitment of adaptor proteins and activation of the downstream signaling pathway (**Figure 9**). These signaling pathways downstream of RANK play an important role in mammary gland development[152,173].

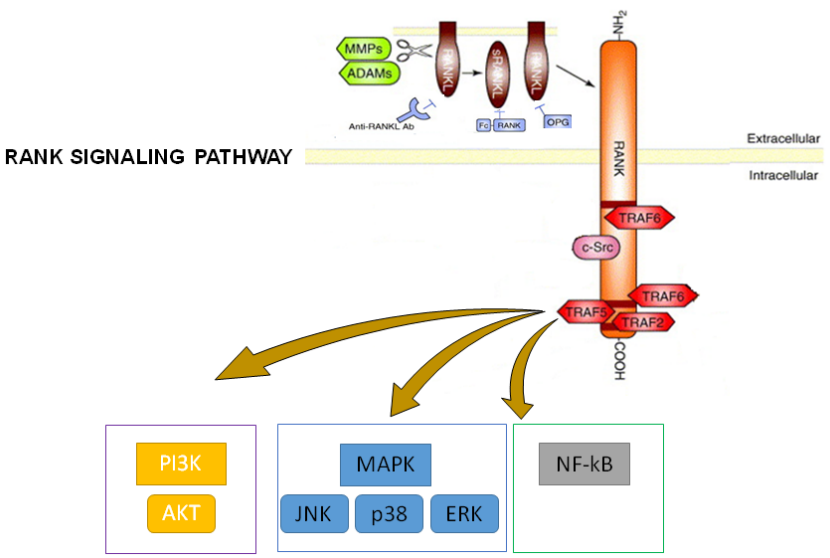

Figure 9: Signaling pathways activated downstream of RANK/RANKL. Adapted from Wada et.al. Trends in Molecular Medicine 2006.

3.7.1 MAPK signaling pathway

The mitogen-activated protein kinase (MAPK) pathway is involved in fundamental cellular processes such as cellular growth, proliferation, differentiation, migration and apoptosis[172,174,175]. Deregulation of this pathway leads to increased or uncontrolled cell proliferation and resistance to apoptosis[176]. Ras, Raf, MEK and ERK are key MAPK pathway signaling proteins. Extracellular growth factors activate the pathway by binding to receptor tyrosine kinases originating a signaling cascade via MEK signaling molecules. Finally, activation of the MAPK pathway leads to the transcription of genes that encode proteins involved in the regulation of essential cellular functions[174,177,178]. Extracellular regulated kinase (ERK), p38 MAPK and Jun N-terminal kinase (JNK) intracellular signaling cascades regulate the proliferation of MECs. Besides, it has been described that ERK signaling pathway is necessary for ductal morphogenesis, pregnancy-induced alveolar morphogenesis[179] and plays an essential role in breast cancer, enhancing tumor cell proliferation and invasiveness, preventing apoptosis and inducing resistance to tamoxifen[173,179]. Several developed drugs targeting this pathway, including humanized monoclonal antibodies (as EGFR inhibitors) and small molecule inhibitors (RAS, RAF and MEK inhibitors), are currently being tested in clinical trials[177,180].

The JNK pathway is mainly activated by cytokines, UV radiation, growth factor deprivation and DNA-damaging agents. JNK role has been reported in the normal MECs organization during acinus development, in cell polarization and the formation of tight junctions and lumen cleareance[181]. Moreover, JNK contributes to mammary tumor cell proliferation by participating in the cell cycle[182]. A small molecule inhibitor (SP600125) of JNK was reported to inhibit JNK activity *in vitro* and reduces inflammatory responses *in vivo*[183].

Together with the JNK family, p38 MAPKs are known as stress-activated MAP kinases (SAPK)[184]. p38 pathway is activated in response to stress signals or inflammatory cytokines. p38 MAPK signaling pathway plays essential roles in the regulation of cell proliferation, differentiation, development, apoptosis and response to stress[185–187]. Indeed, p38 MAPK contributes to breast cancer cell progression, invasion and metastasis, but also the activation of p38 MAPK signaling cause resistance to tamoxifen in $HER2^+$ breast tumors[175]. The anti-inflammatory drug SB203580 is a selective inhibition of p38 MAPK[188].

3.7.2 NF-κB signaling pathway

Stimulation of RANK pathways results in strong NF-κB pathway activation[189]. Nuclear NF-κB transcription factors regulate a broad range of biological processes including innate and adaptive immunity response, inflammation, stress responses, cell growth, survival and development[190,191]. The NF-κB family of proteins is composed of two subfamilies: NF-κB and Rel proteins. NF-κB /Rel proteins include NF-κB2 (p52 and its precursor p100), NF-κB1 (p50 and its precursor p105), c-Rel, RelA/p65 and RelB[192]. All proteins from the NF-κB family can form homo or heterodimers, except for RelB, which only forms heterodimers[193].

The activity of NF-κB proteins is regulated by the interaction with inhibitory IκB proteins. As in NF-κB family, there are several IκB proteins such as IκBα, IκBβ, IκBγ,and IκBε[192,194]. There are two well described pathways leading to the activation of NF-κB, canonical and non-canonical or alternative pathways. The common upstream mechanism of regulation is the activation of an IκB kinase (IKK) complex, which consists of IKKα and IKKβ. The phosphorylation of NF-κB dimers causes the degradation of the IκB inhibitor, allowing the nuclear import of the p65-p50 heterodimer to activate specific target gene expression. In most cases, the activation of NF-κB is transient and cyclical in the presence of a continuous inducer. A selective inhibitor of IKK, known as IKK-16, shows an anti-inflammatory and endothelial protective effect likely mediated by inhibiting the inflammation promoted by NF-κB[195].

NF-κB pathway is not only involved in mammary gland proliferation, architecture and branching during early post-natal development[196,197], but also participates in the initiation and progression of breast cancer[198]. Genetic deletion of the classical NF-κB pathway in PyMT mouse model showed an increase in tumor latency[199]. In MMTV-Neu mice, blockage of NF-κB activity leads to a decrease in tumor formation ability and reduces mammosphere growth *in vitro*[200].

3.7.3 PI3K-AKT signaling pathway

The pathway PI3K-AKT-mammalian target of rapamycin (mTOR) is frequently activated in breast cancer, in around 70% of breast tumors[201,202]. PI3K is activated by the binding of growth factors to receptor tyrosine kinases (RTKs) and catalyzes the production of the phosphatidylinositol 3,4,5-triphosphate (PIP3) at the cell membrane[203]. PIP3 recruits and activates a wide range of downstream targets, including the serine-threonine protein kinase AKT[204]. Phosphatase and tensin homologue deleted on chromosome ten (PTEN) is a tumor suppressor which negatively regulates the pathway by dephosphorylating PIP3 to PIP2[205]. PI3K-AKT signaling pathway regulates many cellular processes such as metabolism, inflammation, cell survival, motility and cancer progression[206]. Constitutive activation of Akt in the mammary epithelium (MMTV-Akt) enhances the accumulation of lipids droplets in pregnancy and delays post-weaning mammary involution by inhibiting the apoptosis process[207].

The PI3K-AKT signaling pathway has been implicated in therapy resistance in preclinical breast cancer models[208,209]. In HER2-overexpressing breast cancer, it has been shown that PI3K/AKT pathway promotes trastuzumab resistance[210]. Reducing PTEN in breast cancer cells confers trastuzumab resistance *in vitro* and *in vivo*. Patients with PTEN-deficient breast cancer have a significantly weaker response to trastuzumab-based therapy than with normal PTEN[211]. TNBC tumors, show a high frequency of PTEN loss, which correlates with AKT pathway activation[212]. Inhibitors against RTKs have been an active area of drug development to fight cancer and some of them have entered clinical trials for breast cancer[213]. These RTKs inhibitors allow shutting off upstream signaling to the PI3K/AKT pathway.

4 Senescence

Decades ago, Hayflick and Moorhead[214] first described the phenomenon of "replicative senescence" as a stable cell cycle arrest when a certain finite number of divisions has been reached, leading to a mitogen-refractory growth arrest of metabolically active cells.

4.1 Features of cellular senescence

Senescence, or irreversible cell cycle arrest, is characterized by morphological, epigenetic and enzymatic cellular changes (**Figure 10**). As mentioned, cellular senescence was first described as the finite proliferative capacity of human fibroblasts in culture and it has also been implicated as a major cause of age-related disease[215,216]. Later, it was demonstrated that this "replicative senescence", was due to telomere shortening, induction of the DNA damage response (DDR)[217] and cell cycle arrest[218].

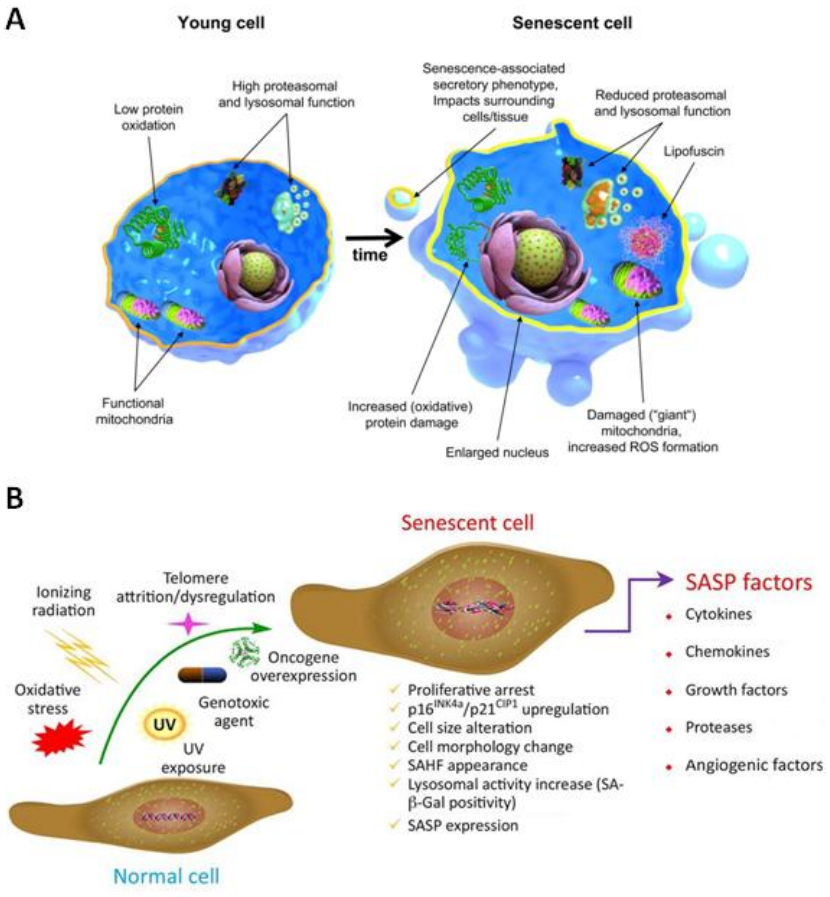

Figure 10: Characteristics of Cellular Senescence. **A**) Comparing young to aged cells. Adapted from Höhn, et.al. Redox Biology 2017. **B**) Cells exposed to various types of interior and/or exterior stress can go to senescence. Adapted from Sun, et. al. Trends in Molecular Medicine 2018.

In vitro, morphologic characteristics of cellular senescence are easily observed. Cells appear enlarged, flattened, and granulated, whereas cell growth rate decreases[219–222].

However, the identification of senescent cells *in vivo* has technical limitations. *In vivo*, senescent cells appear normal without clear morphological changes[223,224]. Therefore, senescence cellular markers have emerged as a tool for *in vivo* identification of senescent cells[225,226]. Several features were identified as characteristic of the senescence state, being the "gold-standard" marker of senescence the presence of senescence-associated β-galactosidase(SA-βGal) activity[227,228]. This marker allows the identification of senescent cells due to an increased level of lysosomal β-Gal activity[227]. Cells under normal growth conditions produce acid lysosomal β-Gal, which is localized in the lysosome. β-Gal enzymatic activity can be detected at the optimal pH conditions, using the chromogenic substrate 5-bromo-4-chloro-3-indolyl β D-galactopyranoside (X-Gal)[229], that turns into an insoluble blue precipitate upon cleavage by β-Gal. During senescence, the lysosomal mass is increased and leads to higher levels of β-Gal activity. The abundant senescence-associated enzyme is detectable over background despite the less favorable pH conditions[225]. The SA-βGal positive cells are thus stained as blue-green cells, which can be scored under bright-field microscopy. Moreover, these cells have high levels of autofluorescence due to lipofuscin accumulation[230] and they are characterized as well by the loss of lamin B1[231]. Based on their stable growth arrest, markers of proliferation like Ki-67 staining and 5-bromodeoxyuridine (BrdU) incorporation are also used for the detection of cellular senescence[232]. Other surrogate markers of senescence are DNA damage-related proteins, such as γH2AX, senescence-associated heterocromatin foci (SAHF), p53/p21, $p16^{INK4A}$, macroH2A and several secreted proteins such as interleukins 6 and 8 (IL-6 and IL-8)[220,233–237]. An important feature of senescent cells is that although they are growth arrested, they remain metabolically active[215]. Therefore, senescent cells are characterized by the secretion of cytokines and chemokines -the senescence-associated secretory phenotype (SASP) [238,239] can affect the surrounding neighbouring cells or cause changes to the tissue microenvironment. Finally, senescent cells produce high levels of reactive oxygen species (ROS) and contain elevated levels of oxidative DNA damage[240](**Figure 10**). However, these markers are not unique or specific of senescent cells, and novel and distinctive features are still being actively explored.

4.2 Role of senescence during cancer initiation and progression

During the process of epithelial cell transformation into malignant and tumorigenic cells, the cells need to overcome several biological processes that trigger growth arrest and/or programmed cell death[58]. Several tumor suppressor genes regulate cancer development. Some of these genes permanently halt cell cycle progression and cells, no longer able to divide, enter cellular senescence[241,242]. Essentially, growth arrest is controlled by the activation of p53/p21 and $p16^{INK4A}$/pRB tumor suppressor networks.

Senescent cells have been shown to inhibit tumorigenesis, acting as a potent tumor-suppressive mechanism[243,244]. Senescence is induced by activation of oncogenes and certain oncogenic stimuli such as dysfunctional telomeres and DNA damage[242].

Mutations in p53 or $p16^{INK4A}$/pRB pathways cause resistance to senescence and increase cancer risk[245]. In mice and humans, the senescence response prevents premalignant lesions from progressing to malignant cancers[246]. Some years ago, it was believed that senescent cells would not be found in malignant tumors because of their decreased ability to divide. However, the characterization of several senescence, epithelial and mesenchymal cell markers reported the presence of numerous senescent cells in tumors[247,248]. Despite the concept that senescence acts as an anti-tumor mechanism, it has also been suggested to have deleterious effects for cancer progression[239,249,250]. Thus, cellular senescence can have a positive or negative effect depending on the physiological context[251].

4.3 Senescence-Associated Secretory Phenotype

The senescence-associated secretory phenotype (SASP) is one of the several hallmarks of senescence[252,253].

As already mentioned, the SASP can be beneficial or deleterious, depending on the context, as it can help to eliminate damaged cells[254], but can also generate a pro-inflammatory microenvironment that plays an essential role in promoting the growth and/or the invasion of cancer cells[255,256]. One of the primary functions of the SASP is to recruit and activate the adaptative and innate immune cells to eliminate senescent cells[254]. In contrast, the SASP can stimulate tumorigenesis by promoting angiogenesis[257,258] or tumor growth[259], among other mechanisms. Some of the factors secreted by senescent cells can reinforce the senescence phenotype, potentially during aging, being IL-8, IL-6, GROα and IGBP-7 specific SASP components reinforcing senescence[253,260,261]. SASP factors can also induce senescence in neighboring cells in a paracrine manner[262], which together with the autocrine reinforcement, could potentially explain some of the effects due to the aberrant accumulation of senescent cells. Consequently, cellular senescence constitutes a barrier against tumor progression but, if senescence cells are not removed quickly, they become deleterious due to the SASP and reinforce tumorigenesis, being senescence a double-edged sword in cancer[263] (**Figure 11**).

The SASP components have been classified based on their molecular features[264]. The first group is composed by soluble signaling molecules such as cytokines, chemokines and growth factors able to bind to a cell receptor[260]. The best-known representatives of this group are the cytokines IL-6, IL-8 and IL-1α; the chemokines GROα, GROβ, CCL-2, CCL-5, CCL-16, CCL-26 and CCL-20; and the growth factors HGF, FGF, TGFβ and GM-CSF. Another group of SASP factors are those able to cleave membrane-bound proteins, modifying signaling molecules and remodeling the extracellular matrix in order to modify the microenvironment[265]. This group includes matrix metalloproteases MMP-1, MMP-10, MMP-3 and serine proteases, as well as reactive oxygen and nitrogen species[266]. The third group is composed by regulatory factors which lack

enzymatic activity and their mode of action is through the binding to factors from the first and second groups regulating their function. This group includes tissue inhibitors of metalloproteases (TIMPs), the plasminogen activator inhibitor (PAI), and insulin-like growth factor binding proteins (IGFBPs).

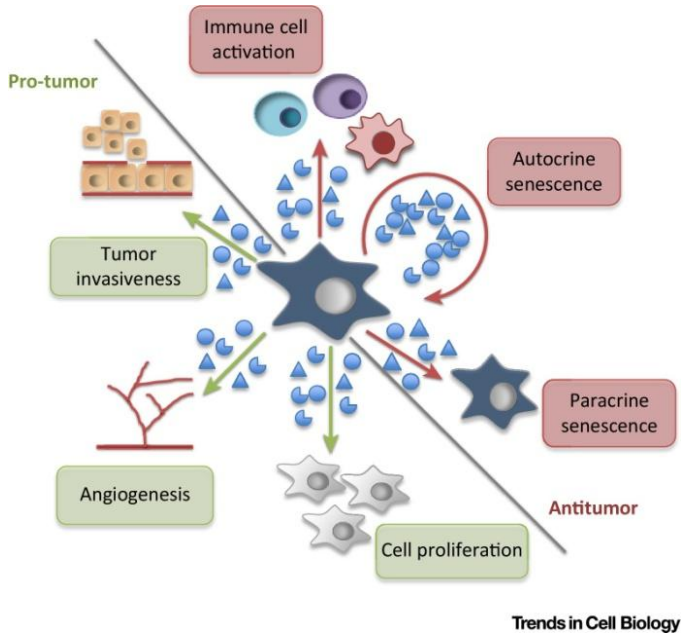

Figure 11: Pro-tumorigenic and anti-tumorigenic effects of Senescence-Associated Secretory Phenotype (SASP). From di Mitri D, et.al. Trends in Cell biology 2016.

The SASP has been described as a phenomenon that arises over time[267] and develops in several phases [268]. The SASP is initiated by several genotoxic senescence-inducing stress such as telomere shortening, cytotoxic drugs, radiation, oncogene activation or oxidative stress[269]. Genotoxic stress trigger multiple types of DNA lesions, but severe stress is strong enough to generate DNA double-strand breaks (DSBs), which activate the DDR[270]. This first phase is not sufficient to determine the initiation of senescence, as the damage could be repaired or cells could enter apoptosis[267]. After senescence induction, not all SASP factors begin to be secreted at the same time; it is a gradual transition conserved among cell types and senescence inducers. Genetic alterations, such as loss of p53 or gain of oncogenic RAS, lead to faster acquisition of the SASP, suggesting that the SASP is triggered by genotoxic stress.

Multiple signaling pathways, including but not limited to p38MAPK[271], cGAS-STING[272,273], TGF-β[274], JAK-STAT[275], PI3K-AKT-mTOR[276], as well as transcription factors such as NF-κB[277] and C/EBP-β[260] regulate and orchestrate the SASP, at least *in vitro*.

4.4 The Guardians of the Senescence-Associated Secretory Phenotype: Tumor suppressor pathways

Senescence is established and maintained by p53 and $p16^{INK4A}$/pRB tumor suppressor pathways[278,279](**Figure 12**). Briefly, when activated, p53 inhibits cell proliferation through the activation of its transcriptional target p21[241]. p21 and p16 keep the protein pRB in its hypophosphorylated and active state[241,280]. Active pRB inhibits E2F1 (a transcription factor) that regulates the expression of genes responsible for the progression of the G1/S phase of the cell cycle, thereby blocking cell cycle entry[281]. Remarkably, if senescence occurrs by the activation of the p53-p21 pathway, the senescent cell could reenter the cell cycle; however, cells that enter to senescence via p16-pRB pathway are unable to resume proliferation[235].

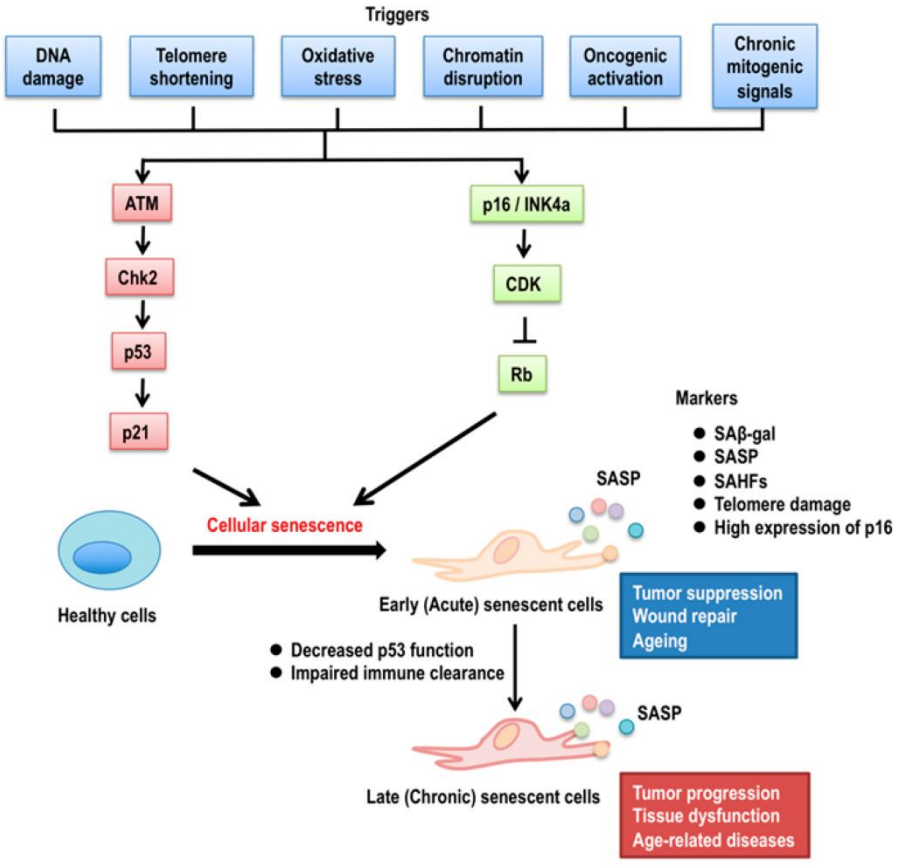

Figure 12: Schematic Schematic model of p53 and p16/pRB pathways regulating senescence. From Fujita International Journal of Molecular Science 2019.

p53 (encoded by TP53 gene) is mutated in almost 50% of human tumors, while the remaining 50% present alterations in the p53 signaling pathway, confirming its essential role in cancer protection[282,283]. p53 tumor suppressor guards genomic integrity regulating numerous cellular processes, such as cell cycle arrest, DNA repair, apoptosis and cellular senescence activated by numerous stressors [284–287]. The induction of p53-dependent senescence has been described to play an essential role in limiting tumor progression *in vivo*[286,287]. This pathway is regulated at multiple points by proteins such as the E3 ubiquitin-protein ligase HDM2 (MDM2 in mice), which promotes p53 degradation, and the alternative-reading frame protein (ARF), which inhibits HDM2 activity[288]. p21 is a transcriptional target of p53 and mediator of p53-

dependent senescence[289]. Moreover, loss of p53 activity by senescing or damaged fibroblasts enhances the SASP and the stimulatory effects of the SASP on malignant epithelial cells[269] (**Figure 13*A***).

The *INK4A/ARF* locus encodes for three tumor suppressor genes: ARF ($p19^{Arf}$ in mouse and $p14^{ARF}$ in human; $p16^{INK4A}$, encoded by the *CDKN2A* gene; and $p15^{INK4B}$, encoded by *CDKN2B*[245]. Both $p16^{INK4A}$ and $p19^{Arf}$ have separate promoters that generate two different transcripts with different reading frames; Ink4a from exons 1α, 2 and 3 and ARF from exons 1β, 2 and 3, resulting in non-homologous protein products (**Figure 13*B***). $p16^{INK4A}$ is a G1 cyclin-dependent kinase (CDK) inhibitor that binds to CDK4 and CDK6[290] and prevents their association with D-type cyclins, in that way allows CDK4/6-cyclinD-mediated phosphorylation and inactivation of retinoblastoma protein (RB) and S-phase entry. $p19^{Arf}$ inhibits MDM2-mediated degradation of p53; so, loss of $p19^{Arf}$ thus results in lower p53 protein levels[291] (**Figure 13*A***).

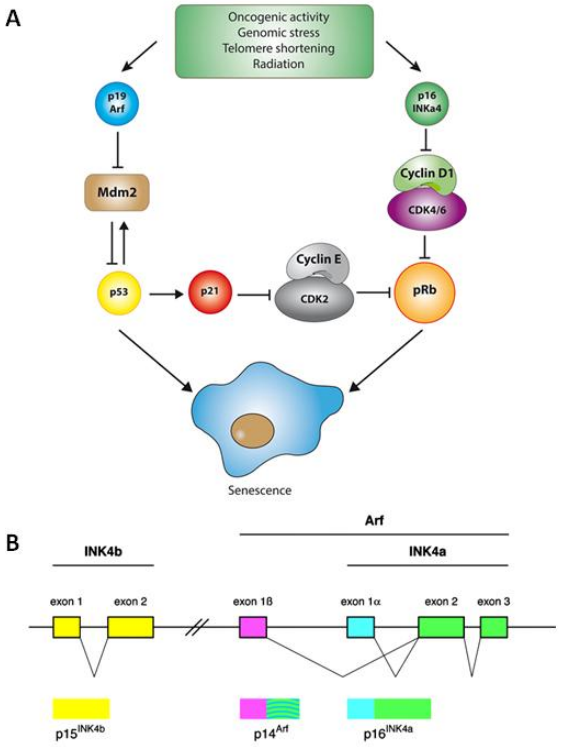

Figure 13: Molecular pathways involved in senescence. **A**) The p53 and pRB pathways during senescence. From Valenzuela C. et.al. Frontiers in Oncology 2017. **B**) Structure of the INK4b and INK4a/Arf genes.From Collins C. et.al. Aging Cell, 2003.

Importantly, if the stress that triggers senescence is transient, p53 induction can drive the cells through a quiescence state and activate DNA repair processes. Upon resolution of the stress, cells can resume cell cycle progression[235]. However, persistent stress or additional insults to the cells can activate $p16^{INK4A}$ contributing to a long-lasting arrest[235]. It has been suggested that the role of p53/p21 may be limited to the onset of senescence, whereas $p16^{INK4A}$ maintains a permanent growth arrest. In addition, although *p21* induction is important for senescence initiation, its expression does not necessary persist in senescent cells[292]. In line with this, the upregulation of

p21, but not of *p53* or *p16^{INK4A},* is the driver of developmental senescence, the type of cellular senescence that occurs during mammalian embryonic development[293,294].

4.5 Premature senescence

Besides the replicative senescence dependent on telomere length, a premature senescence has been also described, which is telomere length-independent and occurs as a consequence of DNA damage and DDR caused by stress, such as elevated ROS, activation of oncogenes, telomere dysfunction and cell-cell fusion[242] (**Figure 14**).

4.5.1 Stress-Induced Premature Senescence

Acute or chronic sublethal doses of exogenous or endogenous stressors could be responsible for causing a state of "stress-induced premature senescence"(SIPS)[295]. Irrespective of the inducer, SISP-cells are irreversibly growth-arrested and positive for the expression of markers such as SA-βGal, *p16^{INK4A}* and telomere-associated persistent DNA damage foci[296]. SIPS is the most important form of cellular senescence *in vivo*, since many cell types never exhaust their maximum replicative potential during organism life-span and thus, do not enter replicative senescence. Nevertheless, these cells are exposed to varios exogenous and endogenous stressors throughout life, which include ROS produced by the cell itself, cytotoxic compounds from the environment, or radiation among others (**Figure 14**).

4.5.2 Oncogene-Induced Senescence

Oncogene-induced senescence (OIS) was first described more than 20 years ago by Serrano, Collado and coworkers[297,298]. OIS does not only occur in cell culture *in vitro*, but also in tumors *in vivo*[299]. In the tumor context, senescent cells are detectable in early-points, but in later invasive tumor stages they are no longer detectable[300]. OIS leads to SIPS *in vivo*[299] and can favour tumor growth by impacting on surrounding stroma cells through the SASP, which depends on the type of cancer (**Figure 14**). OIS results from the hyperactivation of oncogenes like H-Ras or the inactivation of tumor suppressors such as PTEN[297,301]. Active mitogenic signaling can also induce DNA damage via replication stress, which triggers the collapse of replication forks. OIS is conserved not only in fibroblasts[302], but also in epithelial cells of human and murine origin[303,304]. The tumor suppressors *p16^{INK4A}* (inactivates D-type cyclins) and *p19^{Arf}* (inactivates p53) together with the main cell cycle regulators such as pRb among others, play a key role in Ras-induced senescence[297,305–307]. In the case of human fibroblasts, *p16^{INK4A}* seems to have a more prominent role than *p19*^{Arf} in both Ras-induced senescence and replicative senescence. However, mouse fibroblasts depend on *p19^{Arf}*, but not on *p16^{INK4A}*, for replicative senescence and Ras-induced senescence[308–310]. Recent evidence suggests the relevance of OIS in the context of induced pluripotency *in vitro*. At least, two oncoporteins, c-Myc and Klf4, are required for the generation of induced pluripotent stem cells (iPSCs). As the INK4a/ARF proteins and p53 limit the efficiency of iPSC formation, it has been suggested that cellular

senescence counteracts the induced conversion of primary cells into pluripotent stem cells[311–316]. Alternatively, increased proliferation rates associated with p53 loss may result in accelerated kinetics of iPSC formation. To the extent that this can be extrapolated to an *in vivo* setting, one could imagine that cancer stem cells arise from a similar reprogramming process[317]. Thus, cellular senescence might suppress tumor formation not only by inducing a persistent cell cycle arrest, but also by limiting the generation of cancer stem cells.

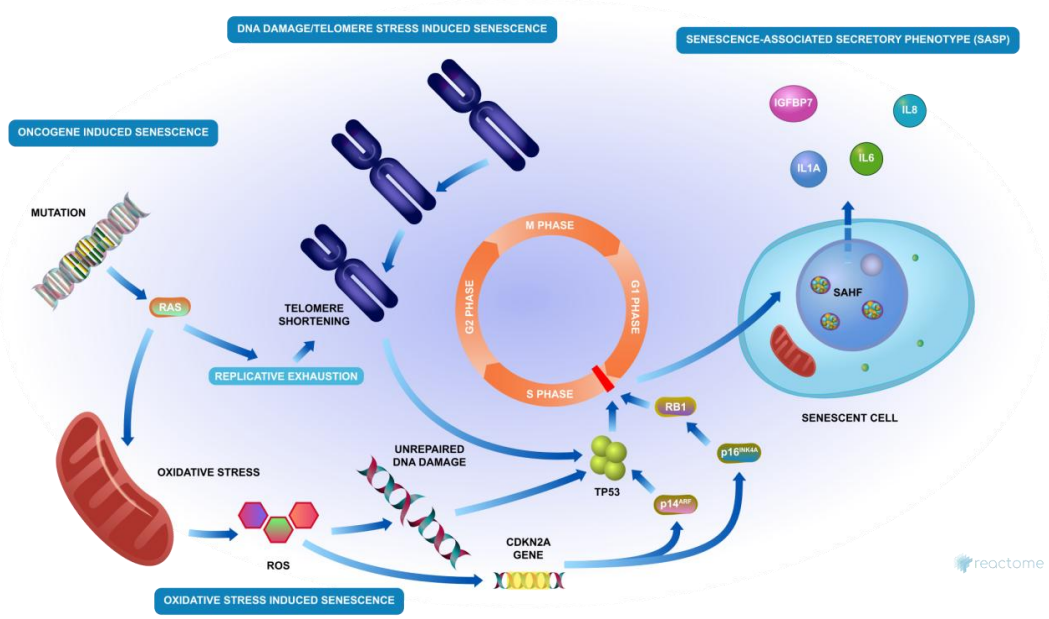

Figure 14: Induction of cellular senescence by various stimuli. From Reactome database.

4.5.3 Therapy-Induced Senescence

The progression to malignancy involves bypassing or inhibiting crucial mediators of senescence; however, this does not mean that malignant cells have completely lost their capacity to undergo senescence[318]. Therapy-induced senescence (TIS) is another type of cellular senescence that has been described to be caused by genotoxic agents such as irradiation and chemotherapeutic drugs[319] and shares most of the features with OIS (**Figure 15**). In line with this, pharmacological CDK4 inhibitors promote senescence in many cancer cells and show promising activity in breast cancer clinical trials[320–322]. However, chemotherapeutic treatments can promote disease progression through the induction of senescence and SASP[323].

In a cancer context, senescent cells have an active DDR and rely on antiapoptotic pathways, such as the PI3K pathway[324], involved in survival regulation, and the Bcl-2/Bcl-xL proteins which regulate apoptosis[325,326]. Thus, senescent cells are more dependent on pro-survival pathways than non-senescent analogous cells and are resistant to apoptosis[327]. These features are determinant for the rationale behind the

development of senolytic drugs, aimed at eliminating senescent cells without affecting quiescent and proliferative cells[328] and thus avoiding undesirable side effects on healthy tissue. Senolytics will be discussed below.

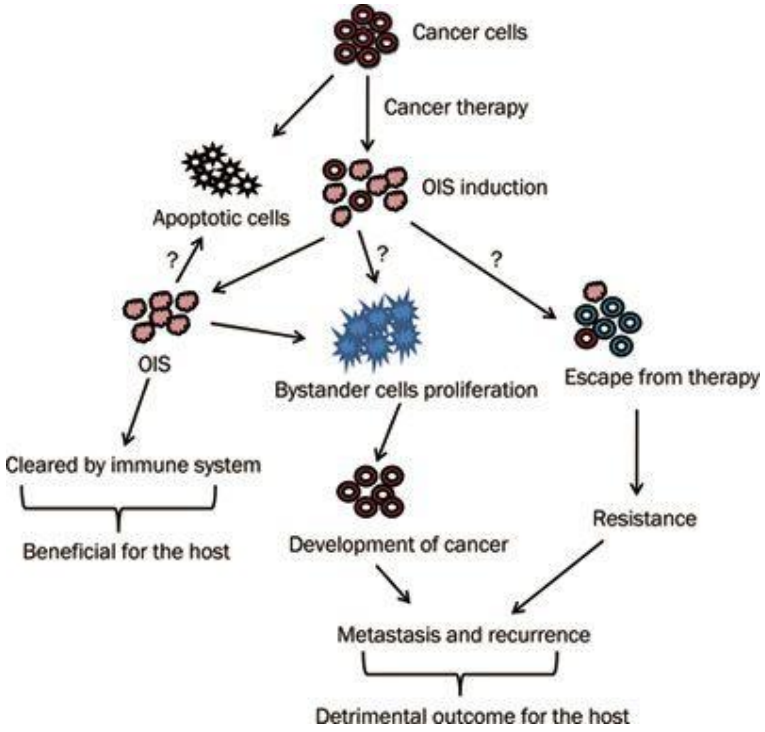

Figure 15: *T*herapy-induced Senescence, a double-edged sword?. From Zhang Y. et.al. Acta Pharmacologica Sinica 2011.

4.6 Cellular senescence and stemness

Recently, it has been postulated the relevance of OIS in the context of induced pluripotency *in vitro*, since senescent cells accumulating in response to tissue damage can also promote stemness and reprogramming[329]. Key senescence-relevant signaling proteins (such as $p16^{INK4A}$, p21 or p53) have critical roles in stem cell maintenance, suggesting an underexplored interplay between senescence-and stemness-controlling signaling networks[330,331]. Mosteiro et al.[332] reported that the induction of the reprogramming factors OSKM (Oct3/4, Sox2, Klf4 and c-Myc) triggers two divergent cellular outcomes in tissues, cellular reprogramming and damage-induced cellular senescence. Expression of the four reprogramming factors triggers senescence by up-regulating *p53*, *p21* and $p16^{INK4A}$. They find that SASP promotes *in vivo* reprogramming, as pharmacological elimination of senescent cell decreases the number of pluripotent cells and they identify IL-6 as a critical mediator of senescence and *in vivo* reprogramming[332]. Chiche et al.[333] also found a beneficial paracrine effect of tissue-injury-induced SASP on reprogramming *in vivo,* where senescence in the muscle enhances plasticity in muscle stem cells.

In addition, Schmitt and colleagues showed that cellular senescence induced by chemotherapy leads to the acquisition of "stemness-like features" by cancer cells, which allows them to escape senescence and promote tumor growth[334]. Interestingly, such cells gain elevated tumor-initiating capacity compared with cells that have never undergone senescence. The authors used a genetically engineered tumor in mice in which a state of cell-cycle arrest could be maintained by the administration of the drug tamoxifen. They showed that cells exiting senescence upon tamoxifen removal had greater capacity to drive tumor growth than do control tumor cells that did not go through a senescent phase. These findings suggest that senescence induction in cancer could have an unexpected "dark side" if tumour cells break through the cell-cycle-arrest barrier.

Nevertheless, additional confirmation and insights on the connection of this both cellular processes and the mechanisms involved are still needed.

4.7 Cellular senescence and aging

Cellular senescence has also been linked to aging, because senescent cells can not proliferate and gradually deplete the renewal capacity of tissues by exhausting the supply of progenitor stem cells. Among others hallmarks described, the senescent cells can also contribute to ageing by disrupting the integrity, function and/or homeostasis os tissues[335] and by secreting degradative enzymes and inflammatory cytokines (***Figure 16***).

Furthermore, the expression of $p16^{INK4A}$ and $p19^{ARF}$ increases with age[336–338]. High levels of $p16^{INK4A}$ in adult stem cells have been shown to impair self-renewal and the proper function of some adult stem cell compartments, leading to a decrease in regenerative potential[335,339]. Senescent cells are present at sites of certain age-related pathologies, including atherosclerotic lesions, skin ulcers and arthritic joints, as well as bening and preneoplasic hyperproliferative lesions in the prostate and liver[340].

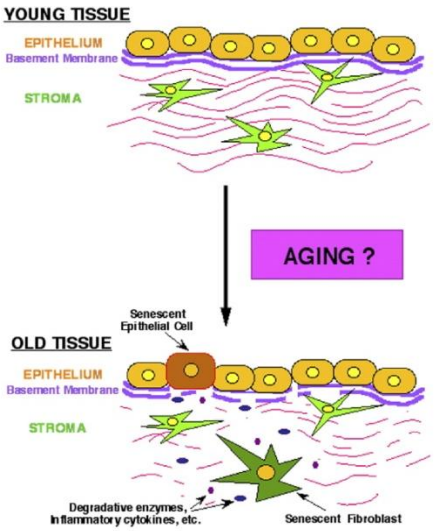

Figure 16: Senescent cells contribute to aging.

4.8 Pharmacological approaches: Senolytics

Despite the tumor-suppressive role of senescence, the long-term exposure of senescence cells is potentially detrimental. Thus, elimination of senescent cells may be fundamental in the therapeutic strategies in cancer[341]. As mentioned before, there are two important problems for the identification, isolation, and characterization of senescent cells. First, many of the senescence-associated molecular and morphological features are present in other cellular states and conditions[342]. Second, the phenotype of senescent cells is highly heterogeneous and dynamic, possibly a consequence of various distinct senescence programs.

A number of senolytic drugs have been identified (**Figure 17**), such as quercetin, which targets the PI3K pathway, dasatinib, which interferes with EPHB1 receptor, and ABT263 or navitoclax, which targets Bcl-2/Bcl-xL proteins[328,343]. Senolytics present a wide range of beneficial effects for senescence-related indications *in vitro* and *in vivo* and could be crucial to treat disorders related to senescent cell accumulation, for instance, atherosclerosis, pulmonary fibrosis, osteoarthritis, cancer, diabetes, kidney dysfunction, chronic obstructive lung disease and neurodegenerative diseases[279,344–346]. Besides promising results, senolytics are not effective for all senescence cell types, and each senolytic has to be tested in each senescent cell type of interest. Therefore, finding a safe and effective senolytic drug to use in standard treatments is still under development.

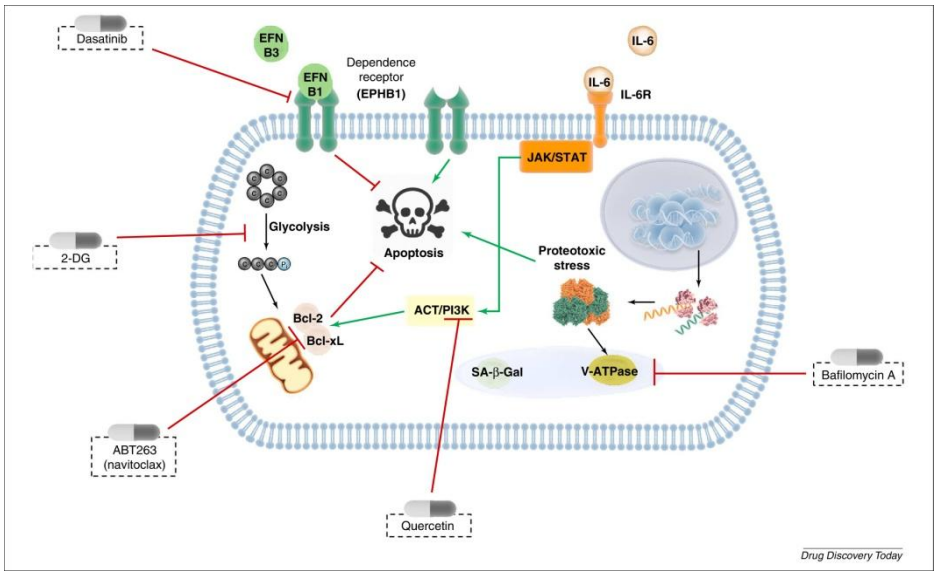

Figure 17: Targetting senescence cells. Various drugs have been shown specifically to lead senescent cells to apoptosis. Particularly, interference with the phosphoinositide 3 kinase (PI3K), Bcl and metabolic pathways seems the most effective, but still effectiveness is highly cell-type dependent. From Soto-Gamez et al. Drug Discovery Today 2017.

OBJECTIVES

OBJECTIVES

The main purpose of this PhD thesis is to characterize the role of RANK overexpression in mammary epithelial homeostasis and cancer. We previously demonstrated that RANK overexpression delays tumorigenesis in oncogene-driven mouse models of breast cancer but increased tumor aggressiveness once tumors developed. Preliminary results evidenced SA-beta-galactosidase staining in preneoplastic mammary lesions of the double transgenic Rank/PyMT and Rank/Neu mice. SA-beta-galactosidase is the most accepted marker of senescence.

Hence, we hypothesize that Rank-induces senescence attenuating tumor initiation but increases tumor growth through the paracrine action of senescent cells. To test this hypothesis the following specific objectives were defined:

1. Evaluate the ability of RANK signaling pathway to induce senescence in non-transformed mammary epithelial cells
2. Evaluate the ability of RANK signaling pathway to induce senescence in breast cancer cells and the contribution of senescent cells to tumor aggressiveness.
3. Study the putative association between senescence and stemness driven by RANK in the mammary epithelia and in breast cancer. We aim to discriminate between paracrine actions (through senescence associated secretory phenotype) or cell intrinsic mechanisms which may involve reversible senescence.

MATERIALS AND METHODS

MATERIALS AND METHODS

1. Experiments in animals models

1.1 Mouse models and *in vivo* experiments: Rankl and Navitoclax treatments

All research involving animals was performed at the IDIBELL animal facility in compliance with protocols approved by the IDIBELL Committee on Animal Care and following national and European Union regulations. MMTV-Neu mice (N202 Mul; FVB background) and MMTV-PyMT (FVB/N-Tg (MMTV-PyMT) 634Mul) were obtained from Jackson laboratory and have been described previously)[347]. $PyMT^{+/-}$ (FVB) were backcrossed to C57Bl6 mice for at least 15 generations. MECs from $PyMT^{+/-}$ mice in C57Bl6 background were used for infections as tumor onset is delayed in this background compared to $PyMT^{+/-}$ in FVB. MMTV-RANK mice in FVB background were obtained from Amgen Inc. MMTV-$PyMT^{+/-}$; $Rank^{+/tg}$ and MMTV-$Neu^{+/-}$; $Rank^{+/tg}$ mice were obtained by crossing $PyMT^{-/+}$ (FVB) and $Neu^{+/+}$ (FVB) strains with $Rank^{+/tg}$ (FVB) mice. $p16/p19^{-/-}$ mice were obtained through a collaboration with M. Serrano (Institute for Research in Biomedicine, IRB Barcelona). $PyMT^{+/-}$ males were bred with $Rank^{+/tg}$ (FVB) female mice and after birth the pups were fed by a foster mother, as $Rank^{+/tg}$ females cannot lactate[21,144] and $PyMT^{+/-}$ (FVB) females develop early onset tumors. Mice were monitored for tumor formation three times per week and tumors bigger than 1 cm in diameter were considered as endpoint criteria for mice sacrifice.

Treatment with the Bcl-2/Bcl-xL/Bcl-w-inhibitor Navitoclax, also known as ABT-263 (Selleckchem #S1001), was performed by daily oral gavage (o.p.) for 14 days at 25mg/kg once dissolved in 15%DMSO/PEG400. Treatments with sRANKL (Amgen) were performed three times per week during two weeks by intraperitoneal injection (i.p), at 0.75 mg/kg.

1.2 Mammary epithelial and tumor cell isolation

Single cells were isolated from mammary glands or tumors as previously described[348]. Briefly, fresh tissues were mechanically dissected with McIlwain tissue chopper and enzymatically digested with appropriate medium (DMEM F-12, 0.3% Collagenase A, 2.5U/mL dispase, 20 mM HEPES, and Penicillin/Streptomycin (P/S)) 45 min at 37°C. Samples were washed with Leibowitz L15 medium 10% fetal bovine serum (FBS) between each step. Erythrocytes were eliminated by treating samples with hypotonic lysis buffer, and fibroblasts were excluded by short-term cultures (1 hour at 37°C) with DMEM high glucose containing 10% FBS (the majority of fibroblasts attach to tissue culture plastic while most of the epithelial organoids do not). Single epithelial cells were isolated by treating with trypsin for 2 min at 37°C. Cell aggregates were

dissociated by incubation with 2.5 U/mL dispase (GIBCO), 20U/ml DNase (Invitrogen) for 5 min at 37°C. The obtained cell suspension was filtered with a 40 µm filter and cells were counted before further processing.

2. Cell culture protocols

2.1 Primary cells and cell lines cultures

All cells were grown in a 37°C 5% CO_2 cell culture incubator. MECs were cultured in DMEM/F12, 5% FBS (Gibco), epidermal growth factor (EGF) 100µg/mL (Sigma), insulin 10mg/mL (Sigma), cholera toxin 1mg/L and 1X P/S (PAA Laboratories). MEFs and MCF7 human breast carcinoma cells were cultured in DMEM high glucose containing 10% FBS and 1X P/S. Primary p16/p19$^{-/-}$ and WT MEFs were donated by Dr M. Serrano (IRB,Barcelona). For RANKL treatments *in vitro*, 1µg/mL of RANKL-LZ, (obtained from Amgen Inc. Thousand Oaks, CA.USA) was used.

MEFs were prepared essentially as described[302]. Briefly, each embryo was dispersed and trypsinized in a 10 cm diameter plate and incubated for 2 days in DMEM high glucose containing 10% FBS and 1X P/S. At this point, most of the attached cells had the appearance of fibroblasts. These cells were frozen in aliquots and considered passage 0 (P0). Human breast cancer cell lines were purchased from the American Type Culture Collection (ATCC, Rockville, MD). ATCC provides molecular authentication in support of their collection through their genomics and proteomic cores by using DNA barcoding and species identification, quantitative gene expression and transcriptomic analyses. All lines were expanded and frozen within 2 weeks of purchase and used for a maximum of 4 months after recovery of frozen aliquots. Cell lines were routinely tested for mycoplasma (Biotools, B&M Labs, #4542) every month and experiments were done with mycoplasma free cells.

2.2 Lentivirus production and cell infection

Lentiviral infection was done following the manufacturer's indications (Invitrogen). HEK 293T cells were transfected with lentiviral empty, Rank or RAS overexpressing plasmids and packaging (gag-pol, vsvg, rev) plasmids (Addgene) by the calcium phosphate method. 25 mM HEPES was added 16h later. The supernatant containing the viral particles was harvested 72h post-transfection, centrifuged at 1500rpm 5min and filtered with 0.22µm filters. Non-transformed MECs, MEFs, tumor cells derived from Neu$^{+/-}$ or PyMT$^{+/-}$ tumors and human breast cancer cell lines were transduced in a ratio 1:4 of the virus and fresh growth medium and 8µg/mL polybrene was added. Plates were centrifuged 1h at 600g at 32°C to improve infection and infected cells were selected with 5µg/mL of blasticidin (pLenti6/V5-DEST) or 1.5µg/mL puromycin (psd69, HRas (G12V)-pcw107 and pCW57.1). After selection, infected cells were maintained in 0.75µg/mL puromycin or 2.5µg/mL blasticidin.

2.3 *In vitro* reprogramming assays

For the reprogramming of Rank-overexpressing MEFs, we transfected HEK 293T ($2x10^6$) cells with Tet-O-FUW-OSKM (Addgene #20321) and packaging vectors using Fugene HD (Roche). Viral supernatants were collected twice a day on two consecutive days starting 24h after transfection and were used to infect MEFs, previously plated at a density of $2x10^5$ cells/well in 6-well plates. Previous to infection, polybrene was added to the viral supernatants at a final concentration of 8 µg/mL. Infected MEFs were cultured in iPSC medium (DMEM high glucose supplemented with KSR (15% Invitrogen), LIF (1 U/mL), non-essential aminoacids, 1X P/S, glutamax and β-mercaptoethanol) with 1 µg/mL doxycycline and medium was changed every 48h until iPSC colonies appeared (between 7 and 14 days).

Reprogramming plates were stained for alkaline phosphatase activity (AP detection Kit, Sigma Aldrich), and AP positive (AP^+) colonies were counted.

2.4 Mammospheres assay

MECs were isolated as described previously and filtered to obtain single cells. As $Rank^{+/tg}$ mammary glands contain more epithelia than WT mice, $CD326^+$ ($EPCAM^+$) cells were isolated using the EpCAM Microbeads and LS Columns (Miltenyi Biotec), to ensure that the same number of epithelial cells were plated. Briefly, the $EPCAM^+$ cells are magnetically labeled with EpCAM Microbeads. Then, the cell suspension is loaded onto the MACS® Column, which is placed in the magnetic field of a MACS separator and thus magnetically labeled $EPCAM^+$ cells are retained within the column. The unlabeled cells run through; being this cell fraction depleted of $EPCAM^+$ cells. After removing the column from the magnetic field, the magnetically retained $EPCAM^+$cells are eluted as the positively selected cell fraction. $EPCAM^+$cells (25.000 cells/mL in 2mL) were resuspended in serum-free DMEM/F12 mammosphere medium containing 20 ng/mL EFG, 2% B27, 1% P/S and 1% glutamine in ultra-low attachment multiwell culture plates. Medium was replenished three times a week with or without Navitoclax (0.2 or 0.6µM) or Rankl (1µg/mL). After 7 days, primary mammospheres were isolated by 5 min treatment with accutase (Gibco) at 37°C and 25.0000 cells/well were plated in triplicates for secondary mammospheres formation. Individual spheres from each replicate well were counted under a bright field microscope.

3. Molecular biology techniques and immunostaining

3.1 Generation of expression plasmids

Rank overexpressing plasmids were generated using Gateway® cloning system strategy following manufacture's instructions[349]. The BP Reaction allows the recombination of an attB-plasmid (Rank/RANK) with an attP donor vector (pDONR 201, Invitrogen).

Briefly, the ORFeome collaboration sequence of human RANK or mouse Rank inserted in a pENTR223.1 vector was transferred to the following attR destination vectors by a LR reaction: pwpi-GW (modified from the original Addgene plasmid # 12254 to insert the gateway cassette by H. Kendrick and M. Smalley), psd69 (donated by M. Bentires-Alj and S. Duss), pLenti6/V5-DEST (Invitrogen #V49610) or pCW57.1 (Addgene plasmid # 41393). The expression plasmids were verified by restriction enzymes and RT-PCR analyses. Lentiviral vectors with different strength promoters were used in order to achieve different levels of Rank/RANK overexpression: pwpi (EF1a promoter, contains GFP expression gene for FACS selection), plenti6/V5-DEST (CMV promoter, blasticidin selection), psd69 (PGK promoter, puromycin selection) and inducible vector pCW57.1 (TRE promoter doxycycline inducible, puromycin selection).
In addition, the following plasmids were generously provided: (i) pEIZ-PyMT[350] (modified from the Addgene plasmid #18121, HIV-ZSGreen) by B. Welm (Huntsman Cancer Institute, UT, USA) (ii) pwpi-NeuN (pSV2) by M. Smalley (Stem Cells Institute, Cardiff UK) and HRas-(G12V)-pcw107 by M. Collado (IDIS, Santiago de Compostela) modified from the original Addgene plasmid #64603.

3.2 RNA isolation, RT-PCR and gene expression analyses

Total RNA from MECs, MEFs, mouse and human breast cancer cells was extracted using the RNeasy Mini Kit (Cat.No.74106, Qiagen), sorted cells with RNAeasy Micro kit (Cat.No.74004, Qiagen) and reverse-transcribed with SuperScript® II Reverse Transcriptase (Cat. No. 18064014, Thermo Fisher Scientific). Quantitative PCR (qPCR or qRT-PCR) was performed using the LightCycler® 480 SYBR green (Roche Diagnostics). Primer sequences are indicated below. Ct analysis was performed using LightCycler 480 software (Roche).

3.3 Primers used for quantitative RT-PCR (qPCR) analyses and for genotyping

Primers for SYBR GREEN qPCR

Rank Fwd	5’ CAAACCTTGGACCAACTGCA 3’
Rank Rev	5’ AGGAGCAGAACGATGAGACT 3’
Rankl Fwd	5’ CCCACAATTGTGTTGCAGTTC 3’
Rankl Rev	5’ TCCTGAGACTCCATGAAAACG 3’
Krt14 Fwd	5’ TGAGAGCCTCAAGGAGGAGC 3’
Krt14 Rev	5’ TCTCCACATTGACGTCTCCAC 3’
Krt8 Fwd	5’ ATTGACAAGGTGCGCTTCCT 3’
Krt8 Rev	5’ CTCCACTTGGTCTCCAGCATC 3’
p16-Ink4a Fwd	5’ TACCCCGATTCAGGTGAT 3’
p16-Ink4a Rev	5’ TTGAGCAGAAGAGCTGCTA 3’
p19-Arf Fwd	5’ GCCGCACCGGAATCCT 3’
p19-Arf Rev	5’ TTGAGCAGAAGAGCTGCTA 3’

RAS Fwd	5’ TTTGAGGACATCCACCAGTACA 3’
RAS Rev	5’ GCCGAGATTCCACAGTGC 3’
PyMT Fwd	5’ GGAAGCAAGTACTTCACAAGGG 3’
PyMT Rev	5’ GGAAAGTCACTAGGAGCAGGG 3’
NeuRat Fwd	5’ CCCAGATCTCCACTGGCTCC 3’
NeuRat Rev	5’ TTCAGGGTTCTCCACAGCACC 3’
mCXCL1 Fwd	5’ CTGGGATTCACCTCAAGAACATC 3’
mCXCL1 Rev	5’ CAGGGTCAAGGCAAGCCTC 3’
mCXCL2 Fwd	5’ CCAACCACCAGGCTACAGG 3’
mCXCL2 Rev	5’ GCGTCACACTCAAGCTCTG 3’
mIL6 Fwd	5’ GTTCTCTGGGAAATCGTGGA 3’
mIL6 Rev	5’ GGTACTCCAGAAGACCAGAGGA 3’
mIL1α Fwd	5’ TCCATAACCCATGATCTGGAA 3’
mIL1α Rev	5’ TTGGTTGAGGGAATCATTCAT 3’
mCCL2 Fwd	5’ CATCCACGTGTTGGCTCA 3’
mCCL2 Rev	5’ GATCATCTTGCTGGTGAATGAGT 3’
mVEGF Fwd	5’ AAAAACGAAAGCGCAAGAAA 3’
mVEGF Rev	5’ TTTCTCCGCTCTGAACAAGG 3’
mPAI1 Fwd	5’ CCAACATCTTGGATGCTGAA 3’
mPAI1 Rev	5’ GCCAGGGTTGCACTAAACAT 3’
mNanog Fwd	5’ CAAGGGTCTGCTACTGAGATGCTCTG 3’
mNanog Rev	5’ TTTTGTTTGGGACTGGTAGAAGAATCAG 3’
mSox9 Fwd	5’ TCAGCAAGACTCTGGGCAAG 3’
mSox9 Rev	5’ GTCCGTTCTTCACCGACTTC 3’
HK Hprt Fwd	5’ TCAGTCAACGGGGGACATAAA 3’
HK Hprt Rev	5’ GGGGCTGTACTGCTTAACCAG 3’
HK Pp1a Fwd	5’ CAAATGCTGGACCAAACACAAACG 3’
HK Pp1a Rev	5’ GTTCATGCCTTCTTTCACCTTCCC 3’
HRANK Fwd	5’ GCAGGTGGCTTTGCAGAT 3’
HRANK Rev	5’ GCATTTAGAAGACATGTACTTTCCTG 3’
HPP1A Fwd	5’ ATGGTCAACCCCACCGTGT 3’
HPP1A Rev	5’ TCTGCTGTCTTTGGGACCTTG 3’
HTP53 Fwd	5’ GTCTGGGCTTCTTGCATTCT 3’
HTP53 Rev	5’ AATCAACCCACAGCTGCAC 3’
HP21 Fwd	5’ GACTCTCAGGGTCGAAAACG 3’
HP21 Rev	5’ TAGGGCTTCCTCTTGGAGAA 3’
HIL6 Fwd	5’ AGACAGCCACTCACCTCTTC 3’
HIL6 Rev	5’ ACCAGGCAAGTCTCCTCATT 3’
HTNFα Fwd	5’ AAGCCTGTAGCCCATGTTGT 3’
HTNFα Rev	5’ TGAGGTACAGGCCCTCTGAT 3’

Primers for genotyping

Rank Fwd	5’ GGGAGCAGTGGTGGAATGCCT 3’
Rank Rev	5’ TCAGGTTCAGGGGGAGGTGTG 3’
Neu Fwd	5’ TTTCCTGCAGCAGCCTACGC 3’
Neu Rev	5’ CGGAACCCACATCAGGCC 3’
HK B965S Fwd	5’ CCTAGCTGTCACCAACCCTTT 3’
HK N1227AS Rev	5’ GACGAAGAGCATCACAAGGAG 3’
PyMT Fwd	5’ GGAAGCAAGTACTTCACAAGGG 3’
PyMT Rev	5’ GGAAAGTCACTAGGAGCAGGG 3’
HK PyMT Fwd	5’ TTTCCTGCAGCAGCCTACGC 3’
HK PyMT Rev	5’ CGGAACCCACATCAGGCC 3’
p16/p19$^{+/+}$ WT-allele	
mp16.1	5’ATG ATG ATG GGC AAC GTT C 3’
mp16.2	5’ CAA ATA TCG CAC GAT GTC 3’
p16/p19$^{-/-}$ KO-allele	
oIMR038	5’ CTA TCA GGA CAT AGC GTT GG 3’
R1	5’ AGT GAG AGT TTG GGG ACA GAG 3’

3.4 Cell sorting by flow cytometry

Single cells were labeled with antibodies against CD24-PE or CD24-FITC (5 µg/mL, M1/69 BD Pharmingen, San Diego, CA, http://www.bdbiosciences.com), CD29-FITC (1,25 µg/mL, HMb1-1, BD Pharmingen), CD49f-a647 (2,5 µg/mL, GoH3, BD Pharmingen), CD61-PE or CD61-FITC (2,5 µg/mL, 2C9.G2, BD Pharmingen), Sca-1-APC or Sca-1-PE (0,5 µg/mL, Ly-6A/E, BD Pharmingen), and CD49b-a647 (1,25 µg/mL, HMa2 Biolegend, San Diego, CA, http://www.biolegend.com). Lymphocytes and endothelial cells were excluded in flow cytometry using CD45-PECy7 (0,125 µg/mL, 30-F11 Biolegend) and CD31-PECy7 (0,5 µg/mL, 390 Biolegend) antibodies, respectively.
FACS analyses were performed using FACS Canto (Becton Dickinson, San Jose, CA) and Diva software package. Cell sorting was performed using MoFlo (Beckman Coulter) at 25psi and using a 100 mm tip.

3.5 Cell apoptosis assessments

Apoptosis was evaluated using the Annexin A5 Apoptosis Detection Kit from Biolegend. The cells were stained with APC Annexin V and 7-amino-actinomycin (7-AAD) according to the manufacturer’s instructions to detect early apoptotic cells (7AAD$^-$ Annexin V$^+$), dead cells (7AAD$^+$Annexin V$^+$) and live cells (7AAD$^-$Annexin V$^-$).Cells were analyzed by flow cytometry using a FACS Canto and Diva software for analysis.

3.6 RNA sequencing

MECs were isolated as previously described, and basal ($CD24^{lo}$ $CD49f^{hi}$) and luminal ($CD24^{hi}$ $CD49f^{lo}$) cells within the Lin- population were sorted by FACS from WT and $Rank^{+/tg}$ mice.

Raw sequencing reads in the fastq files were mapped with STAR version 2.6.1b[351] to the Gencode release 17 based on the GRCm38.p6 reference genome and the corresponding GTF file. The table of counts was obtained with FeatureCounts function in the package subread, version 1.5.[352] The differential expression gene analysis (DEG) was assessed with voom+limma in the limma package version 3.40.6[352] and R version 3.6.0. Genes having less than 10 counts in at least 3 samples were excluded from the analysis. Raw library size differences between samples were treated with the weighted "trimmed mean method" TMM[353] implemented in the edgeR package[354]. The normalized counts were used in order to make unsupervised analysis, PCA and clusters. For the differential expression (DE) analysis, read counts were converted to log2-counts-per-million (logCPM) and the mean-variance relationship was modelled with precision weights using voom approach in limma package.

3.7 GSEA analysis

Pre-Ranked Gene Set Enrichment Analysis (GSEA) (GSEA 2017) was used in order to retrieve functional pathways. The ranked list of genes was generated using the -log(p.val)*signFC for each gene from the statistics obtained in the DE analysis with limma[353]. Functional annotation was obtained based on the enrichment of gene sets belonging to gene set collections (MSigDB 2017). The collections used in this project are:

- c2.all: Gene sets collected from various sources such as online pathway databases, publications in PubMed, and knowledge of domain experts.
- c5.bp: Gene sets derived from the Biological Process Gene Ontology (GO).
- Hall: Hallmark gene sets. Coherently expressed signatures derived by aggregating many MSigDB gene sets to represent well-defined biological states or processes.

3.8 Mouse cytokine array

The cytokine array was performed using the Mouse Cytokine Array C100 Kit (RayBiotech) to measure the relative levels of proteins in mammary epithelial cells lysates and cell culture supernatants. The assay was performed according to the manufacturer's instructions. Cell lysates were pooled and an equal amount of total protein (500µg) was loaded onto the array kit. Blot images were analyzed with ImageJ software.

3.9 Tissue histology and immunostaining

For tissue fixation within histology cassettes samples were fixed in 4% formaldehyde overnight at room temperature. After fixation, cassettes were placed in 70% ethanol

for long term storage. For analyses, the samples were dehydrated following ethanol immersions as indicated:

1. 70% ethanol for 1h at room temperature;
2. 96% ethanol for 1h at room temperature;
3. 96% ethanol 45 min at room temperature;
4. 100% ethanol two times for 45 min each at room temperature;
5. 2-propanol (isopropanol) (in case of tissues previously processed for SA-βGal staining) or in Xylene 45 min at room temperature; and
6. 2-propanol (in case of tissues previously processed for SA-βGal staining) or in Xylene 45 min at 65 C.

   Finally, samples were embedded overnight in paraffin at 65°C.

For histological analysis, 3 μm sections from paraffin-embedded mammary glands were cut and stained with hematoxylin and eosin (H&E). For immunohistochemistry (IHC) staining of Ki-67 (Thermo Scientific), 3 μm sections from paraffin embedded mammary glands were sectioned, dewaxed and rehydrated. Antigen retrieval was performed with citrate buffer (pH6) in a pressure cooker (20 min) prior to overnight antibody incubation at 4°C. The antigen-antibody complex was detected with streptavidin-horseradish peroxidase (Vector Laboratories) and revealed with DAB substrate (DAKO).

Immunofluorescence (IF) was also performed in 3 μm tumor sections. Antigen heat retrieval was performed as described above for K8 (TROMA, dshl, Developmental Studies Hybridoma Bank, Iowa City, Iowa), K5 (AF-138, Covance, Princeton, NJ) and K14 (AF-64, Covance). Suitable fluorochrome-conjugated secondary antibodies were added upon incubation with primary antibodies. Cell nuclei were stained with DAPI (Sigma) and slides mounted with Prolong ® Gold Antifade (Life Technologies).

3.10 Senescence-associated β-galactosidase staining

For SA-βGal staining in culture, MECs, MEFs and human breast cancer cell lines were seeded in 24-well plates with growth medium (50.000cells/well for MECs and 25.000 cells/well for MEFs and human cells lines). After 8 days, cells were washed in PBS, fixed for 15 min (room temperature) in 2% formaldehyde/0.2% glutaraldehyde, washed, and incubated overnight at 37°C with fresh SA-βGal staining solution: 1 mg/mL of 5-bromo-4-chloro-3-indolyl beta-D-galactoside (X-Gal) (Fisher Scientific), 40 mM citric acid/sodium phosphate pH 5.5, 5 mM $K_3Fe[CN]_6$, 5 mM $K_4Fe[CN]_6$, 150 mM NaCl, and 2 mM $MgCl_2$.

For whole-mount SA-βGal staining, mammary glands and tumors were washed in PBS, fixed for 30min (room temperature in 2% formaldehyde/0.2% glutaraldehyde, washed, and incubated overnight at 37°C with fresh SA-βGal staining solution: 1 mg/mL of X-Gal (Fisher Scientific), 40 mM citric acid/sodium phosphate pH 5.5 (in case of human samples pH 6), 5 mM $K_3Fe[CN]_6$, 5 mM $K_4Fe[CN]_6$, 150 mM NaCl, and 2 mM $MgCl_2$[225].

Stained mammary glands/tumors were dehydrated in ethanol and embedded in paraffin (see below 3.9).
SA-βGal stained mammary glands and cells were photographed on a bright field microscope and the number of positive cells was quantified using ImageJ software.

3.11 Immunofluorescence analysis of primary MECs from mammary glands and MEFs

MECs, MEFs and human breast cancer cell lines were seeded in 8-well chamber slides (LabTek) with growth medium (50.000 cells/well for MECs and 25.000 cells/well for MEFs and human cell lines). After 48h, the medium was removed and cells were fixed in 2% paraformaldehyde and permeabilized using 0.5% Triton X-100 before blocking. Cells were incubated overnight at room temperature with the primary antibodies; ki67 (Thermo Scientific), p19 ARF (5-C3-1, Santa Cruz), anti-phospho-Histone γH2A.X (Ser139) (Millipore) and then with Alexa-564-647 conjugated secondary antibodies (1:750; Molecular Probes) for 45 min at room temperature or DAPI for nuclear staining. Slides were mounted with Prolong® Gold Antifade Reagent. Confocal analyses were carried out using a Leica confocal microscope. Images were captured using LasaF software (Leica).

3.12 Protein isolation and western blot analysis

For total cell extracts, cells were lysed with RIPA buffer (50 mM Tris-HCl pH 7.4, 150mM NaCl, 1% NP-40, 0,25% Sodium deoxycholate, 0,1% SDS) 30 min at 4°C. Phosphatases and proteases inhibitors (Roche 04906837001 and 11697498001) were added fresh to the lysis buffer. Total protein quantification was performed with Bio-Rad DC Protein assay following manufacturer's instructions (BioRad). A total of 12μg whole protein extracts were loaded with Loading Buffer (20% β-Mercaptoethanol, 40% glycerol, 200 mM Tris pH 6.8, 10% SDS, 0,4% bromophenol blue) and separated on 8,5% SDS-PAGE at 110V and transferred to PVDF membranes (Millipore) during 1 h at 400mA. Membranes were first blocked with blocking buffer (5M NaCl, 2mM Tris-HCl pH 7.4, 1% Tween 20, 5% BSA) and then incubated overnight at 4°C with primary antibodies against anti-phospho-NF-κB p65 (#3033), anti- NF-κB p65 (#8242), anti-phospho-p38 MAPK (#4631), anti-p38 MAPK (#9218), anti-phospho p44/42 MAPK (phospho Erk1/2) (#9101), anti-p44/42 MAPK (Erk1/2) (#9102), anti-phospho-IκBα (#9246), anti-IκBα (#4814), anti-phospho-SAPK/JNK (#4668), anti-SAPK/JNK (#9252). Anti-mRANK (AF692) and anti-hRANK (AF683) antibodies were purchased from R&D, and anti-β-tubulin antibody from Abcam (ab21058). After washing, blots were incubated with horseradish peroxidase-conjugated secondary antibodies (1:2000; DAKO) for 1h. Blots were developed with the ECL detection kit (Amersham Biosciences).

4. Statistical analysis

Statistical analyses were performed using GraphPad Prism software. Analysis of the differences between two mouse cohorts or conditions was performed with a two-tailed Student's t-test *** $p < 0.001$; ** $p < 0.01$; * $p < 0.05$; n.s. not significant. Two-way analysis of variance (ANOVA) was used to analyze tumor growth curves.

RESULTS

RESULTS

PART 1

ROLE OF RANK OVEREXPRESSION IN MAMMARY EPITHELIAL CELLS

The long latency in mammary tumor formation observed in Rank$^{+/tg}$ mice[138] suggests that the cooperation of RANK overexpression with oncogenic events may be required to induce tumorigenesis. Unexpectedly, previous data from our laboratory (included in the thesis of A.Cordero; 2015) showed a longer latency of tumor formation in double transgenic mice Neu$^{+/-}$; Rank$^{+/tg}$ and PyMT$^{+/-}$; Rank$^{+/tg}$ as compared to the corresponding single mutants: Neu$^{+/-}$Rank$^{+/tg}$ (414 ± 115 days), compared to Neu$^{+/-}$ mice (261 ± 87 days) and PyMT$^{+/-}$Rank$^{+/tg}$ mice (67 ± 16 days), compared to PyMT$^{+/-}$ mice (41 ± 7 days) (**Figure 18**). Moreover, Neu$^{+/-}$; Rank$^{+/tg}$ mice showed a reduction in tumor incidence (only 58% of mice developed tumors), compared to Neu$^{+/-}$, where 100% mice developed tumors (**Figure 18**).

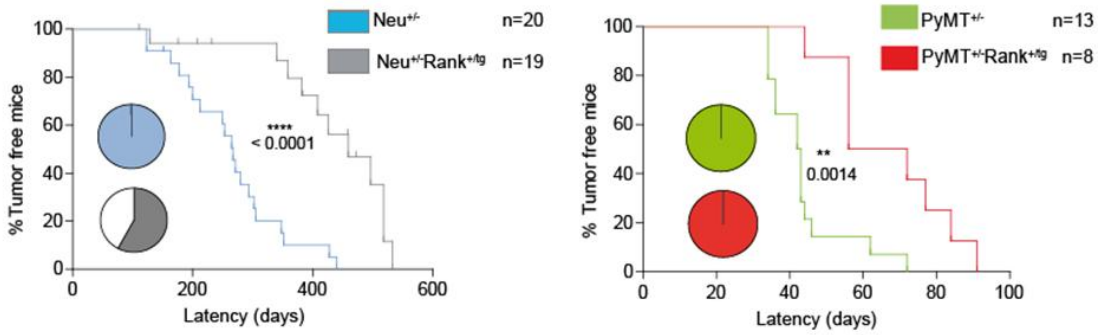

Figure 18: Kinetics of palpable tumor onset with age in the indicated genotypes. Statistical difference between groups was evaluated by log-Rank test. Pie charts represent the total frequency of mice with tumors at sacrifice. Note that some Neu$^{+/-}$Rank$^{+/tg}$ mice died or had to be sacrificed without tumors.

These observations suggest that high levels of RANK interfere with tumor initiation in these oncogene-driven mouse models and may protect from breast cancer. In this thesis, we aimed to determine the mechanism underlying these unexpected effects.

1.1. Histological analysis of mammary glands from Neu$^{+/-}$, PyMT$^{+/-}$ and double transgenic Neu$^{+/-}$; Rank$^{+/tg}$ and PyMT$^{+/-}$; Rank$^{+/tg}$ adult mice

Histological analysis at different time points (40-55-week-old mice) revealed that Neu$^{+/-}$; Rank$^{+/tg}$ had a higher incidence of hyperplasias compared to Neu$^{+/-}$ mice (**Figure 19*A***), mimicking the mammary glands of Rank$^{+/tg}$ mice[138]. Mammary intraepithelial neoplasias (MINs) were almost abscent in the single Neu$^{+/-}$ transgenic mice while easily detectable in Neu$^{+/-}$; Rank$^{+/tg}$ double transgenic.

PyMT$^{+/-}$; Rank$^{+/tg}$ mammary glands contained multiple hyperplasias but a similar number of MINs compared to the mammary glands from single transgenic PyMT$^{+/-}$ mice (**Figure 19*B***).

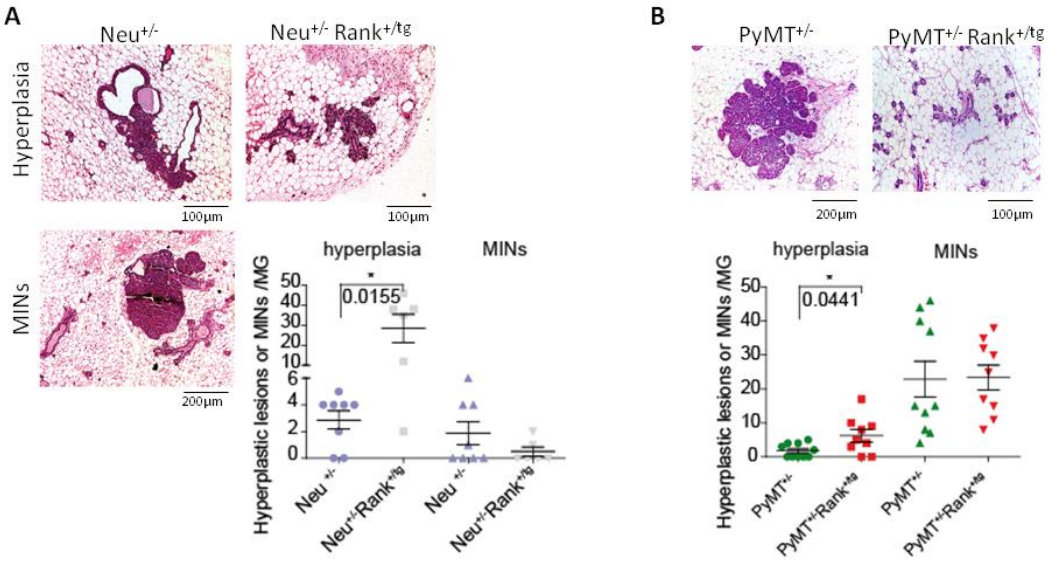

Figure 19: A) Representative images of hematoxylin and eosin (H&E) stained sections and quantification of hyperplastic lesions and mammary intraepithelial neoplasias (MINs) in mammary glands from 40-55 week-old Neu$^{+/-}$ (n=7) and Neu$^{+/-}$; Rank$^{+/tg}$ (n=6) females. Only mammary glands without palpable lesions were considered. **B**) Representative H&E images showing preneoplastic lesions in 12 week-old PyMT$^{+/-}$ and/or PyMT$^{+/-}$; Rank$^{+/tg}$ mice.

These observations suggest that constitutive activation of RANK in the mammary gland blocks the progression from hyperplasic lesions to MINs, leading to a significant delay in tumor onset.

1.2. Rank overexpression enhances senescence in preneoplasic lesions

Given the strong delay in tumor latency observed in double transgenic mice that overexpress RANK we decided to evaluate the mechanisms responsible for the delayed tumor latency observed in mice. For this purpose, proliferation (ki67) and apoptosis (cleaved caspase 3) were analyzed by immunohistochemistry in mammary gland samples collected from the different mouse models[355,356]. No clear differences in proliferation or apoptosis were observed between single and double transgenic mice at the stage of hyperplasias (**Figure 20*A***).

Multiple studies suggest that senescence can be an efficient anti-tumor mechanism[318,327]. To investigate whether the delayed latency observed in RANK overexpressing mice could be explained by the induction of senescence, we performed senescence-associated beta-gal (SA-βGal) staining analyses of mammary glands from the different transgenic mice[225]. In fact, strong SA-βGal staining was detected in the Neu$^{+/-}$; Rank$^{+/tg}$ and PyMT$^{+/-}$; Rank$^{+/tg}$ mammary glands, mainly within the hyperplasic lesions and early MINs. Senescent cells were located in preneoplasic lesions but not in

invasive carcinomas from Neu$^{+/-}$; Rank$^{+/tg}$ and PyMT$^{+/-}$; Rank$^{+/tg}$ mammary gland epithelia (**Figure 20*B***). A significant increase in the frequency of SA-βGal positive cells was found in the mammary glands from the double transgenic mice as compared to the single Neu or PyMT mice (**Figure 20*B***).

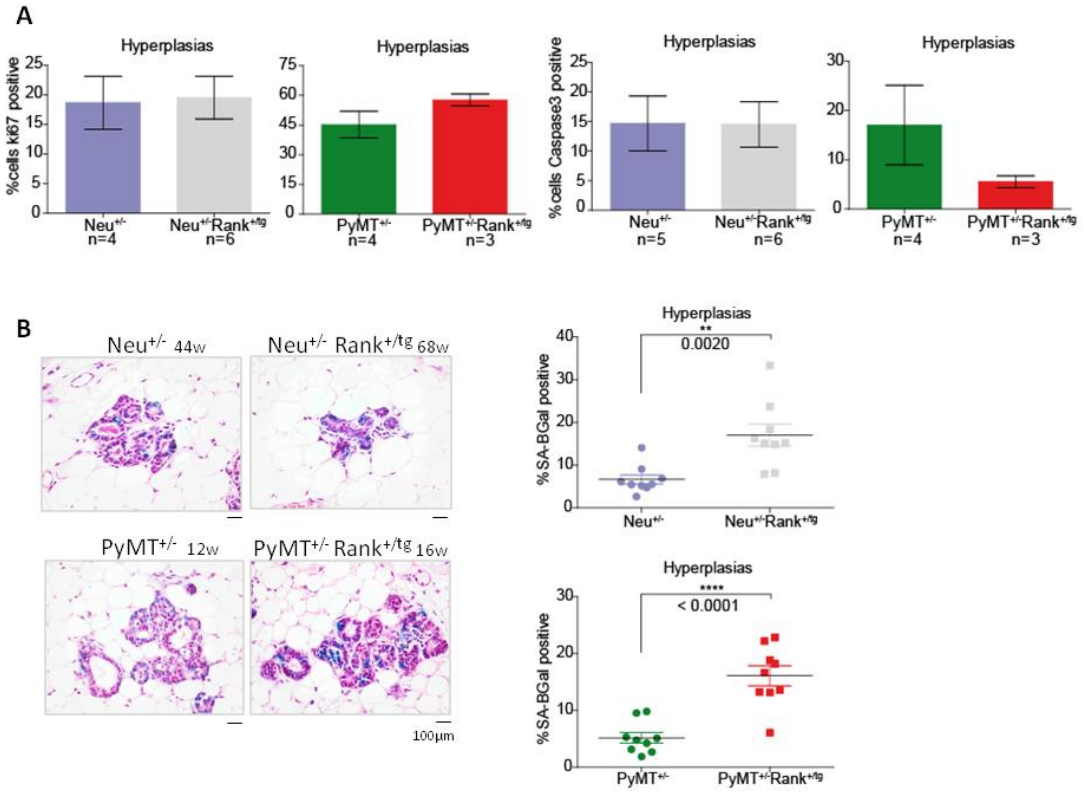

Figure 20: A) Quantification of ki67 and cleaved caspase-3 staining within hyperplasias from mammary glands from Neu$^{+/-}$, Neu$^{+/-}$; Rank$^{+/tg}$, PyMT$^{+/-}$and PyMT$^{+/-}$; Rank$^{+/tg}$ mice. **B**) Representative images of H&E with SA-βGal staining and corresponding quantification (right panel, frequency of SA-βGal positive cells relative to MECs) in mammary glands of the indicated genotypes containing ducts or preneoplasic lesions. Age of the mice is indicated. Note that double transgenic mice are older than single mutants. Three representative pictures of the indicated number of mammary glands were quantified and mean and p values are shown. Each dot indicates quantification of a picture.

We therefore hypothized that RANK overexpression induces senescence in the mammary epithelium. To address this hypothesis we performed histopathological analysis of normal and hyperplasic epithelium from Rank$^{+/tg}$ mammary glands and observed multiple senescent structures (**Figure 21*A***). No overlap between senescence and the proliferation marker ki67 was observed in the preneoplasic lesions of the mammary glands independently of the genotype of the mice (**Figure 21*B***), further supporting the senescent status of these cells. A significant increase in the frequency of SA-βGal positive senescent cells was found in Rank$^{+/tg}$ MECs plated *in vitro* (30% of the total number of cells), which showed high *Rank* mRNA expression (**Figure 21*C,D***).

These results suggest that Rank overexpression is enough to induce senescence in MECs.

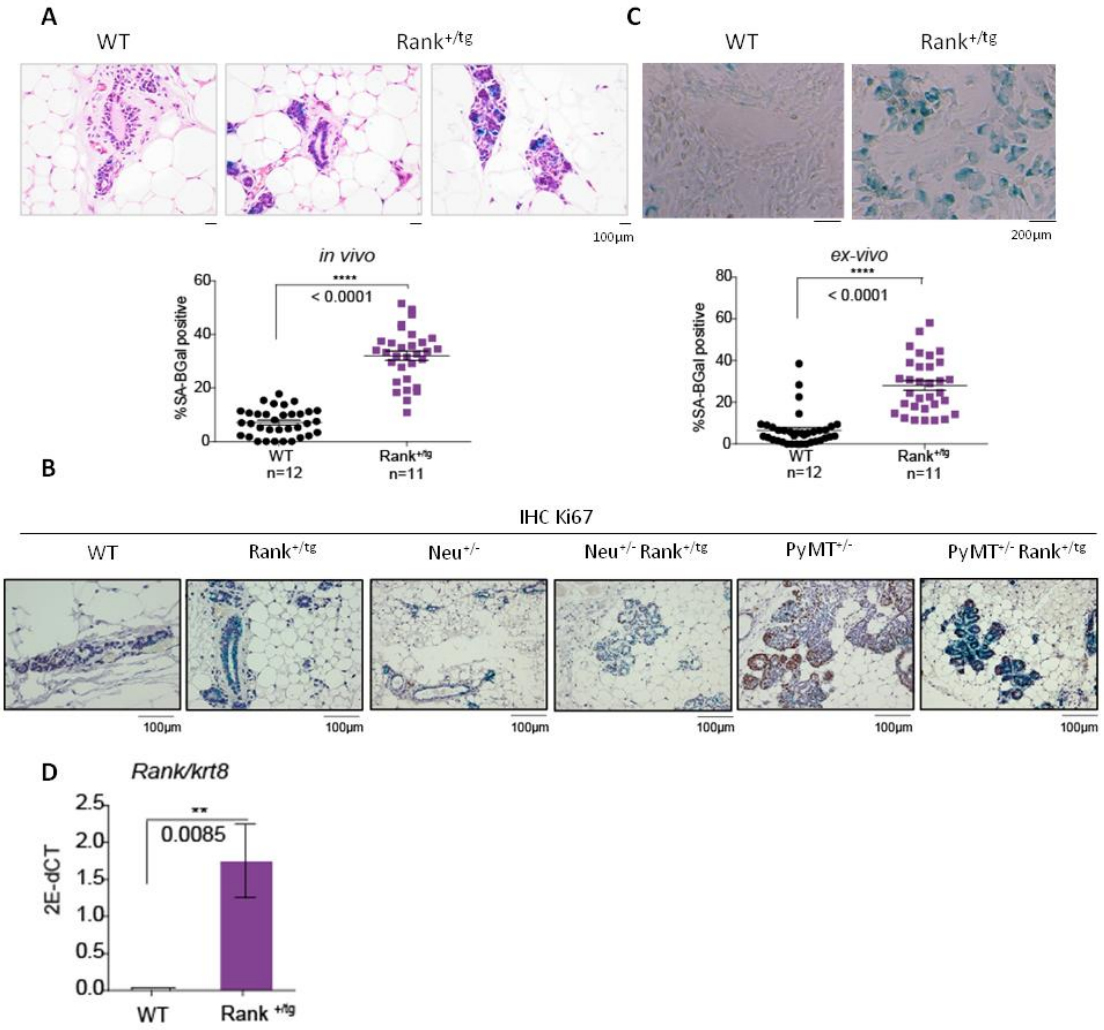

Figure 21: A) Representative images of H&E with SA-βGal staining and corresponding quantification of WT and Rank$^{+/tg}$ mammary glands containing ducts or preneoplasic lesions. Three representative pictures of the indicated number of mammary glands were quantified and mean and p values are shown in the graph below. Each dot indicates the quantification from one picture. **B**) Representative images of ki67 immunohistochemistry (brown) and SA-βGal (blue) staining in preneoplasic lesions of the indicated genotypes. No overlap between ki67 and SA-βGal staining was found. **C**) Representative images of SA-βGal positive cells in MECs isolated from WT (n=12) and Rank$^{+/tg}$ (n=11) females cultured for 8 days and corresponding quantification (right panel). Quantifications were performed in triplicates and each dot indicates a replica. Mean, SEM and t test p values are shown. **D**) mRNA expression of *Rank* relative to *krt8* measured by RT-PCR in MECs isolated from WT and Rank$^{+/tg}$ mice (n=3). SA-βGal staining is shown in Fig. 4A.

1.3. Overexpression of PyMT or Neu oncogenes did not induce senescence

To investigate the contribution of PyMT and Neu oncogenes to senescence in Rank$^{+/tg}$ mouse models, MECs of Rank$^{+/tg}$ mice were infected with lentivirus carrying PyMT (pEIZ-PyMT) and Neu (pwpi-NeuN) oncogenes. PyMT and Neu overexpression was confirmed by qRTPCR (**Figure 22*A***). Next, we analyzed the levels of senescence by SA-βGal staining of these infected cells. Overexpression of PyMT or NeuN did not induce senescence neither in WT, nor had any impact in Rank$^{+/tg}$ MECs (**Figure 22*B***).

Given the strong senescent phenotype of Rank$^{+/tg}$ mammary epithelia and Rank$^{+/tg}$ MECs, we decided to infect non-transformed Neu and PyMT MECs and their corresponding WT controls with Rank-overexpressing plasmids. PyMT$^{+/-}$ mice in the C57BL6 background were used, as the tumor onset is significantly longer than in the FVB background. No differences in the percentage of senescent cells among WT, Neu and PyMT MECs were observed (**Figure 22*C***), whereas overexpression of Rank induced senescence to a similar extent in MECs of the three genotypes (**Figure 22*C***).

Altogether, these data show that overexpression of Rank (but not of NeuN or PyMT) *in vivo* and *in vitro,* irrespective of the presence of other oncogenic stimuli, leads to senescence of the mammary epithelial cells (MECs).

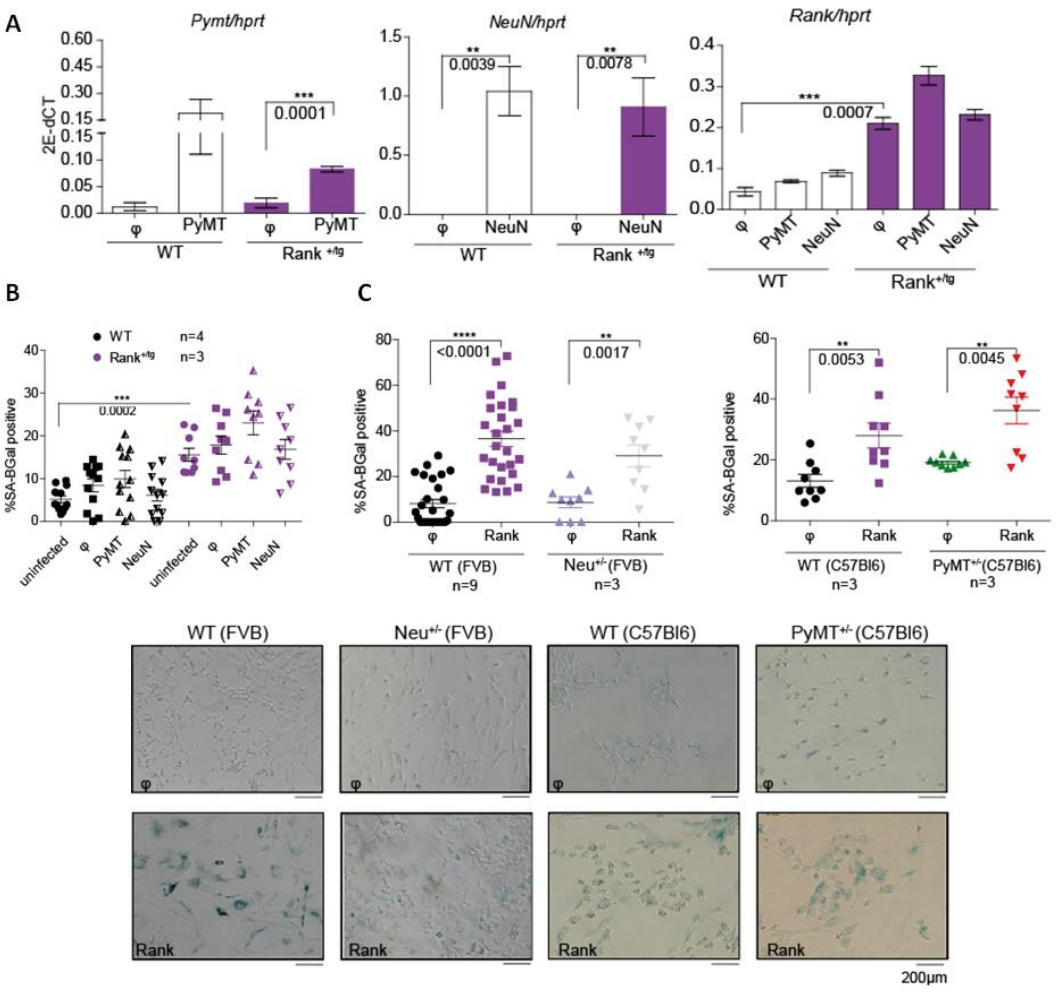

Figure 22: **A**) mRNA expression of *PyMT*, *NeuN* and *Rank* relative to *hprt* measured by RT-PCR in cultured Rank+/tg and WT MECs six days after infection with NeuN and PyMT overexpressing plasmids and control (ϕ) vectors. Mean, SEM and t-test p value for 3 independent experiments are shown. Quantifications were performed in triplicate and mean values were used in the calculations. **B**) Quantification of SA-βGal positive cells in cultured $Rank^{+/tg}$ and WT MECs 6 days after infection with PyMT and NeuN overexpressing and control (ϕ) vectors, as well as non-infected cells. Each dot indicates a replica, quantifications were performed in triplicates and mean, SEM and t test p values for 3 independent experiments are shown. **C**) Frequency (top panel) and representatives images (down panel) of SA-βGal positive cells in non-transformed MECs isolated from $Neu^{+/-}$ (FVB), $PyMT^{+/-}$ (C57BL6) and corresponding WT MECs six days after the infection with Rank-overexpressing or control (ϕ) plasmids. Total number of infections is shown. For each experiment the mammary gland of an independent mouse was used. Quantifications were performed in triplicates and each dot indicates a replica. Mean and t test p values are shown.

1.4. Rank overexpression leads to and "oncogene-induced senescence" phenotype in MECs and MEFs through p16/p19

Although SA-βGal is the most widely accepted marker of senescence, we next analyzed additional senescence markers and further address the oncogene-induced senescence (OIS) potential of Rank in other cell types. For that, mouse embryonic fibroblasts (MEFs) (as one of the most extended cell types to study senescence[357,358]), as well as non-transformed MECs isolated from WT mice were infected in parallel with Rank and H-RAS-overexpressing vectors, since RAS is the best-characterized oncogene prompting OIS[301,302]. We evaluate SA-βGal staining of these MECs and MEFs six days after the infection. RAS and Rank overexpression led to senescence in MECs and MEFs (***Figure 23A***). Quantification of SA-βGal staining showed that Rank and RAS overexpression triggered similar rates of senescent cells in both cell types (about 35% in MECs and 40% in MEFs) (***Figure 23A,B***).

Three different vectors, that achieved different levels of Rank overexpression, were used to transduce Rank in MECs and MEFs by lentiviral infection (***Figure 23C***). Senescence was observed in all cases suggesting that even low levels of Rank expression can induce senescence (***C***). Moreover, a doxycycline dependent inducible vector was used to overexpress Rank. Despite the fact that the levels of Rank overexpression were much lower than those achieved with the constitutive vectors, senescence was found in both MECs and MEFs, although a dose dependent effect was observed (**Figure 23*D***).

The tumor suppressor $p16^{INK4a}$ and $p19^{ARF}$ proteins (encoded by the genetic locus *Cdkn2a* or *Ink4a/Arf*) are main regulators of senescence, often used as senescent markers due to their upregulation in senescent cells[300]. For this reason, we analyzed the expression of both genes in Rank overexpressing MECs and MEFs. We found a higher expression of both *Cdkn2a* or *Ink4a/Arf*) in Rank overexpressing cells compared to the controls as observed after RAS overexpression (**Figure 24*A***). Indeed, expression of p19 protein was detected by immunofluorescence in $Rank^{+/tg}$ plated MECs as opposed to WT (**Figure 24*B***). Moreover, double immunofluorescence for ki67 and p19

in Rank-overexpressing MECs, showed that approximately 20% of cells were positive for p19, twice more than in control MECs; very few MECs were proliferating (less than 3% were ki67+), and there was no overlap between p19 and ki67 (**Figure 24*C***). In MEFs, upon Rank overexpression, p19 was detected in 50% of MEFs compared to 20% in control cells. The frequency of proliferating cells (ki67+) decreased from 20 to 3% in Rank overexpressing cells and no overlap between p19 and ki67 was observed, consistent with a growth-arrested phenotype (**Figure 24*D,E***).

Next, we assessed whether Rank-driven senescence is mediated by p16/p19. To this end, infections with Rank-overexpressing lentivirus were performed on p16/p19 deficient MEFs (p16/p19$^{-/-}$). Inded, neither Rank nor RAS were able to induce senescence in the absence of p16 and p19 (**Figure 24*E***). Together, these results indicate that Rank is a potent inductor of senescence comparable to RAS both in MECs and MEFs and that Rank overexpression *in vitro* induces senescence through p16/p19.

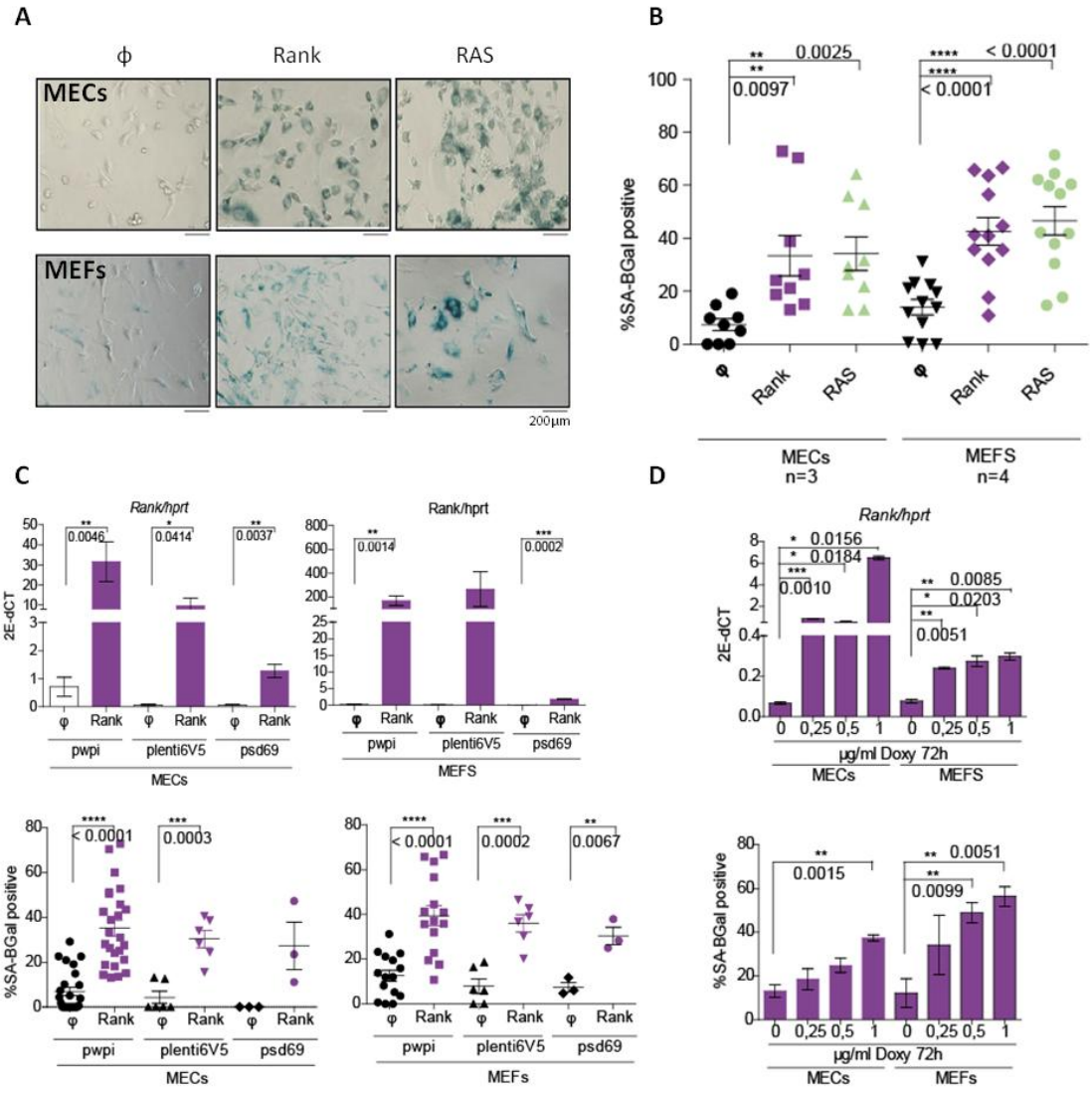

Figure 23: A-B) Representatives images (**A**) and quantification (**B**) of SA-βGal staining in MECs isolated from WT mammary glands and WT MEFs 6 days after infection with Rank or RAS overexpressing and control (ϕ) plasmids. Quantifications were performed in triplicates and each dot represents a replica of the indicated number of experiments. Mean, SEM and t-test p values are shown. **C**) mRNA expression of *Rank* relative to *hprt* (top panel) in MECs and MEFs 6 days after the infection with the indicated Rank-overexpressing plasmids and control (ϕ) vectors and quantification of the corresponding SA-βGal positive cells (bottom panel). Mean, SEM and t-test p values for the indicated independent experiments in MECs (pwpi (n=9), plenti6-V5 (n=2) and psd69 (n=1)) and in MEFs (pwpi (n=5), plenti6-V5 (n=2) and psd69 (n=1)) are shown. RT-PCR quantifications were performed in triplicate and mean values were used in the calculations. SA-βGal quantifications were performed in triplicate and each dot indicates a replica. **D**) mRNA expression of *Rank* relative to *hprt* (top panel) and quantification of SA-βGal staining (bottom panel) in MECs and MEFs infected with Rank-doxycycline dependent inducible vector, treated with the indicated concentrations of doxycycline for 72h. Mean, SEM and t test p values from one representative out of two independent experiments are shown. RT-PCR quantifications were performed in duplicates and mean values were used in the calculations.

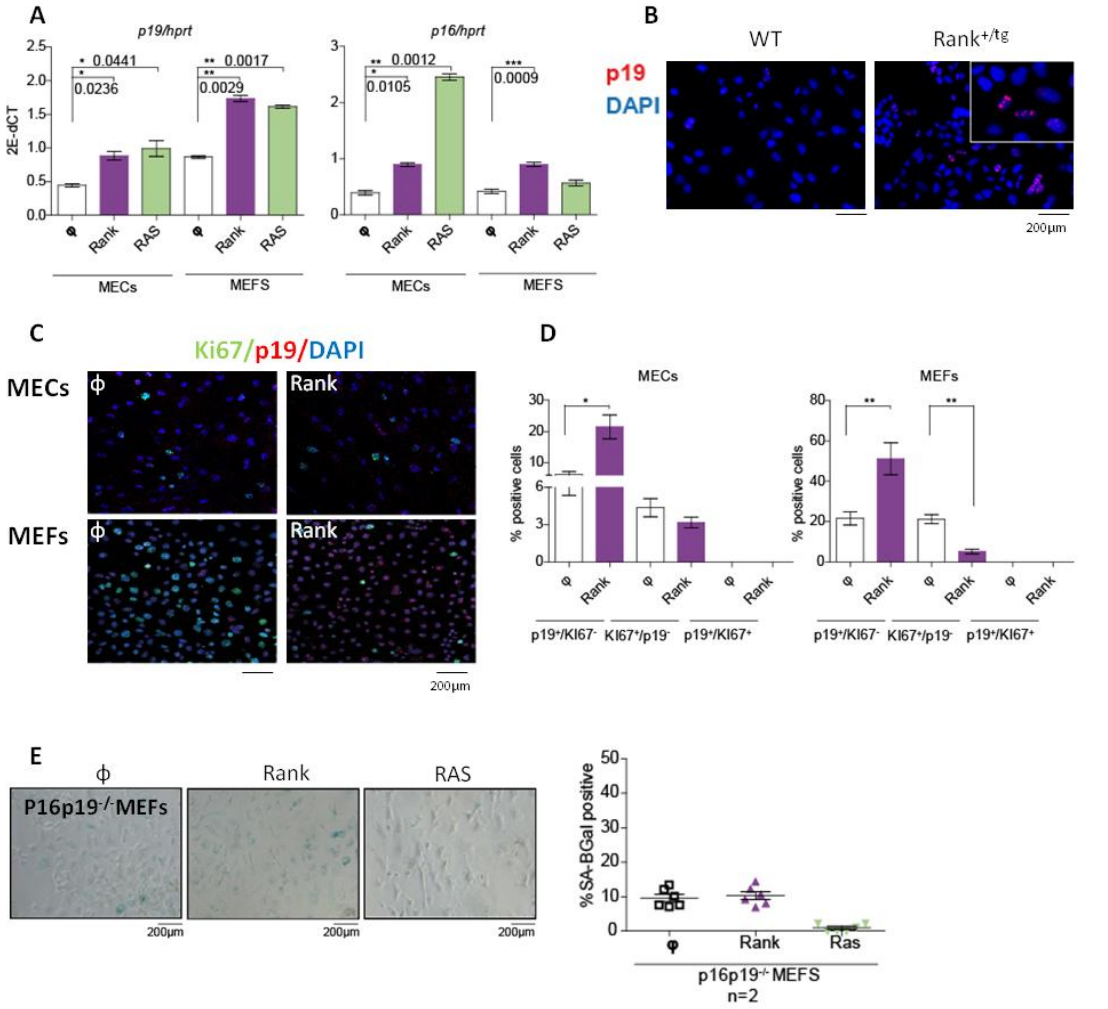

Figure 24: A) mRNA expression of *p19* and *p16* relative to *hprt* measured by RT-PCR in MECs and MEFs 6 days after the infection with Rank and RAS overexpressing plasmids and control (ϕ) vectors. Mean, SEM and t test p values for three independent experiments are shown. Quantifications were performed in triplicate and mean values were used in the calculations. Corresponding SA-βGal quantifications are shown in Fig. 6B. **B**) p19 (red) immunostaining in WT (FVB) and Rank$^{+/tg}$ MECs. Nuclei were counterstained with DAPI. Insets (2x) are included to highlight the staining in Rank$^{+/tg}$ MECs. **C-D**) Representative images (**C**) and corresponding quantifications (**D**) of ki67 (green) and p19 (red) immunofluorescence of MECs and MEFs six days after infection with Rank overexpressing and control (ϕ) plasmids. Nuclei are counterstained with DAPI (blue). **E**)Representatives images and quantification of SA-βGal staining in p16p19KO MEFs 6 days after the infection with Rank or RAS overexpressing and control (ϕ) lentivirus. Quantifications were performed in triplicates and each dot represents a replica of the indicated number of experiments. Mean, SEM and t-test p values are shown.

To confirm that p16/p19 were also mediators of Rank-driven senescence "in vivo", we crossed Rank$^{+/tg}$ with p16/p19$^{-/-}$ mice[308,310] and analyze the mammary glands. SA-βGal staining in p16/p19$^{-/-}$ and Rank$^{+/tg}$; p16/p19$^{-/-}$ mammary glands revealed similar levels of senescence in both genotypes (**Figure 25*A***) and a significant decrease of senescence in Rank$^{+/tg}$; p16/p19$^{-/-}$ MECs compared to Rank$^{+/tg}$ MECs (**Figure 25*B***). Thus, Rank-drives senescence through p16/p19 *in vitro* and *in vivo*.

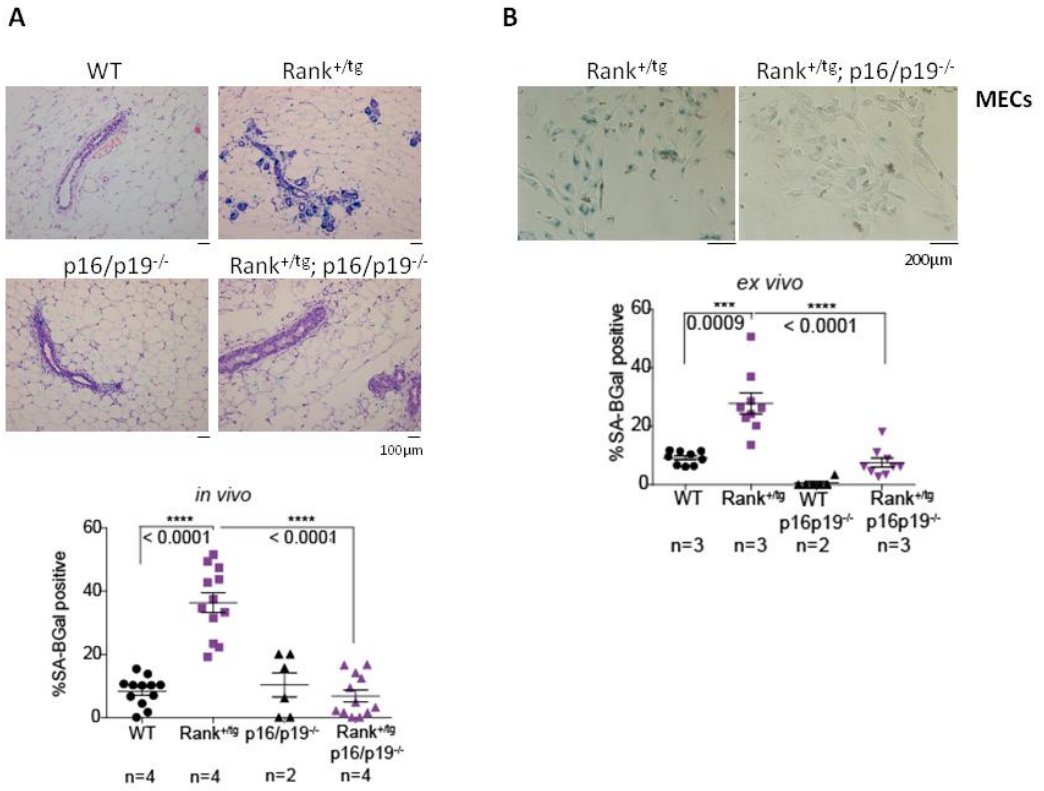

Figure 25: A) Representatives images and quantification (lower panel) of the SA-βGal staining in WT, Rank$^{+/tg}$, p16/p19$^{-/-}$ and Rank$^{+/tg}$ p16/p19$^{-/-}$ mammary glands. Three representative pictures of the indicated number of mammary glands were quantified and mean and p values are shown. Each dot indicates the quantification from one picture. **B**) Representative images and quantification (lower panel) of SA-βGal staining in MECs isolated from Rank+$^{/tg}$ and Rank$^{+/tg}$; p16/p19$^{-/-}$ MGs (ex-vivo) cultured for 8 days. Quantifications were performed in triplicates and each dot represents a replica from three independent MGs/mice. Mean, SEM and t test p values are shown.

1.5. How does Rank overexpression induces senescence?

The activation of the DNA damage response is associated to OIS[217] and regarded as a hallmark of the senescence phenotype[342]. Thus, the presence of DNA damage was analyzed by the immunofluorescence detection of γH2A.X foci (a marker of DNA double strand breaks) on WT and Rank$^{+/tg}$ MECs cultured *in vitro.* We found that Rank-overexpression induces a significant accumulation of DNA damage in MECs and MEFs that might result in OIS (**Figure 26**).

Besides growth arrest and DNA damage, a significant feature of senescent cells is the senescence-associated secretory phenotype (SASP)[268,359]. Thus, we analyzed the cytokine profiles of mammary lysates, as well as supernatants from *in vitro* cultured WT and RANK$^{+/tg}$ MECs for 8 days (**Figure 27**). Proteins involved in senescence[360] such

as Mmp2, Timp2 and Cxcl15 (one of the murine IL8 homologues) were upregulated in RANK$^{+/tg}$ MECs, as well as Mmp3, bFgf , Il7 and Ccl20 compared to WT mammary lysates (***Figure 27***). To validate this signature, we analyzed gene expression patterns of selected genes by qPCR (***Figure 28***). Increased expression of multiple genes known to be involved in SASP, was found in the RANK$^{+/tg}$ MECs (***Figure 28***).

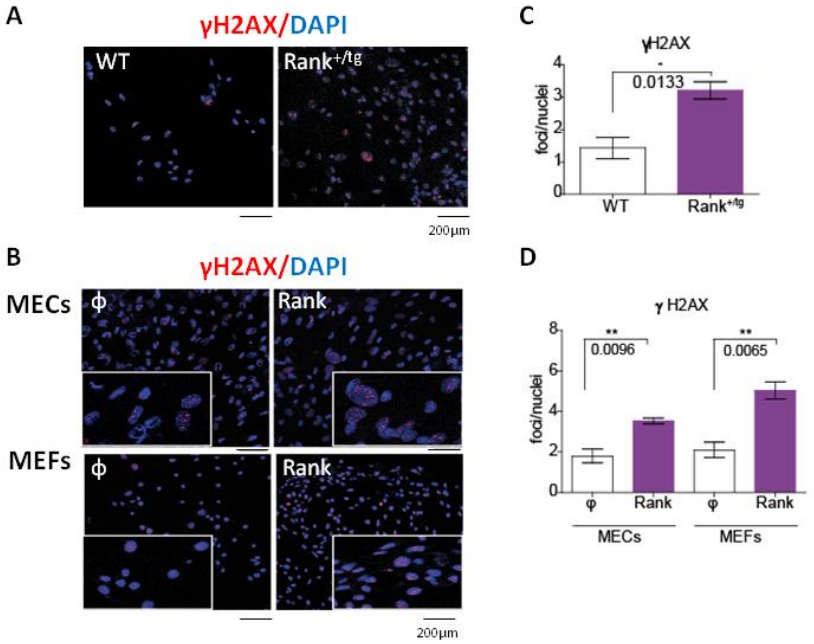

Figure 26: **A-B**) Representative images and quantification (**C-D**) of γH2AX+ (red) foci in WT, Rank$^{+/tg}$ and non-transformed MECs and MEFs 6 days after infection with Rank overexpressing and control (ϕ) lentivirus. The number of γH2AX+ foci per nuclei was quantified by ImageJ and nuclei were counterstained with DAPI. Three representative pictures of three independent experiments were quantified and mean and p values are shown.

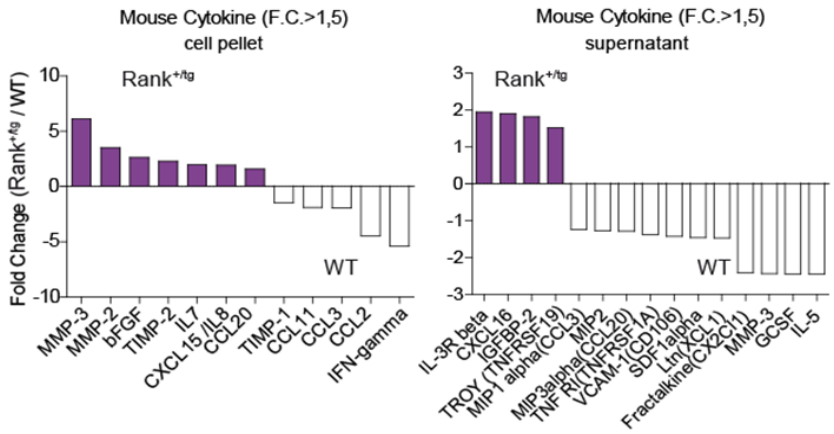

Figure 27: Cytokine array analysis of WT and Rank$^{+/tg}$ MECs lysates and supernatants from in vitro cultured WT and Rank$^{+/tg}$ MECs. Fold change of relative expression in Rank$^{+/tg}$ MECs relative to WT, calculated as the mean of the dot density of the two different spots per cytokine. Cytokines are shown form the highest to the lowest fold change (only fold chages ≥ 1.5 are represented).

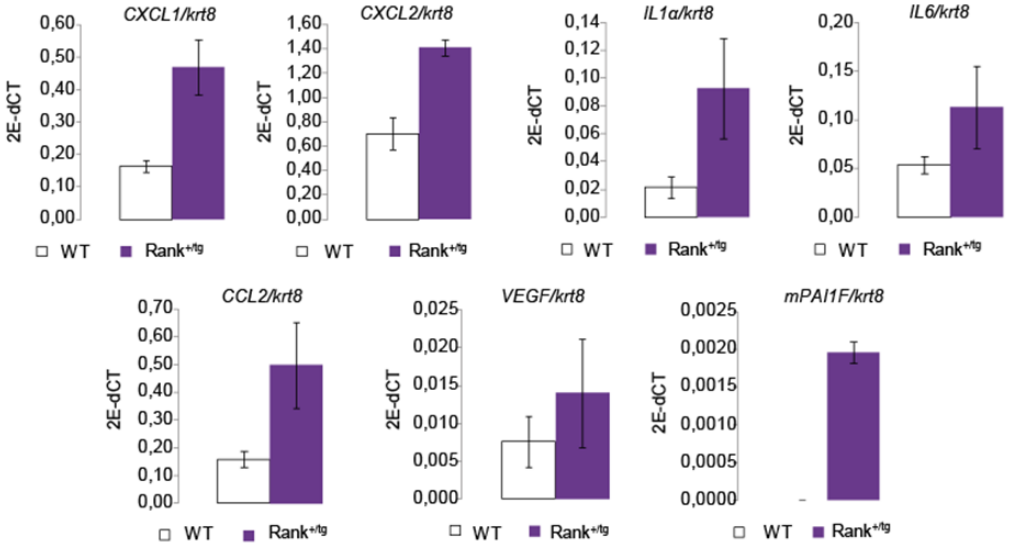

Figure 28: mRNA expression of the indicated genes relative to *krt8* measured by RT-PCR in Rank$^{+/tg}$ and WT MECs. Mean, SEM and t-test p value for 3 or 2 in case of Rank$^{+/tg}$ MECs independent experiments are shown. Quantifications were performed in triplicate and mean values were used in the calculations.

1.6. The senolytic drug Navitoclax targets Rank-induced senescent cells

Despite the tumor-suppressive role of senescence, the long-term accumulation of senescent cells is potentially detrimental and might favor cancer progression[361]. Thus, elimination of senescent cells is nowadays contemplated as a novel therapeutic strategy against cancer[341]. Senolytics are regarded as drugs with wide range of beneficial effects for senescence-related indications and could be crucial to treat age related disorders linked to senescence[362]. In the last years, several senolytic drugs have been developed, such as ABT263 (Navitoclax), a small molecule inhibitor that specifically targets Bcl-2/Bcl-xL pro-apoptotic proteins[328,343].

We assessed the sensitivity of Rank-overexpressing cells to the senolytic drug Navitoclax (ABT263)[363]. Rank$^{+/tg}$ MECs cultured *in vitro* are more sensitive to Navitoclax than WT MECs (**Figure 29**) which is consistent with the abundance of senescent cells. In fact, less SA-βGal staining was detected in Rank$^{+/tg}$ MECs upon Navitoclax treatment (**Figure 29*A,B***). Senescence structures were no longer observed in the mammary glands of Rank$^{+/tg}$ mice treated *in vivo* during 14 days with 25mg/Kg of Navitoclax (**Figure 29*C***) and the total number of viable MECs isolated show a greater reduction in Rank$^{+/tg}$ mice compared to WT mice (**Figure 29*D***). SA-βGal analyses of cultured WT and Rank$^{+/tg}$ MECs isolated from Navitoclax-treated mice demonstrated that the frequency of senescent cells in MECs from Rank$^{+/tg}$ mice after Navitoclax treatment was comparable to those detected in WT MECs demonstrating that Navitoclax preferentially kills the senescent cells induced by Rank overexpression (**Figure 29*E***). Thus, Rank induced senescent cells are sensitive to the senolytic Navitoclax.

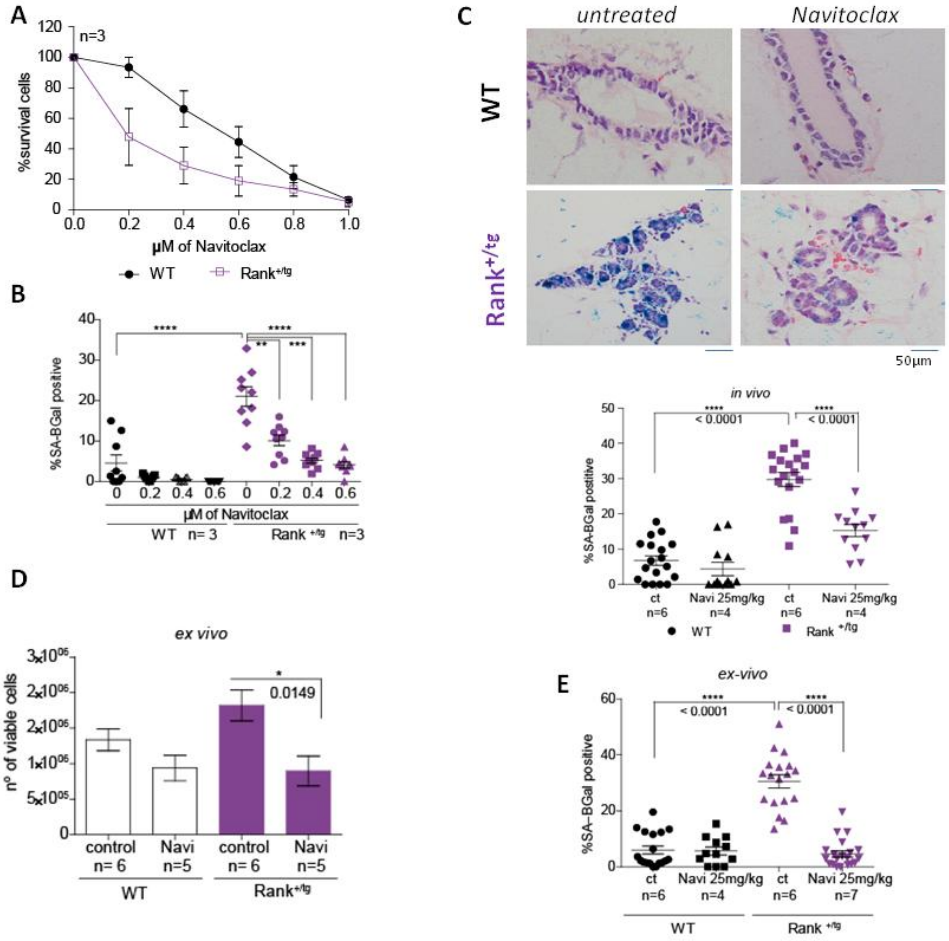

Figure 29: A-B) Percentage of surviving cells (**A**) and SA-βGal positive cells (**B**) of WT and Rank$^{+/tg}$ MECs treated *in vitro* with the indicated doses of Navitoclax for 48h. Quantifications were performed in triplicates and mean and SEM for 3 independent experiments are shown. Each dot indicates a replica of each experiment. **C**) Representative images and quantification (bottom panel) of the SA-βGal staining in WT and Rank$^{+/tg}$ mammary glands after 14 days of treatment with Navitoclax (25 mg/Kg). Three representative pictures of the indicated number of mammary glands were quantified and mean and p values are shown. Each dot indicates quantification of a picture. Mean, SEM and t test p values are shown. **D**) Number of viable MECs isolated from the MGs of WT and Rank$^{+/tg}$ mice after Navitoclax treatment (25mg/kg mice) administered by daily oral gavage for 14 days. The total number of treated mice is shown. **E**) Quantification of SA-βGal staining of WT and Rank$^{+/tg}$ MECs isolated from Navitoclax-treated mice and cultured *ex vivo* for 8 days. Quantifications were performed in triplicates and each dot represents a replica.

1.7. Rank-induced senescence is required for Rank driven stemness

Previous results from our group have established that Rank induces stemness in mouse[138] and human[148] MECs, as well as in mammary tumor cells. Since we have now established that Rank induces senescence in mammary epithelia, we decided to analyze whether there is a link, regulated by Rank, between senescence and stemness. Indeed, recent findings support that senescence and reprogramming/stemness are associated [329,332,364]. A significant increase in the amount of secondary mammospheres derived from Rank$^{+/tg}$ mammary epithelia compared to WT was observed (**Figure 30*A***), confirming the previously reported stemness phenotype driven by Rank in MECs[138,148].

RNAseq analysis was performed in basal and luminal MECs isolated from WT and Rank$^{+/tg}$ mice. Single cells were FACs-sorted based on the cell surface markers CD24 and CD49f following exclusion of lymphocytes and endothelial cells using CD45 and CD31 antibodies, respectively. As expected, a 14-fold increase in *Rank* mRNA expression was found in Rank$^{+/tg}$ luminal cells compared to luminal WT cells, while 1124 genes were differentially expressed (897 up and 227 downregulated in luminal Rank$^{+/tg}$ cells compared to WT luminal cells) **Supplementary Table 1** . GSEA analyses revealed a decrease in the luminal mature signature in luminal Rank$^{+/tg}$ cells as compared to luminal WT in accordance with the "stemness" phenotype observed in Rank$^{+/tg}$ cells[138]; a higher expression levels of Wnt related genes (*Rspo1, Axin2)* and a reduction in luminal differentiation markers (*Pr, PrlR, Csn)*. The most prominent signatures increased in luminal Rank$^{+/tg}$ were related to cell cycle, proliferation, p53 senescence/apoptotic pathway, Rb and DNA repair pathway (**Figure 30*B,* Supplementary Table 1**). An increase in *Cdkn2a* was also found in luminal Rank$^{+/tg}$ cells compared to WT. TLX and EzH2 targets were enriched in luminal Rank$^{+/tg}$ suggesting that the stemness/senescence phenotypes may be controlled by epigenetic mechanisms[327,365,366].

In the basal compartment, even though no significant differences in the expression of *Rank* mRNA were found between Rank$^{+/tg}$ and WT cells, 476 genes were differentially expressed **Supplementary Table 1** , highlighting the relevance of the crosstalk between basal and luminal populations. Interestingly, an increase in cell cycle and E2F targets was found in Rank$^{+/tg}$ basal cells, whereas the p53 pathway, ROS, and p53 senescence targets were downregulated, including *cdkn1a* (p21) **Supplementary Table 1** . These results suggest that senescence in the luminal compartment may stimulate proliferation in basal cells. RNA sequencing results have been uploaded in GEO. To review GEO accession GSE139675:

Go to https://www.ncbi.nlm.nih.gov/geo/query/acc.cgi?acc=GSE139675
Enter token yretmeoqppqdhsv into the box.

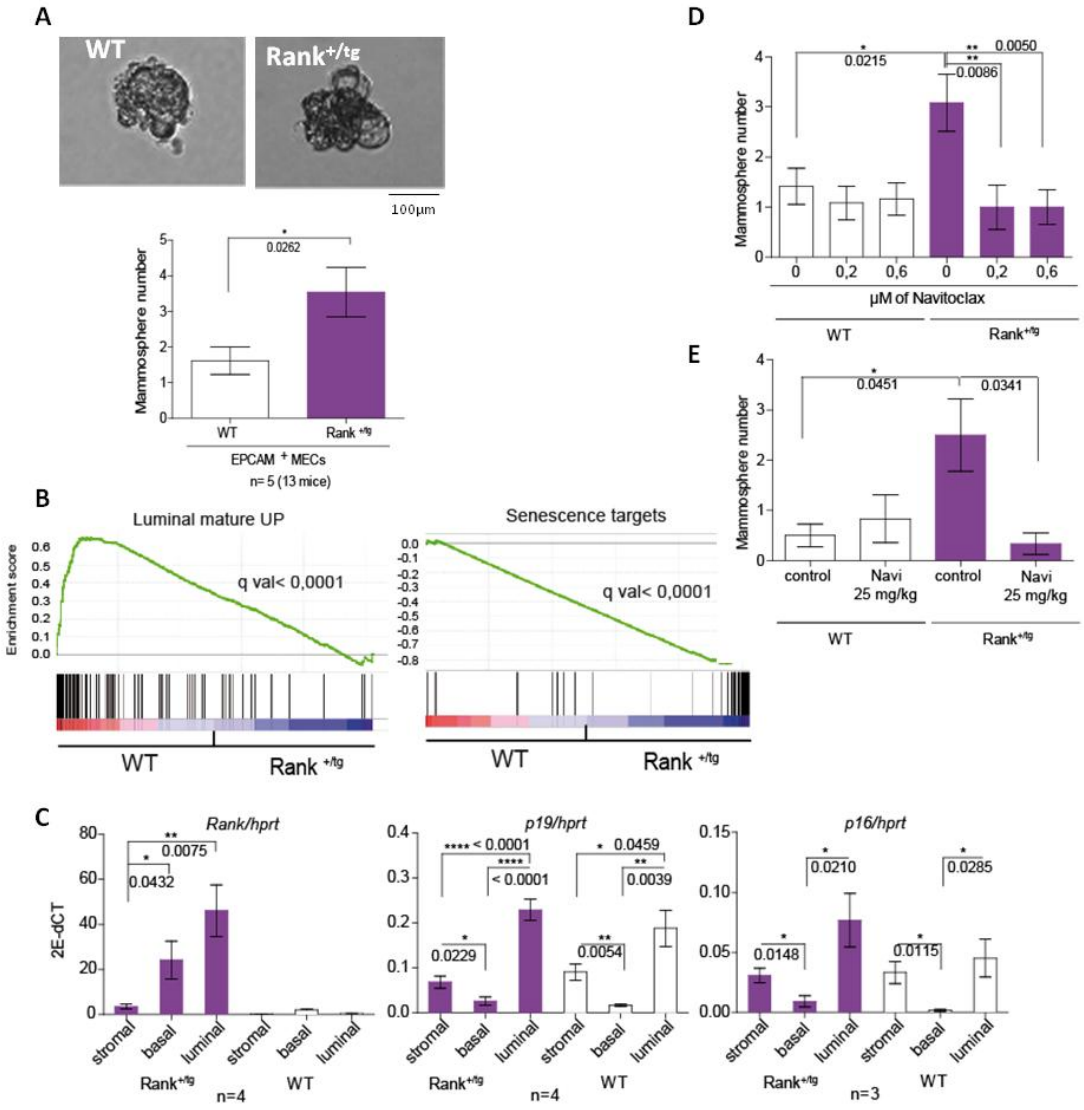

Figure 30: A) Representative images of secondary mammospheres and quantification (bottom) derived from WT and Rank$^{+/tg}$ EpCAM^{+} MECs. Mean and t test p value for 5 independent experiments are shown. For each experiment pools of MECs from 2-3 independent mice were used (13 mice per genotype). **B**) GSEA graphical outputs for the association analysis between RNAseq results from WT and Rank$^{+/tg}$ luminal MECs. Each signature was analyzed using the gene subsets corresponding to over-or under-expression. The GSEA enrichment score and nominal p values are shown. **C**) mRNA expression of *Rank*, *p16* and *p19* relative to *hprt* measured by RT-PCR in sorted cells of the basal and luminal populations from the mammary epithelial cell compartment from WT and Rank$^{+/tg}$ mice. Mean, SEM and t-test p values for the indicated independent experiments are shown. **D**) Number of secondary mammospheres of WT and Rank$^{+/tg}$ EpCAM^{+} MECs after Navitoclax (Navi) treatment *in vitro* (14 days). Mean and SEM for 4 independent experiments is shown. **E**) Number of secondary mammospheres obtained from WT and Rank$^{+/tg}$ EpCAM^{+} MECs after Navitoclax treatment *in vivo* (25mg/kg*)*. Mean and SEM for 2 independent experiments are shown. Quantifications for each experiment were done in triplicates. MECs from 3 mice per genotype and treatment were pooled for each experiment.

In addition, mRNA extracted from sorted luminal, basal and stromal cells from Rank$^{+/tg}$ and WT was analyzed by RT-quantitative PCR for *p16* and *p19* expression. Higher expression levels of both genes were found in the luminal compared to the basal cells, not only in Rank$^{+/tg}$ but also in WT cells (**Figure 30*C***).

Although Rank expression levels in basal Rank$^{+/tg}$ are higher than in the stroma, a reduction in *p19* and *p16* mRNA expression is observed, confirming that there is no senescence in the basal population, where mammary stem cells are located. These results suggest that senescent cells in the luminal compartment might enhance stemness in the basal cells through paracrine mechanisms.

Next, we directly tested whether Rank-induced senescence is involved in the activation and/or acquisition of stemness features. In order to study the functional connection between both cellular processes, mammosphere ability was assessed after treatment *in vitro* and *in vivo* with Navitoclax. The increased frequency of secondary mammospheres derived from Rank$^{+/tg}$ epithelia in the presence of 0.2 and 0.6 µM of Navitoclax was no longer observed (***Figure 30D***). Accordingly, whereas Navitoclax treatment *in vivo* did not alter the number of secondary mammospheres in WT, in Rank$^{+/tg}$ a significant reduction in mammosphere potential was observed (**Figure 30*E***). In fact, similar numbers of mammospheres derived from WT and Rank$^{+/tg}$ MECs isolated from Navitoclax-treated mice were observed in contrast with those derived from mock-treated control mice (**Figure 30*E***). These results demonstrate that Rank-induced senescence in MECs is essential for stemness.

1.8. Activation of Rank signaling by Rankl leads to senescence in WT MECs

We then studied whether senescence in MECs could also be achieved by the exposure to Rankl. For that purpose, we stimulated WT and Rank$^{+/tg}$ MECS with Rankl *in vitro* and *in vivo* settings. Rankl treatment (1µg/ml) in cultured WT MECs significantly increased senescence to levels comparable to those observed in Rank$^{+/tg}$ MECs (**Figure 31*A*,*B***). Strikingly, Rank$^{+/tg}$ MECs showed a reduction in senescent cells upon Rankl treatment (**Figure 31*A*,*B***). No changes in survival and apoptosis were found in treated WT and Rank$^{+/tg}$ MECS *in vitro* (**Figure 31*C***). A trend to a reduction in mammosphere forming ability of Rank$^{+/tg}$ was detected after Rankl treatment, whereas in WT no changes were found (**Figure 31*D***).

A decrease in the mRNA expression levels of *p19* and *p16* genes was found in Rank$^{+/tg}$ MECs cells upon Rankl treatment compared to the control cells, whereas in WT MECs the trend was opposite (**Figure 33**). Interestingly, upon Rankl treatment the expression levels of *Rankl* mRANK increase in both genotypes (**Figure 33**). After 8 days of culture in the presence of Rankl, *Rank* expression levels decrease in Rank$^{+/tg}$ (**Figure 33**) which might explain the observed reduction in senescence markers.

Accordingly, multiple senescent cells were observed in the mammary glands of WT mice treated with Rankl (0.75 mg/kg, three times per week) for 14 days *in vivo* (**Figure 32*A,B***). Hyperplasic structures were observed in these glands recapitulating the phenotype seen in Rank$^{+/tg}$ epithelia, with several senescent cells located within the luminal cell compartment (**Figure 32*A***). Quantification of SA-βGal staining in cultured MECs isolated from Rankl-treated WT mice revealed senescence in 20% of the cells as

compared to 3% in non-treated controls (**Figure 32*C***). In contrast, in Rank$^{+/tg}$ mammary glands a non-significant decrease in senescent cells was observed upon Rankl treatment and quantification of SA-βGal staining in cultured MECs isolated from Rankl-treated Rank$^{+/tg}$ mice revealed a similar trend: a decrease in the number of senescent cells upon Rankl; however, these changes did not reach significance (**Figure 32*A-C***).

The lower levels of senescence in the Rank$^{+/tg}$ MECs after Rankl treatment could indicated that overactivation of Rank signaling could prevent or rescue senescence. To further explore this hypothesis, non-transformed MECs and MEFs were transduced with Rank overexpressing plasmids and cultured in the presence of Rankl for 48h or 6 days.. In this case no differences in SA-βGal staining were found (**Figure 32*D***). Moreover, non-transformed MECs and MEFs were transduced with Rank overexpressing lentivirus and after 6 days of infection, these cells were treated with Rankl and the expression of genes such as p19 and p16, as well as, survival and proliferation assays, are currently being analyzed to explain these controversial results. It is important to consider that unlike Rank$^{+/tg}$, where Rank expression is driven by the MMTV promoter, which can be modulated in the infections, the cells infected with Rank-overexpressing plasmids cannot downregulate Rank (CMV promoter associated to antibiotic selections).

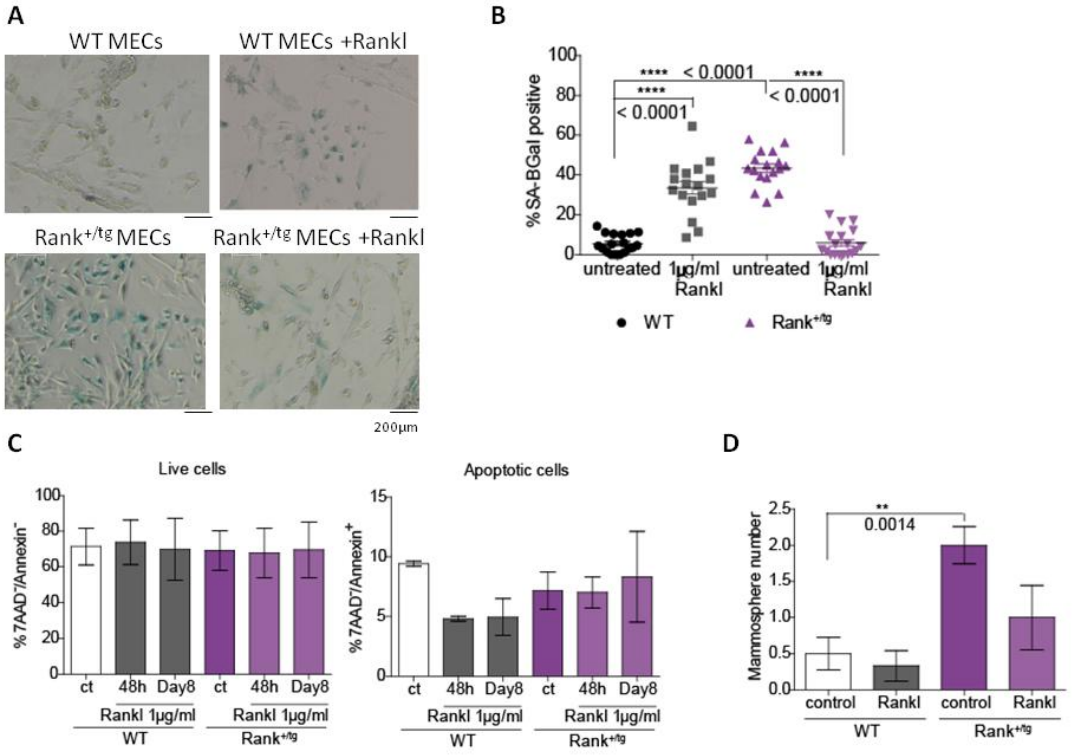

Figure 31: A-B) Representatives images (**A**) and quantification **(B**) of SA-βGal staining in WT and Rank$^{+/tg}$ MECs cultured *in vitro* in the presence of Rankl (1µg/ml, 7days). Quantifications were performed in triplicates. Each dot indicates a replica of 6 independent experiments and mean, SEM and t test p values are shown. **C**) Graphs showing the percentages of live (7AAD$^-$AnnexinV$^-$) and apoptotic (7AAD$^-$AnnexinV$^+$) WT and Rank$^{+/tg}$ MECs cultured *in vitro* in the presence of Rankl (1µg/ml). **D**) Number of secondary mammospheres obtained from WT and Rank$^{+/tg}$ EpCAM$^+$ MECs upon Rankl treatment *in vitro* (1µg/ml*)*. Mean and SEM for 2 independent experiments are shown. Quantifications for each experiment were done in triplicates. MECs from 3 mice per genotype and treatment were pooled for each experiment.

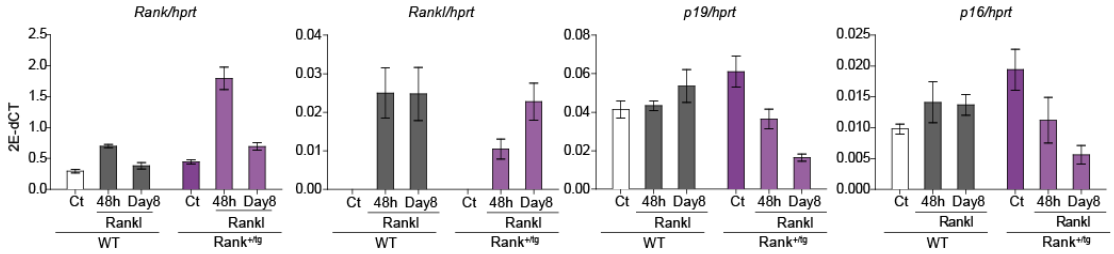

Figure 33: mRNA expression of *Rank*, *Rankl*, *p19* and *p16* relative to *hprt* measured by RT-PCR in WT and Rank$^{+/tg}$ MECs cultured *in vitro* in the presence of Rankl (1µg/ml). Mean and SEM for one experiment are shown.

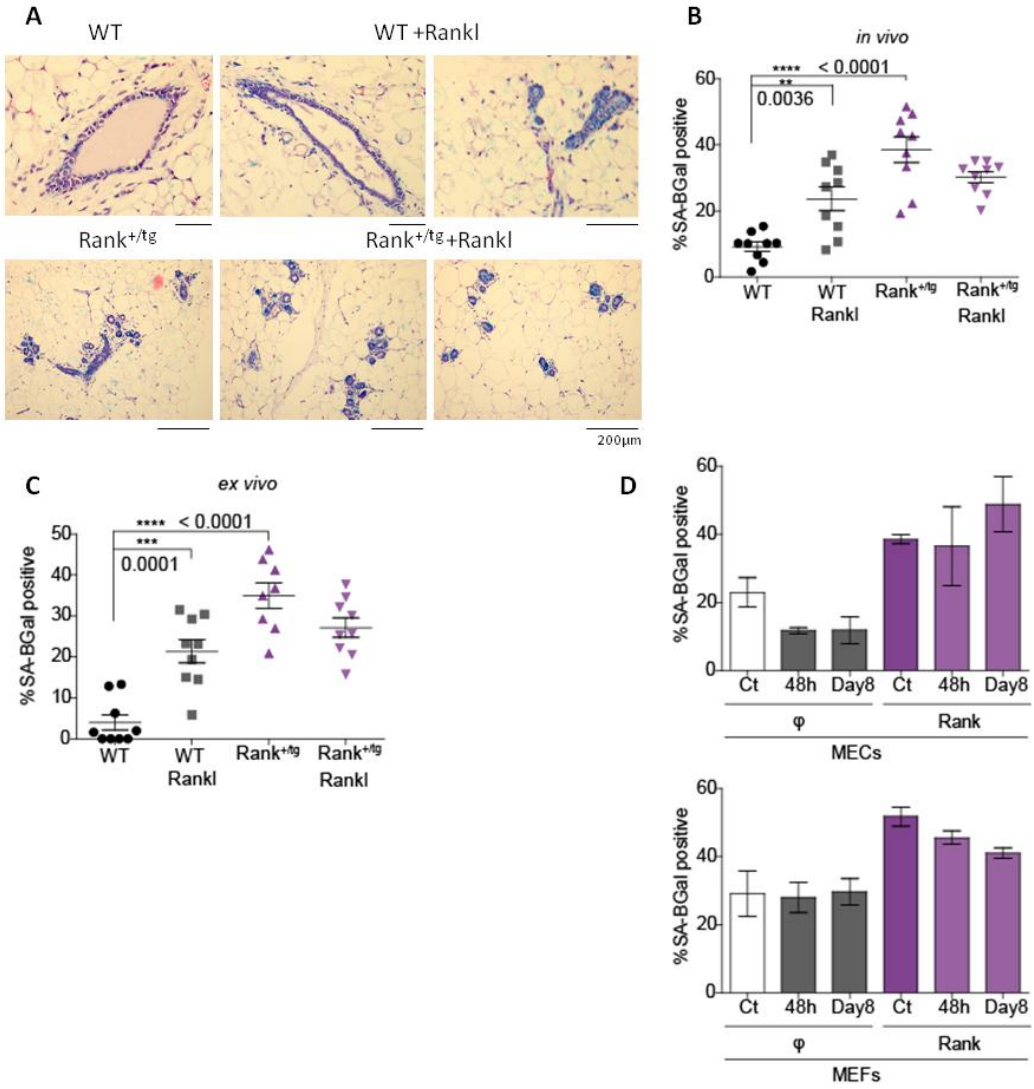

Figure 32: A) Representatives images and quantification (**B**) of SA-βGal staining in WT and Rank$^{+/tg}$ mammary glands after 14 days of Rankl (0.75mg/kg, 3 times per week) or mock (CT) (n=3) *in vivo* treatment. Quantifications were done in triplicate. Each dot indicates a replica. Mean, SEM and t test p values are shown. **C**) Quantification of SA-βGal staining of MECs isolated from Rankl-treated (0.75mg/Kg, three times per week by intraperitoneal injection for two weeks) WT and Rank$^{+/tg}$ mice (n=3) cultured for 8 days (*ex vivo*). Mean, SEM and t test p values are shown. **D**) Quantification of SA-βGal staining in MECs and MEFs infected with Rank overexpressing plasmids cultured *in vitro* in the presence of Rankl (1µg/ml) for the indicated time. Quantifications were performed in triplicates. Mean and SEM are shown (n=1)

The fact that the activation of Rank signaling upon Rankl treatment leads to senescence in WT MECs, indicates that Rank-induced senescence could play a role not only during the early stages of mammary tumor initiation but also during mammary gland development. Rank and Rankl expression increase during pregnancy, thus, we speculate that it may result in senescence and that senescence may pay a role in mammary gland development during pregnancy. Preliminary results have shown that in the early stages of gestation (8.5 and 10.5days, where the gland resembles those of $Rank^{+/tg}$ mice) SA-βGal is observed (**Figure 34*A***). Rank, but not Rankl expression was expressed at involution (day 0-3). However, Rank expression decreased at later involution timepoints and did not seem to correlate with SA-βGal staining which was strongly expressed at involution day 7 (**Figure 34*B***).

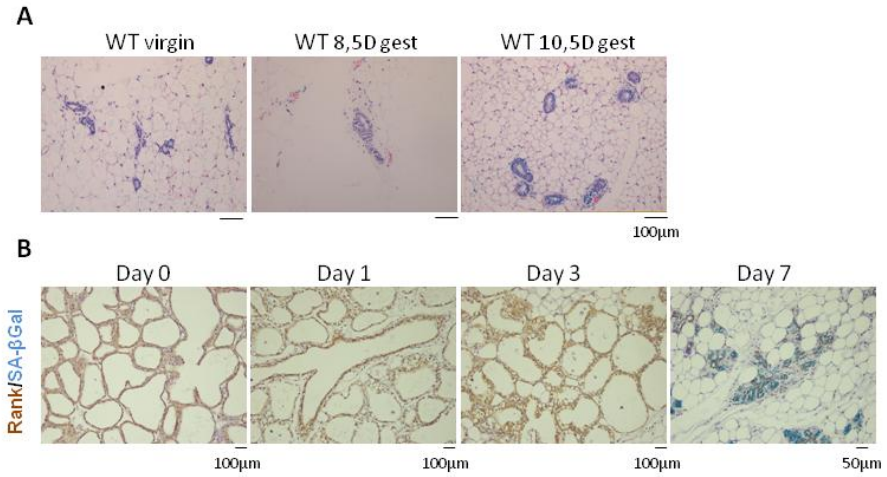

Figure 34: A) Representative images of H&E with SA-βGal staining in MG of WT mice at the indicated gestation time point. **B**) Representative images of Rank (brown) and SA-βGal (blue) staining in involuted WT MGs at the indicated involution days .

1.9. Rank downstream pathways involved in Rank induce senescence

We next sought to investigate the signaling pathways that could mediate the RANK-induced senescence. We analyzed whether the Rank-downstream signaling pathways: NF-κB, MAPK and PI3K are altered in Rank overexpressing cells compared to WT cells and/or upon Rankl treatment *in vitro*. Mitogen-Activated Protein Kinase (MAPK) and Nuclear Factor kappa-light-chain-enhancer of activated B cells (NF-κB) pathways are involved in proliferation[367], oncogenesis[368,369] and oncogene-induced senescence[370,371]. Moreover, the mitogen activated protein kinases (MAPK) ERK and p38 are active in MECs and regulate cell proliferation, differentiation and survival[372,373], and recent studies indicated that p38 MAPK pathway also mediates OIS and tumor suppression[374,375]. The expression of the main proteins involved in these pathways was analyzed by western blot in WT and $Rank^{+/tg}$ MECs, but no clear differences were found between genotypes were found (**Figure 35 *A***). Lack of differences may result from the

contamination of non-senescent MECs and other cell types or from the kinetics of activation MECS.

Next, we analyzed by western blot putative changes in these signaling pathways in WT and Rank$^{+/tg}$ MECs cultured in the presence of Rankl (1µg/ml) for 48h or 8 days. Preliminary results show a moderate increase in p-p65 and p-ERK in WT and Rank$^{+/tg}$ MECs cultured in the presence of Rankl (**Figure 35*B***). In untreated MECs, higher levels of p-Akt were observed in Rank$^{+/tg}$ compared with WT MECS and these levels decreased in the presence of Rankl in both genotypes. The levels of P-p38 were a bit higher in untreated Rank$^{+/tg}$ MECs, compared with the other conditions (**Figure 35*B***).

Finally, we analyzed the downstream pathways in MECs and MEFs infected with Rank overexpressing constitutive and inducible vectors. Rank was only detected in MECs and MEFS infected with constitutive plasmids (pWPI-Rank) but not in those infected with the inducible vector, irrespectively of doxycycline treatment (**Figure 35*C,D***). Accordingly, P-p65 levels are higher in MECs and MEFs infected with constitutive Rank-overexpression vectors. In contrast, a reduction in pERK, P-JNK and P-p38 expression were observed in MECs with Rank constitutive expression (**Figure 35*C***). In MECs infected with inducible vectors, a clear increase in P-Akt and a slight increase in and P-JNK and P-p38, was observed 24h after the induction of Rank expression; these changes disappear at later timepoints and a late induction of P-ERK (6 days of culture), revealing complex kinetics mediating the Rank-induced senescence phenotype. These results are preliminary and further experiments and additional markers are required to clarify the role of the downstream pathway in Rank-induced senescence.

Since the NF-κB pathway plays a pivotal role in promoting the secretory phenotype of senescent cells[376–378] and increased levels of NF-κB activation were observed in MECs and MEFs expressing high levels of RANK, we hypothesized that NF-κB could contribute to the RANK driven senescence phenotype observed in these cells. To test this hypothesis, we used an inhibitor (IKK-16) of the IKKs, the core kinases of the NF-κB cascade[379]. Thus, we treated WT and Rank$^{+/tg}$ MECs with IKK-16 for 8days in culture with several doses of these inhibitor (0.2,0.5,1 and 2.5µM) and analyzed the impact on senescence evaluated by SA-βGal staining (**Figure 36**). A significant decrease in SA-βGal staining in Rank$^{+/tg}$ MECs was observed upon NF-κB inhibiton demonstrating that RANK induced senescence in MECS partially through NF-κB activation.

In addition, a slight increase in P-ERK was observed in Rank$^{+/tg}$ MECs or after induction of RANK expression in MECs infected with the inducible vector. Moreover, analyses by IHC in the mammary gland of Rank$^{+/tg}$ and WT, revealed increased levels of P-ERK (**Figure 36*A,B***) and P-ERK is involved in other OIS models, such as RAS. Thus, we treated WT and Rank$^{+/tg}$ MECs with the MEK inhibitor (PD98059), 0.2,0.4,0.6 and 1 µM for 8 days and senescence cells were quantified (**Figure 36*C***). We observed that treatment with PD98059, caused a reduction in SA-βGal staining in cultured Rank$^{+/tg}$

but not WT MECs (**Figure 36*C***). Differences in our results may be related to the sensitivity of the techniques, changes during cell isolation, and will be clarified in the future.

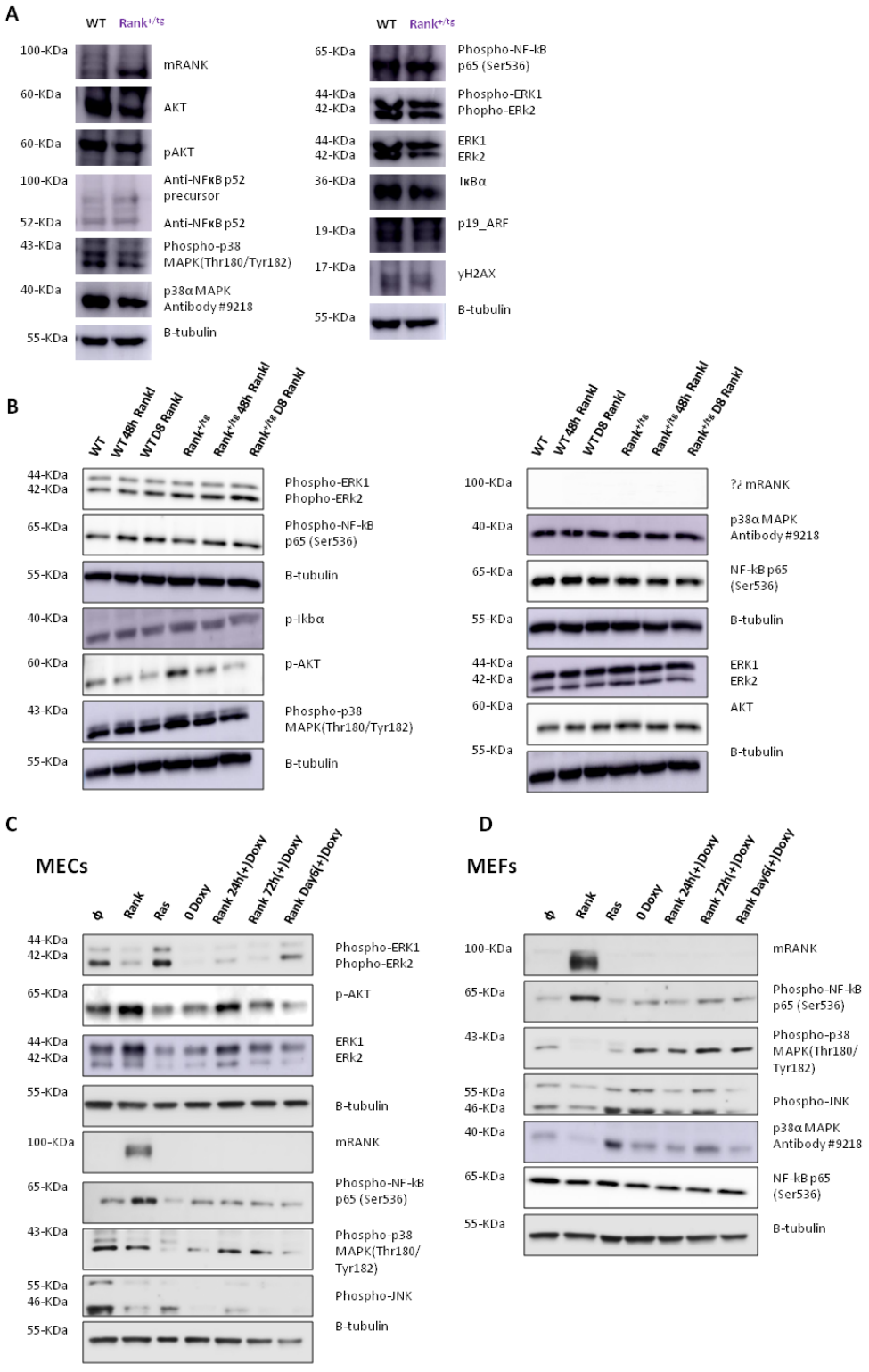

Figure 35: A-B) Western blot analysis of the indicated proteins in whole extracts from WT and Rank$^{+/tg}$ MECs (**A**) and from WT and Rank$^{+/tg}$ MECs cultured with Rankl for 48h or 8 days and untreated controls (**B**). **C-D**) Western blot analysis of the indicated proteins in constitutive (pwpi) and inducible Rank-overexpressing MECs and MEFs. Tubulin is shown as a loading control.

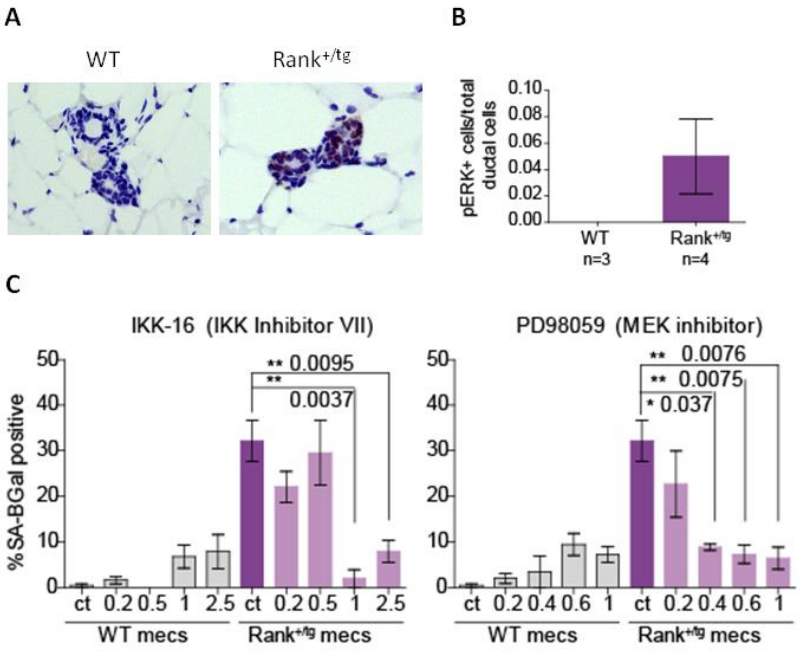

Figure 36: A) Representative images and quantification (**B**) of pERK (brown) and SA-βGal staining in WT and Rank$^{+/tg}$ mammary glands. **C)** Quantification of SA-βGal staining of MECs isolated from WT and Rank$^{+/tg}$ mice and plated *in vitro* during 8 days treated with the indicated doses of the corresponding inhibitors. Mean, SEM and t-test p values are shown.

1.10. Impact of Rank overexpression in reprogramming

Senescence is activated in response to different types of cellular damage, characterized by an abundant production of cytokines and other molecules that cause, together with the recruitment of inflammatory cells, tissue remodeling[251,380]. Serrano and colleagues report that senescence plays an active role in facilitating an *in vivo* reprogramming through the paracrine action of the SASP[332,333]. Several scientific reports demonstrated that the activation of the reprogramming factors OSKM (Oct4, Sox2, Klf4 and c-Myc)[381] also results in cellular damage and senescence, both *in vitro*[311] and *in vivo*[332,333].

Once determined that Rank overexpression induces stemness and senescence, in collaboration with Noelia Alcazar and Manuel Serrano (Cellular Plasticity and Disease Group, IRB), we evaluated the impact of Rank modulation to *in vitro* reprogramming. To address the effect of Rank on the process of cellular reprogramming, we overexpressed *Rank* in MEFs by lentiviral infection and then we transduced Rank-overexpressing MEFs whith a tetracycline-inducible cassette expressing the reprogramming factors: Oct4, Sox2, Klf4 and c-Myc[382] (**Figure 37*A***).

After 10 days in doxycycline to induce the expression of the reprogramming factors, we evaluated the efficiency and kinetics of the reprogramming in MEFs with different levels of RANK expression, which was measured by alkaline phosphatase (AP) staining of the resulting iPSCs colonies. The number of colonies increased when MEFs

overexpressed Rank compared with control vector (**Figure 37*B***). To verify pluripotency, colonies were picked and expanded for further analysis. As expected, *Rank* mRNA levels were increased in Rank-transduced MEFs. However, embryonic stem cell markers such as *Nanog* and *Sox9* showed similar expression levels between Rank overexpressing and control MEFs (**Figure 37*C***). Although preliminary, these results suggest that MEFs transduced with Rank and reprogramming factors generated induced pluripotent stem cells (iPSCs), but these do not uphold increased pluripotency features than those generated in the absence of Rank overexpression.

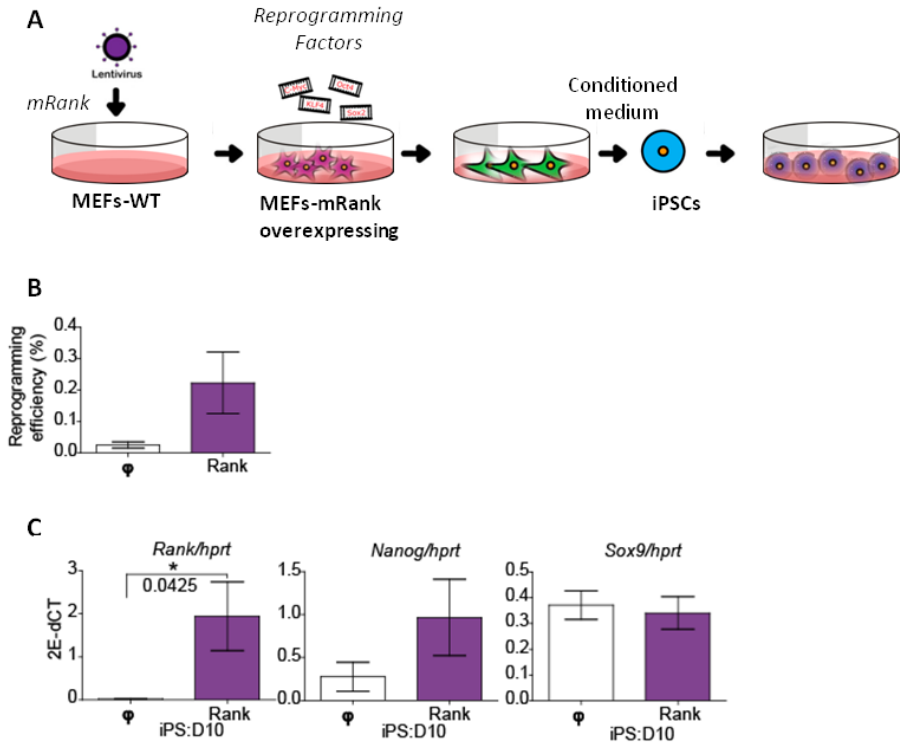

Figure 37: **A)** Schematic representation of the experimental setup to test the effect of Rank overexpression during reprogramming on WT MEFs. **B)** Reprogramming efficiency of iPSCs resulted from the *in vitro* reprogramming of Rank overexpressing MEFs cultured in the presence of 1µg/ml doxycycline (to induce the pruripotency factors) compared to control MEFs carrying an empty vector(ϕ). Alkaline phosphatase (AP) positive colonies were counted on day 10. **C)** mRNA expression of *Rank*, *Nanog* and *Sox9* relative to *hprt* in Rank overexpressing MEFs after reprogramming with inducible OSKM compared to control MEFs carrying an empty vector(ϕ).

PART 2

ROLE OF RANK ON MAMMARY TUMOR CELLS

Even though $Rank^{+/tg}$ mice spontaneously develop mammary tumors, the long tumor latency observed [138,152], suggests that additional oncogenic events are required to induce tumorigenesis. Unexpectedly, we observed that Rank overexpression delays tumor initiation in oncogene-driven mouse models (Neu and PyMT) while promoting tumor aggressiveness and enrichment in the cancer stem cell compartment (results included in the PhD thesis of Alex Cordero). During the execution of this PhD thesis, we found that in non-transformed mammary epithelium, Rank overexpression also induces senescence. Indeed, Rank-driven senescence recapitulates the main characteristics of a typical "oncogene-induced senescence" (OIS)[244]phenotype in both MECs and MEFs: reduced proliferation, increased SA-βGal staining, dependency on p16/p19, DNA damage, SASP induction and sensitivity to senolytics.

Encouraging previous results from our group showed in A.Cordero thesis 2015, revealed that, despite the delayed tumor initiation and reduced incidence, after tumor appearance in double transgenic mice ($PyMT^{+/-}$; $Rank^{+/tg}$), tumors grew significantly faster than in single PyMT mice. These results suggest that increased Rank expression in tumor cells favors tumor aggressiveness in the presence of the PyMT oncogene (**Figure 38*A***). Moreover, Rank overexpression led to the accumulation of $CK14^{+}/CK8^{+}$ cells in the $PyMT^{+/-}$; $Rank^{+/tg}$ tumors (**Figure 38*B***), but no changes in $CK5^{+}/CK8^{+}$ cells compared with the single $PyMT^{+/-}$ tumors (**Figure 38*B***), in accordance with previous observations in spontaneous $Rank^{+/tg}$ tumors[138]. Moreover, $PyMT^{+/-}$; $Rank^{+/tg}$ mice presented 100% lung metastasis incidence, with all mice showing more than 10 metastatic foci per lung; by contrast, only 70% $PyMT^{+/-}$ mice presented lung metastasis, and 40% showed less than 10 metastatic foci per lung (**Figure 38*C***).

FACS analysis revealed a significant increase in $CD61^{+}$ and $CD49b^{+}$ cells within the Lin^{-} ($CD45^{-}$ $CD31^{-}$) $CD24^{+}$ epithelial cell population in $PyMT^{+/-}$ $Rank^{+/tg}$ tumors, compared to $PyMT^{+/-}$ (**Figure 38*D***). As $CD61^{+}$ and $CD49b^{+}$ cells are described to identify luminal progenitors in untransformed MG[383,384], their increase in $PyMT^{+/-}$ $Rank^{+/tg}$ tumors may indicate an enhanced stem cell population. In fact, more and bigger secondary tumorspheres (**Figure 38*E***), and a significantly higher frequency of metastasis initiating cells (MICs) (1 in 1064 cells) was observed in $PyMT^{+/-}Rank^{+/tg}$ compared to $PyMT^{+/-}$ (1 in 6264 cells) (**Figure 38*F***). In contrast, within the Neu background, no clear changes in tumor growth (**Figure 38*G***) or in cell populations discriminated by CK staining were observed between both genotypes (**Figure 38*H***), but the incidence of lung metastasis was higher in $Neu^{+/-}$; $Rank^{+/tg}$ mice compared with single $Neu^{+/-}$ mutants (**Figure 38*I***). All $Neu^{+/-}Rank^{+/tg}$ mice developed lung metastasis (10% of the mice with more than 50 metastatic foci) as compared to 80% of $Neu^{+/-}$ mice (**Figure 38*I***). Together, these

results indicate that once tumor develop, Rank overexpression increases tumor aggressiveness.

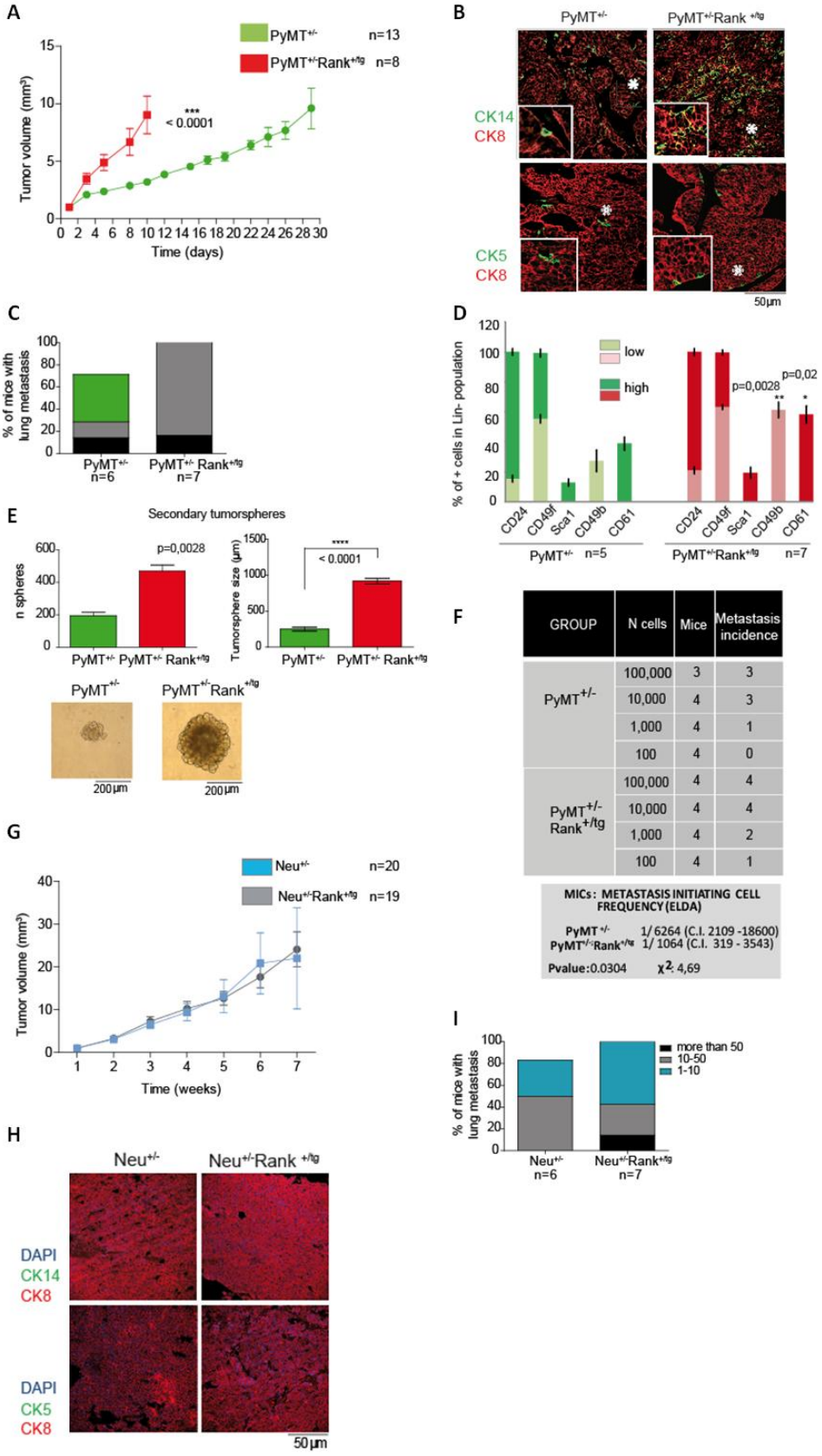

GROUP	N cells	Mice	Metastasis incidence
PyMT+/-	100,000	3	3
	10,000	4	3
	1,000	4	1
	100	4	0
PyMT+/- Rank+/tg	100,000	4	4
	10,000	4	4
	1,000	4	2
	100	4	1

MICs: METASTASIS INITIATING CELL FREQUENCY (ELDA)

PyMT+/- 1/ 6264 (C.I. 2109 -18600)
PyMT+/-Rank+/tg 1/ 1064 (C.I. 319 - 3543)

Pvalue:0.0304 χ^2: 4,69

Figure 38: : **A**) Tumor growth curves of the $PyMT^{+/-}$ and $PyMT^{+/-}Rank^{+/tg}$ spontaneous tumors. Mean tumor volume +/- SEM at each time point relative to their volume on the first day of detection and statistical t-test are shown. **B**) Representative CK14 or CK5 (green) and CK8 (red) immunostaining in $PyMT^{+/-}$ and $PyMT^{+/-}Rank^{+/tg}$ spontaneous adenocarcinomas. Asterisks indicate magnifications (2X) to highlight double positive $CK14^{+}CK8^{+}$ cells. No $CK5^{+}CK8^{+}$ cells were found. **C**) Percentage of $PyMT^{+/-}$ and $PyMT^{+/-}Rank^{+/tg}$ females with lung metastasis. Entire lungs were step-sectioned at 75 µm intervals and individual metastases identified histologically. Total number of metastasis foci per mouse is indicated. **D**) Frequency of indicated cells in Lin- ($CD45^{-}$ $CD31^{-}$) population found in $PyMT^{+/-}$ and $PyMT^{+/-}Rank^{+/tg}$ spontaneous tumors analyzed by FACS. Positive/negative and $high^{(hi)}$/$low^{(lo)}$ populations were set according to populations in the normal mammary gland. Mean, SEM and t-test p values for each marker for 5-7 independent tumors for each genotype are shown. **E**) Number and size of secondary tumorspheres derived from $PyMT^{+/-}$ and PyMT+/-$Rank^{+/tg}$ tumor cells isolated from established tumors. Each bar is representative of a pool of 3 independent tumors. 5.000 cells/ml from primary mammospheres were plated in triplicate in anchorage-independent conditions, and tumorspheres were quantified after 2 weeks. Mean, SEM and t-test p value are shown. Representative pictures of secondary tumorspheres derived from each genotype are also shown. **F**) Table showing limiting dilution assay to test the metastasis-initiating ability of $PyMT^{+/-}$ and $PyMT^{+/-}Rank^{+/tg}$ tumor cells. Cells from two independent tumors per genotype were pooled for injections in limiting dilution in the tail vein of $Foxn1^{nu}$ females. Presence of lung metastasis was scored 8 weeks after injection. Entire lungs were step-sectioned at 100µm and individual metastases identified histologically. The metastasis-initiating cell frequencies (with confidence intervals) for each group were calculated by ELDA; p- and chi-square values are shown. **G**) Tumor growth curves of the $Neu^{+/-}$ and $Neu^{+/-}Rank^{+/tg}$ spontaneous tumors. Mean tumor volume +/- SEM at each time point relative to their volume on the first day of detection are shown. **H**) Representative CK8 (red) and CK14/CK5 (green) immunostaining in $Neu^{+/-}$ and $Neu^{+/-}$ $Rank^{+/tg}$ tumor lesions. **I**) Percentage of $Neu^{+/-}$ and $Neu^{+/-}Rank^{+/tg}$ females with lung metastasis. Entire lungs were step-sectioned at 75 µm intervals and individual metastases identified histologically. Total number of metastasis foci per mouse is indicated.

2.1. Rank overexpression induces senescence in mouse breast tumor cells

Despite higher levels of Rank expression are detected in $Neu^{+/-}$; $Rank^{+/tg}$ and $PyMT^{+/-}$; $Rank^{+/tg}$ compared to $Neu^{+/-}$, and $PyMT^{+/-}$ invasive adenocarcinomas or in cultured tumor cells (*ex vivo*), SA-βGal staining showed similar levels of senescence among genotypes (**Figure 39*A,B***). Senescent cells were mainly located in preneoplasic lesions but not in the adenocarcinomas of $Neu^{+/-}$; $Rank^{+/tg}$ and $PyMT^{+/-}$; $Rank^{+/tg}$ (**Figure 20*B***, **Figure 39*A***). These findings suggest that eventually senescence is overcome with full transformation. However, when Neu and PyMT tumor-derived MECs were infected with Rank overexpressing vectors, an increase in senescence was observed (**Figure 39*C***).

As mentioned before, multiple studies suggest that triggering senescence can represent an efficient anti-tumor mechanism[318]. Nonetheless, the persistence of senescence cells and the release of pro-inflammatory cytokines via SASP might eventually contribute to tumor progression and aggresiveness[359,385]. We have performed gene expression analyses of several spontaneous $Rank^{+/tg}$, $PyMT^{+/-}$; $Rank^{+/tg}$, $PyMT^{+/-}$, $Neu^{+/-}$; $Rank^{+/tg}$ and $Neu^{+/-}$ tumors to further understand the mechanisms underlying the effects observed in tumor latency and growth. RNA seq analyses were performed in tumoral cells from $Rank^{+/tg}$, $PyMT^{+/-}$; $Rank^{+/tg}$, $PyMT^{+/-}$, $Neu^{+/-}$; $Rank^{+/tg}$ and $Neu^{+/-}$ mice. Upon data examination, 134 genes were commonly found between $Neu^{+/-}$; $Rank^{+/tg}$ and $Neu^{+/-}$ tumors compared to $PyMT^{+/-}$; $Rank^{+/tg}$, $PyMT^{+/-}$ tumors. According to GSEA, signatures increased in $PyMT^{+/-}$; $Rank^{+/tg}$ tumors were related to the p53 senescence/apoptotic dependent pathway as well as DNA damage[386]. One of the most prominent pathways found upregulated in $Neu^{+/-}$; $Rank^{+/tg}$ tumors is related to E2F

transcription factors and TLX-negative targets, suggesting that Rank overexpression in these tumor cells drives senescence in accordance with the role proposed for these factors in the regulation of senescence[387,388](**Supplementary Table 2**).

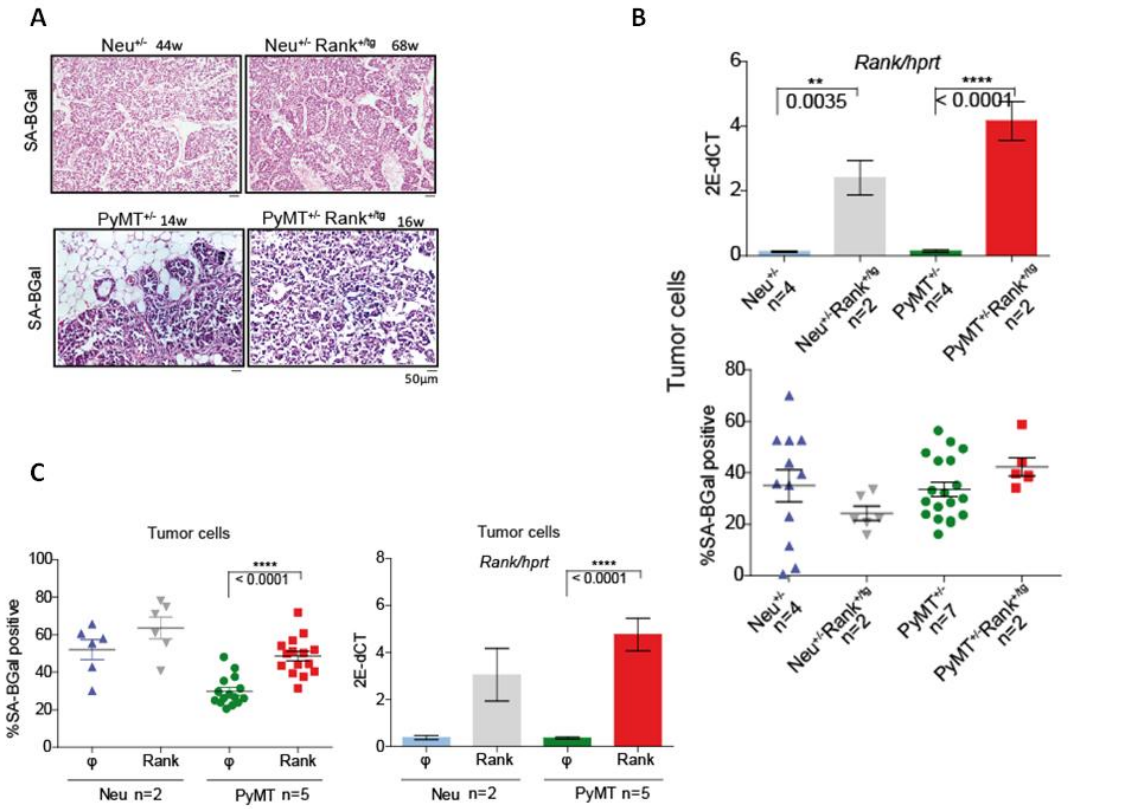

Figure 39: A) Representative images of SA-βGal staining of Neu$^{+/-}$, Neu$^{+/-}$ Rank$^{+/tg}$, PyMT$^{+/-}$ and PyMT$^{+/-}$ Rank$^{+/tg}$ tumors. Age of the mice is indicated. Note that double transgenic mice are older than single mutants and senescent cells are scarce. Non-specific SA-βGal staining was found at the edge of the sections. **B**) *Rank* mRNA expression relative to *hprt* (top panel) and quantification of SA-βGal staining (bottom panel) in Neu$^{+/-}$, Neu$^{+/-}$Rank$^{+/tg}$, PyMT$^{+/-}$ and PyMT$^{+/-}$Rank$^{+/tg}$ tumor cells cultured for 8 days. Quantifications were performed in triplicates. Each dot represents a replica and mean and SEM for the indicated independent experiments is shown. C) SA-βGal staining quantification (left panel) and mRNA expression of *Rank* relative to *hprt* (right panel) in Neu+/- and PyMT+/- (FVB) tumor-derived MECs infected with Rank overexpressing and control (ϕ)lentivirus 6 days after the infection. Quantifications were performed in triplicates and each dot indicates a replica. Mean, SEM and t test p values for the indicated independent experiments are shown.

In order to investigate whether the differences in tumor growth detected between PyMT$^{+/-}$and PyMT$^{+/-}$; Rank$^{+/tg}$ mice are tumor cell autonomous[389] or influenced by the senescent microenvironment[390–393], PyMT$^{+/-}$ and PyMT$^{+/-}$; Rank$^{+/tg}$ tumor cells were transplanted to WT mice (**Figure 40*A***). We could not detect differences in tumor latency in mice transplanted with PyMT$^{+/-}$or PyMT$^{+/-}$; Rank$^{+/tg}$ tumor cells , tumors from both genotypes initially grew at similar rates but a later time points PyMT$^{+/-}$; Rank$^{+/tg}$ tumors grew faster (**Figure 40*A,B***). Additional experiments will be performed to confirm these results.

To address whether the removal of senescent cells affects tumor onset and growth we treated PyMT$^{+/-}$; Rank$^{+/tg}$ mice and controls with the senolytic drug Navitoclax

(ABT263). Mice were treated before palpable lesions were detected (4-6 weeks of age), during 14 days with 25mg/kg of Navitoclax. As we are not avoiding senescence, no differences in tumor onset were observed (***Figure 40C,D***); however, tumor growth rates were attenuates in PyMT$^{+/-}$; Rank$^{+/tg}$ mice pretreated with the senolytic drug Navitoclax compared to untreated mice, indicating that the senescent cells present in the preneoplasic lesions are indeed favouring tumor growth.

Treatments with the senolytic drug in PyMT$^{+/-}$; Rank$^{+/tg}$ mice after tumor palpation and additional transplants, injecting PyMT tumor cells injected in WT and Rank$^{+/tg}$, as well as PyMT/RANK and PyMT injected in WT mammary glands will be performed to determine how senescent cells influence tumor growth.

Finally, to confirm that Rank-induced senescence could explain this delay in tumor onset observed in double transgenic mice for Rank and PyMT we are currently crossing p16/p19$^{-/-}$ mice with PyMT$^{+/-}$; Rank$^{+/tg}$.

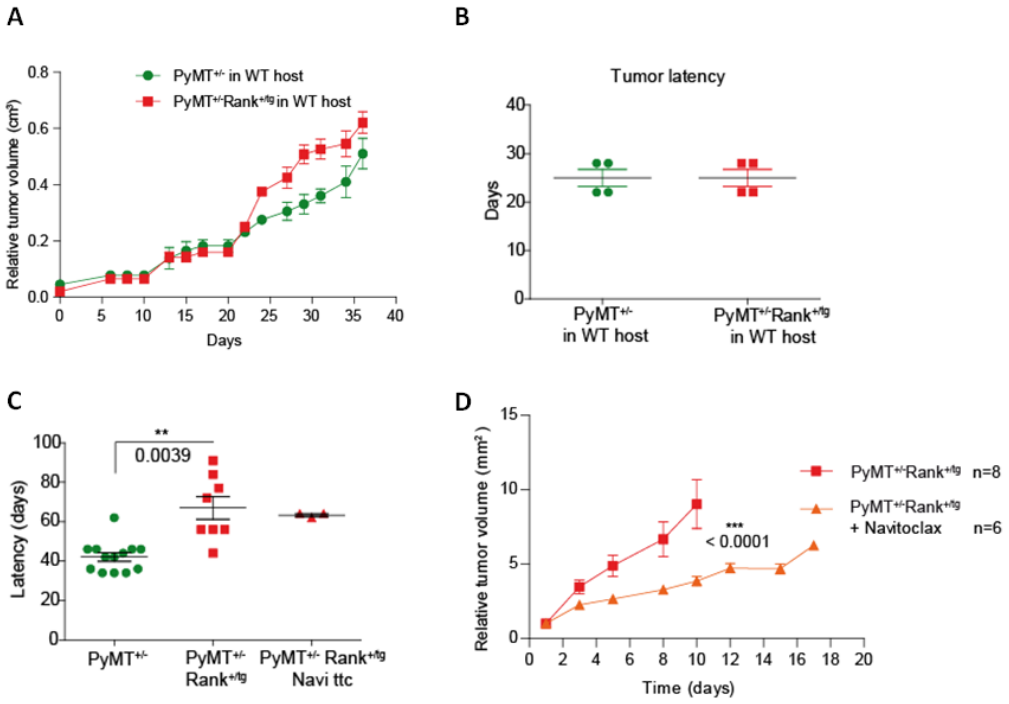

Figure 40: A) Tumor volume growth normalized to the first day of size assessment in 2 WT mice bearing tumors (4 tumors from each condition: PyMT$^{+/-}$ or PyMT$^{+/-}$ Rank$^{+/tg}$ transplanted tumor cells). Mean and SEM are shown. **B)** Tumor latency of PyMT$^{+/-}$ and PyMT$^{+/-}$ Rank$^{+/tg}$ tumor cells orthotopically implanted in 2 WT mice. **C)** Latency of PyMT$^{+/-}$(n=13), PyMT$^{+/-}$;Rank$^{+/tg}$ (n=8), and PyMT$^{+/-}$; Rank$^{+/tg}$ tumors from mice that received treatment with Navitoclax (Navi ttc) (n=6). Mean, SEM and t-test p values are shown. **D)** Tumor growth curves PyMT$^{+/-}$; Rank$^{+/tg}$ mice treated or not with Navitoclax (25mg/kg) for 14 days. Mean tumor volumne +/- SEM at each time point relative to their volumne on the first day of detection and statistical t-test are shown. The number of mice is indicated, and each mouse developed multiple tumors.

Altogether, our results reveal unexpected insights and a complex role of RANK signaling in mammary tumorigenesis of the oncogene-driven mouse models, MMTV-PyMT and MMTV-Neu. Mice that overexpress Rank in the mammary gland are more susceptible to mammary tumorigenesis driven by carcinogens and spontaneously develop mammary tumors after multiple pregnancies with long latency[138,152].

However, double transgenic mice for Rank and Neu or PyMT have a significant delay in tumor onset. These results indicate that eventually Rank-overexpressing MECs evade or escape senescence allowing tumor formation. Moreover, tumors derived from MECs in double transgenic mice that have undergone senescence are more aggressive (faster tumor growth, more metastasis and increased metastasis initiating ability).

2.2. Rank overexpression induces senescence in human breast cancer cells

Next, we assessed whether Rank was able to induce senescence in human breast cancer cells. To this end, the human luminal-like breast cancer cell line MCF7[394], was infected with RANK overexpressing constitutive or inducible lentivirus.

RANK overexpression (either constitutive or inducible) in the luminal breast cancer cell line MCF7 also led to senescence (**Figure 41*A,B***). Even low levels of RANK expression, as those achieved by the inducible system, rapidly led to senescence in MCF7 cells (**Figure 41*B,C***). Moreover, no changes in survival and apoptosis (measured as $7AAD^-/AnnexinV^-$ and $7AAD^-/AnnexinV^+$ by flow cytometry, respectively) were found upon RANK overexpression (**Figure 41*D***).

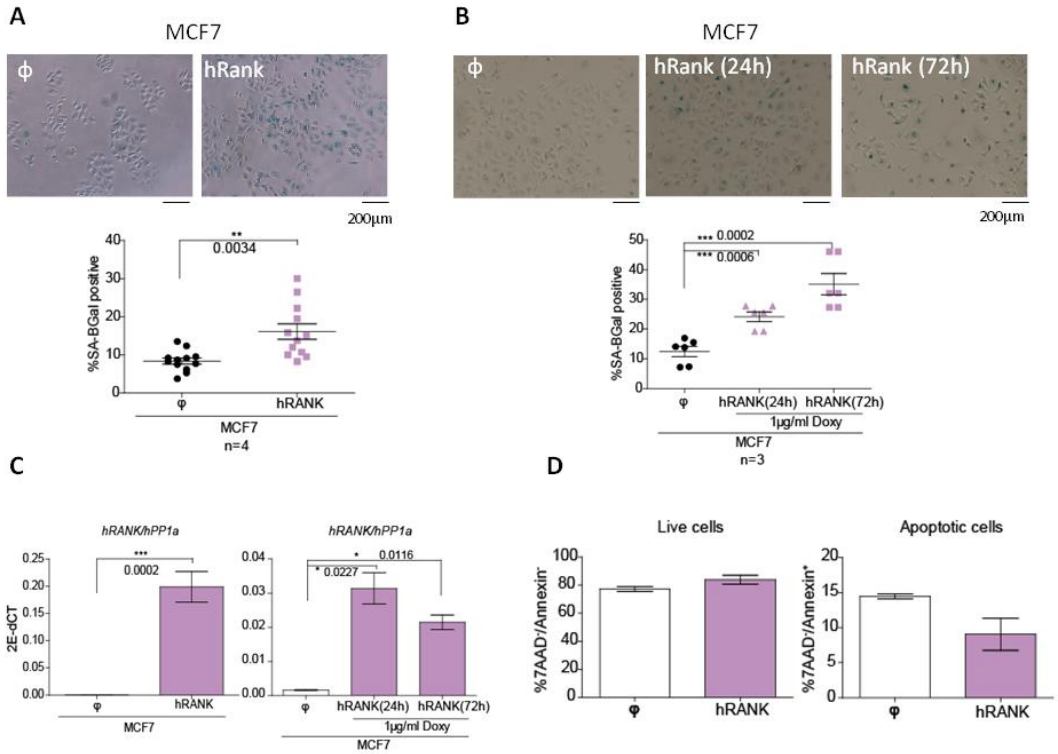

Figure 41: A) Representative images of SA-βGal staining and quantification (bottom panel) of MCF7 human breast cancer cells two weeks after infection with RANK overexpressing and control (ϕ) vectors. Quantifications for each experiment were done in triplicate. Each dot indicates a replica. Mean, SEM and t text p values are shown. **B**) Representative images and quantification (bottom panel) of SA-βGal staining in MCF7 cells infected with RANK overexpressing inducible lentivirus, 24h and 72h after RANK induction (1µg/ml of doxycycline). Quantifications for each experiment were done in triplicate. Each dot indicates a replica. Mean, SEM and t text p values are shown. B) mRNA expression of *RANK* related to *PP1a* measured by RT-PCR in MCF7 human breast cancer cells 2 weeks after the infection with RANK overexpressing and control (ϕ) and/or with RANK-doxycycline inducible lentivirus (1 µg/ml of doxycycline for 24h or 72h). Mean, SEM and t-text p value for 6 independent experiments are shown. Note that, in the inducible graph, data of a representative experiment (out of three independent experiments) is shown and mean, SEM and t-test p-value was performed for the replicates. **D**) Graphs showing the percentage of live ($7AAD^-$ $AnnexinV^-$) and apoptotic ($7AAD^-AnnexinV^+$) MCF7 human breast cancer cells with RANK overexpressing and control (ϕ) lentivirus.

As described in the literature, *p16*^{INK4a} and *p14*^{ARF} (*p19*^{Arf} in mouse) genes are deleted in the MCF7 cell lines[395–397]. For this reason, in MCF7 cells RANK drives senescence independently of the cell cycle inhibitors *p16*^{INK4a} and *p14*^{ARF}. Thus, we checked the expression of *p53* and *p21* cell cycle inhibitors that can also lead to growth arrest and senescence[282,283]. Our results showed a slight increase in *p53* and *p21* mRNA levels in RANK-overexpressing cells compared to the control ones (**Figure 42*A***). An increased expression level of these cell cycle inhibitors may not only denote growth arrest.To confirm the senescence phenotype, these changes should be accompanied with other senescence markers such as SASP[268,359]or DNA damage[217], in line with our previous findings in MECs and MEFs. So, we analyzed the expression of *IL6*, a one well-known senescence-trigger often comprised in the SASP[260] and *TNFα*[398], an important pro-inflammatory cytokine secreted by the senescent cells. Gene expression levels of these cytokines reveal an increase of their expression in RANK overexpressing MCF7 cells (**Figure 42*B***). Besides, we also detected an accumulation of γH2AX foci per cell in RANK overexpressing MCF7 cells (**Figure 42*C***). Together, these results suggest that RANK overexpression also induces senescence in human breast cancer cells.

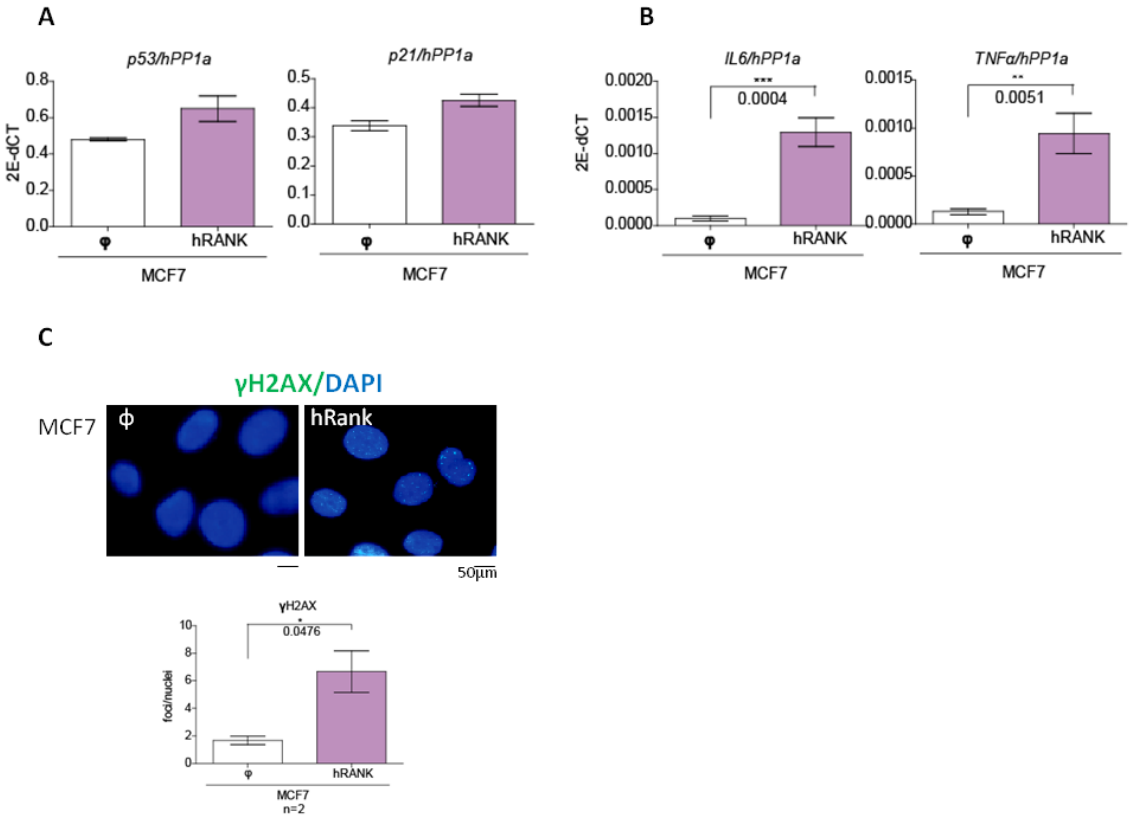

Figure 42: A) mRNA expression of *p53* and *p21* related to *PP1α* measured by RT-PCR in control (ϕ) and RANK overexpressing MCF7 cells 2 weeks after the infection. Data of a representative experiment (out of 3 independent experiments) is shown and mean, SEM and t-test p-value was performed for the replicates. **B**) mRNA expression of *IL6* and *TNFα* related to *PP1α* measured by RT-PCR in MCF7 cells collected 2 weeks after the infection with RANK overexpressing and control (ϕ) lentivirus. Mean, SEM and t-test p value for 7 independent experiments are shown. **C**) Representative images and quantification (bottom panel) of γH2AX (green) foci per nuclei (DAPI) in RANK overexpressing or control (ϕ) MCF7 cells.

2.3. RANK-induced senescence is required for the increased frequency of cancer stem cells

In order to address the connection between senescence and stemness in a human setting, tumorsphere ability was assessed in MCF7 cells after treatment *in vitro* with Navitoclax. An increased frequency of secondary tumorspheres was observed in RANK overexpressing MCF7 cells, confirming that RANK drives stemness in these breast cancer cells; however, no differences between genotypes were observed in the presence of 0.6 µM Navitoclax (***Figure 43A,B***). Importantly, whereas Navitoclax treatment *in vitro* did not alter the number of secondary tumorspheres in the control cells, in RANK overexpressing cells a significant reduction in tumorsphere potential was observed. Thus RANK driven senescence is required for Rank drive stemness also in MCF7 cells. To gain further insights into the mechanisms involved in this regulation the tumorsphere ability of RANK overexpressing MCF7 cells and controls was evaluated in the presence of conditioned media from senescent and non senescent cells. Preliminary analysis evidence that control MCF7 cultured with conditioned-medium extracted from senescent RANK-overexpressing MCF7 plated during 8 days, show more secondary tumorspheres than those cultured in their own conditioned media (***Figure 43C***). Conversely, the frequency of secondary tumorspheres in RANK-overexpressing cells cultured with conditioned-medium from control cells was reduced (**Figure 43*C***).

These results demonstrate that RANK-induced senescence enhances stemness in MCF7 through paracrine mechanisms.

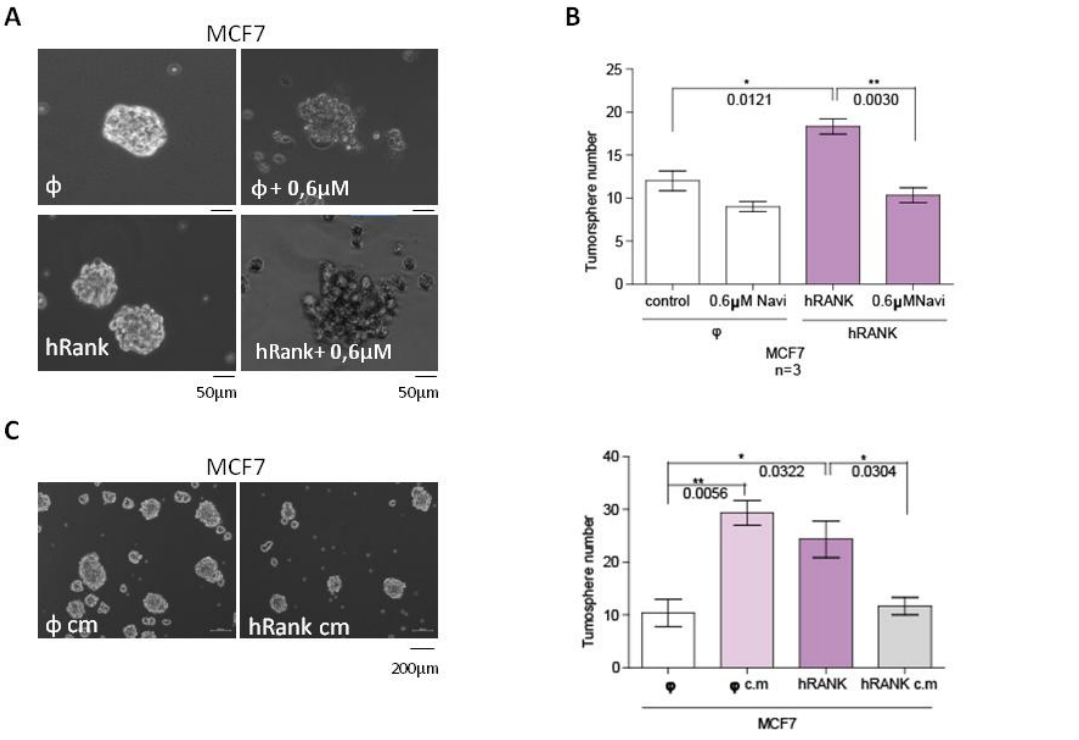

Figure 43: **A-B**) Representatives images (**A**) and quantification (**B**) of secondary tumorspheres of RANK overexpressing or control (ϕ) MCF7 cells treated or untreated *in vitro* with Navitoclax (14 days). Quantifications were performed in triplicate and mean, SEM and t text p-values for 3 independent experiments are shown. **C**) Representative images and number of secondary mammospheres derived from RANK overexpressing or control (ϕ) MCF7 cells cultured with condition medium. Note that in control cells medium contained the supernatant extracted from RANK-overexpressing MCF7 cells and in RANK-overexpressing cells the condition medium contained the supernatant obtained from the control cells 8 days postplate. Quantifications were performed in triplicate and mean, SEM and t text p-values for 1 preliminar experiment is shown.

2.4. Analysis of RANK downstream signaling pathway

We next evaluated whether RANKL treatment changes senescence or RANK downstream pathways.

The frequency of senescent cells increased from 10% to 25% SA-βGal positive in RANK overexpressing cells but no changes after the treatment with RANKL were detected (**Figure 44*A***). The expression of *p53*, *p21*, *IL6* and *TNFα* was determined by quantitative RT-PCR (**Figure 44*B,C***). In line with the results mentioned above (**Figure 44*A,B***), in RANK-overexpressing cells, higher levels of p53, p21, IL6 and *TNFα* were found (**Figure 44*B*,*C***).

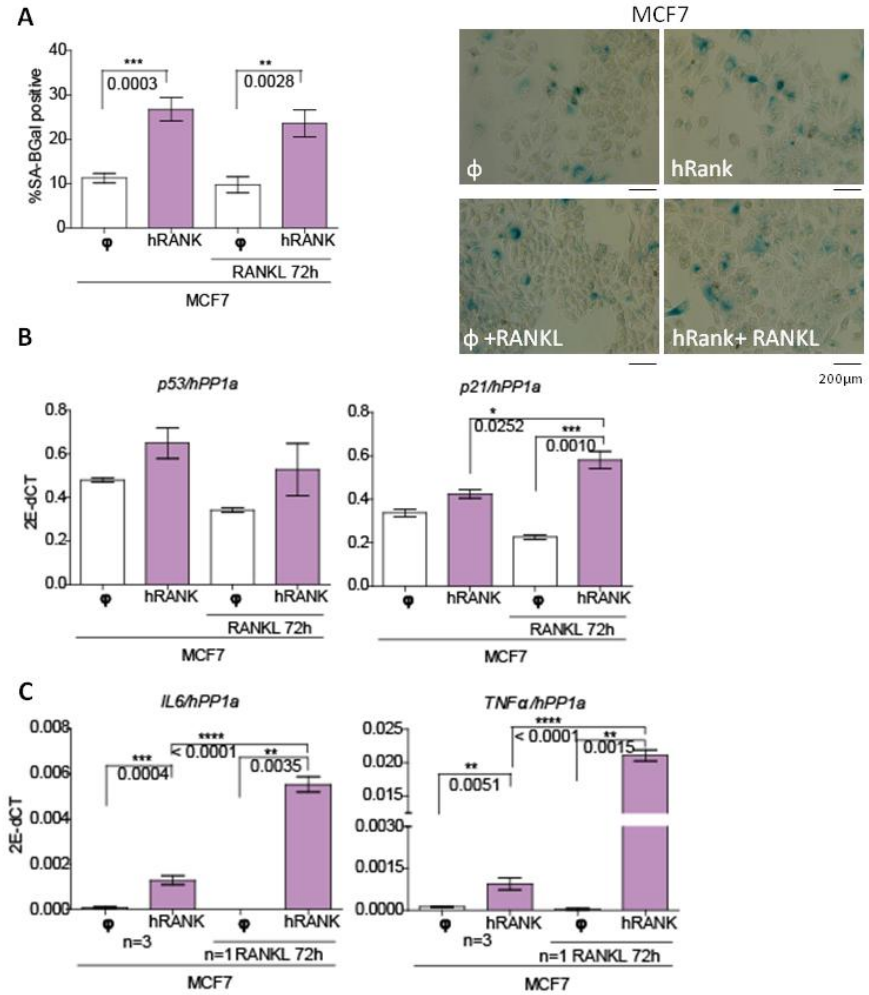

Figure 44: A) Quantification of SA-βGal staining and representative images of MCF7 control (ϕ) and RANK overexpressing cells treated with RANKL (100ng/ml). Mean, SEM and t-test p values for two independent experiments are shown. **B**) mRNA expression of *p53* and *p21* related to *PP1α* measured by RT-PCR in control (ϕ) and RANK overexpressing MCF7 cells upon RANKL treatment. Data of a preliminary experiment is shown. Mean, SEM and t-test p-value was performed for the replicates. **C**) mRNA expression of *IL6* and *TNFα* related to *PP1α* measured by RT-PCR in MCF7 cells upon RANKL treatment. Mean, SEM and t-test p value for the indicated independent experiments are shown.

2.4.1. Activation of RANK signaling pathway leads to NF-kB and MAPK activation

Next, we evaluated RANK downstream pathways in MCF7 cells infected with RANK overexpressing and control lentivirus and treated with RANKL 100ng/ml for 1min, 10min, 30min and 24h, in order to activate RANK signaling pathway.

In line with the previous results described in WT and $Rank^{+/tg}$ MECS, we first investigated whether NF-κB pathway could be altered in RANK overexpressing MCF7 cells compared to control cells and/or upon Rankl treatment *in vitro.* As shown in **Figure 45*A***, RANK was properly upregulated in MCF7 cells infected with RANK-overeexpressing vectors. We found activation of NF-κB canonical pathway after RANKL stimulation, as demonstrated by phosphorylation of p65 and IKBα (**Figure 45*B***). p65 is phosphorylated after short incubation times (1 and 10 min) with RANKL (**Figure 45*B***). After 30 min stimulation with RANKL, p65 is still phosphorylated in RANK-overexpressing MCF7 cells (**Figure 46*B***) and its phosphorylation decreases after long term exposure (24h) to RANKL, when IKBα is re-expressed again (**Figure 46*B***). IKBα phosphorylation leads to polyubiquitination and proteasomal degradation of IKBα[399]. As shown in **Figure 45*C***, upon 1 and 10 min of RANKL incubation (100 ng/ml) induces IKBα degradation, which is not detected after 30min and it is resynthesized after 24h incubation with RANKL (**Figure 46*B***).

In summary, RANKL activates canonical NF-κB downstream signaling in RANK overexpressing MCF7 cells, but not in the parental line, in accordance with the absence of RANK expression in these cells.

Western blot analyses of control and RANK-overexpressing MCF7 cells, treated with RANKL, showed activation of ERK, p38 and JNK after 1 and 10 min of RANKL treatment (**Figure 45*D***), as determined by their phosphorylation[374,400]. Upon 24h incubation with RANKL, there is a decrease in the phosphorylation levels of ERK, p38 and JNK (**Figure 46*C,D***).

Finally, we tried to functionally address the contribution of MAPK to the senescence phenotype induced by RANK in MCF7 cells. First, PD98059 (MEK inhibitor) was tested at several doses to avoid cell toxicity and cell death. Reduced levels of SA-βGal staining in RANK overexpressing cells were observed upon PD98059 treatment *in vitro*, whereas MEK inhibition did not alter SA-βGal staining and cell viability in the control

cells. In MCF7 cells treated with IKK-16, an inhibitor of the NF-κB signaling pathway, a trend to reduced SA-βGal staining was observed in RANK-overexpressiong MCF7 cells but changes did not reach significance(**Figure 47**).

Overall, further investigations are required to elucidate the molecular mechanism that contributes to the RANK-induced senescence in human breast cancer cell lines.

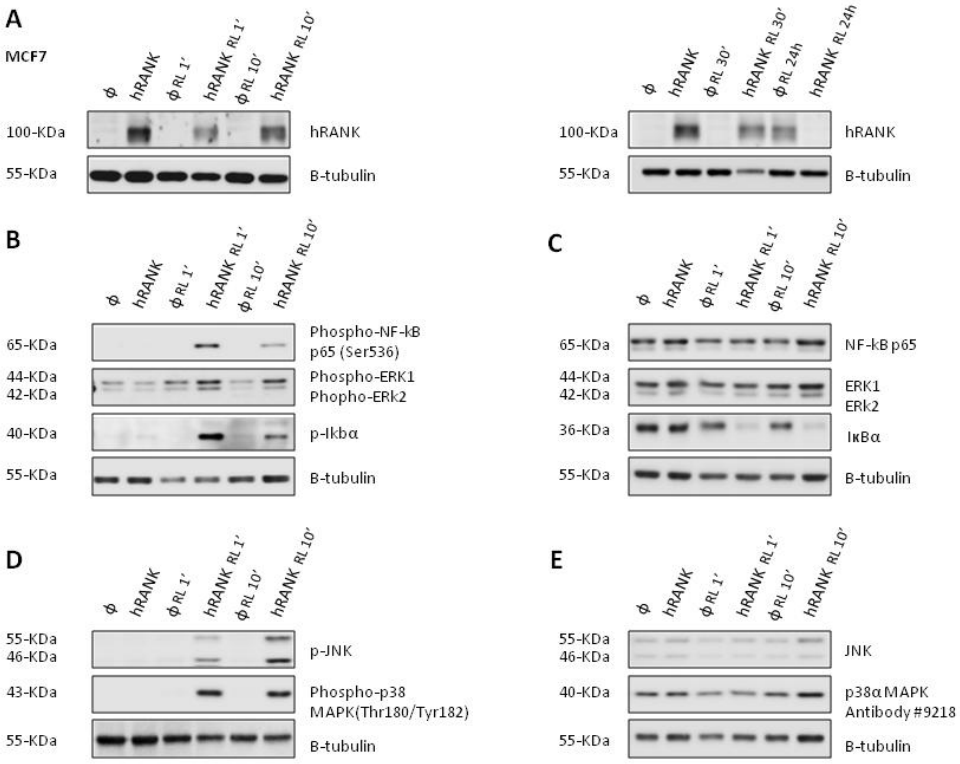

Figure 45: A-E) Western blot analyses of the indicated proteins in whole cell extracts from control (ϕ) or RANK overexpressing MCF7 cells upon RANKL treatment. Tubulin is shown as a loading control.

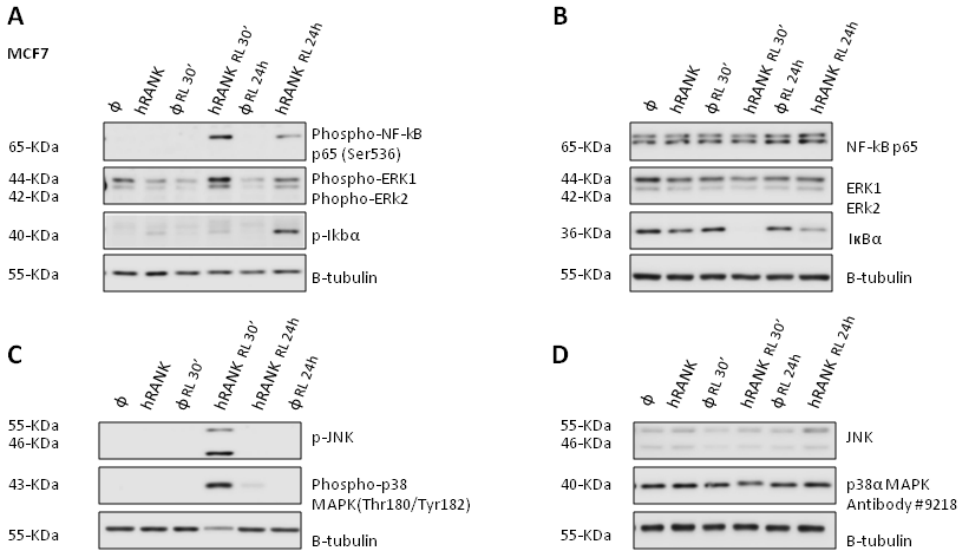

Figure 46: A-D) Western blot analyses of the indicated proteins in whole cell extracts from control (ϕ) or RANK overexpressing MCF7 cells upon RANKL treatment. Tubulin is shown as a loading control.

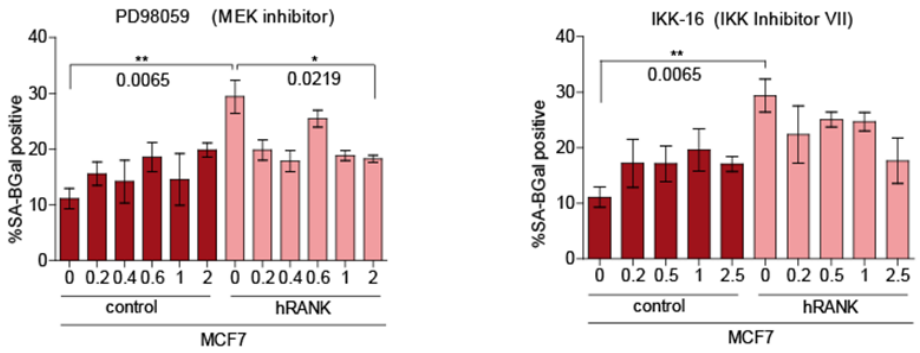

Figure 47: Quantification of SA-βGal staining of MCF7 control and RANK overexpressing cells plated in vitro for 8 days and treated with the indicated doses (μM) of the corresponding inhibitors. Data of a preliminary experiment is shown. Mean, SEM and t-test p-value was performed for the replicates.

DISCUSSION

DISCUSSION

The TNF superfamily members RANK/RANKL have play a key role in mammary gland biology, being required for normal mammary function (lactation) and playing a crucial role in breast cancer development. Our group has previously found that high levels of Rank increase proliferation and interfere with differentiation of MECs[21,138,144]. Moreover, we have shown that RANK signaling inhibition could become an efficient strategy for breast cancer prevention and treatment as it delays or avoids tumor initiation and reduces recurrence and metastasis. Surprisingly, in this thesis we show that RANK overexpression also delays mammary tumorigenesis through the induction of a potent OIS response; these findings place RANK as a classical oncogene[401,402].

In order to characterize the role of RANK in oncogene driven models of breast cancer, we used RANK gain-of-function mouse models as well as *in vitro* tools. Our previous results indicated that RANK pathway activation leads to a significant delay in the appearance of tumors in transgenic mice concomitantly overexpressing Rank together with Neu or PyMT oncogenes. The objective of this thesis was to elucidate the molecular mechanism underlying these paradoxical findings.

We unveiled that the activation of RANK signaling leads to a potent OIS response that acts as a barrier for tumorigenesis, similarly to what has been reported for other oncogenes[401,402].

1. Rank loss or overexpression in the mammary epithelia delays tumor onset

Mice that overexpress Rank in the mammary gland (driven by the MMTV promoter) are more susceptible to carcinogen-induced tumorigenesis, showing shorter tumor latency compared to WT mice treated with DMBA and MPA carcinogenic protocol[146,152]. Moreover, Rank overexpression in the mammary gland leads to the accumulation of bipotent progenitors ($CK5^+CK8^+$ or $CK14^+CK8^+$), favoring spontaneous tumor formation after multiple gestations[138]. Conversely, pharmacological inhibition of RANKL with RANK-Fc, which binds to RANKL and blocks the activation of the pathway, completely prevents MPA/DMBA-induced mammary tumor formation in WT mice[152]. Simultaneously, tumor formation upon DMBA/MPA treatment was shown to be delayed in mice lacking Rank in the mammary epithelia (MMTV-Cre $Rank^{flox}$)[146].

Despite multiple evidence supporting a pro-tumorigenic role for RANK pathway activation, here we found that double transgenic mice that overexpress Rank and the oncogenes Neu or PyMT show a significant delay in the appearance of tumors and a reduced tumor incidence. Delayed tumor appearance and a reduction in tumor and metastasis incidence were observed after genetic deletion of Rank or pharmacological

inhibition of the pathway in the Neu and PyMT tumor models[152,403]. Thus, either Rank loss or Rank overexpression significantly reduced mammary tumor onset and incidence. However, the mechanisms underlying this tumor reduction are different.

Rank pathway is tightly regulated during mammary gland biology; Rank deletion or overexpression result in impaired lactation. Rank deletion impairs alveologenesis through reduced MECs proliferation and survival. It leads to lactation failure by interfering with progesterone signaling[20]. On the other hand, Rank overexpression enhances MECs proliferation and disrupts mammary cell fate resulting in the accumulation of MaSCs and intermediate progenitors and induces changes in the luminal population (decrease in $CD61^+$ and $Sca1^+$ luminal cells)[138]. Activation of RANK signaling also prevents lactogenesis by interfering with prolactin signaling[21,144]. Thus, RANK plays a dual role on mammary gland development: acting as a positive mediator of progesterone but negatively regulating prolactin-driven Stat5 phsophorylation[144].

Given the role of RANK signaling in promoting MEC proliferation and stemness, we were surprised to find that despite the accumulation of epithelial hyperplasias driven by Rank overexpression in the mammary gland of MMTV-Neu mice ($Neu^{+/-}$; $Rank^{+/tg}$), the frequency of mammary intraepithelial neoplasias (MIN) and invasive carcinomas was reduced compared to those in control $Neu^{+/-}$ mice. An increase in hyperplasias and reduction in MINs and tumors was also observed in $PyMT^{+/-}$; $Rank^{+/tg}$ compare to $PyMT^{+/-}$ mice. Thus, constitutive activation of Rank in the mammary glands of oncogene-driven models blocks the transition from hyperplasic lesions to MINs and adenocarcinomas, leading to a significant delay in tumor formation. These findings point to the possibility that Rank behaves as an oncogene, inducing senescence or apoptosis.

2. Rank is a potent inductor of senescence

During the development of this PhD thesis we have demonstrated that the activation of Rank signaling leads to a potent OIS response that prevents or delays tumorigenesis, as previously shown for other oncogenes[401,402]. Several studies have reported that certain oncogenes could induce premature cell senescence in a process called oncogene-induced senescence (OIS)[404,405]. OIS can be induced by oncogenes such as *Ras*, $BRAF^{V600E}$, *E2F1*, *Cdc6*, and by the inactivation of tumor-suppressor genes like *PTEN*, *p53*, *p16*, *p19* or *p21*, suggesting that OIS is not driven by a unique pathway[406]. Thus, several mechanisms, not necessarily mutually exclusive, have been proposed to mediate OIS. Multiple mechanisms possibly cooperate to promote or maintain the senescence response in any given cell type. Nevertheless, some signals leading to OIS may be restricted to specific genetic events and/or in different tissue types[406,407].

In fact, Rank overexpression leads to OIS in MECs and MEFs similar to the widely reported OIS driven by RAS, and share multiple characteristics including induction of

p16/p19, DNA damage response and SASP[393,404,408]. In contrast, neither NeuN nor PyMT overexpression could induce senescence in MECs, despite being strong oncogenes. RANK overexpression in human breast cancer cells also induces DNA damage and senescence. Even low levels of Rank expression, result in senescence in MECs, MEFs and MCF7 cells. Previous results from our group showed a significant increase in Rank expression in the aged mammary epithelia, as well as during transformation in Neu and PyMT mouse models[138,403]. Our present data suggest that enhanced Rank expression could represent a key mechanism to prevent breast cancer development in mouse and human, since we show that Rank is highly expressed in preneoplasic lesions and significant increase during aging[138]. Additionally, we have found that activation of Rank signaling pathway, either upon Rank overexpression or by stimulation with Rankl, is enough to induce senescence and support a role for senescence during mammary gland development and breast cancer initiation, as senescence is observed in WT MECs with physiological Rank expression exposed to Rankl. Importantly, to confirm that Rank-induced senescence could explain the delay in tumor onset observed in double transgenic mice ($PyMT^{+/-}$; $Rank^{+/tg}$), experiments to analyze tumorigenesis in $p16/p19^{-/-}PyMT^{+/-}$; $Rank^{+/tg}$ mice are currently in progress.

Senolytic drugs selectively induce senescent cells death by apoptosis and have been proposed as wide-ranging beneficial drugs due to their senescence-related indications. Senolytic therapy is already included in several clinical trials to treat age-related disorders such as Alzheimer´s disease or cardiac dysfunction[362]. We assessed the effect of the senolytic drug Navitoclax[363], a Bcl2 inhibitor, on Rank-overexpressing cells. *In vitro* treatment demonstrated that cultured $Rank^{+/tg}$ MECs are more sensitive to Navitoclax than WT MECs, consistent with an increased number of senescent cells driven by Rank overexpression. In fact, a decrease in SA-βGal staining was observed in $Rank^{+/tg}$ MECs upon Navitoclax treatment. Moreover, senescent structures were no longer detected in the mammary glands from $Rank^{+/tg}$ mice treated with Navitoclax and the total number of viable $Rank^{+/tg}$ MECs was reduced compared to WT. Finally, SA-βGal analyses of cultured $Rank^{+/tg}$ MECs isolated from Navitoclax-treated mice indicated that senescence dropped to similar levels as those detected in WT MECs. Thus, Rank-induced senescent cells are exquisitely sensitive to Bcl2 inhibitors such as Navitoclax.

Rank-induced senescence promotes stemness

We previously described that high levels of Rank in mouse and human MECs enhance stemness, based on functional assays (mammary reconstitution in limited dilution assays (LDA) and colony-forming assays)[138,148]. Accordingly, now we show that RANK overexpression enhances mammospheres and tumorsphere forming ability and leads to the accumulation of stem/progenitor populations ($CD49b^{+}$, $Sca1^{-}$) and double-

positive CK14/CK8^{+} cells, confirming the stemness phenotype of Rank overexpressing normal and tumor MECs.

The ability of Rank to concomitantly increase senescence and stemness seems contradictory; however, in the last few years, the relationship between senescence and stemness has been explored, and senescence has been shown to promote the occurrence of stem cells in their vicinity by paracrine mechanisms[329]. Stemness is regulated by several signals and genes that influence tumor development[293,294,409]. Strikingly, senescence was described as a physiological mechanism in embryonic development and as a mechanism of tissue regeneration[329,410,411]. Thus, senescence cells express stem-cell related genes. However, cellular senescence is a non-proliferative steady state, so senescent cells do not have self-renewal and cannot sustain clonogenicity. The SASP promotes an environment in which neighboring cells are favored to express stemness markers[329]. Similar results were found by Chiche and Mosteiro[332], showing that senescence in the muscle enhances plasticity in muscle stem cells[329,333,364]. Moreover, conditioned media from senescent cells promotes clonogenicity and cancer stemness[412].

Several studies have identified genes that allow to bypass senescence, whereas less evidences support a true escape of senescence[413]. There is a cellular state of light senescence (characterized by low p16 levels), that allow cells to resume proliferation following p53 inactivation[235], that is different from a deep senescence state, which is irreversible. Cells in a state of senescence express a latent adult stem cell signature and present stem cell properties[334]. Here we found that Rank-induced senescence is essential for Rank-driven stemness: upon elimination of senescence cells, the enhanced stemness phenotype observed in Rank overexpressing cells is lost. Histological and GSEA analyses of RNAseq experiments evidenced that senescence occurs in the luminal compartment of Rank$^{+/tg}$ mice, which is in agreement with the fact that the MMTV promoter drives Rank expression mainly in luminal cells. In accordance with the senescence inhibitory role of TLX[387,414], TLX-negative targets and EzH2 targets were enriched in luminal cell populations from Rank$^{+/tg}$ mice, suggesting that the stemness/ senescence phenotypes may be sustained by epigenetic mechanisms[327,365,366]. Functional assays using WT and Rank$^{+/tg}$ derived MECs show enhanced progenitor/stemness activity in both basal (increased mammary reconstitution ability) and luminal cell compartments (increased colony-forming ability)[138], pointing to paracrine mechanisms regulating the link between senescence and stemness upon Rank overexpression.

3. Senescent cells contribute to the enhanced tumor growth and cancer stemness observed upon Rank overexpression

The expression patterns of Rank and Rankl in Neu and PyMT mammary carcinomas resemble those found in human breast ER^{-}PR^{-} adenocarcinomas[138,403], and therefore

these mouse models represent suitable tools to investigate the role of RANK signaling in hormone receptor-negative late-stage carcinomas. Inhibition of RANK pathway using genetic and pharmacological approaches decreased the incidence of spontaneous preneoplasic lesions, tumor, and lung metastasis in PyMT and Neu mice breast cancer models[152,403], demonstrating that activation of Rank signaling enhances tumor growth and cancer stemness.

$Rank^{+/tg}$ mice are more susceptible to mammary tumorigenesis driven by carcinogens and spontaneously develop mammary tumors after multiple pregnancies with long latency[138,152]. These Rank-overexpressing tumors are enriched in progenitor-like tumor cells $CK14^{+}/CK8^{+}$. Despite the initial delayed in tumor onset, tumors from double transgenic mice $Neu^{+/-}$; $Rank^{+/tg}$ and $PyMT^{+/-}$; $Rank^{+/tg}$, form more metastasis and grow faster (in the case of the PyMT) than the single mutants. Tumor cells double positive for $CK14^{+}/CK8^{+}$ were more abundant in $PyMT^{+/-}$; $Rank^{+/tg}$ compared with the single PyMT tumors, pointing to an increase in tumor stemness. Indeed, $PyMT^{+/-}$; $Rank^{+/tg}$ tumor cells formed more tumorspheres and show a higher frequency of metastasis initiating cells. Thus, Rank overexpression promotes cancer stemness and inhibition of Rank signaling could help to attenuate tumor progression or metastasis in this context.

However, no differences in the frequency of senescent cells were found between single and double mutants, indicating that Rank-overexpressing MECs eventually evade or escape senescence allowing tumor formation. As explain above, tumors derived from MECs in double transgenic mice that have undergone senescence are more aggressive (faster tumor growth, more metastasis and increase metastasis initiating ability). These findings are in agreement with results describing that senescent cells able to escape senescence upon inactivation of suv39h1 or p53[334]. Besides, it is well-established that senescence promotes the appearance of tumor cells with stemness features and favors EMT[359,415]. In addition, the senescence secretome from tumor and primary cells promotes the optimal microenvironment for the invasion of adjacent tissues and migration to distant sites. Among the factors secreted by senescent cells, those described as crucial for the metastatic process are extracellular matrix remodelers[359,416,417]and angiogenic factors, especially the vascular endothelial growth factor (VEGF)[418,419]. In this direction, targeting cellular senescence and SASP was described to reduce metastasis[420].

Alternatively, senescent MECs in the vicinity of $PyMT^{+/-}$; $Rank^{+/tg}$ tumors could contribute to tumor progression and metastasis through SASP as extensively reported in other systems[238,421]. Despite the tumor suppressive role of senescence, the long-term accumulation of senescent cells is potentially detrimental and might ultimately favor cancer progression[361]. Up until now, whether the induction of cellular senescence protects from aberrant growth or represents an integral part of tumor progression remains to be elucidated. Additionally, the SASP enhances

immunosuppressive signaling, preventing the recognition of tumor cells by the immune system and thus favoring tumor progression[422].

Treatment of PyMT$^{+/-}$; Rank$^{+/tg}$ mice with Navitoclax, which eliminates senescent cells, led to an attenuation in tumor growth rate and a reduction in the progenitor-like CK14^{+}/CK8^{+}cells. No differences were observed in tumor onset after navitoclax treatment, as it does not interfere with RANK-driven senescence. Accordingly, our findings using conditioned media from senescent cells support that these senescent cells promote cancer stemness by paracrine mechanisms.

However, we cannot discard that tumor cell-intrinsic mechanisms also contribute to the faster tumor growth and metastasis observed in the double transgenic PyMT$^{+/-}$; Rank$^{+/tg}$ mice after senescence is bypassed. Lineage tracing studies will be required to determine whether Rank-induced senescence contribute to Rank-driven stemness only by paracrine mechanisms or whether there is a direct conversion of senescent cells into mammary or cancer stem cells.

Finally, highlighting the relevance of our findings in clinical breast cancer, we found that high levels of RANK expression associate with stemness and senescence in luminal breast tumors[138]. Activation of Rank signaling in combination with senolytic drugs to eliminate the senescent cells could help to attenuate tumor progression or metastasis.

Together these results support that activation of Rank signaling in combination with anti-Bcl2 senolytic drugs to eliminate the senescent cells, could attenuate tumor progression and metastasis.

4. Concluding remarks

Rank signaling pathway has recently emerged as a novel target for breast cancer prevention and treatment. Paradoxically, we have found that high levels of Rank attenuate and delay mammary tumor initiation, based on the ability of Rank to induce senescence. Moreover, we have demonstrated that Rank-induced senescence is required for Rank-driven stemness in the non-transformed mammary gland as well as in cancer (**Figure 48**). These results open the possibility to use Rank agonists in combination with senolytics for breast cancer prevention and treatment.

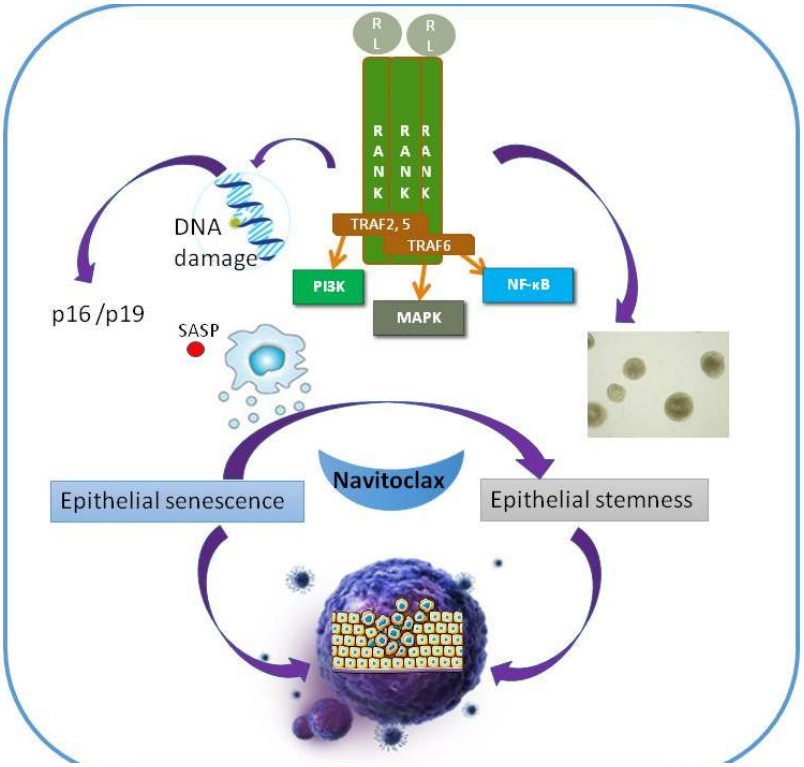

Figure 48: *Graphical summary of the proposed role of Rank in senescence and stemness. Rank signaling leads to a potent OIS response that acts as a barrier for tumorigenesis. Rank-induced senescence is essential for Rank-driven stemness: upon elimination of senescent cells the enhanced stemness phenotype is lost.*

CONCLUSIONS

CONCLUSIONS

1. Rank overexpression in an oncogenic Neu and PyMT background delays tumor onset.

2. Rank induces potent oncogene induced senescence (OIS) response that acts as barrier for carcinogenesis in oncogene-driven breast cancer models.

3. Activation of the Rank signaling pathway induces senescence in mammary epithelial cells (MECs) and mouse embryonic fibroblasts (MEFs), even in the absence of other oncogenes.

4. Rank induced senescence in non-transformed cells, MECs and MEFs, is dependent on p16&p19 and causes an accumulation of DNA damage.

5. Rank induced senescence in MECs is essential for Rank driven stemness.

6. Once senescence is overcome Rank promotes tumor growth and metastasis. Rank driven senescence in MECs promotes mammary tumor growth and cancer stemness.

7. RANK overexpression induces senescence and stemness in mouse and human breast cancer cells (MCF7).

8. Rank induced senescence contributes to cancer stemness and tumor growth through paracrine mechanisms.

BIBLIOGRAPHY

BIBLIOGRAPHY

1. Medina, D. The mammary gland: a unique organ for the study of development and tumorigenesis. *J. Mammary Gland Biol. Neoplasia* **1**, 5–19 (1996).
2. Watson, C. J. *et al.* Mammary development in the embryo and adult: a journey of morphogenesis and commitment. *Development* **135**, 995–1003 (2008).
3. Hassiotou, F. & Geddes, D. Anatomy of the human mammary gland: Current status of knowledge. *Clin. Anat.* **26**, 29–48 (2013).
4. Kordon, E. C. & Smith, G. H. An entire functional mammary gland may comprise the progeny from a single cell. *Development* **125**, 1921–30 (1998).
5. Russo, J. & Russo, I. H. Development of the human breast. *Maturitas* **49**, 2–15 (2004).
6. GEDDES, D. Inside the Lactating Breast: The Latest Anatomy Research. *J. Midwifery Womens. Health* **52**, 556–563 (2007).
7. Cowin, P. & Wysolmerski, J. Molecular mechanisms guiding embryonic mammary gland development. *Cold Spring Harb. Perspect. Biol.* **2**, a003251 (2010).
8. Inman, J. L., Robertson, C., Mott, J. D. & Bissell, M. J. Mammary gland development: cell fate specification, stem cells and the microenvironment. *Development* **142**, 1028–42 (2015).
9. Hormonal synergism in mammary growth. *Proc. R. Soc. London. Ser. B - Biol. Sci.* **149**, 303–325 (1958).
10. Nandi, S. Endocrine Control of Mammary-Gland Development and Function in the C3H/He Crgl Mouse. *JNCI J. Natl. Cancer Inst.* **21**, 1039–1063 (1958).
11. Williams, J. M. & Daniel, C. W. Mammary ductal elongation: Differentiation of myoepithelium and basal lamina during branching morphogenesis. *Dev. Biol.* **97**, 274–290 (1983).
12. Fata, J. E., Chaudhary, V. & Khokha, R. Cellular Turnover in the Mammary Gland Is Correlated with Systemic Levels of Progesterone and Not 17β-Estradiol During the Estrous Cycle1. *Biol. Reprod.* **65**, 680–688 (2001).
13. Ruan, W. & Kleinberg, D. L. Insulin-like growth factor I is essential for terminal end bud formation and ductal morphogenesis during mammary development. *Endocrinology* **140**, 5075–5081 (1999).
14. Hennighausen, L. & Robinson, G. W. Signaling pathways in mammary gland development. *Dev. Cell* **1**, 467–75 (2001).
15. Gudjonsson, T., Adriance, M. C., Sternlicht, M. D., Petersen, O. W. & Bissell, M. J. Myoepithelial Cells: Their Origin and Function in Breast Morphogenesis and Neoplasia. *J Mammary Gland Biol Neoplasia* **10**, (2005).
16. Watson, C. J. Key stages in mammary gland development - Involution: apoptosis and tissue remodelling that convert the mammary gland from milk factory to a quiescent organ. *Breast Cancer Res.* **8**, 203 (2006).
17. Talhouk, R. S., Chin, J. R., Unemori, E. N., Werb, Z. & Bissell, M. J. Proteinases of the mammary gland: developmental regulation in vivo and vectorial secretion in culture. *Development* **112**, (1991).
18. Brennan, K. R. & Brown, A. M. C. Wnt Proteins in Mammary Development and Cancer. *J. Mammary Gland Biol. Neoplasia* **9**, 119–131 (2004).

19. Callahan, R. & Egan, S. E. Notch Signaling in Mammary Development and Oncogenesis. *J. Mammary Gland Biol. Neoplasia* **9**, 145–163 (2004).
20. Fata, J. E. *et al.* The osteoclast differentiation factor osteoprotegerin-ligand is essential for mammary gland development. *Cell* **103**, 41–50 (2000).
21. Gonzalez-Suarez, E. *et al.* RANK overexpression in transgenic mice with mouse mammary tumor virus promoter-controlled RANK increases proliferation and impairs alveolar differentiation in the mammary epithelia and disrupts lumen formation in cultured epithelial acini. *Mol. Cell. Biol.* **27**, 1442–54 (2007).
22. Jäger, R., Schäfer, S., Hau-Liersch, M. & Schorle, H. Loss of transcription factor AP-2gamma/TFAP2C impairs branching morphogenesis of the murine mammary gland. *Dev. Dyn.* **239**, 1027–1033 (2010).
23. Chadi, S. *et al.* R-spondin1 is required for normal epithelial morphogenesis during mammary gland development. *Biochem. Biophys. Res. Commun.* **390**, 1040–1043 (2009).
24. Shackleton, M. *et al.* Generation of a functional mammary gland from a single stem cell. *Nature* **439**, 84–88 (2006).
25. Clarke, R. B. Isolation and characterization of human mammary stem cells. *Cell Prolif.* **38**, 375–386 (2005).
26. Deome, K. B., Faulkin, L. J., Bern, H. A. & Blair, P. B. *Development of Mammary Tumors from Hyperplastic Alveolar Nodules Transplanted into Gland-free Mammary Fat Pads of Female C3H Mice**. (1959).
27. Smith, G. H. & Medina, D. A morphologically distinct candidate for an epithelial stem cell in mouse mammary gland. *J. Cell Sci.* **90**, 173–183 (1988).
28. Daniel, C. W., De Ome, K. B., Young, J. T., Blair, P. B. & Faulkin, L. J. The in vivo life span of normal and preneoplastic mouse mammary glands: a serial transplantation study. *Proc. Natl. Acad. Sci. U. S. A.* **61**, 53–60 (1968).
29. HOSHINO, K. Morphogenesis and growth potentiality of mammary glands in mice. II. Quantitative transplantation of mammary glands of normal male mice. *J. Natl. Cancer Inst.* **30**, 585–91 (1963).
30. Stingl, J. *et al.* Purification and unique properties of mammary epithelial stem cells. *Nature* **439**, 993–997 (2006).
31. Stingl, J., Eaves, C. J., Zandieh, I. & Emerman, J. T. Characterization of bipotent mammary epithelial progenitor cells in normal adult human breast tissue. *Breast Cancer Res. Treat.* **67**, 93–109 (2001).
32. dos Santos, C. O. *et al.* Molecular hierarchy of mammary differentiation yields refined markers of mammary stem cells. *Proc. Natl. Acad. Sci. U. S. A.* **110**, 7123–30 (2013).
33. Sleeman, K. E., Kendrick, H., Ashworth, A., Isacke, C. M. & Smalley, M. J. CD24 staining of mouse mammary gland cells defines luminal epithelial, myoepithelial/basal and non-epithelial cells. *Breast Cancer Res.* **8**, R7 (2005).
34. Badders, N. M. *et al.* The Wnt Receptor, Lrp5, Is Expressed by Mouse Mammary Stem Cells and Is Required to Maintain the Basal Lineage. *PLoS One* **4**, e6594 (2009).
35. Zeng, Y. A. & Nusse, R. Wnt Proteins Are Self-Renewal Factors for Mammary Stem Cells and Promote Their Long-Term Expansion in Culture. *Cell Stem Cell* **6**, 568–577 (2010).
36. Plaks, V. *et al.* Lgr5-Expressing Cells Are Sufficient and Necessary for Postnatal

Mammary Gland Organogenesis. *Cell Rep.* **3**, 70–78 (2013).
37. Wang, D. *et al.* Identification of multipotent mammary stem cells by protein C receptor expression. *Nature* **517**, 81–84 (2015).
38. Prater, M. D. *et al.* Mammary stem cells have myoepithelial cell properties. *Nat. Cell Biol.* **16**, 942–950 (2014).
39. Sun, P., Yuan, Y., Li, A., Li, B. & Dai, X. Cytokeratin expression during mouse embryonic and early postnatal mammary gland development. *Histochem. Cell Biol.* **133**, 213–21 (2010).
40. Wu, A. *et al.* Characterization of mammary epithelial stem/progenitor cells and their changes with aging in common marmosets. *Sci. Rep.* **6**, 32190 (2016).
41. Bouras, T. *et al.* Notch Signaling Regulates Mammary Stem Cell Function and Luminal Cell-Fate Commitment. *Cell Stem Cell* **3**, 429–441 (2008).
42. Skoda, A. M. *et al.* The role of the Hedgehog signaling pathway in cancer: A comprehensive review. *Bosn. J. Basic Med. Sci.* **18**, 8–20 (2018).
43. Joshi, P. A. *et al.* Progesterone induces adult mammary stem cell expansion. *Nature* **465**, 803–807 (2010).
44. Petersen, O. W., Høyer, P. E. & van Deurs, B. Frequency and distribution of estrogen receptor-positive cells in normal, nonlactating human breast tissue. *Cancer Res.* **47**, 5748–5751 (1987).
45. Sleeman, K. E. *et al.* Dissociation of estrogen receptor expression and in vivo stem cell activity in the mammary gland. *J. Cell Biol.* **176**, 19–26 (2007).
46. Asselin-Labat, M. L. *et al.* Gata-3 is an essential regulator of mammary-gland morphogenesis and luminal-cell differentiation. *Nat. Cell Biol.* **9**, 201–209 (2007).
47. Rios, A. C., Fu, N. Y., Lindeman, G. J. & Visvader, J. E. In situ identification of bipotent stem cells in the mammary gland. *Nature* **506**, 322–327 (2014).
48. Beleut, M. *et al.* Two distinct mechanisms underlie progesterone-induced proliferation in the mammary gland. *Proc. Natl. Acad. Sci. U. S. A.* **107**, 2989–94 (2010).
49. Van Keymeulen, A. *et al.* Distinct stem cells contribute to mammary gland development and maintenance. *Nature* **479**, 189–193 (2011).
50. Li, S. *et al.* Overview of the reporter genes and reporter mouse models. *Anim. Model. Exp. Med.* **1**, 29–35 (2018).
51. Lee, E., Piranlioglu, R., Wicha, M. S. & Korkaya, H. Plasticity and potency of mammary stem cell subsets during mammary gland development. *Int. J. Mol. Sci.* **20**, (2019).
52. Van Keymeulen, A. *et al.* Lineage-Restricted Mammary Stem Cells Sustain the Development, Homeostasis, and Regeneration of the Estrogen Receptor Positive Lineage. *Cell Rep.* **20**, 1525–1532 (2017).
53. Wang, C., Christin, J. R., Oktay, M. H. & Guo, W. Lineage-Biased Stem Cells Maintain Estrogen-Receptor-Positive and -Negative Mouse Mammary Luminal Lineages. *Cell Rep.* **18**, 2825–2835 (2017).
54. Rodilla, V. *et al.* Luminal Progenitors Restrict Their Lineage Potential during Mammary Gland Development. *PLoS Biol.* **13**, (2015).
55. Flier, J. S., Underhill, L. H. & Dvorak, H. F. Tumors: Wounds That Do Not Heal. *New England Journal of Medicine* **315**, 1650–1659 (1986).
56. Liotta, L. A. & Kohn, E. C. The microenvironment of the tumour - Host interface.

Nature **411**, 375–379 (2001).
57. Bogenrieder, T. & Herlyn, M. Axis of evil: Molecular mechanisms of cancer metastasis. *Oncogene* **22**, 6524–6536 (2003).
58. Hanahan, D. & Weinberg, R. A. The hallmarks of cancer. *Cell* **100**, 57–70 (2000).
59. Hanahan, D. & Weinberg, R. A. Leading Edge Review Hallmarks of Cancer: The Next Generation. *Cell* **144**, 646–674 (2011).
60. Kamińska, M., Ciszewski, T., Łopacka-Szatan, K., Miotła, P. & Starosławska, E. Breast cancer risk factors. *Menopausal Rev.* **3**, 196–202 (2015).
61. Nkondjock, A. & Ghadirian, P. Risk factors and risk reduction of breast cancer. *médecine/sciences* **21**, 175–180 (2005).
62. Dumitrescu, R. G. & Cotarla, I. Understanding breast cancer risk -- where do we stand in 2005? *J. Cell. Mol. Med.* **9**, 208–21
63. Newman, B., Austin, M. A., Lee, M. & King, M. C. Inheritance of human breast cancer: evidence for autosomal dominant transmission in high-risk families. *Proc. Natl. Acad. Sci. U. S. A.* **85**, 3044–8 (1988).
64. Claus, E. B., Risch, N. & Thompson, W. D. Genetic analysis of breast cancer in the cancer and steroid hormone study. *Am. J. Hum. Genet.* **48**, 232–42 (1991).
65. Couch, F. J. & Weber, B. L. Mutations and Polymorphisms in the familial early-onset breast cancer (BRCA1) gene. *Hum. Mutat.* **8**, 8–18 (1996).
66. Langston, A. A., Malone, K. E., Thompson, J. D., Daling, J. R. & Ostrander, E. A. *BRCA1* Mutations in a Population-Based Sample of Young Women with Breast Cancer. *N. Engl. J. Med.* **334**, 137–142 (1996).
67. Genetics: Breast Cancer Risk Factors. Available at: https://www.breastcancer.org/risk/factors/genetics. (Accessed: 28th April 2019)
68. Sheikh, A. *et al.* The spectrum of genetic mutations in breast cancer. *Asian Pac. J. Cancer Prev.* **16**, 2177–85 (2015).
69. Perou, C. M. *et al.* Molecular portraits of human breast tumours. *Nature* **406**, 747–752 (2000).
70. Malhotra, G. K., Zhao, X., Band, H. & Band, V. Histological, molecular and functional subtypes of breast cancers. *Cancer Biol. Ther.* **10**, 955–60 (2010).
71. Silverstein, M. J. *et al.* Prognostic classification of breast ductal carcinoma-in-situ. *Lancet (London, England)* **345**, 1154–7 (1995).
72. Prat, A. & Perou, C. M. Mammary development meets cancer genomics. *Nature Medicine* **15**, 842–844 (2009).
73. Inic, Z. *et al.* Difference between Luminal A and Luminal B subtypes according to Ki-67, tumor size, and progesterone receptor negativity providing prognostic information. *Clin. Med. Insights Oncol.* **8**, 107–111 (2014).
74. Prat, A. *et al.* Phenotypic and molecular characterization of the claudin-low intrinsic subtype of breast cancer. *Breast Cancer Res.* **12**, R68 (2010).
75. Prat, A. *et al.* Response and survival of breast cancer intrinsic subtypes following multi-agent neoadjuvant chemotherapy. *BMC Med.* **13**, 303 (2015).
76. Bernard, P. S. *et al.* Supervised risk predictor of breast cancer based on intrinsic subtypes. *J. Clin. Oncol.* **27**, 1160–1167 (2009).
77. Stem Cells and Niches: Mechanisms That Promote Stem Cell Maintenance throughout Life. *Cell* **132**, 598–611 (2008).
78. Beck, B. & Blanpain, C. Unravelling cancer stem cell potential. *Nat. Rev. Cancer* **13**, 727–738 (2013).

79. Al-Hajj, M., Wicha, M. S., Benito-Hernandez, A., Morrison, S. J. & Clarke, M. F. Prospective identification of tumorigenic breast cancer cells. *Proc. Natl. Acad. Sci.* **100**, 3983–3988 (2003).
80. Singh, S. K. *et al.* Identification of a cancer stem cell in human brain tumors. *Cancer Res.* **63**, 5821–8 (2003).
81. Ginestier, C. *et al.* ALDH1 Is a Marker of Normal and Malignant Human Mammary Stem Cells and a Predictor of Poor Clinical Outcome. *Cell Stem Cell* **1**, 555–567 (2007).
82. Weiswald, L.-B., Bellet, D. & Dangles-Marie, V. Spherical cancer models in tumor biology. *Neoplasia* **17**, 1–15 (2015).
83. Yu, Z. *et al.* microRNA, Cell Cycle, and Human Breast Cancer. *Am. J. Pathol.* **176**, 1058–1064 (2010).
84. Nusse, R. *et al.* Wnt Signaling and Stem Cell Control. *Cold Spring Harb. Symp. Quant. Biol.* **73**, 59–66 (2008).
85. DeSano, J. T. & Xu, L. MicroRNA Regulation of Cancer Stem Cells and Therapeutic Implications. *AAPS J.* **11**, 682 (2009).
86. Charafe-Jauffret, E. *et al.* Breast cancer cell lines contain functional cancer stem sells with metastatic capacity and a distinct molecular signature. *Cancer Res.* **69**, 1302–1313 (2009).
87. Velasco-Velázquez, M. A., Popov, V. M., Lisanti, M. P. & Pestell, R. G. The role of breast cancer stem cells in metastasis and therapeutic implications. *American Journal of Pathology* **179**, 2–11 (2011).
88. Geng, S. Q., Alexandrou, A. T. & Li, J. J. Breast cancer stem cells: Multiple capacities in tumor metastasis. *Cancer Letters* **349**, 1–7 (2014).
89. Hennighausen, L. Mouse models for breast cancer. *Breast Cancer Res.* **2**, 2–7 (2000).
90. Richmond, A. & Su, Y. Mouse xenograft models vs GEM models for human cancer therapeutics. *Dis. Model. Mech.* **1**, 78–82 (2008).
91. Cardiff, R. D. *et al.* The mammary pathology of genetically engineered mice: the consensus report and recommendations from the Annapolis meeting. *Oncogene* **19**, 968–88 (2000).
92. Kim, J. B., O'Hare, M. J. & Stein, R. Models of breast cancer: is merging human and animal models the future? *Breast Cancer Res.* **6**, 22 (2003).
93. Bradham, B. M. & Bolander, F. F. The role of sex steroids in the expression of MMTV in the normal mouse mammary gland. *Biochem. Biophys. Res. Commun.* **159**, 1020–1025 (1989).
94. Bolander, F. F. Regulation of the mouse mammary tumor virus (MMTV) binding site in cultured mammary tissue. *Mol. Cell. Endocrinol.* **82**, 137–142 (1991).
95. Haraguchi, S., Good, R. A. & Day, N. K. Prolactin acts on the extreme 5' portion of MMTV LTR involving a mammary cell-specific enhancer. *Mol. Cell. Endocrinol.* **96**, R1-6 (1993).
96. Fantozzi, A. & Christofori, G. Mouse models of breast cancer metastasis. *Breast Cancer Res.* **8**, 212 (2006).
97. Bargmann, C. I., Hung, M. C. & Weinberg, R. A. Multiple independent activations of the neu oncogene by a point mutation altering the transmembrane domain of p185. *Cell* **45**, 649–57 (1986).
98. Menezes, M. E. *et al.* Genetically engineered mice as experimental tools to

dissect the critical events in breast cancer. *Adv. Cancer Res.* **121**, 331–382 (2014).
99. Ursini-Siegel, J., Schade, B., Cardiff, R. D. & Muller, W. J. Insights from transgenic mouse models of ERBB2-induced breast cancer. *Nat. Rev. Cancer* **7**, 389–397 (2007).
100. Yarden, Y. & Sliwkowski, M. X. Untangling the ErbB signalling network. *Nat. Rev. Mol. Cell Biol.* **2**, 127–137 (2001).
101. Taneja, P. *et al.* MMTV mouse models and the diagnostic values of MMTV-like sequences in human breast cancer. *Expert Rev. Mol. Diagn.* **9**, 423–440 (2009).
102. Guy, C. T., Cardiff, R. D. & Muller, W. J. Activated neu induces rapid tumor progression. *J. Biol. Chem.* **271**, 7673–8 (1996).
103. Siegel, P. M., Ryan, E. D., Cardiff, R. D. & Muller, W. J. Elevated expression of activated forms of Neu/ErbB-2 and ErbB-3 are involved in the induction of mammary tumors in transgenic mice: implications for human breast cancer. *EMBO J.* **18**, 2149–2164 (1999).
104. Guy, C. T., Cardiff, R. D. & Muller, W. J. Induction of mammary tumors by expression of polyomavirus middle T oncogene: a transgenic mouse model for metastatic disease. *Mol. Cell. Biol.* **12**, 954–61 (1992).
105. Lin, E. Y. *et al.* Progression to Malignancy in the Polyoma Middle T Oncoprotein Mouse Breast Cancer Model Provides a Reliable Model for Human Diseases. *Am. J. Pathol.* **163**, (2003).
106. Fluck, M. M. & Schaffhausen, B. S. Lessons in Signaling and Tumorigenesis from Polyomavirus Middle T Antigen. *Microbiol. Mol. Biol. Rev.* **73**, 542–563 (2009).
107. Herschkowitz, J. I. *et al.* Identification of conserved gene expression features between murine mammary carcinoma models and human breast tumors. *Genome Biol.* **8**, (2007).
108. Boyce, B. F. & Xing, L. Biology of RANK, RANKL, and osteoprotegerin. *Arthritis Res. Ther.* **9**, S1 (2007).
109. Yasuda, H. *et al. Osteoclast differentiation factor is a ligand for osteoprotegerin osteoclastogenesis-inhibitory factor and is identical to TRANCERANKL*. **95**, (1998).
110. Shimamura, M. *et al.* OPG/RANKL/RANK axis is a critical inflammatory signaling system in ischemic brain in mice. *Proc. Natl. Acad. Sci.* **111**, 8191–8196 (2014).
111. Akiyama, T. *et al.* The Tumor Necrosis Factor Family Receptors RANK and CD40 Cooperatively Establish the Thymic Medullary Microenvironment and Self-Tolerance. *Immunity* **29**, 423–437 (2008).
112. Knoop, K. A. *et al.* RANKL Is Necessary and Sufficient to Initiate Development of Antigen-Sampling M Cells in the Intestinal Epithelium. *J. Immunol.* **183**, 5738–5747 (2009).
113. Duheron, V. *et al.* Receptor activator of NF-κB (RANK) stimulates the proliferation of epithelial cells of the epidermo-pilosebaceous unit. *Proc. Natl. Acad. Sci. U. S. A.* **108**, 5342–5347 (2011).
114. Anderson, D. M. *et al.* A homologue of the TNF receptor and its ligand enhance T-cell growth and dendritic-cell function. *Nature* **390**, (1997).
115. Smith, C. A., Farrah, T. & Goodwin, R. G. The TNF receptor superfamily of cellular and viral proteins: Activation, costimulation, and death. *Cell* **76**, 959–962 (1994).
116. Kanazawa, K. & Kudo, A. Self-assembled RANK induces osteoclastogenesis

ligand-independently. *J. Bone Miner. Res.* **20**, 2053–2060 (2005).
117. Boyle, W. J., Simonet, W. S. & Lacey, D. L. Osteoclast differentiation and activation. *Nature* **423**, 337–342 (2003).
118. Wada, T., Nakashima, T., Hiroshi, N. & Penninger, J. M. RANKL-RANK signaling in osteoclastogenesis and bone disease. *Trends in Molecular Medicine* **12**, 17–25 (2006).
119. Wong, B. R. *et al.* The TRAF family of signal transducers mediates NF-kappaB activation by the TRANCE receptor. *J. Biol. Chem.* **273**, 28355–9 (1998).
120. Ikeda, T., Kasai, M., Utsuyama, M. & Hirokawa, K. Determination of Three Isoforms of the Receptor Activator of Nuclear Factor-κB Ligand and Their Differential Expression in Bone and Thymus [1]. *Endocrinology* **142**, 1419–1426 (2001).
121. González-Suárez, E. & Sanz-Moreno, A. RANK as a therapeutic target in cancer. *FEBS J.* **283**, 2018–2033 (2016).
122. Walsh, N. C. *et al.* Activated human T cells express alternative mRNA transcripts encoding a secreted form of RANKL. *Genes Immun.* **14**, 336–345 (2013).
123. Liu, C. *et al.* Structural and Functional Insights of RANKL–RANK Interaction and Signaling. *J. Immunol.* **184**, 6910–6919 (2010).
124. Luo, J. *et al.* LGR4 is a receptor for RANKL and negatively regulates osteoclast differentiation and bone resorption. *Nat. Med.* **22**, 539–546 (2016).
125. Nelson, C. A., Warren, J. T., Wang, M. W.-H., Teitelbaum, S. L. & Fremont, D. H. RANKL employs distinct binding modes to engage RANK and the osteoprotegerin decoy receptor. *Structure* **20**, 1971–82 (2012).
126. Dougall, W. C., Holen, I. & González Suárez, E. Targeting RANKL in metastasis. *Bonekey Rep.* **3**, (2014).
127. Wright, H. L., McCarthy, H. S., Middleton, J. & Marshall, M. J. RANK, RANKL and osteoprotegerin in bone biology and disease. *Current Reviews in Musculoskeletal Medicine* **2**, 56–64 (2009).
128. Simonet, W. S. *et al.* Osteoprotegerin: a novel secreted protein involved in the regulation of bone density. *Cell* **89**, 309–19 (1997).
129. Wada, T., Nakashima, T., Hiroshi, N. & Penninger, J. M. RANKL–RANK signaling in osteoclastogenesis and bone disease. *Trends Mol. Med.* **12**, 17–25 (2006).
130. Penninger, J. M. *et al.* OPGL is a key regulator of osteoclastogenesis, lymphocyte development and lymph-node organogenesis. *Nature* **397**, 315–323 (1999).
131. Dougall, W. C. *et al.* RANK is essential for osteoclast and lymph node development. *Genes Dev.* **13**, 2412–24 (1999).
132. Yasuda, H. RANKL, a necessary chance for clinical application to osteoporosis and cancer-related bone diseases. *World J. Orthop.* **4**, 207–217 (2013).
133. Stopeck, A. & Brown-Glaberman, U. Role of denosumab in the management of skeletal complications in patients with bone metastases from solid tumors. *Biol. Targets Ther.* **6**, 89 (2012).
134. De Castro, J. *et al.* Therapeutic potential of denosumab in patients with lung cancer: Beyond prevention of skeletal complications. *Clinical Lung Cancer* **16**, 431–446 (2015).
135. Joshi, P. A. *et al.* RANK Signaling Amplifies WNT-Responsive Mammary Progenitors through R-SPONDIN1. *Stem Cell Reports* **5**, 31–44 (2015).
136. Mulac-Jericevic, B., Lydon, J. P., DeMayo, F. J. & Conneely, O. M. Defective

mammary gland morphogenesis in mice lacking the progesterone receptor B isoform. *Proc. Natl. Acad. Sci. U. S. A.* **100**, 9744–9 (2003).
137. Srivastava, S. *et al.* Receptor Activator of NF-κB Ligand Induction via Jak2 and Stat5a in Mammary Epithelial Cells. *J. Biol. Chem.* **278**, 46171–46178 (2003).
138. Pellegrini, P. *et al.* Constitutive activation of RANK disrupts mammary cell fate leading to tumorigenesis. *Stem Cells* **31**, 1954–1965 (2013).
139. Fernandez-Valdivia, R. *et al.* The RANKL signaling axis is sufficient to elicit ductal side-branching and alveologenesis in the mammary gland of the virgin mouse. *Dev. Biol.* **328**, 127–139 (2009).
140. Lydon, J. P. *et al.* Mice lacking progesterone receptor exhibit pleiotropic reproductive abnormalities. *Genes Dev.* **9**, 2266–2278 (1995).
141. Horseman, N. D. Prolactin and mammary gland development. *Journal of mammary gland biology and neoplasia* **4**, 79–88 (1999).
142. Mukherjee, A. *et al.* Targeting RANKL to a specific subset of murine mammary epithelial cells induces ordered branching morphogenesis and alveologenesis in the absence of progesterone receptor expression. *FASEB J.* **24**, 4408–4419 (2010).
143. Tanos, T. *et al.* Progesterone/RANKL is a major regulatory axis in the human breast. *Sci. Transl. Med.* **5**, (2013).
144. Cordero, A. *et al.* Rankl Impairs Lactogenic Differentiation Through Inhibition of the Prolactin/Stat5 Pathway at Midgestation. *Stem Cells* **34**, 1027–1039 (2016).
145. Asselin-Labat, M.-L. *et al.* Control of mammary stem cell function by steroid hormone signalling. *Nature* **465**, 798–802 (2010).
146. Schramek, D. *et al.* Osteoclast differentiation factor RANKL controls development of progestin-driven mammary cancer. *Nature* **468**, 98–102 (2010).
147. Cordero, A. *et al.* Rankl Impairs Lactogenic Differentiation Through Inhibition of the Prolactin/Stat5 Pathway at Midgestation. *Stem Cells* **34**, 1027–1039 (2016).
148. Palafox, M. *et al.* RANK Induces Epithelial-Mesenchymal Transition and Stemness in Human Mammary Epithelial Cells and Promotes Tumorigenesis and Metastasis. *Cancer Res.* **72**, 2879–2888 (2012).
149. Lydon, J. P., Ge, G., Kittrell, F. S., Medina, D. & O'Malley, B. W. Murine mammary gland carcinogenesis is critically dependent on progesterone receptor function. *Cancer Res.* **59**, 4276–4284 (1999).
150. Soyal, S. *et al.* Progesterone's role in mammary gland development and tumorigenesis as disclosed by experimental mouse genetics. *Breast Cancer Research* **4**, 191–196 (2002).
151. Aldaz, C. M., Liao, Q. Y., LaBate, M. & Johnston, D. A. Medroxyprogesterone acetate accelerates the development and increases the incidence of mouse mammary tumors induced by dimethylbenzanthracene. *Carcinogenesis* **17**, 2069–72 (1996).
152. Gonzalez-Suarez, E. *et al.* RANK ligand mediates progestin-induced mammary epithelial proliferation and carcinogenesis. *Nature* **468**, 103–107 (2010).
153. Tan, W. *et al.* Tumour-infiltrating regulatory T cells stimulate mammary cancer metastasis through RANKL–RANK signalling. *Nature* **470**, 548–553 (2011).
154. Ghoncheh, M., Pournamdar, Z. & Salehiniya, H. Incidence and Mortality and Epidemiology of Breast Cancer in the World. *Asian Pacific J. Cancer Prev.* **17**, 43–46 (2016).

155. Bhatia, P., Sanders, M. M. & Hansen, M. F. Expression of receptor activator of nuclear factor-kappaB is inversely correlated with metastatic phenotype in breast carcinoma. *Clin. Cancer Res.* **11**, 162–5 (2005).
156. Jones, D. H. *et al.* Regulation of cancer cell migration and bone metastasis by RANKL. *Nature* **440**, 692–696 (2006).
157. Santini, D. *et al.* Expression pattern of receptor activator of NFκB (RANK) in a series of primary solid tumors and related bone metastases. *J. Cell. Physiol.* **226**, 780–784 (2011).
158. Pfitzner, B. M. *et al.* RANK expression as a prognostic and predictive marker in breast cancer. *Breast Cancer Res. Treat.* **145**, 307–315 (2014).
159. Li, R. *et al.* The rank pathway in advanced breast cancer: Does Src play a role? in *Applied Immunohistochemistry and Molecular Morphology* **24**, 42–50 (Lippincott Williams and Wilkins, 2016).
160. Hu, H. *et al.* RANKL expression in normal and malignant breast tissue responds to progesterone and is up-regulated during the luteal phase. *Breast Cancer Res. Treat.* **146**, 515–523 (2014).
161. Azim, H. A. *et al.* RANK-ligand (RANKL) expression in young breast cancer patients and during pregnancy. *Breast Cancer Res.* **17**, 24 (2015).
162. Reyes, M. E. *et al.* Poor prognosis of patients with triple-negative breast cancer can be stratified by RANK and RANKL dual expression. *Breast Cancer Res. Treat.* **164**, 57–67 (2017).
163. Holen, I. *et al.* Osteoprotegerin (OPG) Expression by Breast Cancer Cells in vitro and Breast Tumours in vivo – A Role in Tumour Cell Survival? *Breast Cancer Res. Treat.* **92**, 207–215 (2005).
164. Bonifaci, N. *et al.* Evidence for a link between TNFRSF11A and risk of breast cancer. *Breast Cancer Res. Treat.* **129**, 947–954 (2011).
165. Sigl, V. *et al.* RANKL/RANK control Brca1 mutation-driven mammary tumors. *Cell Res.* **26**, 761–74 (2016).
166. Thomas, R. J. *et al.* Breast cancer cells interact with osteoblasts to support osteoclast formation. *Endocrinology* **140**, 4451–4458 (1999).
167. Schubert, A., Schulz, H., Emons, G. & Gründker, C. Expression of osteoprotegerin and receptor activator of nuclear factor-κB ligand (RANKL) in HCC70 breast cancer cells and effects of treatment with gonadotropin-releasing hormone on RANKL expression. *Gynecol. Endocrinol.* **24**, 331–338 (2008).
168. Ney, J. T., Fehm, T., Juhasz-Boess, I. & Solomayer, E. F. RANK, RANKL and OPG Expression in Breast Cancer - Influence on Osseous Metastasis. *Geburtshilfe Frauenheilkd.* **72**, 385–391 (2012).
169. Barbaroux, J.-B. O., Beleut, M., Brisken, C., Mueller, C. G. & Groves, R. W. Epidermal Receptor Activator of NF-κB Ligand Controls Langerhans Cells Numbers and Proliferation. *J. Immunol.* **181**, 1103–1108 (2008).
170. Knoop, K. A., Butler, B. R., Kumar, N., Newberry, R. D. & Williams, I. R. Distinct developmental requirements for isolated lymphoid follicle formation in the small and large intestine: RANKL is essential only in the small intestine. *Am. J. Pathol.* **179**, 1861–1871 (2011).
171. Sakaguchi, S. & Sakaguchi, N. Regulatory T cells in immunologic self-tolerance and autoimmune disease. *International Reviews of Immunology* **24**, 211–226 (2005).

172. Han, Q. *et al.* Rac1-MKK3-p38-MAPKAPK2 pathway promotes urokinase plasminogen activator mRNA stability in invasive breast cancer cells. *J. Biol. Chem.* **277**, 48379–48385 (2002).
173. Whyte, J., Bergin, O., Bianchi, A., McNally, S. & Martin, F. Key signalling nodes in mammary gland development and cancer. Mitogen-activated protein kinase signalling in experimental models of breast cancer progression and in mammary gland development. *Breast Cancer Res.* **11**, 209 (2009).
174. Knight, T. & Irving, J. A. E. Ras/Raf/MEK/ERK Pathway Activation in Childhood Acute Lymphoblastic Leukemia and Its Therapeutic Targeting. *Front. Oncol.* **4**, 160 (2014).
175. Galliher, A. J. & Schiemann, W. P. Src Phosphorylates Tyr ^{284} in TGF-β Type II Receptor and Regulates TGF-β Stimulation of p38 MAPK during Breast Cancer Cell Proliferation and Invasion. *Cancer Res.* **67**, 3752–3758 (2007).
176. Santarpia, L., Lippman, S. M. & El-Naggar, A. K. Targeting the MAPK-RAS-RAF signaling pathway in cancer therapy. *Expert Opin. Ther. Targets* **16**, 103–19 (2012).
177. Pratilas, C. A. & Solit, D. B. Targeting the Mitogen-Activated Protein Kinase Pathway: Physiological Feedback and Drug Response. *Clin. Cancer Res.* **16**, 3329–3334 (2010).
178. Cseh, B., Doma, E. & Baccarini, M. "RAF" neighborhood: protein-protein interaction in the Raf/Mek/Erk pathway. *FEBS Lett.* **588**, 2398–406 (2014).
179. McCubrey, J. A. *et al.* Roles of the Raf/MEK/ERK pathway in cell growth, malignant transformation and drug resistance. *Biochim. Biophys. Acta - Mol. Cell Res.* **1773**, 1263–1284 (2007).
180. Downward, J. Targeting RAS signalling pathways in cancer therapy. *Nat. Rev. Cancer* **3**, 11–22 (2003).
181. Murtagh, J., Martin, F. & Gronostajski, R. M. The Nuclear Factor I (NFI) gene family in mammary gland development and function. *J. Mammary Gland Biol. Neoplasia* **8**, 241–54 (2003).
182. Mingo-Sion, A. M., Marietta, P. M., Koller, E., Wolf, D. M. & Van Den Berg, C. L. Inhibition of JNK reduces G2/M transit independent of p53, leading to endoreduplication, decreased proliferation, and apoptosis in breast cancer cells. *Oncogene* **23**, 596–604 (2004).
183. Han, Z. *et al.* c-Jun N-terminal kinase is required for metalloproteinase expression and joint destruction in inflammatory arthritis. *J. Clin. Invest.* **108**, 73–81 (2001).
184. Weston, C. R. & Davis, R. J. The JNK signal transduction pathway. *Curr. Opin. Genet. Dev.* **12**, 14–21 (2002).
185. Adams, R. H. *et al.* Essential role of p38alpha MAP kinase in placental but not embryonic cardiovascular development. *Mol. Cell* **6**, 109–16 (2000).
186. Mudgett, J. S. *et al.* Essential role for p38alpha mitogen-activated protein kinase in placental angiogenesis. *Proc. Natl. Acad. Sci. U. S. A.* **97**, 10454–9 (2000).
187. Hui, L., Bakiri, L., Stepniak, E. & Wagner, E. F. p38α: A Suppressor of Cell Proliferation and Tumorigenesis. *Cell Cycle* **6**, 2429–2433 (2007).
188. Kyriakis, J. M. & Avruch, J. Mammalian Mitogen-Activated Protein Kinase Signal Transduction Pathways Activated by Stress and Inflammation. *Physiol. Rev.* **81**,

807–869 (2001).
189. Santini, D. *et al.* Receptor activator of NF-kB (rank) expression in primary tumors associates with bone metastasis occurrence in breast cancer patients. *PLoS One* **6**, (2011).
190. Hayden, M. S. & Ghosh, S. Shared principles in NF-kappaB signaling. *Cell* **132**, 344–62 (2008).
191. Jost, P. J. & Ruland, J. Aberrant NF- B signaling in lymphoma: mechanisms, consequences and therapeutic implications. *Blood* **109**, 2700–7 (2006).
192. Gilmore, T. D. Introduction to NF-κB: players, pathways, perspectives. *Oncogene* **25**, 6680–6684 (2006).
193. Oeckinghaus, A. & Ghosh, S. The NF-kappaB family of transcription factors and its regulation. *Cold Spring Harbor perspectives in biology* **1**, (2009).
194. Chen, F. E. & Ghosh, G. Regulation of DNA binding by Rel/NF-κB transcription factors: structural views. *Oncogene* **18**, 6845–6852 (1999).
195. Coldewey, S. M., Rogazzo, M., Collino, M., Patel, N. S. A. & Thiemermann, C. Inhibition of IκB kinase reduces the multiple organ dysfunction caused by sepsis in the mouse. *Dis. Model. Mech.* **6**, 1031–42 (2013).
196. Cao, Y. *et al.* IKKalpha provides an essential link between RANK signaling and cyclin D1 expression during mammary gland development. *Cell* **107**, 763–75 (2001).
197. Brantley, D. M. *et al.* Nuclear Factor-κB (NF-κB) Regulates Proliferation and Branching in Mouse Mammary Epithelium. *Mol. Biol. Cell* **12**, 1445–1455 (2001).
198. Sovak, M. A. *et al.* Aberrant nuclear factor-kappaB/Rel expression and the pathogenesis of breast cancer. *J. Clin. Invest.* **100**, 2952–2960 (1997).
199. Connelly, L. *et al.* Inhibition of NF-kappa B activity in mammary epithelium increases tumor latency and decreases tumor burden. *Oncogene* **30**, 1402–1412 (2011).
200. Cao, Y., Luo, J. -l. & Karin, M. I B kinase kinase activity is required for self-renewal of ErbB2/Her2-transformed mammary tumor-initiating cells. *Proc. Natl. Acad. Sci.* **104**, 15852–15857 (2007).
201. Ellis, M. J. & Perou, C. M. The Genomic Landscape of Breast Cancer as a Therapeutic Roadmap. *Cancer Discov.* **3**, 27–34 (2013).
202. Lee, J. J., Loh, K. & Yap, Y.-S. PI3K/Akt/mTOR inhibitors in breast cancer. *Cancer Biol. Med.* **12**, 342–54 (2015).
203. Baselga, J. Targeting the phosphoinositide-3 (PI3) kinase pathway in breast cancer. *Oncologist* **16 Suppl 1**, 12–9 (2011).
204. Zhao, L. & Vogt, P. K. Class I PI3K in oncogenic cellular transformation. *Oncogene* **27**, 5486–5496 (2008).
205. Salmena, L., Carracedo, A. & Pandolfi, P. P. Tenets of PTEN Tumor Suppression. *Cell* **133**, 403–414 (2008).
206. Vanhaesebroeck, B., Guillermet-Guibert, J., Graupera, M. & Bilanges, B. The emerging mechanisms of isoform-specific PI3K signalling. *Nat. Rev. Mol. Cell Biol.* **11**, 329–341 (2010).
207. Chen, C.-C. *et al.* Akt is required for Stat5 activation and mammary differentiation. *Breast Cancer Res.* **12**, R72 (2010).
208. Miller, T. W. *et al.* Hyperactivation of phosphatidylinositol-3 kinase promotes escape from hormone dependence in estrogen receptor–positive human breast

cancer. *J. Clin. Invest.* **120**, 2406–2413 (2010).
209. Boulay, A. *et al.* Dual Inhibition of mTOR and Estrogen Receptor Signaling In vitro Induces Cell Death in Models of Breast Cancer. *Clin. Cancer Res.* **11**, 5319–5328 (2005).
210. Pandolfi, P. P. Breast Cancer — Loss of PTEN Predicts Resistance to Treatment. *N. Engl. J. Med.* **351**, 2337–2338 (2004).
211. Dieras, V. *et al.* [Trastuzumab (Herceptin) and breast cancer: mechanisms of resistance]. *Bull. Cancer* **94**, 259–66 (2007).
212. Koboldt, D. C. *et al.* Comprehensive molecular portraits of human breast tumours. *Nature* **490**, 61–70 (2012).
213. Martini, M., De Santis, M. C., Braccini, L., Gulluni, F. & Hirsch, E. PI3K/AKT signaling pathway and cancer: an updated review. *Ann. Med.* **46**, 372–383 (2014).
214. L.Hayflick. The limited in vitro lifetime of human diploid cell strains. *Exp. Cell Res.* **37**, 614–636 (1965).
215. Hayflick, L. & Moorhead, P. S. The serial cultivation of human diploid cell strains. *Exp. Cell Res.* **25**, 585–621 (1961).
216. Herbert, B.-S. *et al.* Inhibition of human telomerase in immortal human cells leads to progressive telomere shortening and cell death. *Proc. Natl. Acad. Sci.* **96**, 14276–14281 (1999).
217. d'Adda di Fagagna, F. Living on a break: cellular senescence as a DNA-damage response. *Nat. Rev. Cancer* **8**, 512–522 (2008).
218. McHugh, D. & Gil, J. Senescence and aging: Causes, consequences, and therapeutic avenues. *Journal of Cell Biology* **217**, 65–77 (2018).
219. López-Otín, C., Blasco, M. A., Partridge, L., Serrano, M. & Kroemer, G. The Hallmarks of Aging. *Cell* **153**, 1194–1217 (2013).
220. Kuilman, T., Michaloglou, C., Mooi, W. J. & Peeper, D. S. The essence of senescence. *Genes Dev.* **24**, 2463–2479 (2010).
221. HAYFLICK, L. & MOORHEAD, P. S. The serial cultivation of human diploid cell strains. *Exp. Cell Res.* **25**, 585–621 (1961).
222. Denoyelle, C. *et al.* Anti-oncogenic role of the endoplasmic reticulum differentially activated by mutations in the MAPK pathway. *Nat. Cell Biol.* **8**, 1053–1063 (2006).
223. Haugstetter, A. M. *et al.* Cellular senescence predicts treatment outcome in metastasised colorectal cancer. *Br. J. Cancer* **103**, 505–9 (2010).
224. Kim, Y. H. *et al.* Senescent tumor cells lead the collective invasion in thyroid cancer. *Nat. Commun.* **8**, 15208 (2017).
225. Dimri, G. P. *et al.* A biomarker that identifies senescent human cells in culture and in aging skin in vivo. **92**, (1995).
226. Debacq-Chainiaux, F., Erusalimsky, J. D., Campisi, J. & Toussaint, O. Protocols to detect senescence-associated beta-galactosidase (SA-βgal) activity, a biomarker of senescent cells in culture and in vivo. *Nat. Protoc.* **4**, 1798–1806 (2009).
227. David J. Kurz*, Stephanie Decary*, Y. H. and J. D. E. Senescence-associated β-galactosidase reflects an increase in lysosomal mass during replicative ageing of human endothelial cells. *J. Cell Sci.* (2000).
228. Lee, B. Y. *et al.* Senescence-associated β-galactosidase is lysosomal β-galactosidase. *Aging Cell* **5**, 187–195 (2006).

229. Miller, J. H. & Lee, K. Y. Experiments in molecular genetics. *Cold Spring Harb. Lab. Press. Cold Spring Harb.* vi, 546p. : figs. (1984).
230. BOSMANN, H. B., GUTHEIL, R. L. & CASE, K. R. Loss of a critical neutral protease in ageing WI-38 cells. *Nature* **261**, 499–501 (1976).
231. Freund, A., Laberge, R.-M., Demaria, M. & Campisi, J. Lamin B1 loss is a senescence-associated biomarker. *Mol. Biol. Cell* **23**, 2066–2075 (2012).
232. Muñoz-Espín, D. *et al.* Programmed Cell Senescence during Mammalian Embryonic Development. *Cell* **155**, 1104–1118 (2013).
233. LeBrasseur, N. K., Tchkonia, T. & Kirkland, J. L. Cellular Senescence and the Biology of Aging, Disease, and Frailty. in *Nestle Nutrition Institute workshop series* **83**, 11–18 (2015).
234. Helman, A. *et al.* p16Ink4a-induced senescence of pancreatic beta cells enhances insulin secretion. *Nat. Med.* **22**, 412–420 (2016).
235. Beausejour, C. M. Reversal of human cellular senescence: roles of the p53 and p16 pathways. *EMBO J.* **22**, 4212–4222 (2003).
236. Sparmann, A. & Bar-Sagi, D. Ras-induced interleukin-8 expression plays a critical role in tumor growth and angiogenesis. *Cancer Cell* **6**, 447–458 (2004).
237. Ancrile, B., Lim, K. H. & Counter, C. M. Oncogenic Ras-induced secretion of IL6 is required for tumorigenesis. *Genes Dev.* **21**, 1714–1719 (2007).
238. Coppé, J.-P., Desprez, P.-Y., Krtolica, A. & Campisi, J. The senescence-associated secretory phenotype: the dark side of tumor suppression. *Annu. Rev. Pathol.* **5**, 99–118 (2010).
239. Lujambio, A. To clear, or not to clear (senescent cells)? That is the question. *BioEssays* **38**, S56–S64 (2016).
240. Song, Y. S., Lee, B. Y. & Hwang, E. S. Dinstinct ROS and biochemical profiles in cells undergoing DNA damage-induced senescence and apoptosis. *Mech. Ageing Dev.* **126**, 580–590 (2005).
241. Campisi, J. & d'Adda di Fagagna, F. Cellular senescence: when bad things happen to good cells. *Nat. Rev. Mol. Cell Biol.* **8**, 729–740 (2007).
242. Ben-Porath, I. & Weinberg, R. A. When cells get stressed: an integrative view of cellular senescence. *J. Clin. Invest.* **113**, 8–13 (2004).
243. Campisi, J. Cancer and ageing: rival demons? *Nat. Rev. Cancer* **3**, 339–349 (2003).
244. Braig, M. & Schmitt, C. A. Oncogene-Induced Senescence: Putting the Brakes on Tumor Development. *Cancer Res* **66**, 2881–2885 (2006).
245. Collins, C. J. & Sedivy, J. M. Involvement of the INK4a/Arf gene locus in senescence. *Aging Cell* **2**, 145–150 (2003).
246. Collado, M. *et al.* Senescence in premalignant tumours. *Nature* **436**, 642–642 (2005).
247. Kim, Y. H. *et al.* Senescent tumor cells lead the collective invasion in thyroid cancer. *Nat. Commun.* **8**, (2017).
248. Haugstetter, A. M. *et al.* Cellular senescence predicts treatment outcome in metastasised colorectal cancer. *Br. J. Cancer* **103**, 505–509 (2010).
249. Krtolica, A., Parrinello, S., Lockett, S., Desprez, P. Y. & Campisi, J. Senescent fibroblasts promote epithelial cell growth and tumorigenesis: a link between cancer and aging. *Proc. Natl. Acad. Sci. U. S. A.* **98**, 12072–7 (2001).
250. Sun, Y., Coppé, J.-P. & Lam, E. W.-F. Cellular Senescence: The Sought or the

Unwanted? *Trends Mol. Med.* **24**, 871–885 (2018).
251. Muñoz-Espín, D. & Serrano, M. Cellular senescence: from physiology to pathology, Muñoz-Espín & Serrano, 2014. *Nat. Rev. Mol. Cell Biol.* (2014). doi:10.1038/nrm3823
252. Coppé, J.-P. *et al.* Senescence-associated secretory phenotypes reveal cell-nonautonomous functions of oncogenic RAS and the p53 tumor suppressor. *PLoS Biol.* **6**, 2853–68 (2008).
253. Acosta, J. C. *et al.* Chemokine Signaling via the CXCR2 Receptor Reinforces Senescence. *Cell* **133**, 1006–1018 (2008).
254. Kang, T.-W. *et al.* Senescence surveillance of pre-malignant hepatocytes limits liver cancer development. *Nature* **479**, 547–551 (2011).
255. Krtolica, A., Parrinello, S., Lockett, S., Desprez, P.-Y. & Campisi, J. *Senescent fibroblasts promote epithelial cell growth and tumorigenesis: A link between cancer and aging*. *Proceedings of the National Academy of Sciences* **98**, 12072–12077 (National Academy of Sciences, 2001).
256. Sun, Y. *et al.* Treatment-induced damage to the tumor microenvironment promotes prostate cancer therapy resistance through WNT16B. *Nat. Med.* **18**, 1359–1368 (2012).
257. Coppé, J.-P., Kauser, K., Campisi, J. & Beauséjour, C. M. Secretion of vascular endothelial growth factor by primary human fibroblasts at senescence. *J. Biol. Chem.* **281**, 29568–74 (2006).
258. Eyman, D., Damodarasamy, M., Plymate, S. R. & Reed, M. J. CCL5 secreted by senescent aged fibroblasts induces proliferation of prostate epithelial cells and expression of genes that modulate angiogenesis. *J. Cell. Physiol.* **220**, 376–381 (2009).
259. Pazolli, E. *et al.* Senescent Stromal-Derived Osteopontin Promotes Preneoplastic Cell Growth. *Cancer Res.* **69**, 1230–1239 (2009).
260. Kuilman, T. *et al.* Oncogene-Induced Senescence Relayed by an Interleukin-Dependent Inflammatory Network. *Cell* **133**, 1019–1031 (2008).
261. Wajapeyee, N., Serra, R. W., Zhu, X., Mahalingam, M. & Green, M. R. Oncogenic BRAF induces senescence and apoptosis through pathways mediated by the secreted protein IGFBP7. *Cell* **132**, 363–74 (2008).
262. Acosta, J. C. *et al.* A complex secretory program orchestrated by the inflammasome controls paracrine senescence. *Nat. Cell Biol.* **15**, 978–990 (2013).
263. Di Mitri, D. & Alimonti, A. Non-Cell-Autonomous Regulation of Cellular Senescence in Cancer. *Trends Cell Biol.* **26**, 215–226 (2016).
264. Borodkina, A. V, Deryabin, P. I., Giukova, A. A. & Nikolsky, N. N. “Social Life” of Senescent Cells: What Is SASP and Why Study It? *Acta Naturae* **10**, 4–14 (2018).
265. Hornebeck, W. & Maquart, F. X. Proteolyzed matrix as a template for the regulation of tumor progression. *Biomed. Pharmacother.* **57**, 223–30 (2003).
266. Chen, J. H. *et al.* Loss of proliferative capacity and induction of senescence in oxidatively stressed human fibroblasts. *J. Biol. Chem.* **279**, 49439–49446 (2004).
267. Baker, D. J. & Sedivy, J. M. Probing the depths of cellular senescence. *J. Cell Biol.* **202**, 11–13 (2013).
268. Malaquin N, Martinez A, R. F. Keeping the senescence secretome under control: Molecular reins on the senescence-associated secretory phenotype. *Exp.*

Gerontol. **82**, 39–49 (2016).
269. Coppé, J.-P. *et al.* Senescence-Associated Secretory Phenotypes Reveal Cell-Nonautonomous Functions of Oncogenic RAS and the p53 Tumor Suppressor. *PLoS Biol.* **6**, e301 (2008).
270. Jackson, S. P. & Bartek, J. The DNA-damage response in human biology and disease. *Nature* **461**, 1071–1078 (2009).
271. Freund, A., Patil, C. K. & Campisi, J. p38MAPK is a novel DNA damage response-independent regulator of the senescence-associated secretory phenotype. *EMBO J.* **30**, 1536–1548 (2011).
272. Glück, S. *et al.* Innate immune sensing of cytosolic chromatin fragments through cGAS promotes senescence. *Nat. Cell Biol.* **19**, 1061–1070 (2017).
273. Dou, Z. *et al.* Cytoplasmic chromatin triggers inflammation in senescence and cancer. *Nature* **550**, 402–406 (2017).
274. Hoare, M. *et al.* NOTCH1 mediates a switch between two distinct secretomes during senescence. *Nat. Cell Biol.* **18**, 979–992 (2016).
275. Toso, A. *et al.* Enhancing Chemotherapy Efficacy in Pten -Deficient Prostate Tumors by Activating the Senescence-Associated Antitumor Immunity. *Cell Rep.* **9**, 75–89 (2014).
276. Laberge, R. M. *et al.* MTOR regulates the pro-tumorigenic senescence-associated secretory phenotype by promoting IL1A translation. *Nat. Cell Biol.* (2015). doi:10.1038/ncb3195
277. Chien, Y. *et al.* Control of the senescence-associated secretory phenotype by NF- B promotes senescence and enhances chemosensitivity. *Genes Dev.* **25**, 2125–2136 (2011).
278. Bargonetti, J. & Manfredi, J. J. Multiple roles of the tumor suppressor p53. *Curr. Opin. Oncol.* **14**, 86–91 (2002).
279. Baker, D. J. *et al.* Clearance of p16Ink4a-positive senescent cells delays ageing-associated disorders. *Nature* **479**, 232–236 (2011).
280. Narita, M. *et al.* Rb-mediated heterochromatin formation and silencing of E2F target genes during cellular senescence. *Cell* **113**, 703–16 (2003).
281. Gire, V. & Dulić, V. Senescence from G2 arrest, revisited. *Cell Cycle* **14**, 297–304 (2015).
282. Hollstein, M., Sidransky, D., Vogelstein, B. & Harris, C. C. p53 mutations in human cancers. *Science* **253**, 49–53 (1991).
283. Vogelstein, B., Lane, D. & Levine, A. J. Surfing the p53 network. *Nature* **408**, 307–310 (2000).
284. Tyner, S. D. *et al.* p53 mutant mice that display early ageing-associated phenotypes. *Nature* **415**, 45–53 (2002).
285. Maier, B. *et al.* Modulation of mammalian life span by the short isoform of p53. *Genes Dev.* **18**, 306–319 (2004).
286. Chen, Z. *et al.* Crucial role of p53-dependent cellular senescence in suppression of Pten-deficient tumorigenesis. *Nature* **436**, 725–730 (2005).
287. Xue, W. *et al.* Senescence and tumour clearance is triggered by p53 restoration in murine liver carcinomas. *Nature* **445**, 656–660 (2007).
288. Sherr, C. J. & McCormick, F. The RB and p53 pathways in cancer. *Cancer Cell* **2**, 103–12 (2002).
289. Brown, J. P., Wei, W. & Sedivy, J. M. Bypass of senescence after disruption of

p21CIP1/WAF1 gene in normal diploid human fibroblasts. *Science* **277**, 831–4 (1997).
290. Serrano, M., Hannon, G. J. & Beach, D. A new regulatory motif in cell-cycle control causing specific inhibition of cyclin D/CDK4. *Nature* **366**, 704–707 (1993).
291. Lowe, S. W. & Sherr, C. J. Tumor suppression by Ink4a–Arf: progress and puzzles. *Curr. Opin. Genet. Dev.* **13**, 77–83 (2003).
292. Sharpless, N. E. & Sherr, C. J. Forging a signature of in vivo senescence. *Nature Reviews Cancer* **15**, 397–408 (2015).
293. Muñoz-Espín, D. *et al.* Programmed cell senescence during mammalian embryonic development. *Cell* **155**, 1104 (2013).
294. Storer, M. *et al.* Senescence is a developmental mechanism that contributes to embryonic growth and patterning. *Cell* **155**, 1119 (2013).
295. Toussaint, O., Royer, V. Â., Salmon, M. & Remacle, J. Â. *Stress-induced premature senescence and tissue ageing*. *Biochemical Pharmacology* **64**, (2002).
296. Hewitt, G. *et al.* Telomeres are favoured targets of a persistent DNA damage response in ageing and stress-induced senescence. *Nat. Commun.* **3**, 708 (2012).
297. Serrano, M., Lin, A. W., McCurrach, M. E., Beach, D. & Lowe, S. W. Oncogenic ras provokes premature cell senescence associated with accumulation of p53 and p16INK4a. *Cell* **88**, 593–602 (1997).
298. Collado, M., Blasco, M. A. & Serrano, M. Cellular senescence in cancer and aging. *Cell* **130**, 223–33 (2007).
299. Sarkisian, C. J. *et al.* Dose-dependent oncogene-induced senescence in vivo and its evasion during mammary tumorigenesis. *Nat. Cell Biol.* **9**, 493–505 (2007).
300. Collado, M. & Serrano, M. The power and the promise of oncogene-induced senescence markers. *Nat. Rev. Cancer* **6**, 472–476 (2006).
301. Frank Bringold, M. Tumor suppressors and oncogenes in cellular senescence. *Exp. Gerontol.* **35**, 317–329 (2000).
302. Serrano, M., Lin, A. W., McCurrach, M. E., Beach, D. & Lowe, S. W. Oncogenic ras provokes premature cell senescence associated with accumulation of p53 and p16INK4a. *Cell* **88**, 593–602 (1997).
303. Farwell, D. G. *et al.* Genetic and Epigenetic Changes in Human Epithelial Cells Immortalized by Telomerase. *Am. J. Pathol.* **156**, 1537–1547 (2000).
304. Lin, A. W. & Lowe, S. W. *Oncogenic ras activates the ARF-p53 pathway to suppress epithelial cell transformation*.
305. Jones, C. J. *et al.* Evidence for a Telomere-Independent "Clock" Limiting RAS Oncogene-Driven Proliferation of Human Thyroid Epithelial Cells. *Mol. Cell. Biol.* **20**, 5690–5699 (2000).
306. Peeper, D. S., Dannenberg, J.-H., Douma, S., Riele, H. te & Bernards, R. Escape from premature senescence is not sufficient for oncogenic transformation by Ras. *Nat. Cell Biol.* **3**, 198–203 (2001).
307. Carnero, A., Hudson, J. D., Price, C. M. & Beach, D. H. p16INK4A and p19ARF act in overlapping pathways in cellular immortalization. *Nat. Cell Biol.* **2**, 148–155 (2000).
308. Sharpless, N. E. *et al.* Loss of p16Ink4a with retention of p19 predisposes mice to tumorigenesis. *Nature* **413**, 86–91 (2001).
309. Krimpenfort, P., Quon, K. C., Mooi, W. J., Loonstra, A. & Berns, A. Loss of p16Ink4a confers susceptibility to metastatic melanoma in mice. *Nature* **413**,

83–86 (2001).
310. Kamijo, T. *et al.* Tumor suppression at the mouse INK4a locus mediated by the alternative reading frame product p19(ARF). *Cell* **91**, 649–659 (1997).
311. Banito, A. *et al.* Senescence impairs successful reprogramming to pluripotent stem cells. *Genes Dev.* **23**, 2134–9 (2009).
312. Hong, H. *et al.* Suppression of induced pluripotent stem cell generation by the p53-p21 pathway. *Nature* **460**, 1132–1135 (2009).
313. Kawamura, T. *et al.* Linking the p53 tumour suppressor pathway to somatic cell reprogramming. *Nature* **460**, 1140–1144 (2009).
314. Utikal, J. *et al.* Immortalization eliminates a roadblock during cellular reprogramming into iPS cells. *Nature* **460**, 1145–1148 (2009).
315. Marión, R. M. *et al.* A p53-mediated DNA damage response limits reprogramming to ensure iPS cell genomic integrity. *Nature* **460**, 1149–1153 (2009).
316. Li, H. *et al.* The Ink4/Arf locus is a barrier for iPS cell reprogramming. *Nature* **460**, 1136–1139 (2009).
317. Krizhanovsky, V. & Lowe, S. W. Stem cells: The promises and perils of p53. *Nature* **460**, 1085–1086 (2009).
318. Collado, M. & Serrano, M. Senescence in tumours: evidence from mice and humans. *Nat. Rev. Cancer* **10**, 51–57 (2010).
319. Nardella, C., Clohessy, J. G., Alimonti, A. & Pandolfi, P. P. Pro-senescence therapy for cancer treatment. *Nat. Rev. Cancer* **11**, 503–511 (2011).
320. Puyol, M. *et al.* A Synthetic Lethal Interaction between K-Ras Oncogenes and Cdk4 Unveils a Therapeutic Strategy for Non-small Cell Lung Carcinoma. *Cancer Cell* **18**, 63–73 (2010).
321. Finn, R. S. *et al.* The cyclin-dependent kinase 4/6 inhibitor palbociclib in combination with letrozole versus letrozole alone as first-line treatment of oestrogen receptor-positive, HER2-negative, advanced breast cancer (PALOMA-1/TRIO-18): a randomised phase 2 study. *Lancet Oncol.* **16**, 25–35 (2015).
322. Turner, N. C. *et al.* Palbociclib in Hormone-Receptor–Positive Advanced Breast Cancer. *N. Engl. J. Med.* **373**, 209–219 (2015).
323. Sun, Y. *et al.* Treatment-induced damage to the tumor microenvironment promotes prostate cancer therapy resistance through WNT16B. *Nat. Med.* **18**, (2012).
324. Osaki, M., Oshimura, M. & Ito, H. PI3K-Akt pathway: Its functions and alterations in human cancer. *Apoptosis* **9**, 667–676 (2004).
325. Minn, A. J. *et al.* Bcl-xL regulates apoptosis by heterodimerization-dependent and -independent mechanisms. *EMBO J.* **18**, 632–643 (1999).
326. Goldschneider, D. & Mehlen, P. Dependence receptors: a new paradigm in cell signaling and cancer therapy. *Oncogene* **29**, 1865–1882 (2010).
327. Lee, S. & Schmitt, C. A. The dynamic nature of senescence in cancer. *Nat. Cell Biol.* **21**, 94–101 (2019).
328. Zhu, Y. *et al.* The Achilles' heel of senescent cells: from transcriptome to senolytic drugs. *Aging Cell* **14**, 644–658 (2015).
329. Ritschka, B. *et al.* The senescence-associated secretory phenotype induces cellular plasticity and tissue regeneration. *Genes Dev.* **31**, 172–183 (2017).
330. Krizhanovsky, V. & Lowe, S. W. Stem cells: The promises and perils of p53.

Nature **460**, 1085–1086 (2009).
331. Zon, L. I. Intrinsic and extrinsic control of haematopoietic stem-cell self-renewal. *Nature* **453**, 306–313 (2008).
332. Mosteiro, L. *et al.* Tissue damage and senescence provide critical signals for cellular reprogramming in vivo. *Science (80-.).* **354**, aaf4445 (2016).
333. Chiche, A. *et al.* Injury-Induced Senescence Enables In Vivo Reprogramming in Skeletal Muscle. *Cell Stem Cell* **20**, 407–414.e4 (2017).
334. Milanovic, M. *et al.* Senescence-associated reprogramming promotes cancer stemness. *Nature* **553**, 96–100 (2018).
335. Krishnamurthy, J. *et al.* p16INK4a induces an age-dependent decline in islet regenerative potential. *Nature* **443**, 453–457 (2006).
336. Krishnamurthy, J. *et al.* Ink4a/Arf expression is a biomarker of aging. *J. Clin. Invest.* **114**, 1299–1307 (2004).
337. Baker, D. J. *et al.* Naturally occurring p16 Ink4a-positive cells shorten healthy lifespan. *Nature* **530**, 184–189 (2016).
338. Helman, A. *et al.* p16 Ink4a-induced senescence of pancreatic beta cells enhances insulin secretion. *Nat. Med.* **22**, 412–420 (2016).
339. Molofsky, A. V. *et al.* Increasing p16INK4a expression decreases forebrain progenitors and neurogenesis during ageing. *Nature* **443**, 448–452 (2006).
340. Krtolica, A. & Campisi, J. Cancer and aging: A model for the cancer promoting effects of the aging stroma. *International Journal of Biochemistry and Cell Biology* **34**, 1401–1414 (2002).
341. Obenauf, A. C. *et al.* Therapy-induced tumour secretomes promote resistance and tumour progression. *Nature* **520**, 368–372 (2015).
342. Hernandez-Segura, A., Nehme, J. & Demaria, M. Hallmarks of Cellular Senescence. *Trends Cell Biol.* **28**, 436–453 (2018).
343. Zhu, Y. *et al.* Identification of a novel senolytic agent, navitoclax, targeting the Bcl-2 family of anti-apoptotic factors. *Aging Cell* **15**, 428–435 (2016).
344. Galiana, I. *et al.* Preclinical antitumor efficacy of senescence-inducing chemotherapy combined with a nanoSenolytic. *J. Control. Release* **323**, 624–634 (2020).
345. Zhu, Y., Armstrong, J. L., Tchkonia, T. & Kirkland, J. L. Cellular senescence and the senescent secretory phenotype in age-related chronic diseases. *Curr. Opin. Clin. Nutr. Metab. Care* **17**, 324–328 (2014).
346. Palmer, A. K. *et al.* Cellular Senescence in Type 2 Diabetes: A Therapeutic Opportunity. *Diabetes* **64**, 2289–2298 (2015).
347. Guy, C. T., Cardiff, R. D. & Muller, W. J. Induction of mammary tumors by expression of polyomavirus middle T oncogene: a transgenic mouse model for metastatic disease. *Mol. Cell. Biol.* **12**, 954–61 (1992).
348. Smalley, M. J. Isolation, Culture and Analysis of Mouse Mammary Epithelial Cells. in *Methods in molecular biology (Clifton, N.J.)* **633**, 139–170 (2010).
349. Katzen, F. Gateway® recombinational cloning: a biological operating system. *Expert Opin. Drug Discov.* **2**, 571–589 (2007).
350. Ma, J. *et al.* Characterization of mammary cancer stem cells in the MMTV-PyMT mouse model. *Tumor Biol.* **33**, 1983–1996 (2012).
351. Dobin, A. *et al.* STAR: ultrafast universal RNA-seq aligner. *Bioinformatics* **29**, 15–21 (2013).

352. Liao, Y., Smyth, G. K. & Shi, W. featureCounts: an efficient general purpose program for assigning sequence reads to genomic features. *Bioinformatics* **30**, 923–930 (2014).
353. Robinson, M. D. & Oshlack, A. A scaling normalization method for differential expression analysis of RNA-seq data. *Genome Biol.* **11**, R25 (2010).
354. Robinson, M. D., McCarthy, D. J. & Smyth, G. K. edgeR: a Bioconductor package for differential expression analysis of digital gene expression data. *Bioinformatics* **26**, 139–140 (2010).
355. Li, L. T., Jiang, G., Chen, Q. & Zheng, J. N. Predic Ki67 is a promising molecular target in the diagnosis of cancer (Review). *Molecular Medicine Reports* **11**, 1566–1572 (2015).
356. Hadjiloucas & al. Assessment of apoptosis in human breast tissue using an antibody against the active form of caspase 3: relation to tumour histopathological characteristics. *Br. J. Cancer* (2001). doi:10.1054/bjoc.2001.2115
357. Campisi, J. From cells to organisms: can we learn about aging from cells in culture? *Exp. Gerontol.* **36**, 607–18 (2001).
358. Kodama, S. *et al.* Culture condition-dependent senescence-like growth arrest and immortalization in rodent embryo cells. *Radiat. Res.* **155**, 254–262 (2001).
359. Coppé, J.-P. *et al.* Senescence-Associated Secretory Phenotypes Reveal Cell-Nonautonomous Functions of Oncogenic RAS and the p53 Tumor Suppressor. *PLoS Biol.* **6**, e301 (2008).
360. Özcan, S. *et al.* Unbiased analysis of senescence associated secretory phenotype (SASP) to identify common components following different genotoxic stresses. *Aging (Albany. NY).* **8**, 1316–29 (2016).
361. Campisi, J. Aging, Cellular Senescence, and Cancer. *Annu. Rev. Physiol.* **75**, 685–705 (2013).
362. Myrianthopoulos, V. *et al.* Senescence and senotherapeutics: a new field in cancer therapy. *Pharmacology and Therapeutics* **193**, 31–49 (2019).
363. Chang, J. *et al.* Clearance of senescent cells by ABT263 rejuvenates aged hematopoietic stem cells in mice. *Nat. Med.* **22**, 78–83 (2016).
364. Taguchi, J. & Yamada, Y. Unveiling the Role of Senescence-Induced Cellular Plasticity. *Cell Stem Cell* **20**, 293–294 (2017).
365. Franzen, J., Wagner, W. & Fernandez-Rebollo, E. Epigenetic Modifications upon Senescence of Mesenchymal Stem Cells. *Curr. Stem Cell Reports* **2**, 248–254 (2016).
366. Orioli, D. & Dellambra, E. Epigenetic Regulation of Skin Cells in Natural Aging and Premature Aging Diseases. *Cells* **7**, (2018).
367. Taniguchi, K. & Karin, M. NF-B, inflammation, immunity and cancer: Coming of age. *Nature Reviews Immunology* **18**, 309–324 (2018).
368. Hakryul, J. *et al.* NF-κB is required for H-ras oncogene induced abnormal cell proliferation and tumorigenesis. *Oncogene* **19**, 841–849 (2000).
369. Dhillon, A. S., Hagan, S., Rath, O. & Kolch, W. MAP kinase signalling pathways in cancer. *Oncogene* **26**, 3279–3290 (2007).
370. Kwong, J. *et al.* P38α and p38 mediate oncogenic ras-induced senescence through differential mechanisms. *J. Biol. Chem.* **284**, 11237–11246 (2009).
371. Crescenzi, E., De Palma, R. & Leonardi, A. Senescence and NFκB: A Trojan horse

in tumors? *OncoImmunology* **1**, 1594–1597 (2012).
372. Pearson, G. *et al.* Mitogen-activated protein (MAP) kinase pathways: Regulation and physiological functions. *Endocrine Reviews* **22**, 153–183 (2001).
373. Hui, L. *et al.* p38α suppresses normal and cancer cell proliferation by antagonizing the JNK-c-Jun pathway. *Nat. Genet.* **39**, 741–749 (2007).
374. Xu, Y., Li, N., Xiang, R. & Sun, P. Emerging roles of the p38 MAPK and PI3K/AKT/mTOR pathways in oncogene-induced senescence. *Trends in Biochemical Sciences* **39**, 268–276 (2014).
375. Wang, W. *et al.* Sequential Activation of the MEK-Extracellular Signal-Regulated Kinase and MKK3/6-p38 Mitogen-Activated Protein Kinase Pathways Mediates Oncogenic ras-Induced Premature Senescence. *Mol. Cell. Biol.* **22**, 3389–3403 (2002).
376. Chien, Y. *et al.* Control of the senescence-associated secretory phenotype by NF-κB promotes senescence and enhances chemosensitivity. *Genes Dev.* **25**, 2125–2136 (2011).
377. Freund, A., Patil, C. K. & Campisi, J. P38MAPK is a novel DNA damage response-independent regulator of the senescence-associated secretory phenotype. *EMBO J.* **30**, 1536–1548 (2011).
378. Acosta, J. C. *et al.* Chemokine Signaling via the CXCR2 Receptor Reinforces Senescence. *Cell* **133**, 1006–1018 (2008).
379. Israël, A. The IKK complex, a central regulator of NF-kappaB activation. *Cold Spring Harbor perspectives in biology* **2**, (2010).
380. Freund, A., Orjalo, A. V, Desprez, P.-Y. & Campisi, J. Inflammatory networks during cellular senescence: causes and consequences. *Trends Mol. Med.* **16**, 238–46 (2010).
381. Takahashi, K. & Yamanaka, S. Induction of Pluripotent Stem Cells from Mouse Embryonic and Adult Fibroblast Cultures by Defined Factors. *Cell* **126**, 663–676 (2006).
382. Abad, M. *et al.* Reprogramming in vivo produces teratomas and iPS cells with totipotency features. *Nature* **502**, (2013).
383. Shehata, M. *et al.* Phenotypic and functional characterisation of the luminal cell hierarchy of the mammary gland. *Breast Cancer Res.* **14**, R134 (2012).
384. Oakes, S. R. *et al.* The Ets transcription factor Elf5 specifies mammary alveolar cell fate. *Genes Dev.* **22**, 581–586 (2008).
385. Lecot, P., Alimirah, F., Desprez, P.-Y., Campisi, J. & Wiley, C. Context-dependent effects of cellular senescence in cancer development. *Br. J. Cancer* **114**, 1180–1184 (2016).
386. Qian, Y. & Chen, X. Senescence regulation by the p53 protein family. *Methods Mol. Biol.* **965**, 37–61 (2013).
387. Wu, D. *et al.* Orphan nuclear receptor TLX functions as a potent suppressor of oncogene-induced senescence in prostate cancer via its transcriptional co-regulation of the CDKN1A (p21WAF1/CIP1) and SIRT1 genes. *J. Pathol.* **236**, 103–115 (2015).
388. Denchi, E. L., Attwooll, C., Pasini, D. & Helin, K. Deregulated E2F Activity Induces Hyperplasia and Senescence-Like Features in the Mouse Pituitary Gland. *Mol. Cell. Biol.* **25**, 2660–2672 (2005).
389. Wang, M. *et al.* Role of tumor microenvironment in tumorigenesis. *Journal of*

Cancer **8**, 761–773 (2017).
390. Guo, Y. *et al.* Senescence-associated tissue microenvironment promotes colon cancer formation through the secretory factor GDF15. *Aging Cell* **18**, (2019).
391. Dean, J. P. & Nelson, P. S. Profiling influences of senescent and aged fibroblasts on prostate carcinogenesis. *British Journal of Cancer* **98**, 245–249 (2008).
392. Castro-Vega, L. J. *et al.* The senescent microenvironment promotes the emergence of heterogeneous cancer stem-like cells. *Carcinogenesis* **36**, 1180–1192 (2015).
393. Gonzalez-Meljem, J. M., Apps, J. R., Fraser, H. C. & Martinez-Barbera, J. P. Paracrine roles of cellular senescence in promoting tumourigenesis. *Br. J. Cancer* **118**, 1283–1288 (2018).
394. Horwitz, K. B., Costlow, M. E. & McGuire, W. L. MCF-7: A human breast cancer cell line with estrogen, androgen, progesterone, and glucocorticoid receptors. *Steroids* **26**, 785–795 (1975).
395. Jose Serrano, Stephan U. Goebel, Paolo L. Peghini, Irina A. Lubensky, Fathia Gibril, and R. T. J. Alterations in the p16 INK4a /CDKN2A Tumor Suppressor Gene in Gastrinomas. (2000).
396. McGowan, E. M. *et al.* P14ARF post-transcriptional regulation of nuclear cyclin D1 in MCF-7 breast cancer cells: Discrimination between a good and bad prognosis? *PLoS One* **7**, (2012).
397. Liang, J. *et al.* CDKN2A inhibits formation of homotypic cell-in-cell structures. *Oncogenesis* **7**, (2018).
398. Kandhaya-Pillai, R. *et al.* TNFα-senescence initiates a STAT-dependent positive feedback loop, leading to a sustained interferon signature, DNA damage, and cytokine secretion. *Aging (Albany. NY).* **9**, 2411–2435 (2017).
399. Viatour, P., Merville, M. P., Bours, V. & Chariot, A. Phosphorylation of NF-κB and IκB proteins: Implications in cancer and inflammation. *Trends in Biochemical Sciences* **30**, 43–52 (2005).
400. Nishina, H., Wada, T. & Katada, T. Physiological roles of SAPK/JNK signaling pathway. *Journal of Biochemistry* **136**, 123–126 (2004).
401. Prieur, A. & Peeper, D. S. Cellular senescence in vivo: a barrier to tumorigenesis. *Curr. Opin. Cell Biol.* **20**, 150–155 (2008).
402. Mar Vergel, M. del. Cellular Senescence as a Barrier to Environmental Carcinogenesis. *J. Carcinog. Mutagen.* **s3**, 1–5 (2014).
403. Yoldi, G. *et al.* Tumor and Stem Cell Biology RANK Signaling Blockade Reduces Breast Cancer Recurrence by Inducing Tumor Cell Differentiation. *Cancer Res* **76**, 1–13 (2016).
404. Serrano, M., Lin, A. W., McCurrach, M. E., Beach, D. & Lowe, S. W. Oncogenic ras provokes premature cell senescence associated with accumulation of p53 and p16(INK4a). *Cell* **88**, 593–602 (1997).
405. Wajapeyee, N., Serra, R. W., Zhu, X., Mahalingam, M. & Green, M. R. Oncogenic BRAF Induces Senescence and Apoptosis through Pathways Mediated by the Secreted Protein IGFBP7. *Cell* **132**, 363–374 (2008).
406. Courtois-Cox, S., Jones, S. L. & Cichowski, K. Many roads lead to oncogene-induced senescence. *Oncogene* **27**, 2801–2809 (2008).
407. Xu, Y., Li, N., Xiang, R. & Sun, P. Emerging roles of the p38 MAPK and PI3K/AKT/mTOR pathways in oncogene-induced senescence. *Trends in*

Biochemical Sciences **39**, 268–276 (2014).
408. Tu, Z., Aird, K. M. & Zhang, R. RAS, cellular senescence and transformation: The BRCA1 DNA repair pathway at the crossroads. *Small GTPases* **3**, 1–5 (2012).
409. Aponte, P. M. & Caicedo, A. Stem Cells, Cancer Stem Cells, and Their Microenvironment. *Stem Cells Int.* (2017). doi:10.1155/2017/5619472
410. Yun, M. H., Davaapil, H. & Brockes, J. P. Recurrent turnover of senescent cells during regeneration of a complex structure. *Elife* **4**, (2015).
411. Demaria, M. *et al.* An essential role for senescent cells in optimal wound healing through secretion of PDGF-AA. *Dev. Cell* **31**, 722–733 (2014).
412. Cahu, J., Bustany, S. & Sola, B. Senescence-associated secretory phenotype favors the emergence of cancer stem-like cells. *Cell Death Dis.* **3**, e446–e446 (2012).
413. Wang, L. *et al.* High-Throughput Functional Genetic and Compound Screens Identify Targets for Senescence Induction in Cancer. *Cell Rep.* **21**, 773–783 (2017).
414. O'Loghlen, A. *et al.* The nuclear receptor NR2E1/TLX controls senescence. *Oncogene* **34**, 4069–4077 (2015).
415. Tato-Costa, J. *et al.* Therapy-induced cellular senescence induces epithelial-to-mesenchymal transition and increases invasiveness in rectal cancer. *Clin. Colorectal Cancer* **15**, 170–178.e3 (2016).
416. Kaur, A. *et al.* Remodeling of the collagen matrix in aging skin promotes melanoma metastasis and affects immune cell motility. *Cancer Discov.* **9**, 64–81 (2019).
417. Hassona, Y., Cirillo, N., Heesom, K., Parkinson, E. K. & Prime, S. S. Senescent cancer-associated fibroblasts secrete active MMP-2 that promotes keratinocyte dis-cohesion and invasion. *Br. J. Cancer* **111**, 1230–1237 (2014).
418. Oubaha, M. *et al.* Senescence-associated secretory phenotype contributes to pathological angiogenesis in retinopathy. *Sci. Transl. Med.* **8**, 362ra144-362ra144 (2016).
419. Ksiazek, K., Jörres, A. & Witowski, J. Senescence Induces a Proangiogenic Switch in Human Peritoneal Mesothelial Cells. *Rejuvenation Res.* **11**, 681–683 (2008).
420. Luo, X. *et al.* Stromal-Initiated Changes in the Bone Promote Metastatic Niche Development. *Cell Rep.* **14**, 82–92 (2016).
421. Schosserer, M., Grillari, J. & Breitenbach, M. The Dual Role of Cellular Senescence in Developing Tumors and Their Response to Cancer Therapy. *Front. Oncol.* **7**, (2017).
422. Bianchi-Smiraglia, A., Lipchick, B. C. & Nikiforov, M. A. The immortal senescence. *Methods Mol. Biol.* **1534**, 1–15 (2017).

ANNEX

ANNEX

ANNEX 1:

"INHIBITION OF RANK SIGNALING IN BREAST CANCER INDUCES AN ANTI-TUMOR IMMUNE RESPONSE ORCHESTRATED BY CD8+T CELLS "

ANNEX 2:

"RANK SIGNALING INCREASES AFTER ANTI-HER2 THERAPY CONTRIBUTING TO THE EMERGENCE OF RESISTANCE IN HER2-POSITIVE BREAST CANCER"

Inhibition of RANK signaling in breast cancer induces an anti-tumor immune response orchestrated by CD8+ T cells.

Clara Gómez-Aleza[1#], Bastien Nguyen[2,3#], Guillermo Yoldi[1#], Marina Ciscar[1,4], Alexandra Barranco[1,4], Enrique Hernandez[1], Marion Maetens[2], Roberto Salgado[2,5], Maria Zafeiroglou[1], Pasquale Pellegrini[1], David Venet[2], Soizic Garaud[6], Eva M. Trinidad[1], Sandra Benítez[1], Peter Vuylsteke[7], Laura Polastro[8], Hans Wildiers[9], Philippe Simon[10], Geoffrey Lindeman[11], Denis Larsimont[12], Gert Van den Eynden[6], Chloé Velghe[13], Françoise Rothé[2], Karen Willard-Gallo[6], Stefan Michiels[14] , Purificación Muñoz[1], Thierry Walzer[15], Lourdes Planelles[16], Josef Penninger[17,18], Hatem A. Azim Jr[19], Sherene Loi[11], Martine Piccart[8], Christos Sotiriou[2*] and Eva González-Suárez[1,4*]

co-first authors

* co-corresponding authors

[1] Oncobell, Bellvitge Biomedical Research Institute, IDIBELL, Barcelona, Spain

[2] Breast Cancer Translational Research Laboratory J.-C. Heuson, Institut Jules Bordet, Université Libre de Bruxelles, Brussels, Belgium

[3] Marie-Josée and Henry R. Kravis Center for Molecular Oncology, Memorial Sloan Kettering Cancer Center, New York, NY 10065, USA

[4] Molecular Oncology, Spanish National Cancer Research Centre (CNIO), Madrid, Spain

[5] Department of Pathology GZA-ZNA Ziekenhuizen, Antwerp, Belgium

[6] Molecular Immunology Unit, Institut Jules Bordet, Université Libre de Bruxelles, Brussels, Belgium

[7] Department of Medical Oncology, Université Catholique de Louvain, CHU UCL, Namur, site Sainte-Elisabeth, Namur, Belgium

[8] Department of Medical Oncology, Institut Jules Bordet, Université Libre de Bruxelles, Brussels, Belgium

[9] Department of Oncology, KU Leuven-University of Leuven, Leuven, Belgium

[10] Department of Obstetrics and Gynaecology, Erasme, Université Libre de Bruxelles, Brussels, Belgium

[11] Peter MacCallum Cancer Centre, The Walter and Eliza Hall Institute of Medical Research and The Royal Melbourne Hospital, Melbourne, Australia

[12] Department of Pathology, Institut Jules Bordet, Université Libre de Bruxelles, Brussels, Belgium

[13] Clinical Trial Supporting Unit, Institut Jules Bordet, Université Libre de Bruxelles, Brussels, Belgium

[14] Service de Biostatistique et D'Epidémiologie, Gustave Roussy, CESP, U1018, Université Paris-Sud, Faculté de Médcine, Université Paris-Saclay, Villejuif, France

[15] Centre International de Recherche en Infectiologie, CIRI, Inserm U1111, CNRS, Université Claude Bernard Lyon, France

[16] BiOncotech Therapeutics, Parc Cientific Universitat Valencia, Spain

[17] Life Sciences Institute, University of British Columbia, Vancouver, Canada

[18] IMBA, Institute of Molecular Biotechnology of the Austrian Academy of Sciences, Vienna, Austria

[19] Department of Medicine, Division of Hematology/Oncology, American University of Beirut, Beirut, Lebanon.

ABSTRACT

Most breast cancers exhibit low immune infiltration and are unresponsive to immunotherapy. We hypothesized that inhibition of RANK signaling pathway may enhance immune activation. Loss of RANK signaling in mouse tumor cells increases leukocytes, lymphocytes, and $CD8^+$ T cells, and reduces macrophage and neutrophil infiltration. $CD8^+$ T cells mediate the attenuated tumor phenotype observed upon RANK loss, whereas neutrophils, supported by RANK-expressing tumor cells, induce immunosuppression. RANKL inhibition increases the anti-tumor effect of immunotherapies in breast cancer through a tumor cell mediated effect. Comparably, pre-operative single-agent denosumab in premenopausal early-stage breast cancer patients from the Phase-II D-BEYOND clinical trial (NCT01864798) was well tolerated, inhibited RANK pathway and increased tumor infiltrating lymphocytes and $CD8^+$ T cells. Higher RANK signaling activation in tumors and serum RANKL levels at baseline predict these immune-modulatory effects. No changes in tumor cell proliferation (primary endpoint) or other secondary endpoints were observed.

Our preclinical and clinical findings reveal that tumor cells exploit RANK pathway as a mechanism to evade immune surveillance and support the use of RANK pathway inhibitors to prime luminal breast cancer for immunotherapy.

INTRODUCTION

Breast cancer (BC) in young women has a unique biology and is associated with poor prognosis. Previous results support a role for the receptor activator of nuclear factor κB (RANK) signaling pathway in these tumors[1]. RANK pathway plays a crucial role in bone remodeling and mammary gland development[2,3], acting as a paracrine mediator of progesterone for the expansion of mammary stem/progenitor cells, and mediates the early steps of progesterone-driven mammary tumorigenesis[4–7]. Denosumab is a human monoclonal antibody against RANKL, approved for the prevention of skeletal morbidity associated with metastatic bone disease and the management of treatment-induced bone loss in early postmenopausal BC. Preclinical data reinforce the potential role of RANKL inhibitors such as denosumab in BC prevention[4,5,8,9] and treatment due to its ability to reduce recurrence and metastasis[10]. We previously found that RANK loss in the oncogene-driven mammary tumor model MMTV-PyMT (PyMT) significantly reduced tumor incidence and lung metastases[10]. Tumor cells lacking RANK showed delayed tumor onset and a reduced ability to initiate tumors and metastasis. Pharmacological inhibition of RANKL also reduced tumor-initiating ability and led to the lactogenic differentiation of tumor cells[10].

RANK and RANKL are expressed in a wide variety of immune cells[11] and are involved in various immune processes, including lymph node development[12], the activation of dendritic cells, monocytes and T cells, and the establishment of central and peripheral tolerance[11,13–22]. Thus, RANK pathway regulates innate and adaptive immune responses, and may promote or suppress immunity, depending on the context.

Tumor cells develop several strategies to evade immune surveillance: infiltration by cytotoxic T lymphocytes or natural killer (NK) cells is reduced and recruitment of immunosuppressive cells such as regulatory T cells (Tregs) and different myeloid

populations such as tumor-associated macrophages (TAMs) and tumor-associated neutrophils (TANs) is increased[23]. Immune-checkpoint inhibitors (mainly antibodies against cytotoxic T-lymphocyte associated protein 4, CTLA4, and programmed cell death protein 1, PD-1, and its ligand, PD-L1) have emerged as potent therapies against some solid tumors, such as melanoma and advanced non-small cell lung cancer (NSCLC)[24,25]. Nevertheless, in BC the efficacy of immunotherapy remains limited even after the inclusion of radiotherapy or chemotherapy[26], in particular in the immune "cold" luminal tumors.

Here, exploiting complementary genetic and pharmacological approaches in the PyMT tumor model[27], we investigated the effects of RANK pathway inhibition on mammary tumor immune surveillance. RANK and RANKL expression patterns in PyMT tumors resemble those found in human breast adenocarcinomas, with RANK being expressed in tumor cells and myeloid cells and RANKL in tumor-infiltrating lymphocytes (TILs)[4,10,28,29]. We found that RANK deletion in tumor cells, but not in myeloid cells, leads to an increase in immune, lymphocyte and $CD8^+$ T lymphocyte infiltration and a reduction in the infiltration of myeloid cells. TANs and $CD8^+$ T lymphocytes modulate the anti-tumor immune response driven by loss of RANK expression in tumor cells. Systemic RANKL inhibition also increased $CD8^+$ T cell infiltration and reinforced the anti-tumor benefits of checkpoint inhibitors in RANK-positive tumors. Importantly, the immune-modulatory effect of RANK signaling was confirmed in the D-BEYOND clinical trial, a prospective, pre-operative study evaluating denosumab and its biological effects in premenopausal early stage BC. Two courses of denosumab induced an increase in TILs and $CD8^+$ T cell infiltration. Increased activation of RANK signaling pathway in the tumors and circulating serum RANKL at baseline were identified as predictive biomarkers for the denosumab-driven increase in TILs. Together, these

results demonstrate the key role of RANK pathway in the tumor-immune crosstalk support the use of RANKL inhibitors, such as denosumab, for enhancing the immune response in poorly immunogenic luminal BC.

MATERIALS AND METHODS

Animals and *in vivo* treatments

All research involving animals was performed at the IDIBELL animal facility in compliance with protocols approved by the IDIBELL Committee on Animal Care and following national and European Union regulations. MMTV-PyMT (FVB/N-Tg(MMTV-PyVT)634Mul) were acquired from the Jackson Laboratory[30], and $RANK^{+}$/- (C57Bl/6) mice from Amgen Inc[19]. MMTV-PyMT; $RANK^{-/-}$ mice were obtained by backcrossing the MMTV-PyMT (FvB/N) strain with $RANK^{+/-}$ mice into the C57BL/6 background for at least ten generations. RANKflox/flox ($RANK^{fl/fl}$) were provided by Dr. Joseph Penninger[31] and crossed with either MMTV-PyMT-/+ or LysM-cre mice (MGI: 1934631) all in C57Bl/6 background. The athymic nude *Foxn1*^{nu} mice were obtained from Envigo. For RANK depletion in the MMTV-$PyMT^{-/+}$ $RANK^{fl/fl}$ tumors, cells were plated *in vitro* and infected with lentivirus produced in HEK293T cells. Lentiviral packaging plasmids psPAX2 (Adgene, 12260) and pMD2.G (Adgene, 12259), with either control pLVX-IRES-ZsGreen1 vector (Adgene, 632187) or pLVX-Cre-IRES-ZsGreen1, kindly provided by Dr. Alejandro Vaquero, were used, following Adgene's recommended protocol for lentiviral production. Tumor cells were cultured for 16 hours with 1:3 virus-containing medium and 72 h later, infected cells were FACs-sorted for zsGreen expression before being injected into syngeneic hosts.

RANK-Fc (10 mg/kg, Amgen) was injected subcutaneously three times a week[3,4]. Therapeutic anti-RANKL (clone IK22/5), anti-CTLA4 (clone 9D9), anti-PD-L1 (clone 10F.9G2) and isotype control rat IgG2A (clone 2A3) and mouse IgG2b (clone MCP-11) were obtained from BioXCell and 200 μg were administered intraperitoneally twice per week, for treatments starting 72 h after tumor cell injection, or three times per week for treatments of established tumors (size > 0.09 cm^2). For depletion experiments, anti-CD8

(300 μg, clone 53-5.8), anti-NK1.1 (200 μg, clone PK136), anti-Ly6G (first injection 400 μg, 100 μg thereafter, clone 1A8), and isotype controls mouse IgG2a (clone C1.18.4) and rat IgG1 (clone TNP6A7) were injected intraperitoneally. Treatment was administered on days -1, 0, 3, and 7 after tumor cell injection, and then once per week until sacrifice for CD8 and NK depletion. For neutrophil depletion, aLy6G was injected on day -1 and thereafter, three times weekly. In all cases, mice were sacrificed before tumors exceeded 10 mm in any dimension. Euthanasia by CO_2 inhalation was performed. Blood samples were taken flow cytometry analyses to check the depletion 7-10 days and 14-20 days after the first injection. Animals were randomized before beginning the treatment schedule. Mice were kept in individually ventilated and open cages and food and water were provided *ad libitum.*

Mouse tumor-cell isolation and tumor-initiation assays

Draining lymph nodes were removed and fresh tissues were mechanically dissected with a McIlwain tissue chopper and enzymatically digested with appropriate medium (DMEM F-12, 0.3% collagenase A, 2.5 U/mL dispase, 20 mM HEPES and penicillin-streptomycin 1x) for 40 min at 37°C. Samples were washed with Leibowitz L15 medium containing 10% fetal bovine serum (FBS) between each step. Erythrocytes were eliminated by treating samples with hypotonic lysis buffer (Lonza Iberica). Single cells were isolated by treating with trypsin (PAA Laboratories) for 2 min at 37°C. Cell aggregates were removed by filtering the cell suspension with a 70-μm filter and counted. For orthotopic transplants and tumor-limiting dilution assays tumor cells isolated from PyMT;$RANK^{+/+}$ or PyMT;$RANK^{-/-}$ (C57BL/6) mice were mixed 1:1 with Matrigel matrix (BD Biosciences) and orthotopically implanted in the inguinal mammary gland of 6-10-week-old syngeneic females or *Foxn1*^{nu} females. Mammary

tumor growth was monitored by palpation and caliper measurements three times per week. Lymph nodes were treated with hypotonic lysis buffer and then mashed through a 70-μm cell strainer to isolate single cells.

Flow cytometry

Single cells from tumors or lymph nodes were resuspended and blocked with PBS 2% FBS and blocked with FcR blocking reagent (Mylteni Biotec) for 10 min on ice and incubated for 30 min on ice with the corresponding surface antibodies: CD45-APCCy7 (0.125 μg/mL; 30-F11), CD11b-APC (2.5 μg/mL; M1/70), CD11b-PECy7 (2.5 μg/mL; M1/70), CD8-PE (1 μg/mL; 53-6.7), CD8-FITC (8 μg/mL; 53-6.7), CD4-PE-Cy7 (2 μg/mL; RM4-5), CD25-APC (2 μg/mL; PC61), Ly6C-FITC (1.25 μg/mL; HK1.4), Gr1-FITC (2 μg/mL; RB6-8C5), Ly6G-PECy7 (1.25 μg/mL; 1A8), F4/80-PE (1.25 μg/mL; BM8), CD3-PerCPCy5.5 (3.2 μg/mL; 145-2C11), CD3-APC (3.2 μg/mL; 145-2C11), Siglec-F- PerCP-Cy™5.5 (4 μg/mL, E50-2440) , CD19-PE (2.5 μg/mL, 6D5), NK1.1-PE (2.5 μg/mL; PK136), PD-1-PE (10 μg/mL; 29F.1A12), PD-L1-PECy7 (1.25 μg/mL; 10F.9G2) and anti-human CD11b-PECy7 (0.8 μg/mL; M1/70) from BioLegend. Apoptosis and necrosis were evaluated using the Annexin V Apoptosis Detection Kit (640930, BioLegend). 7AAD or LIVE/DEAD™ Fixable Green Dead Cell Stain Kit (488nm) from ThermoFisher was added in the various antibody combinations to remove dead cells. The following antibodies were used for intracellular staining: IFNγ-PE (2 μg/mL; XMG1.2); CTLA4-PerCPCy5.5 (10 μg/mL; UC10-4B9), CTLA4-PECy7 (5 μg/mL; UC10-4B9) from BioLegend, and FOXP3-FITC (10 μg/mL; FJK-16s), IL-12-FITC (2 μg/mL; C17.8) from eBioscience. Single-cell suspensions were stimulated in Leibowitz L15 medium containing 10% FBS, 10 ng/mL PMA, 1 μg/mL ionomycin and 5 μg/mL brefeldin A (for IFNγ and CTLA4) or just 5 μg/mL brefeldin A (for IL-12) for

4 h at 37°C. Surface antibodies were stained first, then fixed with PFA 4% (in the case of cytokines) or Fixation Reagent of the Foxp3/Transcription Factor Staining Buffer Set from eBioscience (in the case of FOXP3), and permeabilized using Permeabilization Buffer of the Foxp3/Transcription Factor Staining Buffer Set from eBioscience. The intracellular proteins were then stained. FACS analysis was performed using FACS Canto and Diva software. Cells were sorted using MoFlo (Beckman Coulter) at 25 psi with a 100-μm tip.

Blood samples were collected in tubes containing heparin and stained with CD45-APC-Cy7 (0.125 μg/mL; 30-F11), CD11b-APC (2.5 μg/mL; M1/70), CD3-PerCPCy5.5 (3.2 μg/mL; 145-2C11), CD8-PE (1 μg/mL; 53-6.7), NK1.1-PE (2.5 μg/mL; PK136), Ly6G-PECy7 (1.25 μg/mL; 1A8) and Gr1-FITC (2 μg/mL; RB6-8C5) for 30 min at RT in the dark. Versalyse (Beckman Coulter) containing 0.1% paraformaldehyde (PFA) was added to the samples and incubated for 10 min at RT in the dark before passing them through the cytometer.

Immunohistochemistry in mouse tumor tissues

Mouse tissue samples were fixed in formalin and embedded in paraffin. 3-μm sections were cut for histological analysis and stained with hematoxylin and eosin. 3-μm tissue sections were used for immunostaining. Primary antibody was incubated overnight at 4°C, detected with biotinylated secondary antibodies and streptavidin horseradish peroxidase (Vector) and revealed with DAB substrate (DAKO). CD3 and CD8 immunostaining was performed in the Histopathology Core Unit of the Spanish National Cancer Research Centre (CNIO, Madrid, Spain), using antibodies CD3 (clone M20 from Santa Cruz Biotechnology) and CD8 (clone 94A from the Monoclonal Antibodies Core Unit of the CNIO). For RANK IHC, antigen retrieval was performed

with Protease XXIV at 5 U/ml for 5 minutes (P8038, Sigma) and the anti-RANK (R&D AF692, 1:200).

Real-time PCR

Total RNA was extracted with Tripure Isolation Reagent (Roche) or Maxwell RSC Simply RNA Tissue kit (AS1340, Promega). Frozen tumor tissues were fractionated using glass beads (Sigma-Aldrich) and the PrecCellys® 24 tissue homogenizer (Berting Technologies) and Polytron PT 1200e (Kinematica). cDNA was produced by reverse transcription using 1 µg of RNA in a 35-µL reaction with random hexamers following the kit instructions (Applied Biosystems). In the case of sorted cells, RNA was retrotranscribed with Superscript II Reverse Transcriptase in a 20-µL reaction carried out according to manufacturer's instructions (ThermoFisher). 20 ng/well of cDNA for whole tumors were analyzed by SYBR green real-time PCR with 10-µM primers using a LightCycler® 480 thermocycler (Roche). Analyses were performed in triplicate. *Hprt1* was used as the reference gene. The following primer sequences were used for each gene:

Gene	Forward primer	Reverse primer
Hprt1	5'-TCAGTCAACGGGGGACATAAA-3'	5'- GGGGCTGTACTGCTTAACCAG-3'
Prf1	5'-CTGGATGTGAACCCTAGGCC-3'	5'-GCGAAAACTGTACATGCGAC-3'
Ifnγ	5'-CACGGCACAGTCATTGAAAG-3'	5'-CCATCCTTTTGCCAGTTCCTC-3'
Il-1β	5'-CAACCAACAAGTGATATTCTCCATG-3'	5'-GATCCACACTCTCCAGCTGCA-3'
Casp4	5'-AATTGCCACTGTCCAGGTCT-3'	5'-CTCTGCACAACTGGGGTTTT-3'

S100a9	5'-TCAGACAAATGGTGGAAGCA-3'	5'- GTCCTGGTTTGTGTCCAGGT-3'

For human cell line samples, the following primer sequences were used:

Gene	Forward primer	Reverse primer
PPIA	5'-GGGCCTGGATACCAAGAAGT-3'	5'-TCTGCTGTCTTTGGGACCTT-3'
BIRC3	5'-GGTAACAGTGATGATGTCAAATG-3'	5'-TAACTGGCTTGAACTTGACG-3'
ICAM1	5'-AACTGACACCTTTGTTAGCCACCTC-3	5'-CCCAGTGAAATGCAAACAGGAC-3
NFkB2	5'-GGCGGGCGTCTAAAATTCTG-3'	5'-TCCAGACCTGGGTTGTAGCA-3'
RELB	5'-TGTGGTGAGGATCTGCTTCCAG-3'	5'-TCGGCAAATCCGCAGCTCTGAT-3'

Mouse RNA labeling and hybridization to Agilent microarrays

Hybridization to the SurePrint G3 Mouse Gene Expression Microarray (ID G4852A, Agilent Technologies) was conducted following the manufacturer's two-color protocol (Two-Color Microarray-Based Gene Expression Analysis v. 6.5, Agilent Technologies). Dye swaps (Cy3 and Cy5) were performed on RNA amplified from each sample. Microarray chips were then washed and immediately scanned using a DNA Microarray Scanner (Model G2505C, Agilent Technologies).

Tumor acinar cultures and cytokine array

Isolated tumor cells coming from $RANK^{+/+}$ or $RANK^{-/-}$ transplants were seeded on top of growth factor-reduced matrigel (1 million cells/well in 6-well plates) in growth medium (DMEM-F12, 5% FBS, 10 ng/mL of EGF, 100 ng/mL cholerin toxin, 5 μg/mL insulin and 1x penicillin/streptomycin).

For cytokine arrays, tumor supernatants were collected 72h after plating. A pool of three supernatants derived from three independent tumor transplants and primary tumors was used for the analyses. Multiplex quantification of cytokines and chemokines of supernatants collected from 3D acinar cultures was performed using the Mouse Cytokine Array C1000 (RayBiotech) following manufacturer's instruction and using the recommended ImageJ plug-in. To detect genes affected by RANK activation, 1 µg/mL RANKL was added 24 h after tumor plating. RNA was extracted 24 h after RANKL stimulation for hybridization to a gene expression microarray, as previously described.

Cell line culture and lentiviral transduction

The human breast cancer cell lines MCF-7 and HCC1954 were purchased from the American Type Culture Collection (ATCC). ATCC provides molecular authentication in support of their collection through their genomics, immunology, and proteomic cores, as described, by using DNA barcoding and species identification, quantitative gene expression, and transcriptomic analyses (ATCC Bulletin, 2010). Cells were grown in DMEM and RPMI 1640 medium, respectively, supplemented with 10% fetal bovine serum (FBS) and 1% penicillin-streptomycin solution (all from Gibco). The cells were grown at 37°C in the presence of 5% CO_2 in humidified incubators and were tested for absence of mycoplasma.

To ectopically express GFP (control) or RANK (*TNFRSF11A*), the corresponding genes were cloned in the lentiviral vector pSD-69 (PGK promoter, generously donated by S Duss and M Bentires-Alj) following Gateway cloning protocols. To knock down the expression of endogenous RANK we used the lenti-viral vector pGIPZ clones V3LHS_307325 and V3LHS_400741 with RANK specific shRNA expression (Dharmacon). As a control (ctrl) we used a verified non-targeting clone (Dharmacon).

Lentiviruses were prepared in HEK293T cells with packaging and envelope plasmids psPAX2 and pMD2.G (AdGene). Transduced cells were selected with 1.5 µg/ml puromycin, starting 3 days after infection.

Human neutrophil and T cell isolation and culture

Peripheral blood was provided by the "Banc de Sang I Teixits" (Hospital Universitari de Bellvitge). Mononuclear cells were isolated from buffy coats using Ficoll-plus gradient (GE Healthcare Bio-Sciences). Neutrophils were isolated from the red fraction, then purified by dextran sedimentation. Purified cells were resuspended at 5 x 10^6 cells/mL in RPMI supplemented with 10% of FBS and 50 U/mL streptomycin and penicillin. FACS analysis was performed to detect CD66b (G10F5, BD Bioscience) to confirm purity (98% average).

Neutrophil apoptosis and activation were analyzed culturing 10^4 neutrophils per well in 96-well plates over 24 h in the indicated medium or CM. Apoptosis was measured using the Annexin AV Apoptosis Detection Kit (640930, BioLegend) and activation was detected by staining for CD11b following the previously described flow cytometry staining protocol.

Clinical trial design and patient characteristics

Twenty-seven patients were enrolled in the D-BEYOND trial between October 2013 and July 2016 (first patient enrolled 2nd October; last patient enrolled 9th June 2016). D-BEYOND was a prospective, single arm, multi-center, open label, preoperative "window-of-opportunity" phase IIa trial (NCT01864798). All patients received two injections of denosumab 120 mg subcutaneously, administered 7 to 12 days apart, prior to surgical intervention. Surgery was performed 10-21 days after the first dose of denosumab (median, 13 days). Post-study treatment was at the discretion of the

311 investigator. Snap-frozen and formalin-fixed, paraffin-embedded (FFPE) tumor and
312 normal tissues were collected at baseline (pre-treatment) and at surgery (post-
313 treatment). Normal tissues (snap-frozen and FFPE) were defined as being at least 1cm
314 away from tumor, another quadrant or contralateral breast biopsies. All samples
315 (including normal) were reviewed by a pathologist to assess epithelial content. Eligible
316 patients were premenopausal women with histologically confirmed newly diagnosed
317 operable primary invasive carcinoma of the breast who had not undergone previous
318 treatment for invasive breast cancer. Other key eligibility criteria included a tumor size
319 > 1.5 cm, any nodal status, and known estrogen receptor (ER), progesterone receptor
320 (PR), human epidermal growth factor receptor 2 (HER2) status. Key exclusion criteria
321 included bilateral invasive tumors, current or previous osteonecrosis or osteomyelitis of
322 the jaw, and known hypersensitivity to denosumab. Evaluation of conventional breast
323 cancer markers including ER, PR, HER2 and Ki-67 were centrally performed at the
324 Institut Jules Bordet (IJB). ER and PR status were defined according to ASCO-CAP
325 guidelines. Breast cancer subtypes were defined according to the St Gallen 2015
326 Consensus Meetings[32] using immunohistochemical surrogates as follows: Luminal A:
327 ER and/or PR(+), HER2(-), Ki-67 < 20%; Luminal B: ER and/or PR(+), HER2(-), Ki-
328 67 ≥ 20; Basal: ER(-), PR(-) and HER2(-), irrespective of Ki-67 score; and HER2:
329 HER2(+), irrespective of ER, PR or Ki-67. All 4 HER2+ patients included in the study
330 were ER+ PR+.
331 Serious and non-serious adverse events (AEs) were collected from the day of signed
332 informed consent until one month after the final administration of the study drug, except
333 for the project-specific AEs, for which the reporting was extended to 3 months after the
334 final dose of denosumab. Safety data were evaluated using the National Cancer Institute
335 Common Terminology Criteria for Adverse Events (NCI-CTCAE v 4.0). AEs were

coded according to the Medical Dictionary for Regulatory Activities (version 20.1). All non-serious AEs are summarized in Table S6, the most frequent one being arthralgia (4/27, 14.8%). This study was approved by the Ethics Committee of the trial sponsor; IJB (N°: 2064) and all the other participant sites. All patients provided written informed consent prior to study entry.

One patient was excluded because she had a ductal *in situ* carcinoma and two patients were excluded because of lack of available tumor tissue. Another patient was excluded from TIL evaluation due to tissue exhaustion. The primary study endpoint was a geometric mean decrease in the percentage of Ki-67-positive cells assessed by immunohistochemistry (IHC). Key secondary endpoints included absolute Ki-67 responders (defined as < 2.7% Ki-67 IHC staining in the post-treatment tumor tissue), decrease in serum C-terminal telopeptide (CTX) levels measured by ELISA, cleaved caspase-3 and change in TIL percentage in tumor tissue evaluated on hematoxylin and eosin (HE) slides. Changes in the infiltration of immune populations as measured by IHC were also performed. Paired samples of breast tumor and normal tissue at baseline and at surgery were required. The limited epithelial content precluded analyses of changes in the paired normal tissues. Gene expression analyses in paired tumor and normal tissue at baseline and at surgery was performed for patients with enough epithelial content. Additional secondary endpoints include: change in RANK/RANKL gene expression and signaling, change in tumor proliferation rates using gene expression, change in expression levels from genes corresponding to mammary progenitor populations, estrogen pathways, immune pathways, gene expression changes in the paired samples of surrounding normal tissue when available. All primary, secondary and exploratory endpoints performed are described in Supplementary file 1.

ELISA

Serum concentrations of human sRANKL (soluble homotrimeric form of RANKL) were centrally assessed at IJB in triplicate, using an enzyme-linked immunosorbent assay (ELISA) according to the manufacturer's instructions (Biomedica, Austria). sRANKL bound to denosumab is not be detected by this assay. Serum CTX levels were routinely evaluated in each center by ELISA.

Pathological assessment and immunohistochemical staining of human tumor samples

Tumor cellularity was centrally assessed on hematoxylin and eosin-stained (HE) tissue sections from FFPE and frozen human tumor samples. For patients with multiple samples, the sample with the highest tumor content was chosen for further analyses. The percentage of intratumoral and stromal TILs was independently evaluated by two trained pathologists (R.S. and G.V.D.E.) who were blinded to the clinical and experimental data on the HE slides, following the International TIL Working Group 2014 methodology, as described elsewhere[33]. Median tumor cellularity ranged between 35 and 90%. TIL proliferation was assessed as the percentage of $Ki67^+$ TILs among all TILs.

Tissue sections (4 μm) from FFPE tissues of human primary breast tissue were used to assess RANK and RANKL. For each patient, representative unstained slides of the primary tumor were shipped to NeoGenomics Laboratories (California, USA) for immunohistochemical staining of RANK (N1H8, Amgen) RANKL (M366, Amgen), blinded to clinical information. The percentage of stained cells and their intensity (0, negative; 1^+, weak; 2^+, moderate; and 3^+, strong) were recorded as described previously[26].

An H-score was calculated using the following formula: H = (% of cells of weak intensity x 1) + (% of cells with moderate staining x 2) + (% of cells of strong staining x 3). The maximum possible H-score is 300, corresponding to 100% of cells with strong intensity.

Serial FFPE tissue sections (4 μm) were immunohistochemically stained for CD3/CD20, CD4/CD8, and FOXP3/CD4 dual-staining as well as single Ki-67 and cleaved caspase-3 staining on a Ventana Benchmark XT automated staining instrument (Ventana Medical Systems) as described previously[34]. The antibodies used for dual IHC are: CD3 (IR503, polyclonal), CD8 (C8/144B, IR623) and CD20 (L26, IR604) from Dako, CD4 (RBT-CD4, BSB5150) from BioSB and FOXP3 (236A/E7, 14-4777-82) from E-Bioscience, Ki-67 (Clone MIB-1) from Dako and cleaved caspase-3 (ab2302) from Abcam. T cells were quantified by CD3 protein expression, B cells by CD20 protein expression, cytotoxic T cells by CD4 negative and CD8 positive expression, and T regulatory cells by simultaneous CD4 and FOXP3 expression. Scoring was defined as the percentage of immune-positive cells among stromal and tumoral area.

For multiplex IHC (mIHC), FFPE tissue sections (4 μm) were processed manually. Briefly, slides were heated at 37°C overnight, deparaffinized and then fixed in neutral-buffered 10% formalin. The presence of helper T cells (CD4), cytotoxic T cells (CD8), B cells (CD20), regulatory T cells (FOXP3), macrophages (CD68), cancer cells (pan-cytokeratin) and cell nuclei (DAPI) was assessed using a serial same-species fluorescence-labeling approach that employs tyramide signal amplification and microwave-based antigen retrieval and antibody stripping in accordance with the manufacturer's instructions (Opal Multiplex IHC, Perkin Elmer). Staining was visualized on a Zeiss LSM 710 confocal microscope equipped with PMT spectral 34-

Channel QUASAR (Carl Zeiss). All IHC slides were centrally reviewed by a breast pathologist (R.S.).

RNA extraction from human samples and RNA sequencing

RNA was extracted from frozen tumor and normal tissue using the AllPrep DNA/RNA Mini kit (Qiagen, Germany) according to the manufacturer's instructions. RNA quality was assessed using a Bioanalyzer 2100 (Agilent Technologies). A total of 22 patients had sufficient tumor RNA quantity from both pre- and post- treatment timepoints. A total of 11 patients had sufficient RNA quantity in normal tissue samples from both pre- and post- treatment timepoints. Among the patients without enough RNA quantity in normal tissue, six had biopsies containing mainly fatty tissue without any epithelial cell. Indexed cDNA libraries were obtained using the TruSeq Stranded Total RNA Kit (Illumina) following the manufacturer's recommendations. The multiplexed libraries were loaded onto a NovaSeq 6000 apparatus (Illumina) using a S2 flow cell, and sequences were produced using a 200 Cycle Kit (Illumina).

Bioinformatic analyses

RNA-sequencing read pairs from the D-BEYOND samples were trimmed using Trimmomatic[35]. Alignment was performed using STAR[31]. The number of reads mapping to each gene was assessed with the Rsamtools package in the R environment. Since gene expression profiles of tissues taken at biopsy and surgery are known to be sensitive to differences in tissue-handling procedures[36], we used a publicly available dataset from the no-treatment arm of The Peri Operative Endocrine Therapy - Individualizing Care (POETIC) study to filter-out differentially expressed genes. This study included 57 pairs of samples from untreated patients taken at diagnosis (baseline)

and surgery (GEO ID: GSE73235[36]). We filtered out 3270/21.931 (14.9%) genes that were differentially expressed between diagnosis and surgery by using a strict cut-off of a raw value of $P < 0.05$ from a non-parametric Mann–Whitney U test. Differential expression was analyzed with DESeq2 v.1.14.1 R/Bioconductor package[37] using raw count data. Significantly differentially expressed genes were selected if they had a qval of < 0.05 and an absolute log2-fold change of > 0.5. We used the GAGE v.2.24.0 R/Bioconductor package[38] to identify significantly enriched biological processes from the Biological Process from Gene Ontology database. CIBERSORT software was used[39] to refine the subsets of immune cells present in each sample. RPKM expression data were uploaded to www.cibersort.standford.edu and CIBERSORT was run using LM22 as a reference matrix and, as recommended for RNA-seq data, quantile normalization was disabled.

All other parameters were set to default values. Output files were downloaded as tab-delimited text files and immune cell subsets that were present in fewer than 10 samples were discarded.

We reported the 10 aggregates as described before [PMID: 29628290]:

T.cells.CD8 = T.cells.CD8,

T.cells.CD4 = T..CD4.naive + T..CD4.memory.resting + T..CD4.memory.activated,

T.reg = T.cells.regulatory..Tregs.

B.cells = B.cells.naive + B.cells.memory,

NK.cells = NK.cells.resting+NK.cells.activated,

Macrophage = Macrophages.M0 + Macrophages.M1 + Macrophages.M2,

Dendritic.cells = Dendritic.cells.resting + Dendritic.cells.activated,

Mast.cells = Mast.cells.resting + Mast.cells.activated,

Neutrophils = Neutrophils,

Eosinophils = Eosinophils

RNAseq data have been deposited under EGA accession number **EGAS00001003252** as a fatsq file (available on request from the IJB Data Access Committee).

The prototype-based co-expression module score for *TNFRSF11A* (RANK metagene) and *TNFSF11* (RANKL metagene) was computed for each sample as; $module\ score = \sum_{i=1}^{100} w_i x_i$. Where x_i is the expression of the top 100 genes positively correlated with *TNFRSF11A* or *TNFSF11* at baseline (before treatment) and w_i is the Pearson correlation coefficient between x_i and *TNFRSF11A* or *TNFSF11*.

The public signatures of RANK/NFκB were retrieved from MSigDB[40] (Cell Systems, PMID:26771021) and computed using the geometric mean and then scaling.

Mouse microarray data were feature-extracted using Agilent's Feature Extraction Software (v. 10.7), using the default variable values.

Outlier features in the arrays were flagged by the same software package. Data were analyzed using the *Bioconductor* package in the R environment. Data preprocessing and differential expression analysis were performed using the *limma* and *RankProd* packages, and the most recently available gene annotations were used. Raw feature intensities were background-corrected using the *normexp* background-correction algorithm. Within-array normalization was done using spatial and intensity-dependent *loess*. *Aquantile* normalization was used to normalize between arrays. The expression of each gene was reported as the base 2 logarithm of the ratio of the value obtained for each condition relative to the control condition. A gene was considered differentially expressed if it displayed a *pfp* (proportion of false positives) < 0.05, as determined by a non-parametric test. Raw microarray data have been deposited in GEO, access number GSE119464.

Statistical analyses

All statistical tests comparing pre- and post-treatment paired values were done using the sign test or Student's paired samples t-test. All IHC values were log-transformed to give values of $\log_{10}(x + 1)$, thereby overcoming the problem of some raw variable values being zero. To compare non-responders and responders, the Mann–Whitney U and Fisher's exact tests were used for continuous and categorical variables, respectively. All correlations were measured using the Spearman's non-parametric *rho* coefficient. All reported P-values were two-tailed. All analyses were performed using R version 3.3.3 (available at www.r-project.org) and Bioconductor version 3.6. No correction was made for multiple testing for exploratory analyses, except for the gene expression analysis, for which the false discovery rate (FDR) was used.

Mouse experimental data were analyzed using GraphPad Prism version 5. Differences were analyzed with a two-tailed Student's t-test, an F-test or an unpaired-samples t-test against a reference value of 1. Tumor growth curves were compared using two-way analysis of variance. Frequency of tumor initiation was estimated using the extreme limiting dilution assay (ELDA) (http://bioinf.wehi.edu.au/software/elda/). Regression analysis of the growth curves' mean for the anti-CTLA4, anti-RANKL, and anti-PD-L1 treatments was performed, and 2 x 2 chi-square contingency tables (two-tailed probabilities) were used to evaluate responses. The statistical significance of group differences is expressed by asterisks: *, $p < 0.05$; **, $p < 0.01$; ***, $p < 0.0001$; ****, $p < 0.0001$).

RESULTS

Loss of RANK in tumor cells leads to increased lymphocyte infiltration

We hypothesized that, beyond its tumor cell-intrinsic effects[10], inhibition of RANK signaling pathway may enhance immune activation in BC. To test this hypothesis, we undertook genetic approaches using the PyMT luminal tumor mouse model. First, we tested whether loss of RANK signaling in myeloid cells could induce changes in immune infiltration, by using LysM-cre/RANK$^{flox/flox}$ mice. Expression of Cre driven by LysM deletes RANK in the myeloid compartment (RANK MC$^{-/-}$)[41]. As expected, lower levels of *Rank* mRNA were found in peritoneal macrophages from RANK MC$^{-/-}$ mice (Figure 1a). PyMT RANK$^{+/+}$ (RANK$^{+/+}$) tumors were orthotopically transplanted in RANK MC$^{-/-}$ mice and corresponding controls (RANK MC$^{+/+}$) (Figure 1a). Analyses of the tumor immune infiltrates revealed no changes in immune infiltration, leukocytes (CD45^{+}), lymphocytes (CD11b^{-} within CD45^{+}), TAMs (F4/80^{+}CD11b^{+} within CD45^{+}) or TANs (Ly6G^{+} CD11b^{+} within CD45^{+}) between genotypes (Figure 1b, S1a-b). The frequencies of infiltrating CD8^{+} T cells (CD11b^{-} CD3^{+} CD8^{+}), CD4^{+} T cells (CD11b^{-} CD3^{+} CD8^{-}), and the CD4/CD8 ratio were also similar in RANK$^{+/+}$ tumors growing in RANK MC$^{-/-}$ or RANK MC$^{+/+}$ mice (Figure S1a-b).

We next tested whether RANK loss exclusively in tumor cells could alter tumor immune infiltration: tumors derived from PyMT/RANK$^{-/-}$ mice (RANK$^{-/-}$ tumors) were orthotopically transplanted in syngeneic C57Bl6 mice and compared with RANK$^{+/+}$ tumor transplants (Figure 1c). RANK$^{-/-}$ tumors showed greater infiltration by leukocytes, lymphocytes and CD8^{+} T cells compared with RANK$^{+/+}$ tumors of similar size (Figure S1a, S1c). Together these results demonstrate that loss of RANK in tumor cells, but not in myeloid cells, induces an increase in tumor-immune infiltrates, TILs and CD8^{+} T cells.

T cells mediate the longer tumor latency of RANK$^{-/-}$ tumors

The increase in TILs observed after loss of RANK in tumor cells, prompted us to investigate the functional contribution of this immune population. To this end, RANK$^{+/+}$ and RANK$^{-/-}$ tumor cells were transplanted in parallel in syngeneic mice and in T cell-deficient *Fox1^{nu}* mice (Figure 1c). We had previously demonstrated that, compared with RANK$^{+/+}$, RANK$^{-/-}$ tumor cells display prolonged latency to tumor formation, increased apoptosis and a lower frequency of tumor-initiating cells when transplanted in syngeneic mice[10].

Strikingly, when transplanted in T cell-deficient *Foxn1^{nu}* mice, no differences in latency to tumor onset were observed between RANK$^{+/+}$ and RANK$^{-/-}$ tumor transplants, while the same tumors transplanted in syngeneic C57BL/6 mice corroborated previous results (Figure 1d and Figure S2a)[10]. Additionally, limiting dilution assays in *Foxn1^{nu}* mice showed no differences in the ability of RANK$^{+/+}$ and RANK$^{-/-}$ tumor cells to initiate tumors (Figure 1e). Further characterization of the tumors revealed that RANK$^{-/-}$ tumor transplants growing in syngeneic hosts contained more apoptotic and necrotic cells than did their RANK$^{+/+}$ counterparts (Figure S2b), corroborating previous findings[10]. However, the frequency of apoptotic cells was similar in RANK$^{-/-}$ and RANK$^{+/+}$ tumor cells growing in *Foxn1^{nu}* mice. Differences in late apoptosis/necrosis (7AAD^{+}/Annexin V^{+} cells) between RANK$^{+/+}$ and RANK$^{-/-}$ tumor cells were observed in both syngeneic and *Foxn1^{nu}* recipients but were less marked in T cell-deficient mice (Figure S2b). These observations suggest that the increased tumor cell death rate in the absence of RANK is due to a combination of tumor cell-intrinsic and T cell-mediated effects, whereas T cells are responsible for the delayed tumor onset and the reduced tumor-initiating ability of RANK-null tumor cells.

Analyses of $RANK^{+/+}$ and $RANK^{-/-}$ tumors confirmed the higher frequency of leukocytes and the enrichment in TILs in $RANK^{-/-}$ compared with $RANK^{+/+}$ tumors (Figure 1f-g; Figure S1c). In contrast, the relative frequency of TAMs and TANs was higher in $RANK^{+/+}$ than in $RANK^{-/-}$ tumors (Figure 1f-g, Figure S1c). These differences were no longer observed in *Foxn1*^{nu} transplants (Figure 1f-g).

To rule out the possibility that immune cells transplanted along with tumor cells were responsible for the observed changes, the $CD45^{-}$ population (tumor cell-enriched) was sorted and transplanted into syngeneic hosts. The longer tumor latency observed in $RANK^{-/-}$ was exacerbated when sorted $CD45^{-}$ cells were injected compared with whole tumor transplants (Figure S2c). Accordingly, differences in immune infiltration were also observed between tumors derived from sorted $CD45^{-}$ $RANK^{+/+}$ and $CD45^{-}$ $RANK^{-/-}$ cells and those derived from whole tumor transplants (Figure S2d).

To confirm that our findings are not affected by differences other than RANK status between $RANK^{+/+}$ and $RANK^{-/-}$ tumors, we infected PyMT/$RANK^{flox/flox}$ tumors with pLVX-Cre-IRES-zsGreen or control lentivirus. Infected tumor populations were FACS-sorted and orthotopically transplanted into C57BL/6 mice. RANK depletion was confirmed by RT-PCR and IHC (Figure S2e). RANK-depleted tumors showed lower tumor growth rate (Figure S2f) and greater infiltration of leukocytes, lymphocytes, and T cells ($CD3^{+}$ $CD11b^{-}$ $CD45^{+}$), corroborating previous findings (Figure S2g). $CD8^{+}$ T cells were more abundant, and TANs were reduced in RANK-depleted tumors, although the differences were not significant (Figure S2g). Thus, RANK loss in tumor cells leads to a significant increase in TILs.

Together, these results demonstrate that RANK loss in tumor cells leads to a significant increase in TILs that restrict $RANK^{-/-}$ tumor cell growth. Reciprocally, they indicate that RANK expression in tumor cells induces an immunosuppressive microenvironment

enriched in TAMs and TANs, allowing tumor cells to escape T cell immune surveillance.

$CD8^+$ T cell depletion rescues the delay in tumor onset of RANK-/- tumors

Further characterization of TIL subsets from syngeneic transplants (Figure S1a), revealed a significant increase in the percentage of $CD3^+$ T lymphocytes and $CD8^+$ T cells in $RANK^{-/-}$ tumors and a lower $CD4^+/CD8^+$ ratio in $RANK^{-/-}$ compared with the $RANK^{+/+}$ tumors (Figure 2a). There were no significant differences between the two groups in the frequencies of NK cells ($NK1.1^+$ $CD3^-$), B cells ($CD19^+$ $CD3^-$ $CD11b^-$) or levels of IFNγ production by tumor-infiltrating $CD4^+$ and $CD8^+$ T cells (Figure S3a). However, TAMs that infiltrated $RANK^{-/-}$ tumors expressed higher levels of IL12/IL23, indicative of an anti-tumor M1 response (Figure S3a). Increased $CD3^+$ T lymphocyte and $CD8^+$ T cell tumor infiltration in $RANK^{-/-}$ tumors compared with $RANK^{+/+}$ was confirmed by IHC (Figure 2b-c) and the mRNA levels of the cytotoxicity markers, namely interferon gamma (*Ifnγ)* and perforin (P*rf1)* were higher in $RANK^{-/-}$ tumors (Figure 2d). Gene expression analysis comparing sorted $CD45^-$ cells (tumor cell-enriched) isolated from $RANK^{+/+}$ versus $RANK^{-/-}$ tumor transplants revealed 604 differentially expressed genes (Table S1). Gene Ontology (GO) and Generally Applicable Gene Set Enrichment (GAGE) analyses revealed that $RANK^{-/-}$ tumor cells overexpressed a subset of genes related to the "intrinsic apoptotic signaling pathway", "antigen processing and presentation" and "positive regulation of T cell-mediated cytotoxicity" (Tables S2-S4). Similar frequencies of $CD3^+$, $CD4^+$ and $CD8^+$ cells were found in draining lymph nodes from $RANK^{+/+}$ and $RANK^{-/-}$ tumor transplants, but a moderate increase in IFN_γ production in the lymph node T cells was observed in the $RANK^{-/-}$ tumor transplants (Figure S3b).

Next, we investigated the effects on the tumor immune infiltrate after systemic pharmacological inhibition of RANKL (RL) (RANK-Fc treatment 10 mg/kg three times per week, for 4 weeks) in serial tumor transplants from PyMT mice (Figure S3c)[42]. No significant changes in the total number of TILs upon RL inhibition were observed (Figure S3d-e). However, after RL inhibition, the frequency of infiltrating $CD8^+$ T cells increased (Figure S3d) and $CD4^+$ T cells decreased (Figure S3e), leading to a lower $CD4^+/CD8^+$ ratio (Figure S3d-e). An increased infiltration by $CD8^+$ T cells in tumors continuously treated with RL inhibitor was also observed by IHC (Figure 2e-f). Together, these evidences demonstrate that genetic or pharmacologic inhibition of RANK signaling increases $CD8^+$ T cell tumor infiltration.

$CD8^+$ T and NK cells have been shown to drive tumor cell cytotoxicity[23], therefore depletion experiments were performed in $RANK^{+/+}$ and $RANK^{-/-}$ tumor transplants to confirm their involvement (Figure 2g). Depletion of $CD8^+$ T cells, but not of NK cells, rescued the delayed tumor formation observed in $RANK^{-/-}$ transplants with minor effects on $RANK^{+/+}$ transplants (Figure 2h). $CD8^+$ T and NK cell depletions were corroborated in blood samples and tumor infiltrates (Figure S4a-b). $CD8^+$ T cell depletion resulted in increased NK cell frequency in tumors and, conversely, NK cell depletion led to increased $CD8^+$ T cell infiltration (Figure 2i). These results suggest that $CD8^+$ T cells mediate the anti-tumorigenic response induced by RANK loss in tumor cells and that the exacerbated T cell response in $RANK^{-/-}$ tumors is responsible for the delay in tumor formation.

RANK+ tumor cells promote immunosuppression through neutrophils

To clarify the intercellular crosstalk involved in the observed phenotypes we cultured 3D tumor acini from $RANK^{+/+}$ and $RANK^{-/-}$ tumor transplants for 72 h and measured

the levels of cytokines and chemokines in the culture supernatants (Table S5). Fewer cytokines/chemokines were more abundant in $RANK^{-/-}$ than $RANK^{+/+}$ tumor supernatants, and included eotaxin 1, which is involved in eosinophil recruitment, CD40, which enhances T cell responses, and BLC, which controls B cell trafficking[43] (Figure 3a). However, no significant differences in the frequencies of eosinophils or B cells were found in $RANK^{-/-}$ as compared to $RANK^{+/+}$ tumor transplants (Figure S3a). In supernatants derived from $RANK^{+/+}$ tumor acini many cytokines were upregulated including SDF-1α, MIP-1α, IL-1α, SCF, TNFα, IL-13, M-CSF, IL-10, IL-4, IL-17 and IL-1β (Table S5, Figure 3a). These various cytokines/chemokines are characteristic of an immunosuppressive microenvironment and have a wide-ranging actions, including myeloid cell recruitment[43]. The mRNA expression levels of *Il-1β* and *Caspase-4*, which mediates the activation of pre-IL1-β in the inflammasome[44] were also higher in $RANK^{+/+}$ tumors, while *s100a9*, a gene related to neutrophil stimulation and migration, showed a tendency to increase[45], (Figure 3b). These changes may contribute to the increased infiltration of TANs observed in $RANK^{+/+}$ tumors (Figure 1f-g, Figure S1c, S2d) and the suppression of T cell immunity as previously reported[46,47]. In fact, the percentage of TANs ($Ly6G^{+}$) and that of $CD8^{+}$ T cells were negatively correlated in the mouse tumors (Figure 3c).

To confirm the crosstalk between RANK activation in BC cells and neutrophils, we adopted an independent experimental approach by modulating RANK expression levels in human BC cells and directly testing in co-culture assays whether this influenced neutrophil survival and activation. MCF7 luminal BC cells that had undetectable RANK expression and were unresponsive to RL stimulation, were infected with RANK-overexpressing vectors (Figure S4c). Conversely, HCC1954 basal-like, $HER2^{+}$ cells, which, despite the low levels of RANK expression, are responsive to RANKL

stimulation, were infected with short-hairpin RNAs to downregulate RANK (Figure S4c). Changes in RANK expression and downstream targets (*BIRC3, ICAM1, NFKB2, RELB*) were confirmed by RT-PCR (Figure S4c).

BC cells were stimulated with RL for one hour before co-culturing with neutrophils, isolated from blood of healthy human donors (Figure S4d). MCF7-RANK tumor cells and HCC1954-shSCR cells increased neutrophil survival more than their corresponding tumor cells lacking RANK did (Figure S4e). Conditioned medium (CM) from BC cells with higher level of RANK expression and activation was enough to increase the survival of neutrophils significantly more than CM from control cells (Figure 3d). These neutrophils also presented a more mature/active phenotype based on the increased CD11b levels (Figure 3e)[48].

Finally, to confirm whether neutrophils are involved in the observed differences in latency between $RANK^{+/+}$ and $RANK^{-/-}$ tumor transplants and the crosstalk with T cells, Ly6G depletion assays were performed (Figure 3f). Neutrophil depletion significantly delayed tumor appearance in $RANK^{+/+}$ transplants with no effects in $RANK^{-/-}$ transplants (Figure 3g). Neutrophil depletion was confirmed in blood samples (Figure S4f-g). The frequency of TANs after depletion was reduced in $RANK^{+/+}$ but not in $RANK^{-/-}$ tumor transplants, in which TAN infiltration was much lower (Figure 3h). Neutrophil depletion led to a significant increase in TILs, $CD4^+$ and $CD8^+$ T cells, and to a decrease in the frequency of TAMs infiltrating $RANK^{+/+}$ transplants to levels comparable with those found in $RANK^{-/-}$ transplants (Figure 3h). A trend to increased levels of total leukocyte infiltration was also observed after neutrophil depletion ($p = 0.06$, Figure 3h).

Altogether, these results suggest that RANK activation in tumor cells induces an immunosuppressive microenvironment that favors neutrophil survival restricting T cell immunity.

RANKL inhibition in tumor cells increases responsiveness to immunotherapy

Despite the stronger anti-tumor immune response, $RANK^{-/-}$ tumors eventually evade the immune response and grow. Increased expression of checkpoint regulators such as PD-1 in lymphoid cells and CTLA4 in $CD4^+$ T cells was found in $RANK^{-/-}$ relative to $RANK^{+/+}$ tumors (Figure 4a). The level of PD-L1 expression in $RANK^{-/-}$ tumor cells was also higher than in $RANK^{+/+}$ tumors (Figure 4a). Tregs ($FoxP3^+$ $CD25^+$ $CD4^+$ $CD11b^-$) were more frequent in $RANK^{-/-}$ than in $RANK^{+/+}$ tumors, possibly as a result of the enhanced cytotoxic response, as reported elsewhere[49] (Figure 4a). These results suggest that the exacerbated T cell response in $RANK^{-/-}$ tumors may facilitate the induction of negative immune checkpoint regulators and Tregs, evading immune surveillance and allowing tumor growth. This prompted us to investigate the effects of anti-PD-L1 and/or anti-CTLA4 checkpoints inhibitors in combination with the loss of RANK signaling. In $RANK^{+/+}$ tumors early treatment (72 h after tumor implantation) with anti-RL did not affect tumor growth; however, anti-CTLA4 combined with anti-RL reduced tumor growth to a greater extent than did single anti-CTLA4 treatment (28.5% of implanted tumors did not even grow) (Figure 4b-c). No benefit of combining anti-RL and anti-PD-L1 compared to anti-PD-L1 alone was observed in $RANK^{+/+}$ tumors in the early setting (Figure 4b-c).

Early treatment with anti-CTLA4, but not with anti-PD-L1 or anti-RL, significantly attenuated $RANK^{-/-}$ tumor growth (66.7% of implanted tumors did not grow) compared with the isotype-treated control (Figure 4d). Addition of anti-RL did not improve the

response to anti-CTLA4 (or anti-PD-L1) in $RANK^{-/-}$ tumors as did in $RANK^{+/+}$ tumors, suggesting that the augmented benefit of the anti-RL/anti-CTLA4 combination was driven by inhibition of RANK signaling in tumor cells (Figure 4d).

Next, we tested the effect of checkpoint inhibitors on the growth of already palpable, actively growing tumors (Figure 4e). None of the $RANK^{+/+}$ tumors responded to anti-PD-L1 or anti-RL as single agents but their combination significantly reduced tumor growth in 50% of the tumors (Figure 4f). Anti-RL did not improve the response to anti-CTLA4 (Figure 4f). In tumors lacking RANK, anti-PD-L1 treatment was more efficient than anti-CTLA4, but no improvement was observed after the addition of anti-RL (Figure 4g), in contrast with the observations on $RANK^{+/+}$ tumors.

Collectively, these results demonstrate that in this luminal-like BC, RL inhibition improves the anti-tumor response to anti-CTLA4 (in the early setting) and anti-PD-L1 (for established tumors) through inhibition of RANK signaling in the tumor cells.

A short course of denosumab treatment in early-stage BC increased TILs

To confirm the immunomodulatory role of RANK pathway inhibition in the clinical setting, we analyzed denosumab-treated BC clinical samples from the D-BEYOND study (NCT01864798): a prospective, preoperative window-of-opportunity, single-arm, multicenter trial assessing the effect of denosumab in premenopausal women with early-stage BC. Twenty-seven patients were included in this study and received two doses of denosumab 120 mg subcutaneously one week apart, followed by surgery. The median time interval between the first administration of denosumab and surgery was 13 days. No serious adverse events (AEs) were reported. All non-serious AEs are summarized in Table S6, the most frequent being arthralgia (4/27 patients, 14.8%). Table 1 summarizes the clinicopathological features of the 24 patients subsequently analyzed. In brief, the

median age at diagnosis was 45 years (range, 35-51 years); tumors of 19 patients were hormone receptor-positive (79.2%), four were $HER2^+$ (16.7%) and one was triple-negative (4.2%). After treatment, serum levels of sRANKL (unbound to denosumab) and CTX, a surrogate marker for denosumab activity, decreased in all patients evaluated ($P < 0.001$, Fig. 5a), confirming the target inhibition. Given its correlation with clinical response in luminal BC[50–52], the primary study endpoint was a geometric mean (GM) decrease in the percentage of Ki-67-positive cells. Secondary endpoints included tumor cell survival assessed by cleaved caspase-3, as well as tumor immune infiltration. There was no significant reduction in the percentage of Ki-67-positive cells (GM change from baseline; 1.07, 95% CI 0.87–1.33; $P = 0.485$, Figure 5a) and no absolute Ki-67 or cleaved caspase-3 responders were identified (Figure 5a, S5a).

Collectively, these data confirm that a short course of denosumab was associated with effective systemic RANKL inhibition, but not with a reduction in tumor proliferation or survival.

Next, we assessed the effect of denosumab on tumor immune infiltration in 24 available paired samples. Of note, similar to our preclinical model, we observed a significant increase in stromal and intratumoral lymphocyte levels after short exposure to denosumab (GM change from baseline: 1.75, 95% CI 1.28–2.39; $P = 0.006$ and 1.59, 95% CI 1.14–2.21, $P = 0.008$, respectively, Figure 5b-c and Figure S5a). In particular, 11/24 patients (45.8%), including 6/14 luminal A, 3/5 luminal B and 2/4 $HER2^+$ cases, showed an immunomodulatory response defined as a $\geq$ 10 percent increase in stromal TILs (sTILs) in tumor samples. Analyses of the percentage of $Ki\text{-}67^+$ TILs suggested a trend to increase after denosumab treatment, particularly in responders (7/11) (Figure 5b).

The composition of the immune infiltrate associated with denosumab treatment was analyzed by IHC in 23 available pairs of pre- and post-denosumab treatment tumor tissues (Figure 5b and Figure S5a-b). These analyses revealed a significant increase in the percentage of T ($CD3^+$) and B ($CD20^+$) cells after denosumab treatment (GM change from baseline: 1.68, 95% CI 1.18–2.40; P = 0.006 and 1.62, 95% CI 1.09–2.40; P = 0.019, respectively) and increased levels of $CD8^+$ T cells, validating our preclinical observations (GM change from baseline: 1.59, 95% CI 1.14–2.21; P = 0.008). Moreover, there was a significant decrease in $FOXP3^+/CD4^+$ T regs cell frequency (GM change from baseline: 0.63, 95% CI 0.49–0.83; P = 0.002, Figure 5b), even in patients with no increase in TILs. No significant differences in macrophage infiltration ($CD68^+$ or $CD163^+$) were observed (Figure 5b and Figure S5a). Intratumoral immune population abundance was also quantified, and an increase of TILs and $CD3^+$ T cells was observed (Figure S5a). These findings were illustrated using multiplex IHC of the top four tumors associated with the highest TIL increase (Figure 5c).

To investigate the biological effect of denosumab in early BC further, we performed RNA sequencing on 22 available pre- and post-treatment tumor samples and identified 379 genes that were differentially expressed (Table S7). Pathway analysis using GO and GAGE revealed the enrichment of several genes related to immune activation, immune cell migration and cytokine-mediated signaling pathways (Figure 5d, Table S9-S10). In line with these findings, the expression levels of several chemokines were increased after treatment, including that of the well-known $CD8^+$ T cell chemoattractants CCL4 and CXCL10[53,54] (Figure S5c). Additionally, we performed RNA sequencing on 11 available pre- and post-treatment normal samples using RNA extracted from normal tissues. Sufficient normal RNA quantity from both pre- and post- treatment was obtained from eleven patients. Only ten genes were differentially expressed between

776 pre- and post-treatment normal samples (Table S8) and all of them were also
777 differentially expressed in tumor tissue (Table S7). No significant changes in
778 RANK/RANKL at the protein (IHC) (Figure S5d-e) or at the gene expression levels
779 (RNAseq) (Table S7 and S8) were found. Of note, no differences in genes related to
780 immature mammary epithelial cell populations (*ALDH1*) or related to estrogen receptor
781 pathway (*ESR1*, *PR*, *BCL2)* both in tumor and normal samples were observed (D-
782 BEYOND secondary endpoints) (Table S7 and S8).
783 To further explore the impact of denosumab treatment on the immune cell landscape of
784 BC we used CIBERSORT[55], a deconvolution method for inferring immune cell content
785 from gene expression data. Consistent with the IHC results, this analysis confirmed the
786 increase in the relative frequencies of $CD8^+$ T cells, B cells and $CD4^+$ T cells, and the
787 decrease in the frequencies of Tregs after denosumab treatment (Figure S5f). Despite
788 the overall increase in immune infiltration the relative frequency of macrophage
789 infiltration was reduced after denosumab, particularly in responders (8/11) (Figure S5f).
790 No significant changes in NK cells, dendritic cells, mast cells, neutrophils and
791 eosinophils were noted, because these populations may be too scarce to be captured
792 properly by this method (Figure S5f). Of note, after denosumab treatment, neutrophils
793 correlated negatively with sTILs (Figure S5g), and the neutrophil chemotaxis and
794 migration pathways were modulated after denosumab treatment (Table S9), supporting
795 the preclinical findings.
796 To ensure that these changes are specific to denosumab treatment and not a
797 consequence of the presurgical biopsy procedure, we interrogated the publicly available
798 gene expression data of patients from the control-arm (untreated) of the POETIC study,
799 a large BC window-of-opportunity study evaluating the role of perioperative aromatase
800 inhibitor for which gene expression data were obtained from presurgical biopsies and

surgical specimens. Similar to the D-BEYOND study, biopsies were taken at diagnosis and 2 weeks later at the time of surgery. The comparison of surgery and biopsy samples from the POETIC study did not reveal any enrichment of immune cells assessed by CIBESORT or an immune pathway, as assessed by GAGE analyses (Figure S5h and Table S11). Together, our results indicate that a short course of denosumab enhances immune infiltration as determined by the increased levels of TILs, B and T lymphocytes, $CD4^+$ and $CD8^+$ T cells in luminal and $HER2^+$ breast tumors, validating the clinical relevance of the findings in the preclinical models.

RANK pathway activation in tumors and circulating sRANKL levels predict Denosumab´s immune effect

Finally, we investigated the baseline features associated with the immunomodulatory effect of denosumab. We identified 11 responder (R) cases, defined by a ≥ 10% increase in TIL infiltration after denosumab treatment and 13 non-responder (NR) cases. No associations were found between any baseline clinicopathological features and the immune modulation induced by denosumab (Table S12). Of the characteristics compared between R and NR patients, high sRANKL serum levels, a high percentage of Tregs measured by CIBERSORT, and the presence of intratumoral FOXP3+ cells measured by IHC, were significantly associated with increased TIL infiltration after denosumab treatment (Figure 5e, Table S12). CD20 IHC staining at baseline was also associated with response, but this finding was not corroborated by CIBERSORT (Table S12). A differential gene expression analysis using RNA-seq data from biopsy samples evidenced 42 genes expressed at higher levels in R than in NR, including *FOXP3*, *IL7R*, *MS4A1* (CD20), *CD28* and *IFNG* (Figure 5f, Table S13) and the enrichment of genes

825 involved in lymphocyte activation and immunoglobulin production in R patients (Table
826 S14 which may be indicative of an enhanced immune response.
827 RANK and RANKL IHC was performed on tumor and normal tissue samples. We did
828 not find any difference between pre and post treatment samples (Figure S5d-e) and
829 neither was predictive of the immunomodulatory effects of denosumab (Figure S6a).
830 However, since it has been reported that RANK IHC is an unreliable tool to detect
831 RANK protein on breast tumor samples[1,56], we computed RANK and RANKL
832 metagenes to increase the potency and reliability of RANK and RANKL detection.
833 These metagenes included the expression levels of the top 100 genes that are co-
834 expressed at baseline with *RANK* and *RANKL* mRNA, respectively (see methods, Table
835 S15). Importantly, high expression level of RANK metagene in the tumors at baseline
836 (Figure 5g), but neither RANKL metagene nor individual gene expression of *RANK* or
837 *RANKL*, is predictive of denosumab-induced immune response (Figure S6b).
838 GO analyses showed that the RANK metagene includes genes associated with NF-κB
839 pathway activation as well as with immune response (Figure S6c). Indeed, the RANK
840 metagene strongly correlated with several public signatures of the RANK and NF-κB
841 pathways, as well as with RANKL-induced genes in mouse mammary epithelial cells
842 (MECs) (WT and Rank overexpressing) and PyMT tumor cells (Figure S6d). These
843 results demonstrate that RANK metagene captures RANK pathway activation and
844 support the relevance of the PyMT model. Accordingly, tumors responding to
845 denosumab presented at baseline higher scores for these RANKL-driven genes in mouse
846 MECs and PyMT tumor cells (Figure 5g; Figure S6e) and RANK and NF-κB pathway
847 gene signatures (Figure S6f). Thus, tumors with increased RANK pathway activation at
848 baseline are more likely to show increased TILs after RANKL inhibition, corroborating

849 the preclinical findings: inhibition of RANK signaling in tumor cells contributes to the
850 immunomodulatory effect of denosumab in BC.
851 Together, these results indicate that higher RANK pathway activation, soluble RANKL
852 and the presence of Tregs at baseline, are predictive biomarkers of the
853 immunomodulatory response induced by denosumab in BC patients.

DISCUSSION

Several studies have shown the prognostic and predictive value of TILs, especially in $HER2^+$ and triple-negative BC[57,58]. However, TILs continue to be infrequent in most luminal breast tumors. The identification of a therapy that could convert immune "cold" tumors into "hot" ones would represent a major step towards the development of immune-related therapies. Based on our clinical and preclinical findings, denosumab appears to be just this type of promising therapeutic agent. This question is particularly relevant for luminal BC which is poorly infiltrated and insensitive to immunotherapies.

The results of the D-BEYOND clinical trial provide strong evidence of the immunomodulatory effect of denosumab in luminal early BC and identify predictive biomarkers of response. The mouse genetic studies demonstrate that inhibition of RANK signaling in the tumor cells increases TILs and $CD8^+$ T cell infiltration and attenuates tumor growth. Mechanistically we found that activation of RANK signaling in tumor cells induces a proinflammatory microenvironment that favors survival of TANs and restricts T cell anti-tumor response.

The strength of our work resides in the fact that two independent studies, a clinical trial and preclinical research on tumor-prone mouse models, equally conclude that the inhibition of RANK signaling increases the anti-tumor immune response and set the basis for additional trials combining denosumab with immunotherapy in presumably immune "cold" luminal BC.

Although the clinical trial primary efficacy endpoint was not met, since tumor cell proliferation was not reduced, a short course of denosumab did induce an increase in the levels of TILs, T and B cells and $CD8^+$ T cell infiltration. In contrast with the increased levels of T cells and $CD8^+$ T cells, which were associated with enhanced TIL infiltration, the reduction of Tregs was observed equally in responders and non-

responders, suggesting that it may be driven by additional systemic effects of denosumab, rather than by the loss of RANK signaling in the tumor cells, as suggested by the different results seen in RANK-/- tumors.

Importantly, preclinical genetic mouse approaches evidence that the main immunomodulatory changes induced by denosumab in D-BEYOND -increased in TILs and CD8+ T cells- are replicated when RANK is lost specifically in the tumor compartment. Additionally, they add functional relevance to the changes in immune infiltration, since T lymphocytes and CD8+ T cells are responsible for the delayed tumor onset and reduction of tumor-initiating ability observed in RANK null tumors. In contrast, RANK loss in myeloid cells does not change the tumor immune infiltration. In the PyMT mouse model the frequency $CD8^+$ T cells also increase after systemic anti-RL treatment and the CD4/CD8 ratio was reduced, but no differences in total leukocyte or lymphocyte infiltration were observed. Differences with the D-BEYOND results might be due to drug specific aspects, treatment schedule or tumor divergences.

RANK expression in tumor cells led to a significant increase in the levels of several cytokines and chemokines involved in macrophage and neutrophil recruitment and polarization[43,59,60], in line with the increased infiltration of TAMs and TANs in $RANK^{+/+}$ tumors. Indeed, we found that RANK-expressing human BC cells promote survival of inflammatory neutrophils. Neutrophil depletion significantly delayed tumor appearance in $RANK^{+/+}$, but not in $RANK^{-/-}$ models, supporting a pro-tumorigenic role for neutrophils recruited by $RANK^{+/+}$ tumor cells. Neutrophils have different polarization states and can promote tumorigenesis and metastasis[61]. Our mouse and human data are consistent with the previously reported negative correlation of neutrophils and $CD8^+$ T cell infiltration in NSCLC[62]. Neutrophils have a well-defined role in the suppression of the action of $CD8^+$ T cells[63]. Our results demonstrate that

RANK activation in tumor cells increases neutrophil survival and activation inducing an immunosuppressive environment which could restrict the cytotoxic T cell response. These findings support the connection between RANK activation in tumor cells, neutrophils and $CD8^+$ T cells (see Figure 6).

A critical aspect of current and future clinical trials is the selection of BC patients who may benefit from denosumab treatment, considering the limitations of the RANK immunohistochemistry. We demonstrate that the RANK metagene we generated captures RANK activation and predicts the denosumab-driven increase in TILs in BC. Higher RANK metagene, RANK/NF-κB activation in the tumors and soluble RANKL at baseline could be better biomarkers than the individual expression levels of RANK or RANKL for the selection of BC patients who might benefit from denosumab treatment.

The D-BEYOND trial has some limitations, such as the small sample size, the inclusion of only premenopausal patients and the limited number of triple-negative and $HER2^+$ cases. Whether the immunomodulatory response associated with RANKL inhibition could also be effective in postmenopausal patients will be addressed in the ongoing trial: D-BIOMARK (NCT03691311). It will be also worth reassessing the clinical outcome of two recent large phase III trials of adjuvant denosumab in early BC, D-CARE and ABCSG-18, according to the predictive biomarkers we defined: baseline RANK metagene, sRANKL levels, and the presence of Tregs. The D-CARE study reported no differences in disease-free survival (DFS), whereas the ABCSG-18 trial showed DFS improvement in postmenopausal patients[64–66].

Results in the $RANK^{-/-}$ mouse tumors suggest that up-regulation of negative checkpoints and Tregs occurs as a consequence of a proinflammatory, anti-tumor IFNγ-enriched microenvironment[49,67] and may allow $RANK^{-/-}$ tumor cells to evade immune surveillance and grow. The blockade of CTLA4 and PD-1/PD-L1 has revolutionized

treatment of highly immunogenic tumors such as melanoma and NSCLC[24,25], but, so far, results in BC have been restricted to basal-like tumors in combination with radiotherapy or chemotherapy[26].

CTLA4 blockade affects mainly the priming phase of the immune response, whereas PD-L1 inhibition works mostly during the effector phase to restore the immune function of previously activated T cells[68]. In both scenarios, we have shown an increased benefit after the addition of RANKL inhibitors to immune checkpoints in $RANK^{+/+}$ tumors, which is highly relevant in poorly immunogenic tumors such as luminal BC. Importantly, the combined treatments show no increased benefit in $RANK^{-/-}$ tumors, indicating that it is driven by the inhibition of RANK signaling in tumor cells. This is a novel mechanism of action, as previous preclinical studies reporting the benefit of the combination were done in melanoma and colon cancer cell lines highly responsive to immunotherapy but lacking RANK expression[69,70]. Although we cannot rule out that denosumab may have additional systemic effects, our findings support that a tumor cell-driven effect contributes to the immunomodulatory effect of denosumab in BC.

The benefit of the combined effect of anti-RANKL and immune checkpoint inhibitors will be investigated in the CHARLI trial (NCT03161756), a phase I/II study of the effect of denosumab in combination with nivolumab (an anti-PD-1), with or without ipilimumab (anti-CTLA4), in metastatic melanoma patients, and in the POPCORN trial (ACTRN12618001121257), which will evaluate immune changes in NSCLC patients treated with nivolumab alone or in combination with denosumab. Clinical and preclinical evidence shown in this work encourage the initiation of similar trials in BC.

In summary, compelling clinical and preclinical data reveal an unexpected immunomodulatory role for RANK pathway in luminal early-stage BC and demonstrate

denosumab to be a promising agent for enhancing the immune response in luminal BC alone or in combination with immune checkpoint inhibitors.

AUTHOR CONTRIBUTIONS

G.Y, C.G.A: Collection and/or assembly of data, data analysis and interpretation, manuscript writing. M.Z, P.P, E.M .T, S.B, M.C, A.B., E.H.: Collection and/or assembly of data, data analysis and interpretation. T.W, L.P: Conception and design, data analysis and interpretation. P.M: data analysis and interpretation, E.G-S: Conception and design of the preclinical study, financial support, collection and/or assembly of data, data analysis and interpretation, manuscript writing. M.P, C.Sotiriou, S.L and H.A.A.: Conception and design of the D-Beyond clinical trial. B.N: Collection and/or assembly of clinical trial and biological samples data, data analysis and manuscript writing. F.R: Experiments on patients' samples supervision, data analysis and interpretation and final approval of manuscript. S.M and D.V: Statistical design and clinical trial data analysis. M.M: collection and/or assembly of the clinical trial data and biological samples. R.S, D.L and G.V.E: Pathology assessment of the biological samples. P.V, L.P, H.W, P.S and G.L: Patient consent and recruitment. S.G and K.W-G: Immunological assessment of the biological samples. C.V: Clinical trial project management. All: interpretation of the data analysis and final approval of the manuscript.

ACKNOWLEDGEMENTS

We thank the patients who contributed to this study and acknowledge the clinical staff for their dedication. This work was supported by grants to E. González-Suárez by MICINN (SAF2014-55997-R, SAF2017-86117-R) co-funded by FEDER funds/ European Regional Development Fund (ERDF) -a way to build Europe-), European

Union ERC-2015- Consolidator Grant LS4-682935 and Fundació La Marató de TV3. P. Pellegrini was, and S Benitez is the recipient of a predoctoral grant from the MICINN. We are grateful to William C Dougall and AMGEN Inc. for supporting the design of the D-BEYOND trial and providing RANKL, RANK-Fc reagents and $RANK^{-/-}$ mice. We thank the IDIBELL Animal Facility for their assistance with mouse colonies, Esther Castaño and the scientific services of the University of Barcelona for their assistance with FACS analyses and P Gonzalez-Santamaria, G Perez-Chacon and M Jimenez for critical reading of the manuscript. Christos Sotiriou and Bastien Nguyen are supported by the National Fund for Research (FNRS) and Televie. This work was also supported in part by the Cancer Center Support Grant of the National Institutes of Health (Grant No. P30CA008748). We thank Samira Majjaj and Delphine Vincent for technical assistance. The authors would like to extend their gratitude to the patients who participated in the D-BEYOND study. This clinical study has been supported by research funding from Amgen.

COMPETING INTEREST

R.S. receive travel support from Roche, Astra Zeneca and Merck and research support from Merck, Puma, Roche. H.A.A. is advisory board at Roche and current employee of Innate Pharma. E.G.S. and G.J.L. have served on advisory boards for Amgen and has received honoraria and research funding from Amgen. S.L. receives research funding from Novartis, Merck, BMS, Roche-Genentech, Puma Biotechnology, Pfizer and uncompensated advisory board of Novartis, Merck, BMS, Roche-Genentech, Puma Biotechnology, Pfizer, Seattle Genetics.

DATA AVAILABILIY

Raw microarray data from preclinical samples have been deposited in GEO, access number GSE119464. RNAseq data have been deposited under EGA accession number EGAS00001003252. The coded data of the study could be accessible to other researchers under the following conditions: 1. A research proposal should be submitted to the sponsor who will evaluate the project and decide whether or not the sponsor gives access to the study data. 2. If the data access is granted, a Data Transfer agreement will be put in place between the sponsor and the reseacher (i.a. to be compliant with the GDPR). 3. Any research project should be approved by an ethics committee. Each request will be analysed on a case by case basis. The study protocol is published as a Supplementary file.

BIBLIOGRAPHY

1. Infante, M. *et al.* RANKL/RANK/OPG system beyond bone remodeling: Involvement in breast cancer and clinical perspectives. *Journal of Experimental and Clinical Cancer Research* **38,** (2019).
2. Fata, J. E. *et al.* The Osteoclast Differentiation Factor Osteoprotegerin-Ligand Is Essential for Mammary Gland Development. *Cell* **103,** 41–50 (2000).
3. Gonzalez-Suarez, E. *et al.* RANK Overexpression in Transgenic Mice with Mouse Mammary Tumor Virus Promoter-Controlled RANK Increases Proliferation and Impairs Alveolar Differentiation in the Mammary Epithelia and Disrupts Lumen Formation in Cultured Epithelial Acini. *Mol. Cell. Biol.* **27,** 1442–1454 (2007).
4. Gonzalez-Suarez, E. *et al.* RANK ligand mediates progestin-induced mammary epithelial proliferation and carcinogenesis. *Nature* **468,** 103–107 (2010).
5. Schramek, D. *et al.* Osteoclast differentiation factor RANKL controls development of progestin-driven mammary cancer. *Nature* **468,** 98–102 (2010).
6. Asselin-Labat, M.-L. *et al.* Control of mammary stem cell function by steroid hormone signalling. *Nature* **465,** 798–802 (2010).
7. Joshi, P. A. *et al.* Progesterone induces adult mammary stem cell expansion. *Nature* **465,** 803–807 (2010).
8. Nolan, E. *et al.* RANK ligand as a potential target for breast cancer prevention in BRCA1-mutation carriers. *Nat. Med.* **22,** 933–939 (2016).
9. Sigl, V. *et al.* RANKL/RANK control Brca1 mutation-driven mammary tumors. *Cell Res.* **26,** 761–774 (2016).
10. Yoldi, G. *et al.* RANK Signaling Blockade Reduces Breast Cancer Recurrence by Inducing Tumor Cell Differentiation. *Cancer Res.* **76,** 5857–5869 (2016).

11. González-Suárez, E. & Sanz-Moreno, A. RANK as a therapeutic target in cancer. *FEBS J.* **283,** 2018–2033 (2016).
12. Dougall, W. C. *et al.* RANK is essential for osteoclast and lymph node development. *Genes Dev.* **13,** 2412–24 (1999).
13. Walsh, M. C. & Choi, Y. Biology of the RANKL-RANK-OPG System in Immunity, Bone, and Beyond. *Front. Immunol.* **5,** 511 (2014).
14. Anderson, D. M. *et al.* A homologue of the TNF receptor and its ligand enhance T-cell growth and dendritic-cell function. *Nature* **390,** 175–179 (1997).
15. Williams, C. B. *et al.* Tumor-associated macrophages: unwitting accomplices in breast cancer malignancy. *npj Breast Cancer* **2,** 15025 (2016).
16. Green, E. A., Choi, Y. & Flavell, R. A. Pancreatic lymph node-derived CD4(+)CD25(+) Treg cells: highly potent regulators of diabetes that require TRANCE-RANK signals. *Immunity* **16,** 183–91 (2002).
17. Seshasayee, D. *et al.* A novel in vivo role for osteoprotegerin ligand in activation of monocyte effector function and inflammatory response. *J. Biol. Chem.* **279,** 30202–30209 (2004).
18. Walsh, N. C. *et al.* Activated human T cells express alternative mRNA transcripts encoding a secreted form of RANKL. *Genes Immun.* **14,** 336–345 (2013).
19. Dougall, W. C. *et al.* RANK is essential for osteoclast and lymph node development. *Genes Dev.* **13,** 2412–2424 (1999).
20. Anderson, D. M. *et al.* A homologue of the TNF receptor and its ligand enhance T-cell growth and dendritic-cell function. *Nature* **390,** 175–179 (1997).
21. Biswas, S. K. & Lewis, C. E. NF-κB as a central regulator of macrophage function in tumors. *J. Leukoc. Biol.* **88,** 877–884 (2010).

22. Green, E. A., Choi, Y. & Flavell, R. A. Pancreatic Lymph Node-Derived CD4+CD25+ Treg Cells: Highly Potent Regulators of Diabetes that Require TRANCE-RANK Signals. *Immunity* **16,** 183–191 (2002).

23. DeNardo, D. G. & Coussens, L. M. Inflammation and breast cancer. Balancing immune response: Crosstalk between adaptive and innate immune cells during breast cancer progression. *Breast Cancer Research* **9,** (2007).

24. Hodi, F. S. *et al.* Improved survival with ipilimumab in patients with metastatic melanoma. *N. Engl. J. Med.* **363,** 711–723 (2010).

25. Owen, D. & Chaft, J. E. Immunotherapy in surgically resectable non-small cell lung cancer. *Journal of Thoracic Disease* **10,** S404–S411 (2018).

26. Adams, S. *et al.* Current Landscape of Immunotherapy in Breast Cancer: A Review. *JAMA Oncology* **5,** 1205–1214 (2019).

27. Guy, C. T., Cardiff, R. D. & Mulle, W. J. Induction of Mammary Tumors by Expression of Polyomavirus Middle T Oncogene: A Transgenic Mouse Model for Metastatic Disease. *Mol. Cell. Biol.* **12,** 954–961 (1992).

28. Palafox, M. *et al.* RANK induces epithelial-mesenchymal transition and stemness in human mammary epithelial cells and promotes tumorigenesis and metastasis. *Cancer Res.* **72,** 2879–2888 (2012).

29. Pfitzner, B. M. *et al.* RANK expression as a prognostic and predictive marker in breast cancer. *Breast Cancer Res. Treat.* **145,** 307–315 (2014).

30. Guy, C. T., Cardiff, R. D. & Muller, W. J. Induction of mammary tumors by expression of polyomavirus middle T oncogene: a transgenic mouse model for metastatic disease. *Mol. Cell. Biol.* **12,** 954–961 (1992).

31. Hanada, R. *et al.* Central control of fever and female body temperature by RANKL/RANK. *Nature* **462,** 505–509 (2009).

32. Coates, A. S. *et al.* Tailoring therapies-improving the management of early breast cancer: St Gallen International Expert Consensus on the Primary Therapy of Early Breast Cancer 2015. *Ann. Oncol.* **26,** 1533–1546 (2015).

33. Salgado, R. *et al.* The evaluation of tumor-infiltrating lymphocytes (TILs) in breast cancer: recommendations by an International TILs Working Group 2014. *Ann. Oncol.* **26,** 259–271 (2015).

34. Buisseret, L. *et al.* Tumor-infiltrating lymphocyte composition, organization and PD-1/PD-l1 expression are linked in breast cancer. *Oncoimmunology* **6,** (2017).

35. Bolger, A. M., Lohse, M. & Usadel, B. Trimmomatic: A flexible trimmer for Illumina sequence data. *Bioinformatics* **30,** 2114–2120 (2014).

36. López-Knowles, E. *et al.* Heterogeneity in global gene expression profiles between biopsy specimens taken peri-surgically from primary ER-positive breast carcinomas. *Breast Cancer Res.* **18,** 39 (2016).

37. Love, M. I., Huber, W. & Anders, S. Moderated estimation of fold change and dispersion for RNA-seq data with DESeq2. *Genome Biol.* **15,** 550 (2014).

38. Luo, W., Friedman, M. S., Shedden, K., Hankenson, K. D. & Woolf, P. J. GAGE: generally applicable gene set enrichment for pathway analysis. *BMC Bioinformatics* **10,** 161 (2009).

39. Newman, A. M. *et al.* Robust enumeration of cell subsets from tissue expression profiles. *Nat. Methods* **12,** 453–457 (2015).

40. Liberzon, A. *et al.* The Molecular Signatures Database Hallmark Gene Set Collection. *Cell Syst.* **1,** 417–425 (2015).

41. Clausen, B. E., Burkhardt, C., Reith, W., Renkawitz, R. & Förster, I. Conditional gene targeting in macrophages and granulocytes using LysMcre mice. *Transgenic Res.* **8,** 265–277 (1999).

42. Yoldi, G. *et al.* RANK Signaling Blockade Reduces Breast Cancer Recurrence by Inducing Tumor Cell Differentiation. *Cancer Res.* **76,** 5857–5869 (2016).
43. Griffith, J. W., Sokol, C. L. & Luster, A. D. Chemokines and Chemokine Receptors: Positioning Cells for Host Defense and Immunity. *Annu. Rev. Immunol.* **32,** 659–702 (2014).
44. Guo, H., Callaway, J. B. & Ting, J. P. Y. Inflammasomes: Mechanism of action, role in disease, and therapeutics. *Nature Medicine* **21,** 677–687 (2015).
45. Ryckman, C., Vandal, K., Rouleau, P., Talbot, M. & Tessier, P. A. Proinflammatory Activities of S100: Proteins S100A8, S100A9, and S100A8/A9 Induce Neutrophil Chemotaxis and Adhesion. *J. Immunol.* **170,** 3233–3242 (2003).
46. Coffelt, S. B., Wellenstein, M. D. & De Visser, K. E. Neutrophils in cancer: Neutral no more. *Nature Reviews Cancer* **16,** 431–446 (2016).
47. Youn, J.-I., Nagaraj, S., Collazo, M. & Gabrilovich, D. I. Subsets of Myeloid-Derived Suppressor Cells in Tumor-Bearing Mice. *J. Immunol.* **181,** 5791–5802 (2008).
48. Shaul, M. E. & Fridlender, Z. G. Cancer-related circulating and tumor-associated neutrophils – subtypes, sources and function. *FEBS Journal* **285,** 4316–4342 (2018).
49. Spranger, S. *et al.* Up-regulation of PD-L1, IDO, and T(regs) in the melanoma tumor microenvironment is driven by CD8(+) T cells. *Sci. Transl. Med.* **5,** 200ra116 (2013).
50. Ellis, M. J. *et al.* Randomized phase II neoadjuvant comparison between letrozole, anastrozole, and exemestane for postmenopausal women with estrogen receptor-rich stage 2 to 3 breast cancer: Clinical and biomarker outcomes and

predictive value of the baseline PAM50-based intrinsic subtype - ACOSOG Z1031. *J. Clin. Oncol.* **29,** 2342–2349 (2011).

51. Horimoto, Y. *et al.* Ki67 expression and the effect of neo-adjuvant chemotherapy on luminal HER2-negative breast cancer. *BMC Cancer* **14,** 550 (2014).

52. Yoshioka, T. *et al.* Prognostic significance of pathologic complete response and Ki67 expression after neoadjuvant chemotherapy in breast cancer. *Breast Cancer* **22,** 185–191 (2015).

53. Dufour, J. H. *et al.* IFN- -Inducible Protein 10 (IP-10; CXCL10)-Deficient Mice Reveal a Role for IP-10 in Effector T Cell Generation and Trafficking. *J. Immunol.* **168,** 3195–3204 (2002).

54. Honey, K. CCL3 and CCL4 actively recruit CD8+ T cells. *Nat. Rev. Immunol.* **6,** 427–427 (2006).

55. Newman, A. M. *et al.* Robust enumeration of cell subsets from tissue expression profiles. *Nat. Methods* **12,** 453–457 (2015).

56. Taylor, C. R. *et al.* Distribution of RANK and RANK Ligand in Normal Human Tissues as Determined by an Optimized Immunohistochemical Method. *Appl. Immunohistochem. Mol. Morphol.* **25,** 299–307 (2017).

57. Salgado, R. & Loi, S. Tumour infiltrating lymphocytes in breast cancer: increasing clinical relevance. *The Lancet Oncology* **19,** 3–5 (2018).

58. Savas, P. *et al.* Clinical relevance of host immunity in breast cancer: From TILs to the clinic. *Nature Reviews Clinical Oncology* **13,** 228–241 (2016).

59. Ramos, C. D. L. MIP-1 [CCL3] acting on the CCR1 receptor mediates neutrophil migration in immune inflammation via sequential release of TNF- and LTB4. *J. Leukoc. Biol.* **78,** 167–177 (2005).

60. Oliveira, S. H. P., Canetti, C., Ribeiro, R. A. & Cunha, F. Q. Neutrophil

migration induced by IL-1β depends upon LTB4 released by macrophages and upon TNF-α and IL-1β released by mast cells. *Inflammation* **31,** 36–46 (2008).

61. Fridlender, Z. G. *et al.* Polarization of Tumor-Associated Neutrophil Phenotype by TGF-β: 'N1' versus 'N2' TAN. *Cancer Cell* **16,** 183–194 (2009).

62. Kargl, J. *et al.* Neutrophils dominate the immune cell composition in non-small cell lung cancer. *Nat. Commun.* **8,** (2017).

63. Michaeli, J. *et al.* Tumor-associated neutrophils induce apoptosis of non-activated CD8 T-cells in a TNFα and NO-dependent mechanism, promoting a tumor-supportive environment. *Oncoimmunology* **6,** e1356965 (2017).

64. Coleman, R. *et al.* Adjuvant denosumab in early breast cancer (D-CARE): an international, multicentre, randomised, controlled, phase 3 trial. *Lancet Oncol.* **21,** 60–72 (2020).

65. Coleman, R. E. *et al.* Adjuvant denosumab in early breast cancer: First results from the international multicenter randomized phase III placebo controlled D-CARE study. *J. Clin. Oncol.* **36,** 501–501 (2018).

66. Gnant, M. *et al.* Adjuvant denosumab in postmenopausal patients with hormone receptor-positive breast cancer (ABCSG-18): disease-free survival results from a randomised, double-blind, placebo-controlled, phase 3 trial. *Lancet. Oncol.* **20,** 339–351 (2019).

67. Taube, J. M. *et al.* Colocalization of Inflammatory Response with B7-H1 Expression in Human Melanocytic Lesions Supports an Adaptive Resistance Mechanism of Immune Escape. *Sci. Transl. Med.* **4,** 127ra37-127ra37 (2012).

68. Buchbinder, E. I. & Desai, A. CTLA-4 and PD-1 pathways similarities, differences, and implications of their inhibition. *American Journal of Clinical Oncology: Cancer Clinical Trials* **39,** 98–106 (2016).

69. Ahern, E. *et al.* Co-administration of RANKL and CTLA4 Antibodies Enhances Lymphocyte-Mediated Antitumor Immunity in Mice. *Clin. Cancer Res.* **23,** 5789–5801 (2017).

70. Ahern, E. *et al.* RANKL blockade improves efficacy of PD1-PD-L1 blockade or dual PD1-PD-L1 and CTLA4 blockade in mouse models of cancer. *Oncoimmunology* **7,** e1431088 (2018).

Table 1. Clinicopathological features of the 24 evaluable patients

N		24
Interval surgery-Denosumab	Median days (range)	13 (9-21)
Age	Median years (range)	44 (35-51)
Size	> 2cm	11 (45.8%)
Nodal status	Positive	4 (16.7%)
Histological grade	High	8 (33.3%)
Molecular subtypes	LumA	10 (41.7%)
	LumB	9 (37.5%)
	HER2	4 (16.7%)
	TNBC	1 (4.2%)
Immune response	Percentage of patients	11 (45.8%)

Figure legends

Figure 1. Loss of RANK in tumor cells, but not in myeloid cells, leads to increased TIL frequency, and T cells drive the delayed tumor formation and the reduced tumor-initiating ability of RANK-null tumor cells.

a. Top panel: Injection scheme showing the implantation of PyMT RANK$^{+/+}$ (RANK$^{+/+}$) tumors in LysM-Cre RANK$^{fl/fl}$ mice (RANK MC$^{-/-}$) and WT (RANK MC$^{+/+}$) (C57BL/6); Bottom panel: *Rank* mRNA expression levels relative to *Hprt1* in peritoneal macrophages of RANK MC$^{-/-}$ and RANK MC$^{+/+}$ mice (n=3).

b. Graphs showing the percentages of tumor-infiltrating leukocytes (CD45^{+}), lymphocytes (CD11b- within CD45^{+}), tumor-associated macrophages (TAMs) (F4/80^{+}CD11b^{+} within CD45^{+}) and tumor-associated neutrophils (TANs) (Ly6G^{+}Ly6C^{-} CD11b^{+} within CD45^{+}) in RANK$^{+/+}$ tumor transplants in RANK MC$^{-/-}$ and RANK MC$^{+/+}$ mice (n=12 tumors).

c. Injection scheme showing the implantation of PyMT RANK$^{+/+}$ and PyMT RANK$^{-/-}$ tumors in C57BL/6 WT animals and *Foxn1*^{nu} mice.

d. Kinetics of palpable tumor onset (left) after tumor transplantation of RANK$^{+/+}$ and RANK$^{-/-}$ tumor cells in syngeneic C57BL/6 (n=6-8) and *Foxn1*^{nu} mice (n=6-8). Log-rank test (****, $p < 0.0001$). One representative experiment out of two is shown.

e. Tumor-initiating frequencies (with confidence intervals) and chi-square values as calculated by ELDA. Cells isolated from RANK$^{+/+}$ and RANK$^{-/-}$ tumors were injected in *Foxn1*^{nu} mice in limiting dilutions.

f. Graphs showing the percentages tumor-infiltrating leukocytes (CD45^{+}), lymphocytes (CD11b- within CD45^{+}), TAMs (F4/80^{+}CD11b^{+} within CD45^{+}), TANs (Ly6G^{+}CD11b^{+} within CD45^{+}) in RANK$^{+/+}$ or RANK$^{-/-}$ tumor transplants in syngeneic C57BL/6 and *Foxn1*^{nu} mice. Between 10 and 14 tumors per condition were analyzed at endpoint (>0.2

1226 cm^2). Mean, SEM and t-test p-values are shown. (*, $p < 0.05$; **, $p < 0.01$; ****, $p <$

1227 0.0001). Two representative primary tumors were used in these experiments.

1228 g. Representative dot blots of leukocytes ($CD45^+$) gated in live cells ($7AAD^-$) and

1229 lymphocytes ($CD11b^-$) gated on $CD45^+$.

1230

1231

1232

1233

1234

1235

1236

1237

Figure 2. RANK loss in tumor cells leads to increased $CD8^+$ T cell tumor infiltration that mediates the delayed tumor latency of $RANK^{-/-}$ tumors

a. Graphs showing the percentage of T cells ($CD3^+CD11b^-$ within $CD45^+$), CD8 ($CD8^+CD3^+CD11b^-$ within $CD45^+$), CD4 ($CD8^-CD3^+CD11b^-$ within $CD45^+$) and the CD4/CD8 ratio in $RANK^{+/+}$ (n=12) or $RANK^{-/-}$ (n=10) tumor cells injected in syngeneic C57BL/6 mice[#].

b-c. Representative images (b) and quantification (c) of $CD3^+$ (n = 4 tumors) and $CD8^+$ cells (n = 6 tumors) in $RANK^{+/+}$ and $RANK^{-/-}$ tumor transplants as assessed by IHC. Scale = 25 μm. Tumors derived from three independent primary tumors were used. Each dot represents one picture[#].

d. *Prf1 and Ifnγ* mRNA levels relative to *Hprt1* of whole tumors from $RANK^{+/+}$ and $RANK^{-/-}$ transplants in syngeneic C57BL/6 mice[#].

e-f. Representative images (e) and quantification (f) of $CD8^+$ cells in $RANK^{+/+}$ control and anti-RANKL-treated tumors from second transplants as assessed by IHC. Scale= 25 μm. Each dot represents one picture (n=3 tumors)[#].

g. Schematic overview of CD8 (300μg, clone 53-5.8) and NK1.1 (200μg, clone PK136) treatments in orthotopic $RANK^{+/+}$ and $RANK^{-/-}$ tumor transplants. Animals were treated i.p. on days -1, 0, 3 and 7 after tumor cell injection, and then once per week until the day of sacrifice, when tumors were > 0.5 cm^2.

h. Latency to tumor onset of $RANK^{+/+}$ and $RANK^{-/-}$ tumor cells implanted in syngeneic C57BL/6 animals and treated with anti-CD8 or anti-NK1.1 depletion antibodies (n=6) or corresponding isotype control (n=4 for $RANK^{+/+}$ and n=6 for $RANK^{-/-}$). Box and whisker plots (minimum to maximum) and significant t test p values are shown (*, $p < 0.05$).

i. Graphs showing the percentage of infiltrating CD8 T cells ($CD8^+CD3^+CD11b$- within $CD45^+$) and NK ($NK1.1^+CD3$- within $CD45^+$). Each dot represents one tumor[#].

[#]Mean, SEM and t test p-values are shown. (*, $p < 0.05$; **, $0.001 < p < 0.01$; ***, $0.001 < p < 0.0001$; ****, $p < 0.0001$). For panels a and d, each dot represents one tumor analyzed at the endpoint (> 0.2 cm^2). Data for tumor transplants derived from two representative primary tumors in two independent experiments.

Figure 3. Neutrophils recruited by the proinflammatory cytokine/chemokine milieu driven by RANK restrict T cell immunity

a. Cytokines/chemokines in the supernatant of $RANK^{+/+}$ and $RANK^{-/-}$ tumor 3D acini cultured during 72 h, expressed as the magnitude of change between $RANK^{+/+}$ and $RANK^{-/-}$ tumor acini. See also Table S5.

b. *Il1b, Casp4 and S100a9* mRNA levels relative to *Hprt1* of whole tumors from $RANK^{+/+}$ and $RANK^{-/-}$ transplants in syngeneic C57BL/6 mice. Two representative primary tumors of two independent experiments were used[#].

c. Correlation between the frequency of TANs ($Ly6G^+$ $Ly6C^+$ $CD11b^+$) and $CD8^+$ T cells ($CD8^+$ $CD3^+$ $CD11b^-$) infiltrates in tumor transplants. Pearson correlation coefficients (r) associated probabilities are shown.

d. Percentage of Annexin-V^-7AAD^- neutrophils (n = 5, 2 healthy donors) cultured with conditioned media (CM) from the indicated RL-treated tumor cells. CM was added (1:1) to human neutrophil cultures for 24 h.

e. Mean fluorescence intensity (MFI) of $CD11b^+$ neutrophils (n=4, 2 healthy donors) cultured in CM from the indicated RL-treated tumor cells. CM was added (1:1) to human neutrophils cultures for 24 h.

f. Schematic overview of TAN ($Ly6G^+$) depletion experiments in orthotopic $RANK^{+/+}$ and $RANK^{-/-}$ tumor transplants. Anti-Ly6G (clone 1A8) was administered i.p. before tumor cell injection (400 µg), and then once per week (100 µg) until the day of sacrifice.

g. Latency to tumor formation of $RANK^{+/+}$ and $RANK^{-/-}$ tumor cells orthotopically implanted in syngeneic C57BL/6 animals and treated with anti-Ly6G depletion antibody or isotype control (n= 4-8). Box and whisker plots (minimum to maximum) and t test p-values are shown. (*, $p < 0.05$; **, $p < 0.01$).

h. Graphs showing the percentage of TANs ($Ly6G^+$ $CD11b^+$), leukocytes ($CD45^+$), lymphocytes ($CD11b^-$), TAMs ($F4/80^+$ $CD11b^+$), $CD8^+$ ($CD8^+$ $CD3^+$ $CD11b^-$) and $CD4^+$ T cells ($CD8^-$ $CD3^+$ $CD11b^-$)[#].

[#]: each dot represents one tumor. Mean, SEM and t test p-values are shown. (*, $p < 0.05$; **, $p < 0.01$; ***, $p < 0.0001$). Tumors of similar size were analyzed at endpoint (> 0.2 cm^2). For panels d-e: each dot represents a technical replicate from healthy donors. Representative dot blots are shown below.

Figure 4. RANKL pharmacological inhibition reinforces anti-CTLA4 and anti-PD-L1 anti-tumor response in $RANK^{+/+}$ but not in $RANK^{-/-}$ tumors.

a. Graphs showing the percentage of $PD\text{-}1^+$ cells within $CD11b^-$ lymphocytes ($PD\text{-}1^+$ within $CD11b^-$ $CD45^+$), CTLA4 within $CD4^+$ T cells (CTLA4 within $CD3^+$ $CD8^-$ $CD11b^-CD45^+$), PD-L1 within tumor $CD45^-$ cells (PD-L1 within $F4/80^+$ $CD11b^+$ $CD45^+$) and Tregs ($FoxP3^+$ $CD25^+$ $CD4^+$ $CD11b^-$ within $CD45^+$) in $RANK^{+/+}$ and $RANK^{-/-}$ transplants in syngeneic C57BL/6 mice. Each dot represents an individual tumor transplant derived from 2-5 different primary tumors. Mean, SEM and t-test p-values are shown. (*, $p < 0.05$; ****, $p < 0.0001$).

b. Experimental scheme for early treatments with anti-RANKL (a-RL), anti-CTLA4, anti-PD-L1 or their respective isotype controls (rat IgG2A and mouse IgG2b). All treatments were administered i.p, two times/week and started 3 days after injection of $RANK^{+/+}$ and $RANK^{-/-}$ tumor cells into the mammary gland of syngeneic C57BL/6 mice.

c-d. Tumor growth curves for early treatments (scheduled as in Fig. 4b) of $RANK^{+/+}$ (c) and $RANK^{-/-}$ (d) tumor cells injected in syngeneic C57BL/6. Each thin curve represents one single tumor. Each thick curve represents the mean of all the tumors that received the specific treatment. Regression analysis of the growth curves' mean from the different treatments is shown (****, $p<0.0001$).

e. Experimental scheme for late treatments with anti-RL, anti-CTLA4, anti-PD-L1, or their respective isotype controls (rat IgG2A and mouse IgG2b). All treatments were administered i.p., three times/week and started when transplanted tumors reached a size of 0.09 cm^2.

f-g. Tumor growth curves for late treatments (scheduled as in Fig 4e) of $RANK^{+/+}$ (f) and $RANK^{-/-}$ (g) tumor cells injected in syngeneic C57BL/6. Each thin curve represents one single tumor. Each thick curve represents the mean of all the tumors that received the specific treatment. Regression analysis of the growth curves' mean from the different treatments was performed (**, $p < 0.01$; ***, $p < 0.001$; ****, $p < 0.0001$).

Figure 5. The immunomodulatory role of anti-RANKL in BC

a. Change from baseline in serum levels of free-sRANKL (n = 23) and CTX (n = 17), (significance assessed by the sign test), the percentage of Ki-67-positive cells and the staining of activated caspase-3 (H-score) (n = 24) (significance assessed by paired t-tests)[#].

b. Each bar-plot shows the change from baseline (Δ; post- minus pre-treatment values) of the immune parameters assessed using HE (TILs) and IHC (CD3, CD20, CD8, FOXP3, proliferative TILs ($TILs^{Ki67+}$), CD68 and CD163). Each bar represents one patient, which are ranked by their increase in stromal TIL levels. Geometric mean changes, 95% CIs and p-values are shown below each bar-plot. For each measured parameter, the corresponding ladder-plot is displayed on the right-hand side. Tumor characteristics and tumor RANK metagene expression at baseline are shown above. p; P-value derived from the paired t-test (*, $p<0.05$)[#].

c. Representative micrographs of multiplex IHC of pre- and post-treatment tumor sections from the four patients with the highest immunomodulatory response. Scale bar, 100 μm.

d. Top 20 significantly enriched pathways after denosumab treatment, identified by GAGE.

e. Comparison of baseline serum levels of sRANKL between non-responders (NR; n = 13) *vs.* responders (R; n = 11) and comparison of baseline percentage of regulatory T cells (Tregs) as inferred from CIBERSORT.

f. Comparison of baseline mRNA expression levels of indicated genes (normalized counts) between non-responder (NR; n = 11) and responder (R; patients with ≥ 10% increase in TILs after denosumab treatment. n = 11) groups.

g. Comparison of baseline RANK metagene and RANKL-treated PyMT tumor acini derived gene signature between non-responder (n = 11) and responder (n = 11) patients. For panels a-b: each colored line represents one patient and indicates increase (red), decrease (blue) or no change (black) relative to baseline. Note that all variables were analyzed for all patients, but values for some lines overlap or the indicated population was not detected.

[#]Responder patients are those with ≥ 10% increase in TIL infiltration after denosumab treatment. Significance determined by the Mann–Whitney U test.

Figure 6. Graphical Abstract

RANK expression in luminal breast cancer cells leads to the expression of pro-inflammatory cytokines/chemokines favoring recruitment of TAMs and TANs, immunosuppressive population which interfere with lymphocyte T cell recruitment and/or activity. Denosumab (anti-RANKL) or RANK signaling inhibition results in increased TILs, lymphocytes and CD8+ T cell infiltration, transforming immune "cold" tumors into "hot" ones and attenuating tumor growth. Eventually the exacerbated immune response driven by RANK inhibition will induce the expression of immune checkpoints evading immune surveillance and allowing tumor growth. These results support the benefit of combining RANKL and immune checkpoint inhibitors in luminal breast cancer.

Figure 1

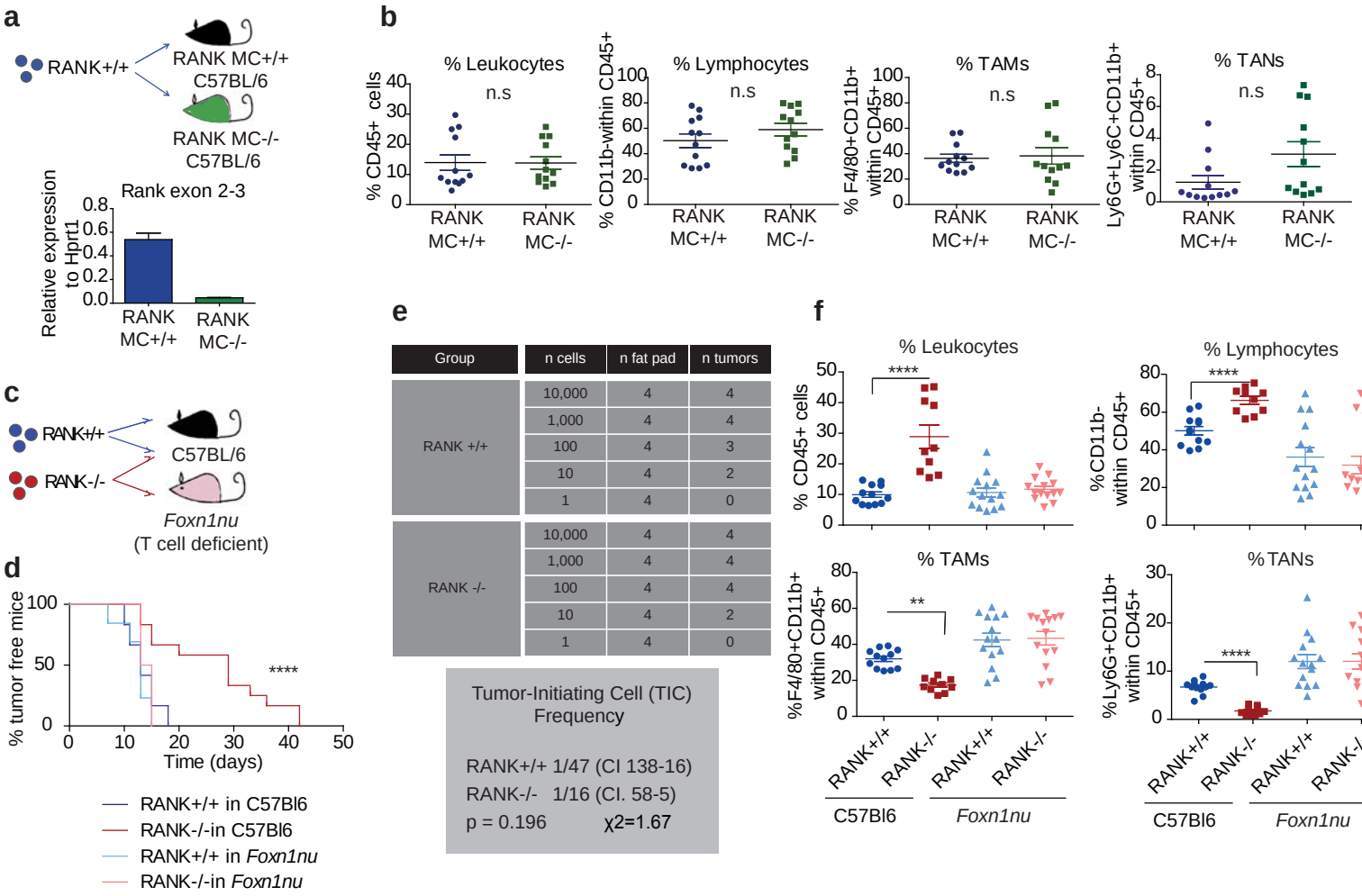
a
RANK+/+
RANK MC+/+ C57BL/6
RANK MC-/- C57BL/6
Rank exon 2-3
Relative expression to Hprt1
RANK MC+/+
RANK MC-/-
b
% Leukocytes
% CD45+ cells
n.s
% Lymphocytes
% CD11b-within CD45+
% TAMs
% F4/80+CD11b+ within CD45+
% TANs
Ly6G+Ly6C+CD11b+ within CD45+
c
RANK+/+
RANK-/-
C57BL/6
Foxn1nu
(T cell deficient)
d
% tumor free mice
Time (days)
****
RANK+/+ in C57Bl6
RANK-/-in C57Bl6
RANK+/+ in Foxn1nu
RANK-/-in Foxn1nu
e
Group
n cells
n fat pad
n tumors
RANK +/+
10,000 4 4
1,000 4 4
100 4 3
10 4 2
1 4 0
RANK -/-
10,000 4 4
1,000 4 4
100 4 4
10 4 2
1 4 0
Tumor-Initiating Cell (TIC) Frequency
RANK+/+ 1/47 (CI 138-16)
RANK-/- 1/16 (CI. 58-5)
p = 0.196 χ2=1.67
f
% Leukocytes
% CD45+ cells
****
% Lymphocytes
%CD11b- within CD45+
% TAMs
%F4/80+CD11b+ within CD45+
**
% TANs
%Ly6G+CD11b+ within CD45+
RANK+/+
RANK-/-
C57Bl6
Foxn1nu
g
Leukocytes
RANK+/+ in C57BL/6
RANK-/- in C57BL/6
RANK+/+ in Foxn1nu
RANK-/- in Foxn1nu
8.8
43.6
3.9
7.6
SSC-A
CD45
Lymphocytes
56.2
69.7
29.9
28.7
CD11b
Tumor-associated neutrophils (TANs)
8.9
0.65
13.4
8.5
Ly6G

Figure 2

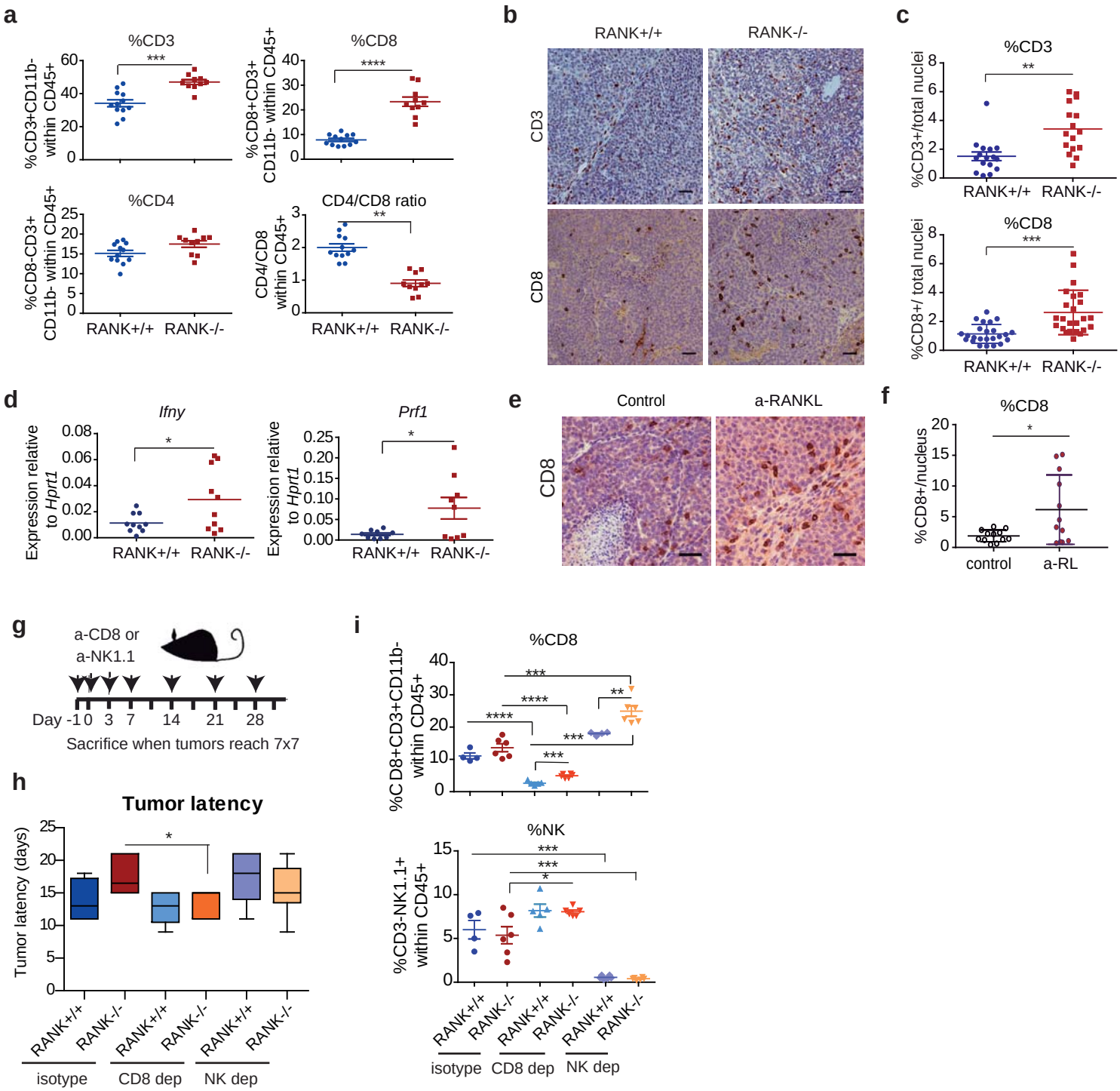
a
%CD3
%CD3+CD11b- within CD45+
%CD8
%CD8+CD3+ CD11b- within CD45+
%CD4
%CD8-CD3+ CD11b- within CD45+
CD4/CD8 ratio
CD4/CD8 within CD45+
RANK+/+
RANK-/-
b
RANK+/+
RANK-/-
CD3
CD8
c
%CD3
%CD3+/total nuclei
%CD8
%CD8+/ total nuclei
d
Ifny
Prf1
Expression relative to Hprt1
e
Control
a-RANKL
CD8
f
%CD8
%CD8+/nucleus
control
a-RL
g
a-CD8 or
a-NK1.1
Day -1 0 3 7 14 21 28
Sacrifice when tumors reach 7x7
h
Tumor latency
Tumor latency (days)
isotype
CD8 dep
NK dep
i
%CD8
%C D8+CD3+CD11b- within CD45+
%NK
%CD3-NK1.1+ within CD45+

Figure 3

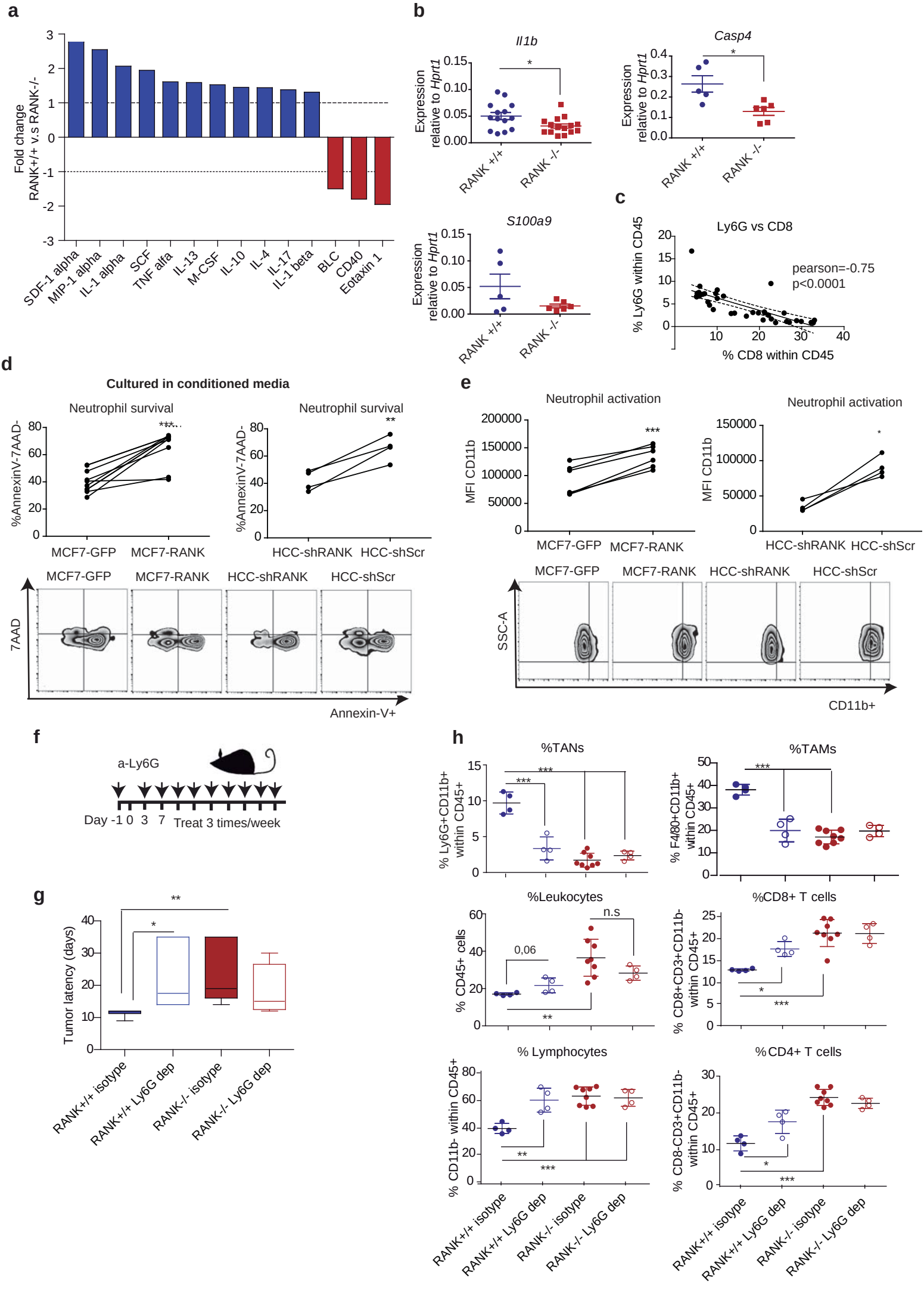
a
Fold change RANK+/+ v.s RANK-/-
SDF-1 alpha
MIP-1 alpha
IL-1 alpha
SCF
TNF alfa
IL-13
M-CSF
IL-10
IL-4
IL-17
IL-1 beta
BLC
CD40
Eotaxin 1
b
Il1b
Casp4
S100a9
Expression relative to Hprt1
RANK +/+
RANK -/-
c
Ly6G vs CD8
% Ly6G within CD45
% CD8 within CD45
pearson=-0.75
p<0.0001
d
Cultured in conditioned media
Neutrophil survival
%AnnexinV-7AAD-
MCF7-GFP
MCF7-RANK
HCC-shRANK
HCC-shScr
7AAD
Annexin-V+
e
Neutrophil activation
MFI CD11b
SSC-A
CD11b+
f
a-Ly6G
Day -1 0 3 7
Treat 3 times/week
g
Tumor latency (days)
RANK+/+ isotype
RANK+/+ Ly6G dep
RANK-/- isotype
RANK-/- Ly6G dep
h
%TANs
% Ly6G+CD11b+ within CD45+
%TAMs
% F4/80+CD11b+ within CD45+
%Leukocytes
% CD45+ cells
0,06
n.s
%CD8+ T cells
% CD8+CD3+CD11b- within CD45+
% Lymphocytes
% CD11b- within CD45+
%CD4+ T cells
% CD8-CD3+CD11b- within CD45+

Figure 4

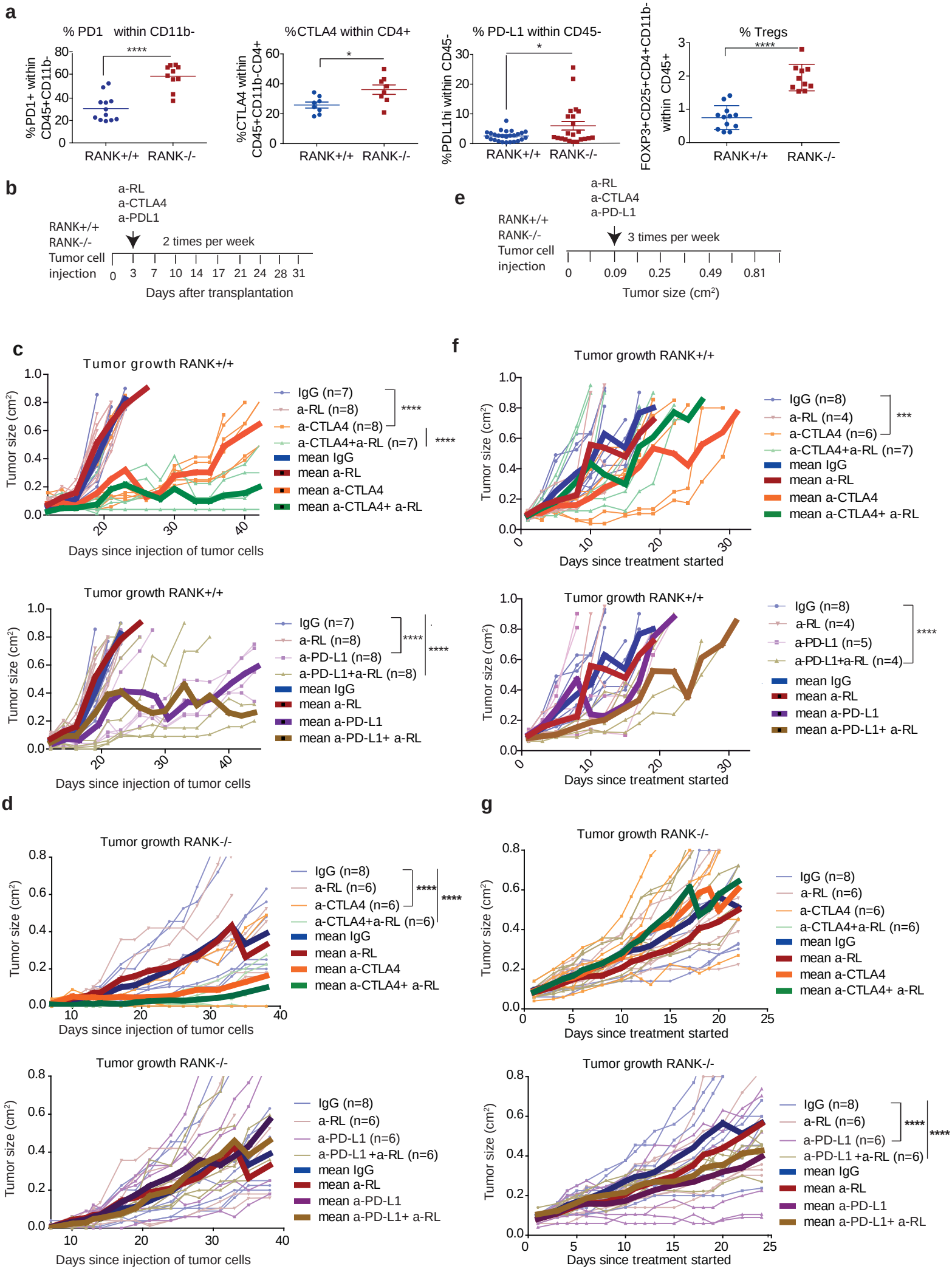
a
% PD1 within CD11b-
%PD1+ within CD45+CD11b-
****
RANK+/+ RANK-/-
%CTLA4 within CD4+
%CTLA4 within CD45+CD11b-CD4+
*
RANK+/+ RANK-/-
% PD-L1 within CD45-
%PDL1hi within CD45-
*
RANK+/+ RANK-/-
% Tregs
FOXP3+CD25+CD4+CD11b- within CD45+
****
RANK+/+ RANK-/-
b
a-RL
a-CTLA4
a-PDL1
RANK+/+
RANK-/-
Tumor cell injection
2 times per week
0 3 7 10 14 17 21 24 28 31
Days after transplantation
e
a-RL
a-CTLA4
a-PD-L1
RANK+/+
RANK-/-
Tumor cell injection
3 times per week
0 0.09 0.25 0.49 0.81
Tumor size (cm²)
c
Tumor growth RANK+/+
Tumor size (cm²)
IgG (n=7)
a-RL (n=8)
a-CTLA4 (n=8)
a-CTLA4+a-RL (n=7)
****
****
mean IgG
mean a-RL
mean a-CTLA4
mean a-CTLA4+ a-RL
Days since injection of tumor cells
Tumor growth RANK+/+
Tumor size (cm²)
IgG (n=7)
a-RL (n=8)
a-PD-L1 (n=8)
a-PD-L1+a-RL (n=8)
****
****
mean IgG
mean a-RL
mean a-PD-L1
mean a-PD-L1+ a-RL
Days since injection of tumor cells
f
Tumor growth RANK+/+
Tumor size (cm²)
IgG (n=8)
a-RL (n=4)
a-CTLA4 (n=6)
a-CTLA4+a-RL (n=7)
***
mean IgG
mean a-RL
mean a-CTLA4
mean a-CTLA4+ a-RL
Days since treatment started
Tumor growth RANK+/+
Tumor size (cm²)
IgG (n=8)
a-RL (n=4)
a-PD-L1 (n=5)
a-PD-L1+a-RL (n=4)
****
mean IgG
mean a-RL
mean a-PD-L1
mean a-PD-L1+ a-RL
Days since treatment started
d
Tumor growth RANK-/-
Tumor size (cm²)
IgG (n=8)
a-RL (n=6)
a-CTLA4 (n=6)
a-CTLA4+a-RL (n=6)
****
****
mean IgG
mean a-RL
mean a-CTLA4
mean a-CTLA4+ a-RL
Days since injection of tumor cells
Tumor growth RANK-/-
Tumor size (cm²)
IgG (n=8)
a-RL (n=6)
a-PD-L1 (n=6)
a-PD-L1 +a-RL (n=6)
mean IgG
mean a-RL
mean a-PD-L1
mean a-PD-L1+ a-RL
Days since injection of tumor cells
g
Tumor growth RANK-/-
Tumor size (cm²)
IgG (n=8)
a-RL (n=6)
a-CTLA4 (n=6)
a-CTLA4+a-RL (n=6)
mean IgG
mean a-RL
mean a-CTLA4
mean a-CTLA4+ a-RL
Days since treatment started
Tumor growth RANK-/-
Tumor size (cm²)
IgG (n=8)
a-RL (n=6)
a-PD-L1 (n=6)
a-PD-L1 +a-RL (n=6)
****
****
mean IgG
mean a-RL
mean a-PD-L1
mean a-PD-L1+ a-RL
Days since treatment started

Figure 5

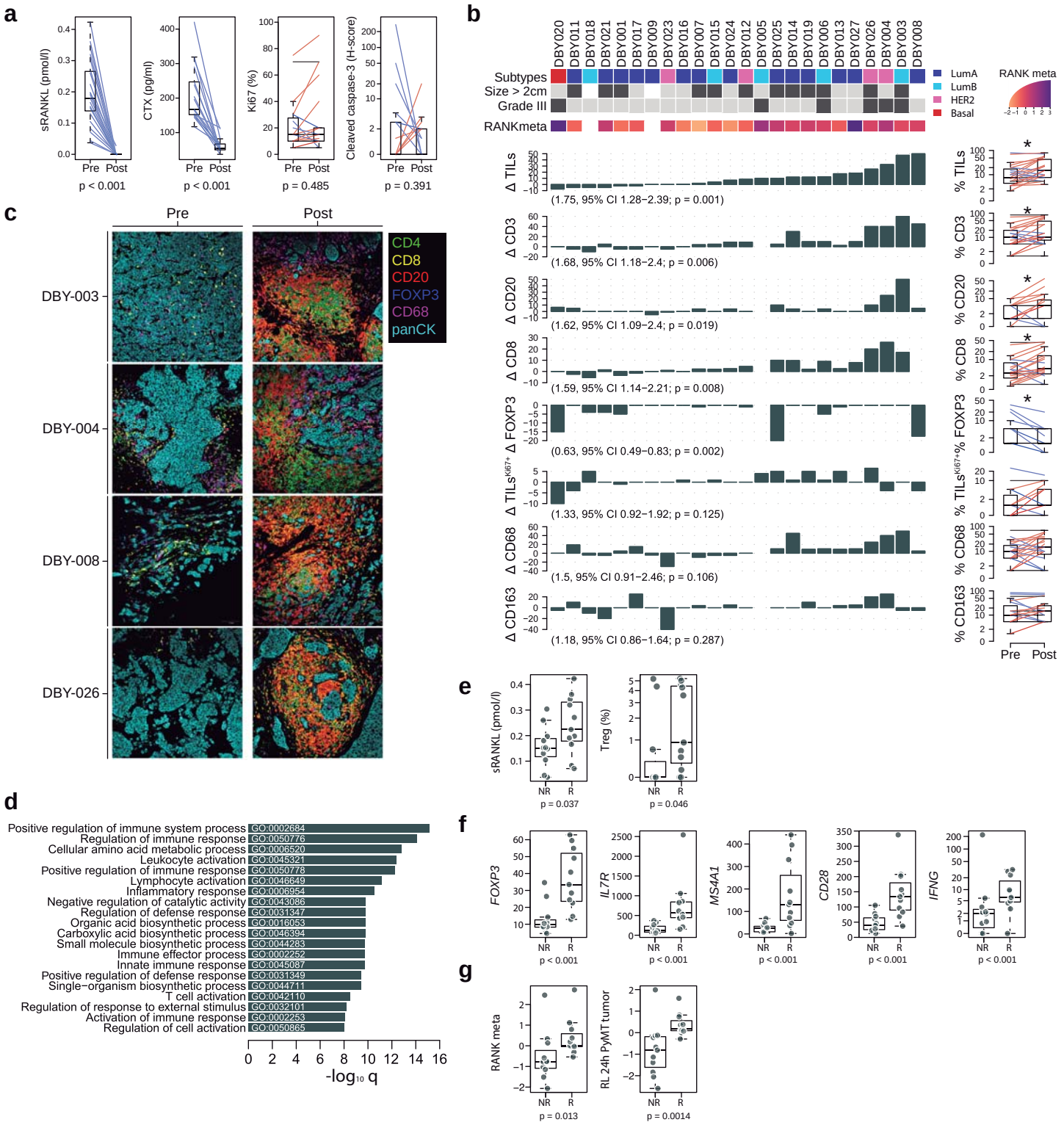
a
sRANKL (pmol/l)
CTX (pg/ml)
Ki67 (%)
Cleaved caspase-3 (H-score)
Pre Post
p < 0.001
p < 0.001
p = 0.485
p = 0.391
b
DBY020 DBY011 DBY018 DBY021 DBY001 DBY017 DBY009 DBY023 DBY016 DBY007 DBY015 DBY024 DBY012 DBY005 DBY025 DBY014 DBY019 DBY006 DBY013 DBY027 DBY026 DBY004 DBY003 DBY008
Subtypes
Size > 2cm
Grade III
RANKmeta
LumA
LumB
HER2
Basal
RANK meta
Δ TILs
(1.75, 95% CI 1.28−2.39; p = 0.001)
Δ CD3
(1.68, 95% CI 1.18−2.4; p = 0.006)
Δ CD20
(1.62, 95% CI 1.09−2.4; p = 0.019)
Δ CD8
(1.59, 95% CI 1.14−2.21; p = 0.008)
Δ FOXP3
(0.63, 95% CI 0.49−0.83; p = 0.002)
Δ TILs Ki67+
(1.33, 95% CI 0.92−1.92; p = 0.125)
Δ CD68
(1.5, 95% CI 0.91−2.46; p = 0.106)
Δ CD163
(1.18, 95% CI 0.86−1.64; p = 0.287)
% TILs
% CD3
% CD20
% CD8
% FOXP3
% TILs Ki67+
% CD68
% CD163
Pre Post
c
Pre Post
DBY-003
DBY-004
DBY-008
DBY-026
CD4
CD8
CD20
FOXP3
CD68
panCK
d
Positive regulation of immune system process GO:0002684
Regulation of immune response GO:0050776
Cellular amino acid metabolic process GO:0006520
Leukocyte activation GO:0045321
Positive regulation of immune response GO:0050778
Lymphocyte activation GO:0046649
Inflammatory response GO:0006954
Negative regulation of catalytic activity GO:0043086
Regulation of defense response GO:0031347
Organic acid biosynthetic process GO:0016053
Carboxylic acid biosynthetic process GO:0046394
Small molecule biosynthetic process GO:0044283
Immune effector process GO:0002252
Innate immune response GO:0045087
Positive regulation of defense response GO:0031349
Single−organism biosynthetic process GO:0044711
T cell activation GO:0042110
Regulation of response to external stimulus GO:0032101
Activation of immune response GO:0002253
Regulation of cell activation GO:0050865
0 2 4 6 8 10 12 14 16
-log10 q
e
sRANKL (pmol/l)
Treg (%)
NR R
p = 0.037
p = 0.046
f
FOXP3
IL7R
MS4A1
CD28
IFNG
NR R
p < 0.001
p < 0.001
p < 0.001
p < 0.001
p < 0.001
g
RANK meta
RL 24h PyMT tumor
NR R
p = 0.013
p = 0.0014

Figure 6

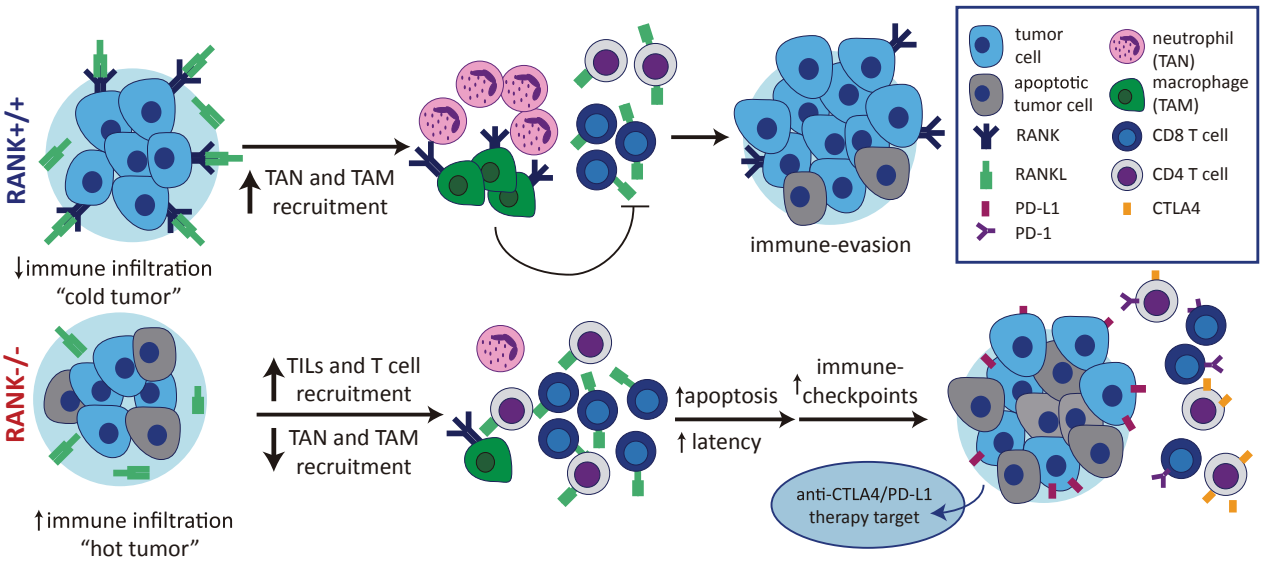
RANK+/+
↓immune infiltration
"cold tumor"
TAN and TAM
recruitment
immune-evasion
tumor cell
apoptotic tumor cell
RANK
RANKL
PD-L1
PD-1
neutrophil (TAN)
macrophage (TAM)
CD8 T cell
CD4 T cell
CTLA4
RANK-/-
↑immune infiltration
"hot tumor"
↑TILs and T cell
recruitment
↓TAN and TAM
recruitment
↑apoptosis
↑latency
immune-
checkpoints
anti-CTLA4/PD-L1
therapy target

RANK signaling increases after anti-HER2 therapy contributing to the emergence of resistance in HER2-positive breast cancer

Sanz-Moreno A[1†], Palomeras S[2†], Pedersen K[1†], Morancho B[3,4], Pascual T[5,6,7], Galván P[5], Benítez S[1], Gomez-Miragaya J[1], Ciscar M[1,8], Pernas S[6,9], Petit A[9,10], Soler-Monsó MT[9,10], Viñas G[2,11], Alsaleem M[12], Rakha EA[12], Green AR[12], Santamaria PG[4,8], Mulder C[13], Lemeer S[13], Arribas J[3,4], Prat A[5,6,7,14], Puig T[2*], Gonzalez-Suarez E[1,8*].

† contributed equally

* corresponding authors

teresa.puig@udg.edu; egonzalez@cnio.es

Affiliations:

1. Oncobell, Bellvitge Biomedical Research Institute (IDIBELL), L'Hospitalet de Llobregat, Barcelona, Spain.
2. New Therapeutics Targets Lab (TargetsLab), Department of Medical Sciences, University of Girona, Girona, Spain.
3. Preclinical Research Program, Vall d'Hebron Institute of Oncology (VHIO), Barcelona, Spain.
4. Centro de Investigación Biomédica en Red de Cáncer (CIBERONC), Spain.
5. Translational Genomics and Targeted Therapeutics in Solid Tumors, August Pi i Sunyer Biomedical Research Institute (IDIBAPS), Barcelona, Spain.
6. SOLTI Breast Cancer Research Group, Barcelona, Spain.
7. Department of Medical Oncology, Hospital Clinic, Barcelona, Spain.
8. Molecular Oncology, Spanish National Cancer Research Centre (CNIO), Madrid, Spain.

9. Department of Medical Oncology, Breast Unit, Catalan Institute of Oncology (ICO), University Hospital of Bellvitge IDIBELL, L'Hospitalet de Llobregat, Barcelona, Spain.

10. Pathology Department, University Hospital of Bellvitge, IDIBELL, Barcelona, Spain.

11. Medical Oncology Department, Catalan Institute of Oncology (ICO), Girona, Spain.

12. Division of Cancer and Stem Cells, School of Medicine, University of Nottingham Biodiscovery Institute, University Park, Nottingham, NG7 2RD, UK.

13. Biomolecular Mass Spectrometry and Proteomics Bijvoet Center, Utrecht University, The Netherlands.

14. Medicine Department, University of Barcelona, Barcelona, Spain.

Abstract

Background

Around 15-20% of primary breast cancers are characterized by HER2 protein overexpression and/or *HER2* gene amplification. Despite the successful development of anti-HER2 drugs, intrinsic or acquired resistance represents a major hurdle. This study was performed to analyze RANK pathway contribution to HER2-positive breast cancer and anti-HER2 therapy resistance.

Methods

RANK and RANKL expression was assessed in samples from HER2-positive breast cancer patients treated with anti-HER2 therapy and treatment naïve patients. Gene expression analyses were performed in paired samples from patients treated with neoadjuvant dual HER2-blockade (lapatinib and trastuzumab) from the SOLTI-1114 PAMELA trial. Additionally, HER2-positive breast cancer cell lines were used to analyze *in vitro* the contribution of RANK signaling to anti-HER2 resistance.

Results

RANK and RANKL proteins are more frequently detected in HER2-positive tumors that have acquired resistance to anti-HER2 therapies than in treatment-naïve ones. *RANK* (but not *RANKL*) gene expression increased after dual anti-HER2 neoadjuvant therapy in the cohort from the SOLTI-1114 PAMELA trial. Results in HER2-positive breast cancer cell lines recapitulate the clinical observations, with increased RANK expression after short-term treatment with the HER2 inhibitor lapatinib or dual anti-HER2 therapy and in lapatinib-resistant cells. After RANKL stimulation, lapatinib-resistant cells show increased NF-κB activation compared to their sensitive counterparts, confirming the enhanced functionality of RANK pathway in anti-HER2 resistant breast cancer. RANK overexpression enhances ERK and NF-κB signaling after stimulation with RANKL and increases lapatinib resistance

in different HER2-positive breast cancer cell lines. Our results indicate that ErbB signaling is required for RANK/RANKL-driven activation of ERK in several HER2-positive cell lines. In contrast, lapatinib is not able to counteract the NF-κB activation elicited after RANKL treatment in RANK-overexpressing cells. Finally, we show that enhanced RANK pathway activation alters HER2 phosphorylation status and RANK binding to HER2 in breast cancer cells.

Conclusions

Our data support a physical and functional link between RANK and HER2 signaling in breast cancer and demonstrate that increased RANK signaling may contribute to the development of lapatinib resistance through NF-κB activation. Whether HER2-positive breast cancer patients with tumoral RANK expression might benefit from dual HER2 and RANK inhibition therapy remains to be elucidated.

Keywords

Breast cancer, HER2, lapatinib, NF-κB, RANK, RANKL, resistance, trastuzumab

Background

The human epidermal growth factor receptor 2 (HER2), known as ErbB2 or Neu, is a tyrosine kinase receptor protein encoded by the *ERBB2* (*HER2*) gene (1). HER2 is a member of the epidermal growth factor (EGF) receptor family along with EGFR/HER1, ERBB3/HER3 and ERBB4/HER4. The four receptors are transmembrane proteins with an intracellular tyrosine kinase domain (although ERBB3/HER3 is considered kinase impaired). While HER2 is the only family member that does not bind to a ligand, it forms heterodimers with the other EGF receptor protein members and shows strong catalytic kinase activity, efficiently triggering downstream signaling through phosphatidylinositol-3 kinase (PI3K) and mitogen-activated protein kinase (MAPK) (1). Approximately 15-20% of

primary breast cancers show HER2 protein overexpression and/or *HER2* gene amplification (2), which is associated with poor prognosis. The development of humanized monoclonal antibodies binding the extracellular domain of HER2 (e.g. trastuzumab, pertuzumab), EGFR-HER2 small molecule kinase inhibitors (e.g. lapatinib, neratinib or tucatinib) and antibody-drug conjugates (e.g. T-DM1 or DS-8201) has revolutionized HER2-positive breast cancer treatment (3). Still, most patients with metastatic disease eventually progress on anti-HER2 therapy due to *de novo* or acquired resistance, and 20-30% of patients with early HER2+ breast cancer relapse (4-6). Therefore, elucidating the mechanisms of resistance to anti-HER2 drugs is pivotal to further improve patients´ survival outcomes.

Receptor activator of nuclear factor kappa-B ligand (RANKL) and its receptor (RANK) belong to the TNF superfamily. The fundamental role of RANK signaling in osteoporosis and bone metastasis inspired the development of denosumab, a monoclonal antibody against RANKL, for the treatment of skeletal-related events (SREs) linked to osteoporosis and cancer (7). RANK signaling activation in the breast epithelium impacts tumor initiation, progression and metastatic spread. Thus, RANK and RANKL have emerged as promising targets for cancer treatment (8). RANKL is expressed in progesterone receptor-positive cells and acts as a paracrine mediator of progesterone in the mammary epithelia (9, 10). Increased RANK receptor expression is more frequent in hormone-receptor negative cells and high-grade breast cancer, but it is also found in a subset of luminal tumors (11, 12). RANK signaling controls proliferation and stemness in BRCA1-mutant and oncogene-driven mammary tumors (13-15). Interestingly, RANK signaling inhibition has been shown to reduce HER2 tumorigenesis in preclinical studies (9, 16). In human tumors, RANKL and HER2 levels predict metastasis to the bone in breast cancer better than RANKL alone (17).

Some of the most common (intrinsic or acquired) resistance mechanisms to trastuzumab and/or lapatinib treatment are impaired HER2 binding, parallel/downstream pathway activation, ER signaling, cell cycle de-regulation or escape from antibody-dependent cellular cytotoxicity (ADCC) (18). Personalized treatment of HER2-positive breast cancer and better predictive biomarkers to anticipate therapy resistance will contribute to the identification of patients that will benefit from new combinatorial therapies, paving the way for HER2-positive breast cancer precision medicine (19).

In this study, we unveiled a functional relationship between RANK and HER2 signaling using HER2-positive breast cancer patient samples and cell lines. Upon analyses of HER2-positive breast cancer samples from treatment-naïve patients, patients treated with trastuzumab-based primary chemotherapy and residual disease at surgery and patients treated with neoadjuvant dual-blockade on the phase II SOLTI-1114 PAMELA trial, we observed that anti-HER2 treatment or acquisition of resistance to anti-HER2 therapy both resulted in increased RANK expression. Besides, when we analyzed the effects of RANK modulation on anti-HER2 treatment, we observed that enhanced RANK signaling led to increased lapatinib resistance in HER2-positive breast cancer cell lines.

Methods

Patient samples

RANK and RANKL expression were assessed in tumor samples from three different cohorts of patients with HER2-positive breast cancer:

Treatment-naïve cohort: patients with primary and operable HER2-positive breast cancer (n = 211) diagnosed from 2003 to 2010 at the Nottingham City Hospital, Nottingham, UK. Tumor samples were collected at surgery prior to any neoadjuvant treatment. Histological grade was assessed by the Nottingham Grading System (20) and other clinicopathological factors such as tumor size, lymph node (LN) status, estrogen receptor (ER), progesterone

receptor (PR) and HER2 expression, as well as patient age and disease progression were analyzed before including the samples into the TMAs, prepared as previously described (21).

Anti-HER2 resistant cohort: patients treated with trastuzumab-based primary chemotherapy and residual disease at surgery (n = 43) diagnosed at the Catalan Institute of Oncology (ICO), Bellvitge University Hospital in l'Hospitalet de Llobregat and Dr. Josep Trueta University Hospital in Girona (Spain) between 2005 and 2014 and described in (22). The selection criterion included patients with early or locally advanced HER2-positive breast cancer (including inflammatory breast cancer) who had received neoadjuvant treatment with trastuzumab-based chemotherapy and had residual invasive disease following surgery (i.e. who had not achieved a pathological complete response at surgery). Neoadjuvant chemotherapy was based on anthracyclines and taxanes given concurrently with weekly-trastuzumab for 24 weeks followed by surgery.

For all patients, hematoxylin and eosin (H&E) stained slides from formalin-fixed paraffin-embedded (FFPE) tumor blocks were examined to determine the representative areas of the invasive tumor. ER, PR, and HER2 positivity were assessed in the initial tumor core-biopsies as well as in the residual disease. For each patient different clinical and histopathological features such as age, tumor stage (TNM classification) and histological grade (Nottingham Grading System) were obtained.

SOLTI-1114 PAMELA cohort: patients treated with neoadjuvant dual-blockade with trastuzumab and lapatinib (n = 151), and in which paired samples were prospectively obtained. The main results of the PAMELA neoadjuvant phase II study have been previously reported (23) and the completed study is registered with ClinicalTrials.gov (number NCT01973660). In this trial, patients with early HER2-positive breast cancer were treated with neoadjuvant lapatinib (1000 mg daily) and trastuzumab (8 mg/kg i.v. loading

dose followed by 6 mg/kg) for 18 weeks. Patients with hormonal receptor-positive breast cancer received letrozole or tamoxifen according to menopausal status. FFPE tumor samples at baseline, at day 14 of treatment and at surgery were collected according to protocol.

Gene expression analyses

RNA samples of the PAMELA trial from tumors at baseline (n = 151) were previously analyzed (23). Here, the nCounter platform (NanoString Technologies, Seattle, Washington, USA) analyzed RNA of 101 residual tumors from surgical samples of the PAMELA trial. A minimum of 100 ng of total RNA was used to measure the expression of 550 genes, including *TNFRSF11A and TNFSF11,* and 5 housekeeping genes (*ACTB, MRPL19, PSMC4, RPLP0* and *SF3A1*). Expression counts were then normalized using the nSolver 4.0 software and custom scripts in R 3.4.3. For each sample, we calculated the PAM50 signature scores (Basal-like, HER2-E, Luminal A and B, normal-like) and the risk of recurrence score (24). Intrinsic molecular subtypes were identified using the research-based PAM50 predictor as previously described (23, 25).

Immunohistochemistry and Tissue Microarray scoring

Immunohistochemistry (IHC) in TMAs was performed using anti-human mouse monoclonal RANK (N-1H8 Amgen) and human RANKL (M366 Amgen) as described in (9). RANK or RANKL staining was scored on a scale of 0 to 3 for intensity (0 = no staining, 1 = weak, 2 = moderate, 3 = intense) and for the percentage of positive stained tumor cells (0–100) as previously reported (26). The result of multiplying staining intensity by positive cell percentage is the H-score value, ranging from 0 to 300. TMA cores were scored if tumor cells represented > 15% of the total TMA core area. Patients were stratified according to RANK or RANKL H-scores as being protein-positive (H-score ≥ 1) or protein-negative (H-score = 0). Statistical analyses were performed with the support of IDIBELL and

Nottingham University Statistical Assessment Services. The ER/PR/HER2 status, grade and tumor stage were known for each case included in the TMAs. Associations between IHC scores and clinicopathological parameters were evaluated using Pearson Chi-square test or Fisher's exact test.

Cell lines and cell culture

The cell lines BT474 parental (BT474) and BT474 with lapatinib resistance (BTLR) were described in (27). SKBR3 parental (SKBR3) and SKBR3 with lapatinib resistance (SKLR) lines were described in (28). The cell line HCC1954 was obtained from ATCC (CRL-2338). BT474 cells were grown in DMEM + GlutaMAX (Gibco) supplemented with 2 mM L-Glutamine (HyClone), 1x penicillin-streptomycin solution (P/S, Gibco) and 7.5% fetal bovine serum (FBS, Gibco). SKBR3 cells were grown in McCoy's 5A + GlutaMAX supplemented with 2 mM L-Glutamine, 1 mM Sodium Pyruvate (HyClone), 1x P/S and 5% FBS. HCC1954 cells were grown in RPMI Medium 1640 + GlutaMAX supplemented with 2 mM L-Glutamine, 1x P/S and 5% FBS. The cells were grown at 37°C in 5% CO_2 humidified incubators. Cell lines were routinely tested for mycoplasma contamination.

Viral transduction

To ectopically express RANK, the *TNFRSF11A* gene was cloned into the lentiviral vector pSD-69 (kindly provided by S. Duss and M. Bentires-Alj) under the control of hPGK promoter. As a control (ctrl), we used empty pSD-69 plasmid generated by removing the BamHI-SalI fragment containing CcdB and CmR genes. Lentiviruses were prepared in HEK293T cells transfected with psPAX2 (Addgene #12260) and pMD2.G (Addgene #12259) by the calcium phosphate method. Virus-containing supernatants were centrifuged at 1500 rpm for 5 min and filtered with 0.45 µm filters (Millipore) and medium from 1 cm^2 production cells was used to infect 2 cm^2 recipient cells at roughly 33% confluence with fresh medium and 8 µg/ml polybrene (Millipore). Plates were centrifuged

for 1 h at 600 g to improve infection. Transduced cells were selected with 1.5 µg/ml puromycin (Sigma), starting 3 days after infection, and subsequently maintained with 1 µg/ml puromycin in the growth media.

Cell Proliferation

To determine cell proliferation, cells were seeded in 96-well plates with 1000-2000 cells in 100 µl per well. After 24 h, 100 µl of medium with or without the indicated concentrations of lapatinib (0-8 µM) was added and cells were incubated for 4 days. The relative number of viable cells each day was determined by adding 50 µl of diluted CCK-8 reagent according to the manufacturer´s protocol (Sigma).

Western blot

Cells were seeded at approximately 33% confluence in 6-well plates. The following day they were washed and incubated in medium without FBS. The next day the medium was changed to 1.8 ml medium with or without 1 µM lapatinib followed by a 2 h incubation. Subsequently, 0.2 ml of medium with or without 300 ng/ml of RANKL (RANKL-LZ Amgen) was added to the wells. 10 min later, extracts for immunoblots were prepared with modified RIPA buffer (50 mM Tris pH 7.4, 150 mM NaCl, 1% Triton NP-40, 0.25% sodium deoxycholate) containing 1x PhosSTOP and Complete protease inhibitor cocktail (Roche), and protein concentrations determined with DC protein assay reagents (BIO-RAD). 15 µg protein were resolved by SDS-PAGE and blotted into Immobilon-P 0.45 µm membranes (Millipore). Antibodies against the following proteins were used for probing: RANK (R&D Systems AF683), p-HER2 (#2249), HER2 (#2165), p-EGFR (#3777), EGFR (#4267), p-ERK1/2 (#9101), ERK1/2 (#9102), p-AKT (#4051), AKT (#9272), p-p65 (#3033), p65 (#8242), p-IκB, IκB (#9246), p-p38 (#9218), p38 (#4631) (from Cell Signaling), β-Actin (sc-47778) and tubulin (Abcam ab21058).

Immunoprecipitation

Cells were washed twice with ice-cold PBS and proteins were extracted with 20 mM Tris-HCl pH 7.4, 137 mM NaCl, 2 mM EDTA, 10% glycerol, 1% Nonidet P-40 supplemented with 50 µg/ml leupeptin, 50 µg/ml aprotinin, 0.5 mM sodium orthovanadate and 1 mM phenylmethylsulfonyl fluoride. Equal amounts of extracts were incubated for 3 h with immunoglobulin G (Abcam ab171870), FLAG (Sigma F3165), HA (Abcam ab9110), V5 (Thermo Scientific #R961-25), HER2 (32H2 in hose antibody described in (29)) or trastuzumab (Hoffmann-La Roche) antibodies and then protein A agarose beads (Calbiochem IP02) were added for 2 h. Immunoprecipitates were washed thoroughly with lysis buffer and boiled in reducing conditions to be analyzed by Western blot.

RNA isolation and RT-qPCR

Cells were seeded at approximately 33% confluence in 6-well plates. The next day the medium was changed to medium with or without 100 ng/ml RANKL (Amgen) followed by an additional 24 h incubation period. To analyze mRNA expression levels, total RNA was purified with Maxwell RSC simplyRNA Tissue kit (AS1340 Promega). For each sample, cDNA was retrotranscribed from 1 µg of RNA using 200U SuperScript II plus random hexamer oligos following manufacturer´s protocol (Invitrogen). 20 ng/well of cDNA for each sample was analyzed by SYBR green real-time PCR (Applied Biosystems) with 10 µM primers using a LightCycler® 480 thermocycler (Roche). Analyses were performed in triplicates using LightCycler® 480 software (Roche). *PP1A* was used as the reference gene. The primer sequences used in the analyses are: *PP1A* (fw ATGGTCAACCCCACCGTT, rev TCTGCTGTCTTTGGGACCTTG); *RANK* (fw GCAGGTGGCTTTGCAGAT, rev 5'GCATTTAGAAACATGTACTTTCCTG); *BIRC3* (fw GGTAACAGTGATGATGTCAAATG, rev TAACTGGCTTGAACTTGACG); *ICAM1* (fw AACTGACACCTTTGTTAGCCACCTC, rev CCCAGTGAAATGCAAACAGGAC); *CCL2* (fw AGGTGACTGGGCATTGAT, rev GCCTCCAGCATGAAAGTCT); *TNFα* (fw

AAGCTGTAGCCCATGTTGT, rev TGAGGTAACAGGCCCTCTGAT) and *IL8* (fw CTGCGCCAACACAGAAATTA, rev CATCTGGCAACCCTACAACA).

Results

RANK is expressed in HER2-positive and anti-HER2 resistant breast cancer patients

The expression of RANK and RANKL in HER2-positive breast cancer patients was analyzed by immunohistochemistry (IHC) in two independent sets of tissue microarrays (TMAs): a collection with tumor samples from treatment-naïve patients (n = 211) and a cohort with tumors resistant to neoadjuvant trastuzumab-based chemotherapy (n = 43) patients with residual invasive disease at surgery).

In the first collection, integrity of the tissue allowed scoring of 67 and 72 HER2-positive treatment-naïve breast cancer patients could be scored for RANK and RANKL expression, respectively. Considering positive samples those with H score ≥ 1, RANK tumor expression was found in 14/67 (20.9%) patients´ samples and transmembrane RANKL staining in just 2/72 (2.8%) of the tumor samples (Fig. 1A). In the anti-HER2 resistant tumor samples, we could score 22 patients for RANK and 21 for RANKL (Fig. 1A). From these, 9/22 (40.9%) were positive for RANK and 2/21 (9.5%) for transmembrane RANKL in tumor cells (Fig. 1A). Representative pictures of RANK and RANKL IHC are shown in Figure 1B.

We then evaluated the clinicopathological factors associated with RANK expression in treatment-naïve HER2-positive tumors (Fig. 1C). RANK expression was significantly associated with tumors from younger patients (less than 50 years old; p = 0.034) and tumors with higher Ki67 proliferation index (p = 0.02). A trend for increased frequency of RANK expression was found in ER/PR negative tumors (p = 0.170 and p = 0.090, respectively), tumors with lymph node positivity (n.s.) and higher histological grade (p =

0.138) (Fig. 1C). Similar patterns were observed in tumors resistant to anti-HER2 treatment (Fig. 1C). In both series, the limited number of samples prevented additional statistically significant associations, but general patterns coincided with those reported in previous studies of RANK/RANKL expression in human breast cancer samples (11, 12, 30). Of note, the frequency of RANK/RANKL-positive samples was higher in anti-HER2 resistant compared to treatment-naïve HER2-positive tumors.

RANK expression increases after anti-HER2 treatment in HER2-positive breast cancer patients (PAMELA clinical trial)

Our previous results suggested that RANK and RANKL expression may increase upon anti-HER2 treatment resistance acquisition in human HER2-positive breast cancer (Fig. 1A). To identify RANK and RANKL changes induced by dual HER2 blockade in patients with HER2-positive disease, gene expression profiling was performed in paired surgical tumor samples obtained before and following treatment with lapatinib and trastuzumab (and endocrine therapy if the tumor was hormone receptor positive) from the PAMELA phase II clinical trial (23). At baseline, the expression of *TNFRSF11A* (*RANK*) was significantly associated with the PAM50 intrinsic subtypes (Additional file 1: Figure S1A; $p < 0.001$), showing non-luminal subtypes (Basal-like and HER2-enriched) the highest *RANK* expression. No significant differences in *TNFSF11* (*RANKL*) gene expression across PAM50 intrinsic subtypes were observed, although RANKL levels were slightly increased in the Luminal A subtype (Additional file 1: Figure S1A), as previously reported (30). As expected, *RANK* gene expression was higher in hormone receptor negative tumor samples ($p < 0.001$) while *RANKL* showed the opposite trend (Fig. 2A) confirming previous findings (12, 31). *ERBB2* gene expression at baseline had a weak positive correlation ($r = 0.16$) with *TNFRSF11A* and the opposite trend ($r = - 0.21$) with *TNFSF11* expression (Additional file 1: Figure S1B and S1C). *RANK* gene expression increased (red lines in

graph) following dual treatment with lapatinib and trastuzumab ($p < 0.001$) while *RANKL* expression did not significantly change when analyzing residual disease samples at surgery (Fig. 2B).

These results confirmed that *RANK* expression increases in HER2-positive breast tumors after dual HER2 blockade. The increased levels of RANK observed in patients upon anti-HER2 treatment suggest that activation of RANK signaling may allow the survival of HER2-positive tumor cells and contribute to resistance to anti-HER2 therapies.

RANK signaling is upregulated after short-term lapatinib treatment and in HER2-positive treatment resistant cell lines

As RANK expression increased after dual lapatinib/trastuzumab treatment in HER2-positive breast cancer patients, we decided to test whether *in vitro* short-term treatment with both anti-HER2 drugs, alone or in combination, would influence RANK expression in three different HER2-positive breast cancer cell lines. While SKBR3 and BT474 cells are sensitive to lapatinib and trastuzumab, HCC1954 cells are less sensitive to lapatinib and resistant to trastuzumab (32).

Lapatinib treatment, alone or in combination with trastuzumab, resulted in higher *RANK* mRNA expression in SKBR3 when compared with non-treated cells (Fig 3A). Lapatinib or trastuzumab treatment, as well as their combination, also increased *RANK* expression levels in BT474 cells. In HCC1954 cells, *RANK* expression increased with lapatinib alone or in combination treatment after 12 h, whereas trastuzumab alone did not alter *RANK* expression levels. Also, we analyzed *RANK* expression in SKBR3 cells, either parental (sensitive to lapatinib and trastuzumab), resistant to trastuzumab (SKTR), to lapatinib (SKLR) or to both (SKTLR and SKLTR; derived from SKTR and SKLR, respectively) (28). RANK gene and protein expression levels were significantly higher in lapatinib-resistant SKLR and dual lapatinib/trastuzumab resistant SKLTR cells when compared to SKBR3

parental cells (Fig. 3B and C). Increased *RANK* mRNA expression was also observed in BT474 cells with acquired lapatinib resistance (LR) as compared to lapatinib-sensitive parental cells in public datasets (platform ID: GPL570; (33)) (Fig. 3D) which we confirmed by RT-qPCR (Fig. 4A).

Taken together, *RANK* expression increased after dual treatment with lapatinib and trastuzumab in HER2-positive human breast cancer cell lines, mimicking the results seen in breast cancer samples from the PAMELA trial (Fig. 2B). Additionally, two HER2-positive cell lines (SKBR3 and BT474) with acquired resistance to lapatinib (SKLR and BTLR) showed increased RANK expression when compared to their respective parental controls (Fig. 3B-D and 4A).

To confirm that the elevated *RANK* expression levels were accompanied by increased activation of RANK signaling pathway, the expression of RANK downstream gene targets *BIRC3, ICAM1, TNFα and IL8,* indicative of NF-κB pathway activation (34, 35), was analyzed in sensitive and lapatinib-resistant (LR) cells treated with or without RANKL. Lapatinib-resistant SKLR cells showed higher gene expression levels of *RANK*, *BIRC3*, *ICAM1*, *TNFα* and *IL8* compared with control SKBR3 cells, and their levels were further increased after pathway stimulation with RANKL, except for *IL8* (Fig. 4A and B). In lapatinib-resistant BTLR, increased expression of *RANK* and its downstream targets *ICAM1* and *IL8* was detected and their levels increased further upon RANKL stimulation compared to sensitive BT474 cells. In these cells, *BIRC3* expression did not change whereas *TNFα* was barely expressed (Fig. 4B). Enhanced NF-κB pathway activation was also evident at the protein level, as RANKL stimulation induced p65 and IκB phosphorylation in lapatinib-resistant SKLR to a greater extent than in SKBR3 cells (Fig. 4C and Additional file 2: Fig. S2), pointing to elevated NF-κB signaling in lapatinib-resistant cells and confirming the enhanced activity of RANK pathway. RANKL treatment did not

significantly alter the phosphorylation status of AKT nor ERK in SKBR3 or SKLR cells (Fig. 4C and Additional file 2: Fig. S2). After lapatinib treatment, HER2, AKT and ERK1/2 protein phosphorylation levels were undetectable, but phosphorylation levels of p65 and IκB were not reduced (Fig. 4C and Additional file 2: Fig. S2), demonstrating that NF-κB activation is not driven by ErbB signaling but may support the survival of HER2-positive breast cancer cells in the presence of lapatinib.

Overactivation of RANK increases NF-κB signaling and resistance to lapatinib

The previous results suggested that increased RANK signaling could contribute to lapatinib resistance. To further test this hypothesis, we stably transduced HER2-positive cell lines with RANK overexpression (psD69-RANK) and empty control (psD69-empty) vectors by lentiviral infection. RANK overexpression was confirmed by increased *RANK* mRNA levels (Fig. 5A) and NF-κB downstream targets (*BIRC3*, *ICAM1*, *TNFα* and *IL8*) in SKBR3, BT474 and HCC1954 cells (Fig. 5B). These RANK overexpressing cell lines showed enhanced expression of all NF-κB targets analyzed after RANKL treatment compared to the corresponding parental cells (Fig. 5B). Next, we tested whether increased activation of RANK signaling would alter the cell response to lapatinib. RANKL stimulation of control cells (empty Ctrl) did not significantly alter lapatinib sensitivity (Fig. 5C). In contrast, RANK overexpression coupled with RANKL treatment resulted in an increased resistance to lapatinib in all HER2-positive cell lines tested (Fig. 5C).

We then analyzed RANK downstream signaling in these cell lines after treatment with lapatinib and/or RANKL. p65 was highly phosphorylated in RANK overexpressing cell lines upon RANKL treatment (Fig. 5D and Additional file 3: Fig. S3), while lapatinib treatment did not affect p65 phosphorylation levels. ERK1/2 and AKT phosphorylation levels increased after RANKL treatment, in both control and RANK overexpressing SKBR3 and BT474 cells (Fig. 5D and Additional file 3: Fig. S3). Interestingly, RANKL-mediated

activation of ERK1/2 and AKT was completely abrogated in the presence of lapatinib. In HCC1954, RANKL treatment increased p-AKT levels to a similar extent in control and RANK overexpressing cells, and again, lapatinib abolished this upregulation. In contrast, p-ERK only increased upon RANKL stimulation in HCC1954 RANK overexpressing cells, which was slightly decreased in the presence of lapatinib (Fig. 5D and Additional file3: Fig. S3).

Taken together, enhanced RANK signaling in HER2-positive cells, after RANK overexpression and RANKL treatment, increases lapatinib resistance and leads to higher NF-κB activation that is not inhibited by lapatinib. Interestingly, ErbB signaling is required for RANK/RANKL-driven activation of ERK and AKT in HER2-positive breast cancer cells.

RANK and HER2 physically and functionally interact

To further investigate the putative crosstalk between RANK and ErbB signaling, we analyzed NF-κB and ErbB signaling after stimulation with ErbB ligands in RANK overexpressing HER2-positive cells lines and corresponding controls. A slight increase in p65 phosphorylation was observed in SKBR3- and BT474- RANK overexpressing cells compared with control cells (Additional file 4: Fig. S4). EGF stimulation faintly increased p-p65 levels in HER2-positive cell lines, but this was not observed after heregulin (HRG) treatment (Additional file 4: Fig. S4). As extensively reported (36), treatment with EGF and HRG efficiently induces ERK phosphorylation in all HER2-positive cell lines (Additional file 4: Fig. S4), but no clear differences were observed between RANK overexpressing cells and corresponding controls. Of note, 5 min after ErbB ligand stimulation, a decrease in HER2 phosphorylation was observed, alongside ERK activation downregulation (Additional file 4: Fig. S4).

To investigate whether RANK/RANKL activation of ERK and AKT might take place, at least partially, via direct crosstalk with ErbB receptors, we compared the phosphorylation

levels of HER2 in cells with and without RANK overexpression upon RANKL stimulation. RANK overexpression led to higher levels of p-HER2 in SKBR3 and BT474, but not in HCC1954 cells, compared with corresponding controls (Fig. 5D and Additional file 3: Fig. S3). Importantly, in all HER2-positive cell lines, concomitant RANK overexpression and stimulation with RANKL resulted in decreased HER2 phosphorylation, indicating that RANKL might impinge on HER2/ErbB signaling pathway (Fig. 5D).

Due to the change in HER2 phosphorylation upon activation of RANK signaling with RANKL, we hypothesized that the two receptors might physically interact. To enable efficient immunoprecipitation and detection, we transiently co-expressed affinity tagged versions of the receptors in HEK293 cells, including an amino (742-NTF) (37) and a carboxy terminal fragment of HER2 (611-CTF) (38). As shown in Figure 6A, RANK-V5 was detected after immunoprecipitation of HER2 or 611-CTF HER2, but not in 742-NTF or any of the control samples (IgG), indicating that RANK interacts with the carboxy-terminal region of HER2. The reverse immunoprecipitation of RANK-V5 corroborated these results (Fig. 6B). To confirm the interaction between the two receptors under endogenous expression levels in the context of breast cancer, we chose SKBR3 cells that, compared to other breast cancer cell lines, express higher levels of HER2 and intermediate/lower levels of RANK. HER2 was immunoprecipitated with the antibody trastuzumab against HER2 extracellular domain and the presence of RANK in the immunoprecipitate was tested by Western blotting. As seen in Figure 6C, trastuzumab precipitated endogenous RANK demonstrating that the two receptors physically interact in breast cancer cells.

Discussion

A crosstalk between RANK and EGFR signaling has been described in the context of osteoclast differentiation (39). In the mammary gland, we found that pharmacological inhibition of RANKL decreases tumorigenesis and lung metastases in the MMTV-ErbB

(Neu) transgenic mouse model (9). In the same line, MMTV-ErbB mice with a heterozygous RANK deletion showed decreased pulmonary metastasis than RANK WT MMTV-ErbB controls (16). In addition, RANKL treatment increased lung metastases in both FVB/N and MMTV-ErbB animals (16). More recently, a review (40) followed by an article with experimental data (41) suggested the combination of RANK and HER2 signaling inhibition as a new strategy for the treatment of HER2-positive breast carcinomas.

In this study, we have shown that *RANK* gene expression is increased after dual treatment with lapatinib and trastuzumab in HER2-positive tumor samples from patients treated on the PAMELA clinical trial (23) and in HER2-positive breast cancer cell lines. These observations would point to increased RANK signaling in patients treated with anti-HER2 drugs. We also observed that the percentage of patients with RANK tumor expression doubled in the context of HER2 resistance when compared to treatment-naïve HER2-positive breast tumors. Furthermore, both SKBR3 and BT474 HER2-positive cell lines with acquired lapatinib resistance displayed increased RANK expression and pathway activation compared to their respective lapatinib-sensitive controls. Thus, our combined analyses of HER2-positive breast cancer tumor samples and HER2-positive cell lines have demonstrated that RANK expression is increased in anti-HER2 treatment resistant breast cancer. Based on these results, one could speculate that anti-HER2 treatment, by enhancing RANK expression, eventually leads to resistance. Moreover, overactivation of RANK signaling increases lapatinib resistance in HER2-positive cell lines (SKBR3, BT474 and HCC1954).

Increased NF-κB activation downstream of RANK (42) may also contribute to lapatinib resistance. Hyperactive NF-κB signaling has been proposed as a possible resistance mechanism after lapatinib treatment in HER2-positive (43) and triple negative breast

cancer (44, 45). In HER2-positive breast cancer, lapatinib-resistant cells show increased NF-κB levels and do not respond to single HER2 or NF-κB inhibitors, but to a combination of both (43). NF-κB expression is normally linked to invasive high-grade tumors and several NF-κB inhibitors are currently being investigated (46, 47). Chen and colleagues showed that lapatinib treatment induced a constitutive activation of NF-κB through Src-dependent p65 and IκBα phosphorylation, sensitizing the cells to proteasome inhibitors (44); our data suggest that increased RANK signaling may also play a role. The phosphorylation of IκBα, leading to its degradation and resulting in p50/p65 heterodimer nuclear translocation, is mediated by the IKK complex (comprising IKKα, IKKβ and IKKγ/NEMO) (48, 49). HER2 itself was shown to activate NF-κB via the canonical pathway involving IKKα in HER2-positive and ER-negative breast cancer cells (50). IKKα also mediates NF-κB activation in mammary cells during pregnancy and after RANKL stimulation (51). In our study, we did not observe clear changes in p65 phosphorylation after stimulation with ErbB ligands and the treatment with lapatinib could not counteract p65 phosphorylation driven by RANKL treatment in RANK overexpressing HER2-positive cell lines. However, we have shown RANK binding to HER2 by co-immunoprecipitation experiments. These results are in agreement with those recently published by Zoi et al. showing the interaction of RANK with ErbB family members by proximity ligation assays (41). In this publication, the authors claim that the number of RANK/HER2 dimers in cells is correlated with HER2 expression levels. Also, denosumab, trastuzumab and/or pertuzumab treatment reduces the number of RANK/HER2 dimers whereas RANKL stimulation leads to an increased number of RANK/HER2 dimers (41). Finally, their data show that RANKL addition decreases the efficacy of HER2 inhibitors (41). In our hands, RANKL stimulation of HER2-positive breast cancer cells overexpressing RANK decreases HER2 phosphorylation, indicating that RANKL influences ErbB2 signaling.

RANKL was shown to promote migration in breast cancer cells after activation of ERK and AKT pathways (52). We have also found increased phosphorylation of ERK1/2 and AKT after RANKL treatment in SKBR3 and BT474 HER2-positive cell lines with both physiological or increased RANK levels upon receptor overexpression. Interestingly, we observed that RANKL-mediated induction of ERK1/2 and AKT phosphorylation was completely abrogated after lapatinib treatment in SKBR3 and BT474 cells, again independently of RANK receptor expression levels. These observations and the fact that RANK and HER2 interact suggest that lapatinib inhibits not only EGFR/HER2 tyrosine phosphorylation but also RANK downstream signaling driven by RANKL (e.g. ERK1/2 and AKT). Importantly, in addition to the direct interaction between RANK and HER2, we observed that RANK signaling is functionally linked to ErbB2 pathway.

Taken together, we showed that anti-HER2 treatment and resistance acquisition both raised RANK expression levels in HER2-positive patients and cell lines. Also, enhanced RANK signaling increased lapatinib resistance in HER2 breast cancer cells. We found that RANK and HER2 physically and functionally interact. Altogether, these results hint to a dual RANK and HER2 inhibition therapy for RANK-expressing HER2-positive breast cancer patients, whose benefit remains to be elucidated.

Conclusions

In summary, we showed that RANK is expressed in HER2-positive breast cancer samples, particularly in patients resistant to anti-HER2 blocking therapy. RANK expression is often associated with younger age, hormone receptor negative status, higher histological grade and proliferation index. Moreover, in HER2-positive breast cancer samples from the PAMELA trial, RANK expression increased upon treatment with lapatinib and trastuzumab. This was confirmed *in vitro* in several HER2-positive human breast cancer cell lines suggesting that RANK signaling may contribute to the development of lapatinib resistance.

Indeed, RANK overexpressing HER2-positive cell lines showed increased resistance to lapatinib and higher NF-κB pathway activation. Finally, we demonstrated that RANK physically and functionally interacted with HER2 suggesting a RANK/HER2 crosstalk whose combined targeting could improve the treatment of RANK-positive HER2 breast cancer patients.

References

1. Moasser MM. The oncogene HER2: its signaling and transforming functions and its role in human cancer pathogenesis. Oncogene. 2007;26(45):6469-87.
2. Slamon DJ, Clark GM, Wong SG, Levin WJ, Ullrich A, McGuire WL. Human breast cancer: correlation of relapse and survival with amplification of the HER-2/neu oncogene. Science. 1987;235(4785):177-82.
3. Pernas S, Tolaney SM. HER2-positive breast cancer: new therapeutic frontiers and overcoming resistance. Ther Adv Med Oncol. T2019;11:1758835919833519.
4. Chumsri S, Li Z, Serie DJ, Mashadi-Hossein A, Colon-Otero G, Song N, et al. Incidence of Late Relapses in Patients With HER2-Positive Breast Cancer Receiving Adjuvant Trastuzumab: Combined Analysis of NCCTG N9831 (Alliance) and NRG Oncology/NSABP B-31. J Clin Oncol. 2019;37(35):3425-35.
5. von Minckwitz G, Huang CS, Mano MS, Loibl S, Mamounas EP, Untch M, et al. Trastuzumab Emtansine for Residual Invasive HER2-Positive Breast Cancer. N Engl J Med. 2019;380(7):617-28.
6. Braso-Maristany F, Griguolo G, Pascual T, Pare L, Nuciforo P, Llombart-Cussac A, et al. Phenotypic changes of HER2-positive breast cancer during and after dual HER2 blockade. Nature communications. 2020;11(1):385.

7. Lacey DL, Boyle WJ, Simonet WS, Kostenuik PJ, Dougall WC, Sullivan JK, et al. Bench to bedside: elucidation of the OPG-RANK-RANKL pathway and the development of denosumab. Nat Rev Drug Discov. 2012;11(5):401-19.

8. Gonzalez-Suarez E, Sanz-Moreno A. RANK as a therapeutic target in cancer. FEBS J. 2016;283(11):2018-33.

9. Gonzalez-Suarez E, Jacob AP, Jones J, Miller R, Roudier-Meyer MP, Erwert R, et al. RANK ligand mediates progestin-induced mammary epithelial proliferation and carcinogenesis. Nature. 2010;468(7320):103-7.

10. Schramek D, Leibbrandt A, Sigl V, Kenner L, Pospisilik JA, Lee HJ, et al. Osteoclast differentiation factor RANKL controls development of progestin-driven mammary cancer. Nature. 2010;468(7320):98-102.

11. Palafox M, Ferrer I, Pellegrini P, Vila S, Hernandez-Ortega S, Urruticoechea A, et al. RANK induces epithelial-mesenchymal transition and stemness in human mammary epithelial cells and promotes tumorigenesis and metastasis. Cancer Res. 2012;72(11):2879-88.

12. Pfitzner BM, Branstetter D, Loibl S, Denkert C, Lederer B, Schmitt WD, et al. RANK expression as a prognostic and predictive marker in breast cancer. Breast Cancer Res Treat. 2014;145(2):307-15.

13. Cuyas E, Corominas-Faja B, Martin MM, Martin-Castillo B, Lupu R, Brunet J, et al. BRCA1 haploinsufficiency cell-autonomously activates RANKL expression and generates denosumab-responsive breast cancer-initiating cells. Oncotarget. 2017;8(21):35019-32.

14. Nolan E, Vaillant F, Branstetter D, Pal B, Giner G, Whitehead L, et al. RANK ligand as a potential target for breast cancer prevention in BRCA1-mutation carriers. Nat Med. 2016;22(8):933-9.

15. Sigl V, Owusu-Boaitey K, Joshi PA, Kavirayani A, Wirnsberger G, Novatchkova M, et al. RANKL/RANK control Brca1 mutation. Cell Res. 2016;26(7):761-74.

16. Tan W, Zhang W, Strasner A, Grivennikov S, Cheng JQ, Hoffman RM, et al. Tumour-infiltrating regulatory T cells stimulate mammary cancer metastasis through RANKL-RANK signalling. Nature. 2011;470(7335):548-53.

17. Shaker OG, Helmy HS. Circulating Bone-related Markers and YKL-40 Versus HER2 and TOPO2a in Bone Metastatic and Nonmetastatic Breast Cancer: Diagnostic Implications. Clin Breast Cancer. 2018;18(3):e321-e8.

18. Vernieri C, Milano M, Brambilla M, Mennitto A, Maggi C, Cona MS, et al. Resistance mechanisms to anti-HER2 therapies in HER2-positive breast cancer: Current knowledge, new research directions and therapeutic perspectives. Crit Rev Oncol Hematol. 2019;139:53-66.

19. Goutsouliak K, Veeraraghavan J, Sethunath V, De Angelis C, Osborne CK, Rimawi MF, et al. Towards personalized treatment for early stage HER2-positive breast cancer. Nat Rev Clin Oncol. 2020;17(4):233-250.

20. Elston CW, Ellis IO. Pathological prognostic factors in breast cancer. I. The value of histological grade in breast cancer: experience from a large study with long-term follow-up. Histopathology. 1991;19(5):403-10.

21. Abd El-Rehim DM, Ball G, Pinder SE, Rakha E, Paish C, Robertson JF, et al. High-throughput protein expression analysis using tissue microarray technology of a large well-characterised series identifies biologically distinct classes of breast cancer confirming recent cDNA expression analyses. Int J Cancer. 2005;116(3):340-50.

22. Pernas S, Gil-Gil M, de Olza MO, Guma A, Climent F, Petit A, et al. Efficacy and safety of concurrent trastuzumab plus weekly paclitaxel-FEC as primary therapy for HER2-positive breast cancer in everyday clinical practice. Breast Cancer Res Treat. 2012;134(3):1161-8.

23. Llombart-Cussac A, Cortes J, Pare L, Galvan P, Bermejo B, Martinez N, et al. HER2-enriched subtype as a predictor of pathological complete response following

trastuzumab and lapatinib without chemotherapy in early-stage HER2-positive breast cancer (PAMELA): an open-label, single-group, multicentre, phase 2 trial. Lancet Oncol. 2017;18(4):545-54.

24. Parker JS, Mullins M, Cheang MC, Leung S, Voduc D, Vickery T, et al. Supervised risk predictor of breast cancer based on intrinsic subtypes. J Clin Oncol. 2009;27(8):1160-7.

25. Prat A, Cheang MC, Galvan P, Nuciforo P, Pare L, Adamo B, et al. Prognostic Value of Intrinsic Subtypes in Hormone Receptor-Positive Metastatic Breast Cancer Treated With Letrozole With or Without Lapatinib. JAMA Oncol. 2016;2(10):1287-94.

26. McCarty KS, Jr., Miller LS, Cox EB, Konrath J, McCarty KS, Sr. Estrogen receptor analyses. Correlation of biochemical and immunohistochemical methods using monoclonal antireceptor antibodies. Arch Pathol Lab Med. 1985;109(8):716-21.

27. Ruprecht B, Zaal EA, Zecha J, Wu W, Berkers CR, Kuster B, et al. Lapatinib Resistance in Breast Cancer Cells Is Accompanied by Phosphorylation-Mediated Reprogramming of Glycolysis. Cancer Res. 2017;77(8):1842-53.

28. Blancafort A, Giro-Perafita A, Oliveras G, Palomeras S, Turrado C, Campuzano O, et al. Dual fatty acid synthase and HER2 signaling blockade shows marked antitumor activity against breast cancer models resistant to anti-HER2 drugs. PloS One. 2015;10(6):e0131241.

29. Parra-Palau JL, Pedersen K, Peg V, Scaltriti M, Angelini PD, Escorihuela M, et al. A major role of p95/611-CTF, a carboxy-terminal fragment of HER2, in the down-modulation of the estrogen receptor in HER2-positive breast cancers. Cancer Res. 2010;70(21):8537-46.

30. Azim HA, Jr., Peccatori FA, Brohee S, Branstetter D, Loi S, Viale G, et al. RANK-ligand (RANKL) expression in young breast cancer patients and during pregnancy. Breast Cancer Res. 2015;17:24.

31. Santini D, Schiavon G, Vincenzi B, Gaeta L, Pantano F, Russo A, et al. Receptor activator of NF-kB (RANK) expression in primary tumors associates with bone metastasis occurrence in breast cancer patients. PloS One. 2011;6(4):e19234.

32. Jernstrom S, Hongisto V, Leivonen SK, Due EU, Tadele DS, Edgren H, et al. Drug-screening and genomic analyses of HER2-positive breast cancer cell lines reveal predictors for treatment response. Breast Cancer. 2017;9:185-98.

33. Liu L, Greger J, Shi H, Liu Y, Greshock J, Annan R, et al. Novel mechanism of lapatinib resistance in HER2-positive breast tumor cells: activation of AXL. Cancer Res. 2009;69(17):6871-8.

34. Pahl HL. Activators and target genes of Rel/NF-kappaB transcription factors. Oncogene. 1999;18(49):6853-66.

35. Yamaguchi N, Yokota M, Taguchi Y, Gohda J, Inoue J. cIAP1/2 negatively regulate RANKL-induced osteoclastogenesis through the inhibition of NFATc1 expression. Genes Cells. 2012;17(12):971-81.

36. Arteaga CL, Engelman JA. ERBB receptors: from oncogene discovery to basic science to mechanism-based cancer therapeutics. Cancer Cell. 2014;25(3):282-303.

37. Morancho B, Parra-Palau JL, Ibrahim YH, Bernado Morales C, Peg V, Bech-Serra JJ, et al. A dominant-negative N-terminal fragment of HER2 frequently expressed in breast cancers. Oncogene. 2013;32(11):1452-9.

38. Parra-Palau JL, Morancho B, Peg V, Escorihuela M, Scaltriti M, Vicario R, et al. Effect of p95HER2/611CTF on the response to trastuzumab and chemotherapy. J Natl Cancer Inst. 2014;106(11).

39. Yi T, Lee HL, Cha JH, Ko SI, Kim HJ, Shin HI, et al. Epidermal growth factor receptor regulates osteoclast differentiation and survival through cross-talking with RANK signaling. J Cell Physiol. 2008;217(2):409-22.

40. Zoi I, Karamouzis MV, Adamopoulos C, Papavassiliou AG. RANKL Signaling and ErbB Receptors in Breast Carcinogenesis. Trends Mol Med. 2016;22(10):839-50.

41. Zoi I, Karamouzis MV, Xingi E, Sarantis P, Thomaidou D, Lembessis P, et al. Combining RANK/RANKL and ERBB-2 targeting as a novel strategy in ERBB-2-positive breast carcinomas. Breast Cancer Res. 2019;21(1):132.

42. Anderson DM, Maraskovsky E, Billingsley WL, Dougall WC, Tometsko ME, Roux ER, et al. A homologue of the TNF receptor and its ligand enhance T-cell growth and dendritic-cell function. Nature. 1997;390(6656):175-9.

43. Bailey ST, Miron PL, Choi YJ, Kochupurakkal B, Maulik G, Rodig SJ, et al. NF-kappaB activation-induced anti-apoptosis renders HER2-positive cells drug resistant and accelerates tumor growth. Mol Cancer Res. 2014;12(3):408-20.

44. Chen YJ, Yeh MH, Yu MC, Wei YL, Chen WS, Chen JY, et al. Lapatinib-induced NF-kappaB activation sensitizes triple-negative breast cancer cells to proteasome inhibitors. Breast Cancer Res. 2013;15(6):R108.

45. Darvishi B, Farahmand L, Eslami SZ, Majidzadeh AK. NF-kappaB as the main node of resistance to receptor tyrosine kinase inhibitors in triple-negative breast cancer. Tumour Biol. 2017;39(6):1010428317706919.

46. Jiang Z, Liu JC, Chung PE, Egan SE, Zacksenhaus E. Targeting HER2(+) breast cancer: the TBK1/IKKepsilon axis. Oncoscience. 2014;1(2):180-2.

47. Wang W, Nag SA, Zhang R. Targeting the NFkappaB signaling pathways for breast cancer prevention and therapy. Curr Med Chem. 2015;22(2):264-89.

48. Israel A. The IKK complex, a central regulator of NF-kappaB activation. Cold Spring Harb Perspect Biol. 2010;2(3):a000158.

49. Rothwarf DM, Karin M. The NF-kappa B activation pathway: a paradigm in information transfer from membrane to nucleus. Science's STKE. 1999;1999(5):RE1.

50. Merkhofer EC, Cogswell P, Baldwin AS. Her2 activates NF-kappaB and induces invasion through the canonical pathway involving IKKalpha. Oncogene. 2010;29(8):1238-48.

51. Cao Y, Bonizzi G, Seagroves TN, Greten FR, Johnson R, Schmidt EV, et al. IKKalpha provides an essential link between RANK signaling and cyclin D1 expression during mammary gland development. Cell. 2001;107(6):763-75.

52. Zhang L, Teng Y, Zhang Y, Liu J, Xu L, Qu J, et al. C-Src-mediated RANKL-induced breast cancer cell migration by activation of the ERK and Akt pathway. Oncol Lett. 2012;3(2):395-400.

Availability of data and materials

Data generated during this study are included in this published article (and its supplementary information files) and datasets generated and analyzed supporting the findings of this study are available from the corresponding authors upon reasonable request.

Abbreviations

EGFR: Epidermal growth factor receptor

ER: estrogen receptor

HER2: Epidermal growth factor receptor 2

IHC: Immunohistochemistry

IP: Immunoprecipitation

NF-κB: Nuclear factor kappa B

PR: Progesterone receptor

RANK: Receptor activator of NF-κB

RANKL: Receptor activator of NF-κB ligand

RT-qPCR: reverse transcriptase quantitative PCR

TMA: Tissue microarray

Acknowledgements

We thank all the patients who contributed to this study. We would like to thank Maria Subijana and Elba López for their contributions, Dr. E. López (Pathology Department Director, Hospital Josep Trueta, Girona, Spain) and the Xarxa de Bancs de Tumors de Catalunya sponsored by Pla Director d'Oncologia de Catalunya (XBTC).

Funding

Work in the laboratory of Eva González Suárez is supported by the Spanish Ministerio de Ciencia, Innovación y Universidades, which is part of Agencia Estatal de Investigación (AEI) (SAF2014-55997-R, SAF2017-86117-R), the ISCIII (PIE13/00022) co-funded by European Regional Development Fund), a Career Catalyst Grant from the Susan Komen Foundation (CCR13262449), an ERC Consolidator grant (LS4-682935) and the Catalan Government 2017SGR00665**.** This work was in part supported by a grant from La Marató de TV3 20131530, to Eva González Suárez and Teresa Puig. The work was in part supported by grants to Teresa Puig from the Spanish Instituto de Salud Carlos III (ISCIII; FIS PI11/00692 and PI14/00329) and the Catalan Government (2017SGR00385). Work in the laboratory of Joaquín Arribas is supported by the ISCIII (PI19/01181) and the Breast Cancer Research Foundation (BCRF-19-008). BM was a recipient of a PERIS fellowship (Departament de Salut, Generalitat de Catalunya). The work in the group of Aleix Prat is supported by GlaxoSmithKline (to SOLTI), the ISCIII (PI16/00904), a Career Catalyst Grant from the Susan Komen Foundation, Banco Bilbao Vizcaya Argentaria (BBVA) Foundation, Pas a Pas, Save the Mama and Breast Cancer Research Foundation. Emad

A Rakha and Andrew R Green are part of the PathLAKE digital pathology consortium supported by a £50m investment from the Data to Early Diagnosis and Precision Medicine strand of the UK government's Industrial Strategy Challenge Fund (UKRI).

Author information

Adrián Sanz-Moreno, Sonia Palomeras and Kim Pendersen contributed equally to this work.

Affiliations

Oncobell, Bellvitge Biomedical Research Institute (IDIBELL), L'Hospitalet de Llobregat, Barcelona, Spain.

Adrián Sanz-Moreno, Kim Pedersen, Sandra Benítez, Jorge Gómez-Miragaya, Marina Ciscar and Eva González-Suárez.

New Therapeutics Targets Lab (TargetsLab), Department of Medical Sciences, University of Girona, Girona, Spain.

Sonia Palomeras, Gemma Viñas and Teresa Puig.

Preclinical Research Program, Vall d'Hebron Institute of Oncology (VHIO), Barcelona, Spain.

Beatriz Morancho and Joaquín Arribas.

Centro de Investigación Biomédica en Red de Cáncer (CIBERONC), Spain.

Patricia G Santamaría, Beatriz Morancho and Joaquín Arribas.

Translational Genomics and Targeted Therapeutics in Solid Tumors, August Pi i Sunyer Biomedical Research Institute (IDIBAPS), Barcelona, Spain.

Tomás Pascual, Patricia Galván and Aleix Prat.

SOLTI Breast Cancer Research Group, Barcelona, Spain.

Sonia Pernas, Tomás Pascual and Aleix Prat.

Department of Medical Oncology, Hospital Clinic, Barcelona, Spain.

Tomás Pascual and Aleix Prat.

Molecular Oncology, Spanish National Cancer Research Centre (CNIO), Madrid, Spain.

Marina Ciscar, Patricia G Santamaría and Eva González-Suárez.

Department of Medical Oncology, Breast Unit, Catalan Institute of Oncology (ICO), University Hospital of Bellvitge IDIBELL, L'Hospitalet de Llobregat, Barcelona, Spain.

Sonia Pernas, Anna Petit and M Teresa Soler-Monsó.

Pathology Department, University Hospital of Bellvitge, IDIBELL, Barcelona, Spain.

Anna Petit and M Teresa Soler-Monsó.

Medical Oncology Department, Catalan Institute of Oncology (ICO), Girona, Spain.

Gemma Viñas.

Division of Cancer and Stem Cells, School of Medicine, University of Nottingham Biodiscovery Institute, University Park, Nottingham, NG7 2RD, UK.

Mansour Alsaleem, Emad A Rakha and Andrew R Green.

Biomolecular Mass Spectrometry and Proteomics Bijvoet Center, Utrecht University, The Netherlands.

Celine Mulder and Simone Lemeer.

Medicine Department, University of Barcelona, Barcelona, Spain.

Aleix Prat.

Contributions

EGS and TP designed the study. ASM, SPa, KM, BM, TP, PG, SB, JGM, MC, SP, AP, MTSM, GV, MA, EAR, ARG, TCM, SML, JA and AP collected the data. ASM, SPa, KM, BM, TP, MC, SP, GV, MA, PGS and EGS assembled the data. All authors analyzed the data. ASM, PGS and EGS wrote the manuscript. All authors critically reviewed the drafts of the manuscript and read and approved the final manuscript.

Corresponding author

Correspondence to Teresa Puig (teresa.puig@udg.edu) and Eva González-Suárez (egonzalez@cnio.es).

Ethics declarations

Ethics approval and consent to participate

This work obtained ethics approval to use the human tissue samples by the North West – Greater Manchester Central Research Ethics Committee under the title; Nottingham Health Science Biobank (NHSB), reference number 15/NW/0685. Informed consent was obtained from all individuals prior to surgery to use their tissue materials in research. This study was performed in compliance with the clinical research guidelines established by the Dr. Josep Trueta University Hospital Ethics Committee. This study was approved by the Institutional Review Board of Hospital Vall d'Hebron (Barcelona) AC/R(AG)110/2013(3755). All patients provided written informed consent.

Consent for publication

Not applicable.

Competing interests

EGS has served on advisory boards for Amgen and has received research funding from Amgen. AP has declared personal honoraria from Pfizer, Novartis, Roche, MSD Oncology, Lilly and Daiichi Sankyo, travel, accommodations and expenses paid by Daiichi Sankyo, research funding from Roche and Novartis, consulting/advisory role for NanoString Technologies, Amgen, Roche, Novartis, Pfizer and Bristol-Myers Squibb. SP has received travel and accommodation grants from Roche and Novartis and holds consulting/advisory roles for Polyphor and Roche.

Figure legends

Figure 1. RANK and RANKL are expressed in treatment-naïve and anti-HER2-resistant HER2 breast cancer tumor samples. **a**. Frequency of HER2-positive patients, treatment-naïve or anti-HER2-resistant, expressing tumoral RANK or RANKL (H-score ≥ 1). The total number of patients scored for RANK or RANKL expression is indicated. **b**. Representative images showing RANK and RANKL IHC. **c**. Frequency of tumoral RANK-positive treatment-naïve HER2 patients and associations with the indicated clinicopathological parameters including those assessed by the Nottingham Grading System (histological grade and proliferation determined by mitotic count and Ki67 as detailed in (20)). The total number of patients analyzed per parameter is indicated in each case. p values were calculated by Chi-Square tests.

Figure 2. *RANK* but not *RANKL* expression increased after dual anti-HER2 therapy in patient samples (n = 151) from the PAMELA trial. **a**. Box plots of *TNFRSF11A/RANK* and *TNFSF11/RANKL* gene expression in HER2-positive tumors at baseline classified by hormone receptor expression. **b**. Ladder plots showing *TNFRSF11A/RANK* and *TNFSF11/RANKL* gene expression in PAMELA HER2-positive tumors before (baseline) and after (surgery) dual anti-HER2 treatment. An increase in gene expression is represented in red and a decrease in blue. Each line represents a tumor sample from one

patient. P values (p) in a were calculated by comparing mean values between both groups and in b were determined by paired two-tailed t-tests. See Additional file 1: Fig. S1 for further analyses.

Figure 3. RANK expression increased in HER2-positive breast cancer cell lines after treatment with anti-HER2 therapies as well as in anti-HER2 resistant cells. **a**. *RANK* gene expression levels determined by RT-qPCR in the indicated HER2-positive cell lines after short-term treatment with lapatinib (Lapa), trastuzumab (Trastu) or the combination of both, relative to corresponding untreated cells (Ctr). **b**. *RANK* gene expression levels determined by RT-qPCR in SKBR3 cell lines resistant to trastuzumab (SKTR), lapatinib (SKLR), or both drugs (SKTLR, SKLTR) compared to untreated SKBR3 control cells. **c**. RANK protein expression in parental SKBR3 cells (SK) or resistant to trastuzumab (SKTR), lapatinib (SKLR), or both (SKTLR, SKLTR). β-actin was used as a loading control. Blots shown are representative of those obtained from 3 independent experiments. **d**. *RANK* gene expression levels in BT474 cells, either control or resistant to lapatinib (according to public datasets (33). a.u.: arbitrary units. *PP1A* expression was used as an internal reference gene (a and b). Mean values for two or three independent experiments are shown. For each experiment determinations were done in triplicates. P (p) values were calculated by ordinary one-way ANOVA (a and b) and by unpaired t-tests (d).

Figure 4. SKBR3 and BT474 lapatinib-resistant cells show increased *RANK* expression and NF-κB activation. **a**. *RANK* mRNA levels relative to housekeeping gene *PP1A* in parental (SKBR3, BT474) and lapatinib-resistant (SKLR, BTLR) HER2-positive cell lines with or without RANKL treatment (24 h). **b**. mRNA expression levels of the RANK/NF-κB downstream gene targets *BIRC3*, *ICAM1*, *TNFα* and *IL8* relative to *PP1A* in cells depicted in a. Gene expression levels were quantified by RT-qPCR. In a and b, determinations were done in triplicates and mean values are used in the calculations. **c**. Western blot showing

the levels of NF-κB (p-p65, p-IκB) and HER2 (p-HER2, p-ERK1/2, p-AKT) pathway activation in control and lapatinib-resistant (SKLR) SKBR3 cells treated with RANKL or lapatinib. Cells were serum starved for 12 h and then treated with lapatinib (2 h) or RANKL (10 min) before processing them. Tubulin was used as a loading control. See Additional file 2: Fig. S2 for total protein levels.

Figure 5. Overactivation of RANK signaling in HER2-positive cell lines increased NF-κB activation and lapatinib resistance. **a**. Expression levels of *RANK* mRNA in HER2-positive SKBR3, BT474 and HCC1954 cells stably transduced with empty or RANK overexpressing (RANK) vectors. *RANK* expression values were quantified by RT-qPCR relative to *PP1A* gene expression. **b**. Expression levels of RANK/NF-κB downstream gene targets *BIRC3*, *ICAM1*, *TNFα* and *IL8* relative to *PP1A* gene expression in cells described in a, with and without RANKL treatment (24 h). Experiments were performed in triplicates and standard error is depicted. **c**. Relative number of alive (relative survival) SKBR3, BT474 and HCC1954 cells stably transduced with control (empty) or RANK overexpressing (RANK) vectors incubated for 4 days with the indicated concentrations of lapatinib and/or stimulated with RANKL. Cells were seeded in growth media with/without 100 ng/ml RANKL; 24 h later lapatinib was added and cells were analyzed with CCK8 after 4 days as detailed in methods. Mean values for three independent experiments are shown. For each experiment data was obtained from triplicates. **d**. Western blot analyses of NF-κB (p-p65) and HER2 (p-HER2, p-ERK1/2 and p-AKT) pathway activation in cells depicted in c. Before collecting the cells, they were cultured in media without FBS for 12 h, pretreated with/without lapatinib for 2 h followed by 10 min stimulation with RANKL. Representative blots from three independent experiments are shown. Tubulin was used as a loading control. See Additional file 3: Fig. S3 for total protein levels and Additional file 4: Fig. S4 for EGF/HRG stimulations.

Figure 6. Co-immunoprecipitation of RANK and HER2. **a**. Immunoprecipitation (IP) against HER2 was performed in HEK293 cells transfected with RANK-V5 and HER2, HER2-FLAG, a carboxy-terminal fragment of HER2 (611-CTF) or an amino-terminal fragment of HER2 (742-NTF). IP was performed using anti-FLAG, anti-HA or control IgG antibodies as indicated. RANK was detected by blotting the immunoprecipitates (IP, left upper panel) or the whole lysates (input, right upper panel) with V5 antibody. HER2 was detected in IPs (left lower panel) and input (right lower panel) using 32H2 antibody that detects all forms of HER2. **b**. IP against RANK-V5 was performed in HEK293 cells transfected with RANK-V5 and GFP, HER2-FLAG, a carboxy-terminal fragment of HER2 (611-CTF) or an amino-terminal fragment of HER2 (742-NTF) using V5 antibody. In the IP and input HER2 was detected using 32H2 antibody. **c**. IP against endogenous HER2 was performed in SKBR3 cells using trastuzumab (Herceptin-HCP) or a control IgG. Endogenous RANK and HER2 were detected in IP (RANK immunoprecipitated by HER2 is indicated by an asterisk * in upper panel) and input samples.

Supplementary information

Additional file 1: Figure S1. *RANK* and *RANKL* expression in breast cancer samples from the PAMELA clinical trial. **a**. Expression of *RANK* (*TNFRSF11A*) and *RANKL* (*TNFSF11*) across the intrinsic molecular subtypes from the PAMELA study. P-values (p) were calculated by comparing mean values across all groups. **b**. Scatter plots of *RANK* (*TNFRSF11A*) and *RANKL* (*TNFSF11*) expression versus *ERBB2* expression for baseline samples in the PAMELA study. Solid line in each figure represents the regression line. Pearson correlation coefficient (r) with significance (p value) is presented in each figure. **c**. Pearson correlation between single genes and gene expression signatures evaluated in baseline samples from the PAMELA study.

Additional file 2: Figure S2. Western blot showing the total levels of p65, IκB**,** HER2, ERK1/2 and AKT in control and lapatinib-resistant (SKLR) SKBR3 cells treated with RANKL or lapatinib as depicted in Fig. 4C. Cells were serum starved for 12 h and then treated with lapatinib (2 h) or RANKL (10 min) before processing them. Tubulin was used as a loading control.

Additional file 3: Figure S3. Western blot analyses of total levels of p65, ERK1/2 and HER2 in whole lysates from SKBR3, BT474 and HCC1954 cells stably transduced with empty or RANK overexpressing (RANK) vectors as depicted in Fig. 5D. Before collecting the cells, they were cultured in media without FBS for 12 h, pretreated with/without lapatinib for 2 h followed by 10 min stimulation with RANKL. Tubulin was used as a loading control.

Additional file 4: Figure S4. Western blot analyses of HER2 (p-HER2, p-ERK1/2) and NF-κB (p-p65) pathway activation in SKBR3, BT474 and HCC1954 cells stably transduced with empty or RANK overexpressing (RANK) vectors. Cells were cultured in media without FBS for 12 h, followed by stimulation with EGF (100 ng/ml) (upper panels) or heregulin (HRG 10 ng/ml) (lower panels) for the indicated times. Tubulin was used as a loading control.

Figure 1

A

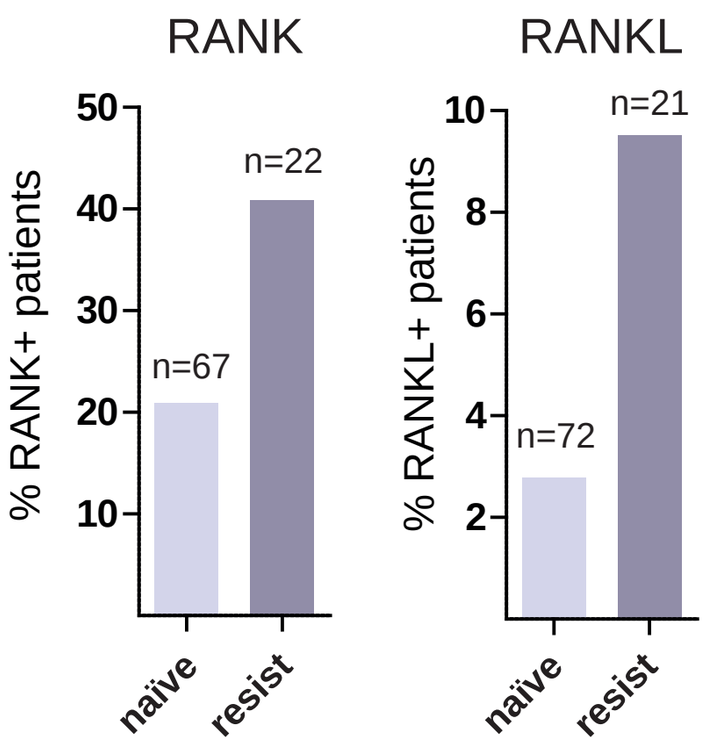

B

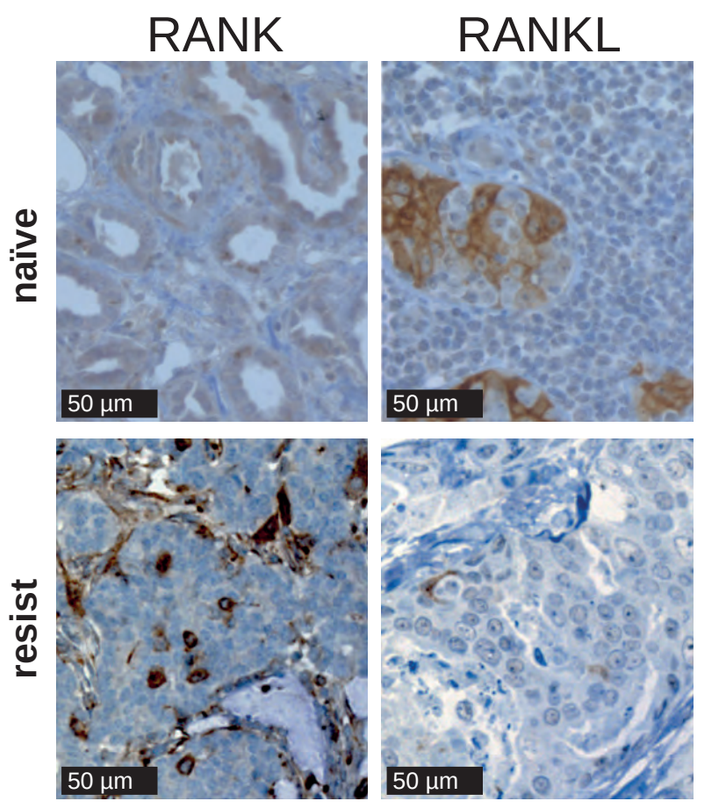

C

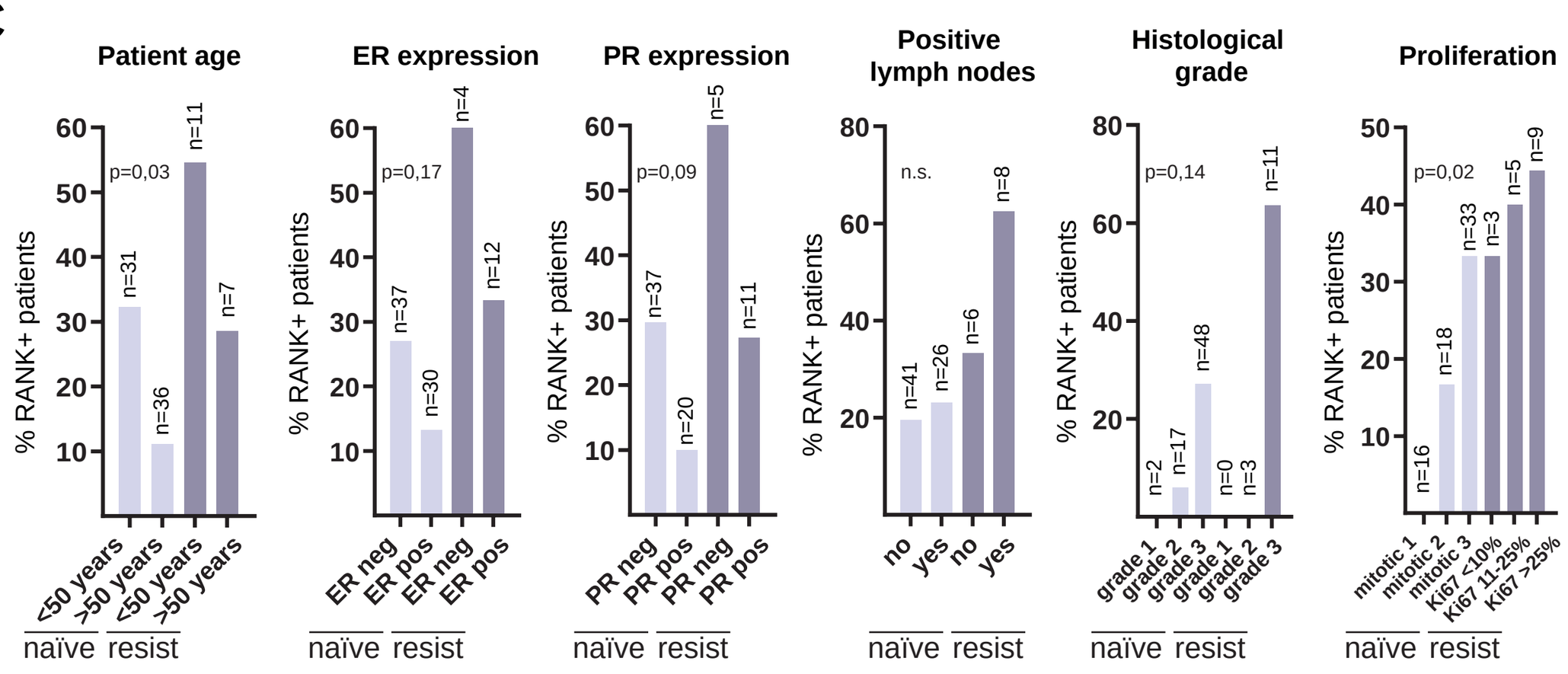

Figure 2

A

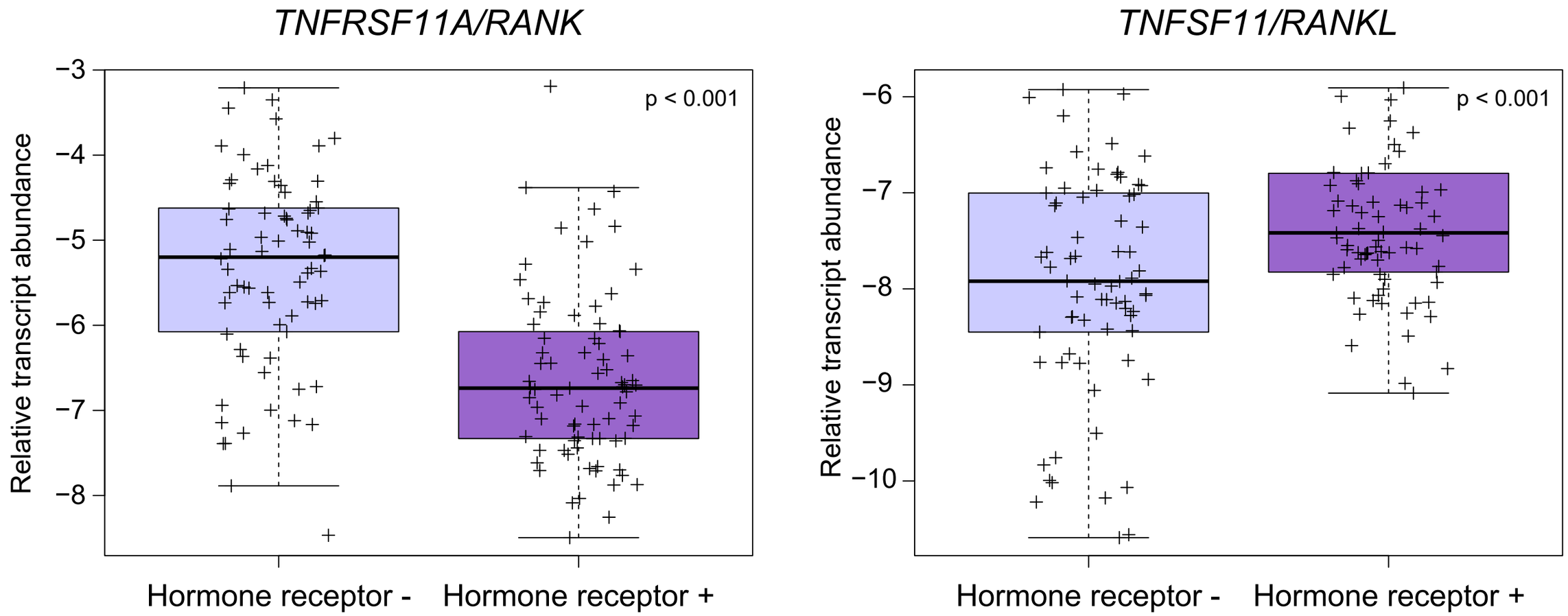
TNFRSF11A/RANK
TNFSF11/RANKL
Relative transcript abundance
p < 0.001
p < 0.001
−3
−4
−5
−6
−7
−8
−6
−7
−8
−9
−10
Hormone receptor -
Hormone receptor +
Hormone receptor -
Hormone receptor +

B

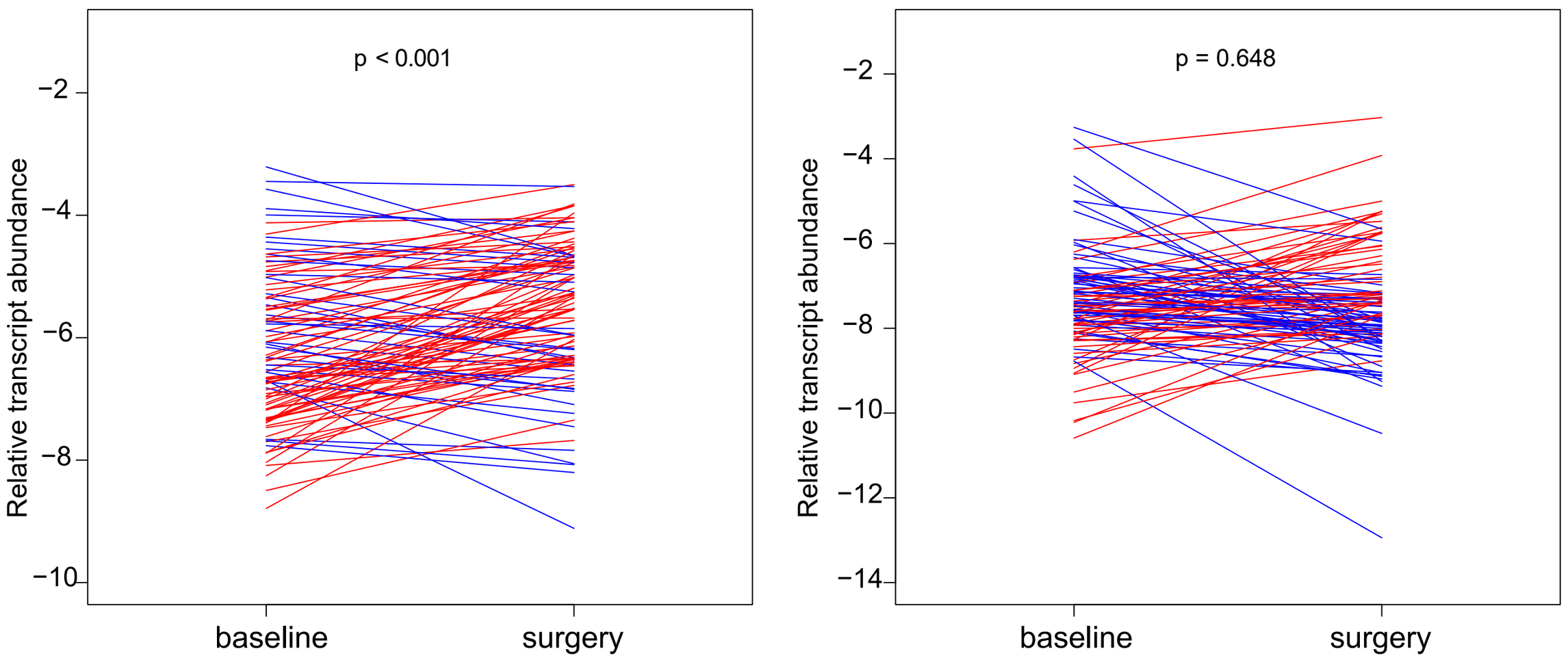
TNFRSF11A/RANK
TNFSF11/RANKL
Relative transcript abundance
p < 0.001
p = 0.648
−2
−4
−6
−8
−10
−2
−4
−6
−8
−10
−12
−14
baseline
surgery
baseline
surgery

Figure 3

A

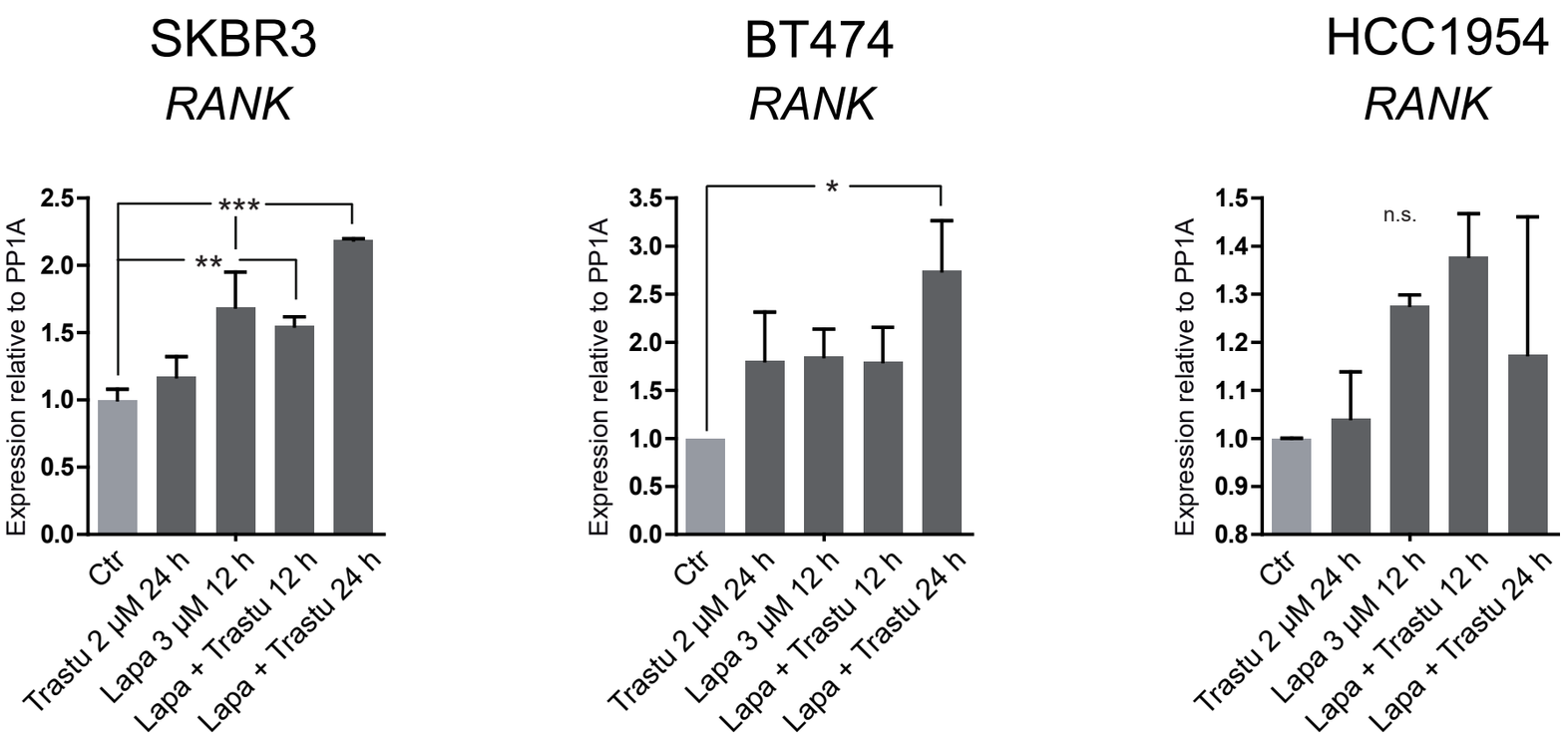

B

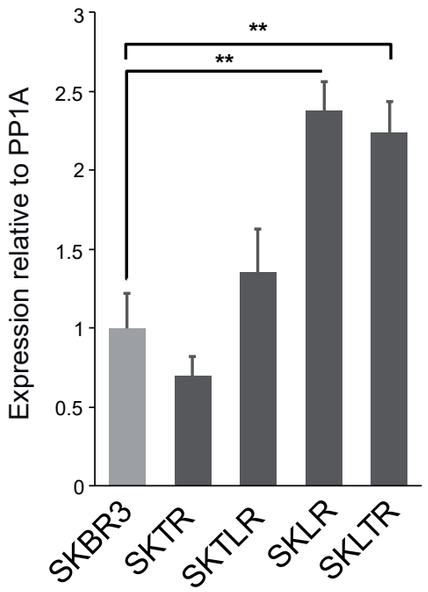

C

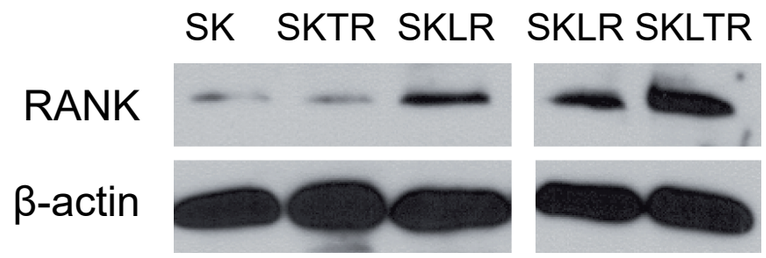

D

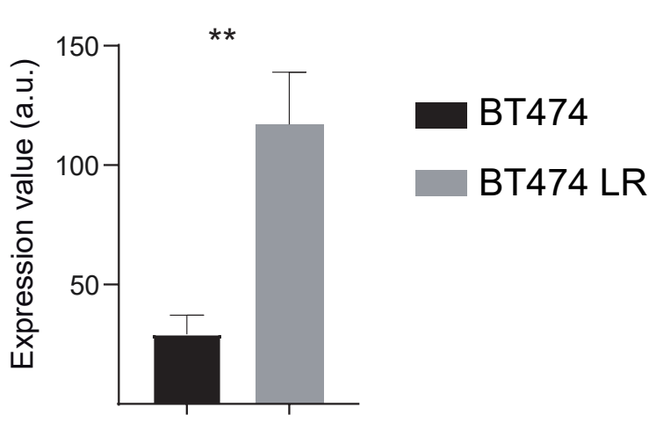

Figure 4

A

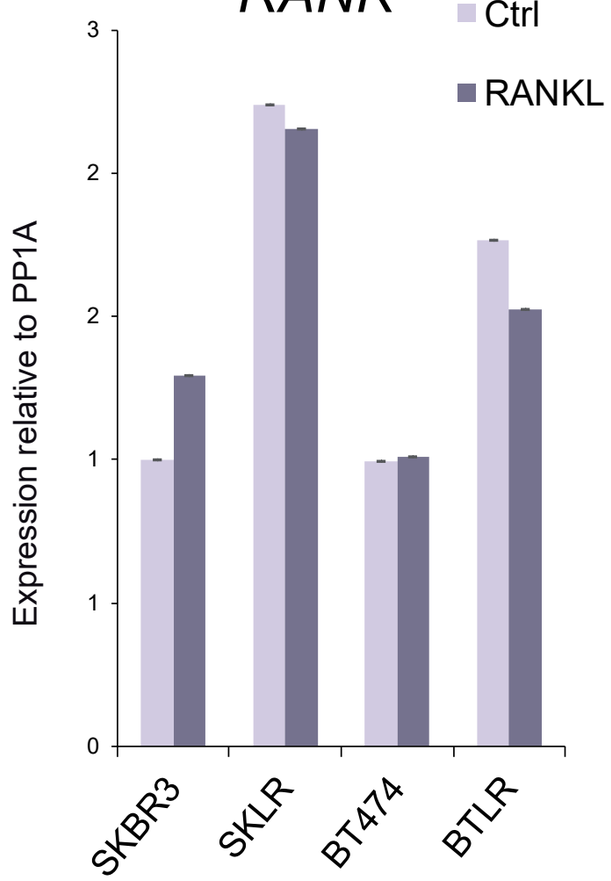
RANK
Ctrl
RANKL
Expression relative to PP1A
0
1
1
2
2
3
SKBR3
SKLR
BT474
BTLR

B

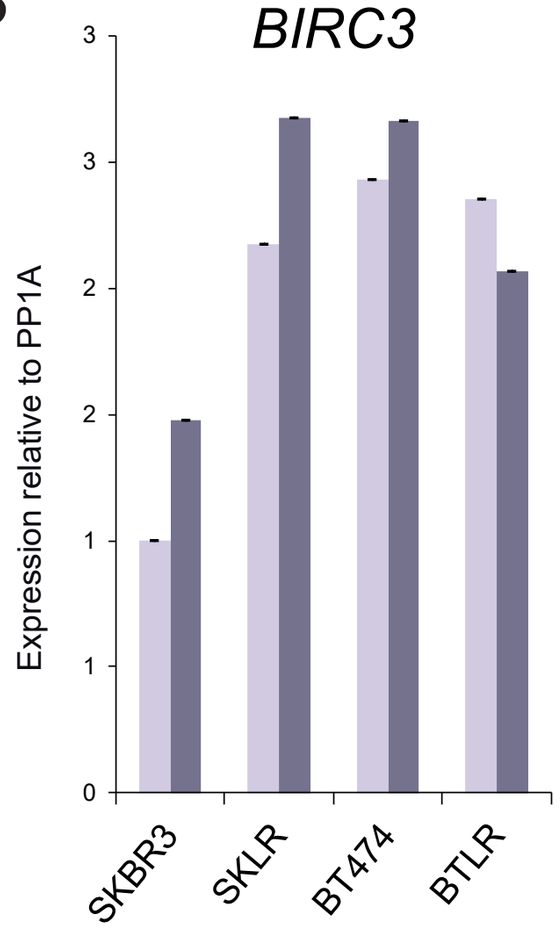
BIRC3
Expression relative to PP1A
0
1
1
2
2
3
3
SKBR3
SKLR
BT474
BTLR

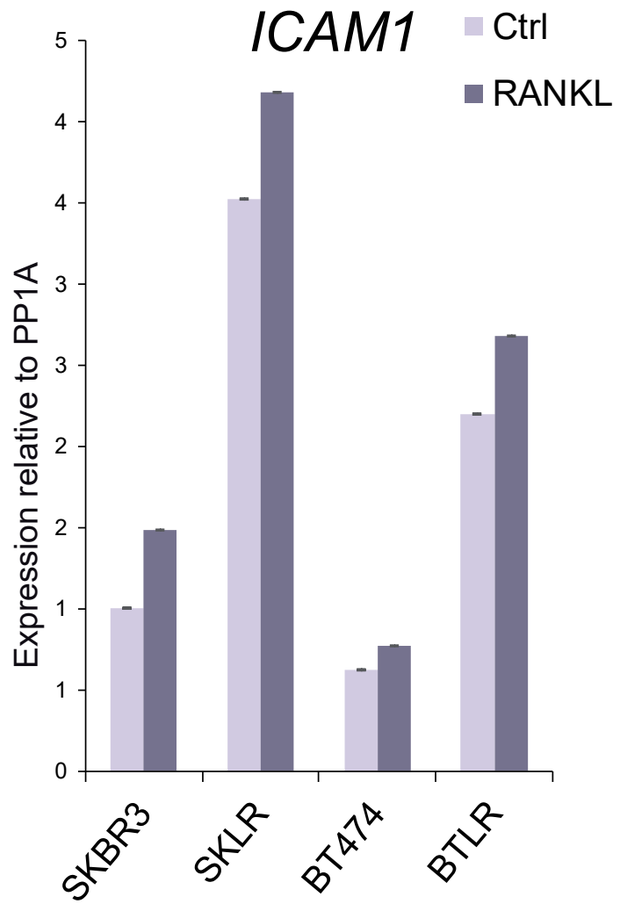
ICAM1
Ctrl
RANKL
Expression relative to PP1A
0
1
1
2
2
3
3
4
4
5
SKBR3
SKLR
BT474
BTLR

C

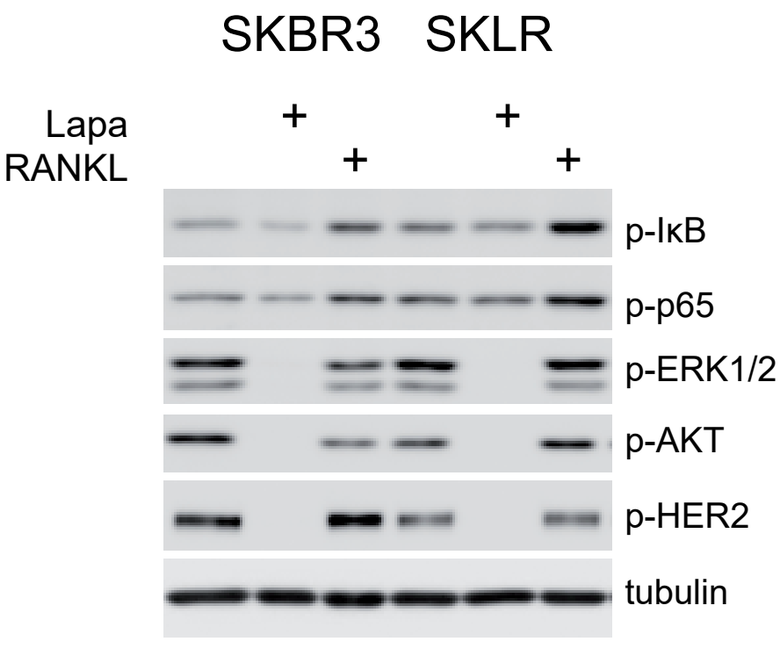
SKBR3
SKLR
Lapa
RANKL
+
+
+
+
p-IκB
p-p65
p-ERK1/2
p-AKT
p-HER2
tubulin

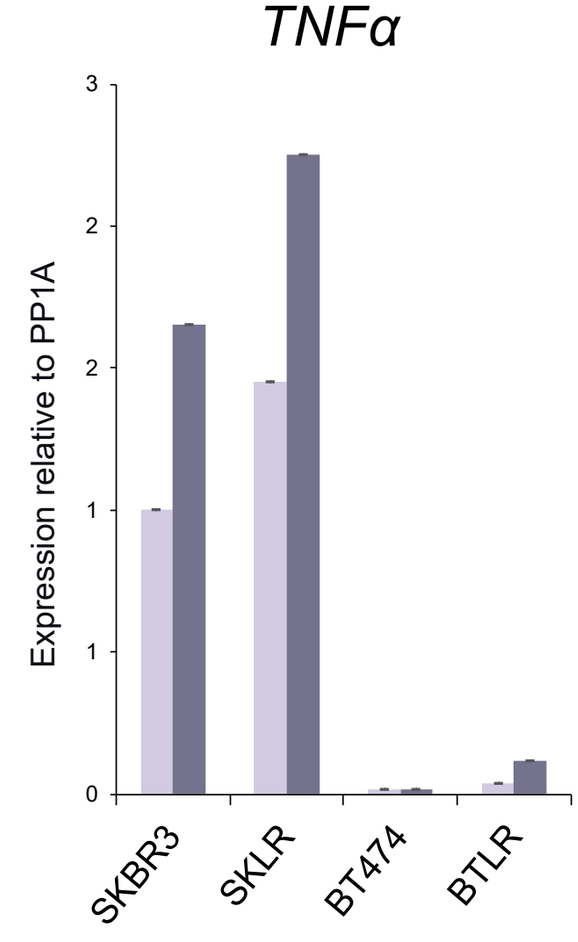
TNFα
Expression relative to PP1A
0
1
1
2
2
3
SKBR3
SKLR
BT474
BTLR

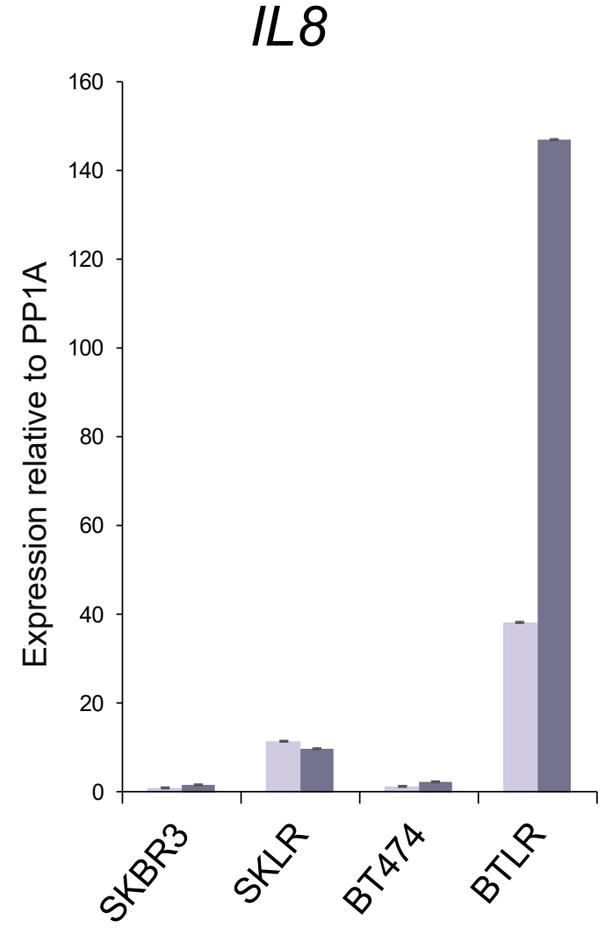
IL8
Expression relative to PP1A
0
20
40
60
80
100
120
140
160
SKBR3
SKLR
BT474
BTLR

Figure 5

A

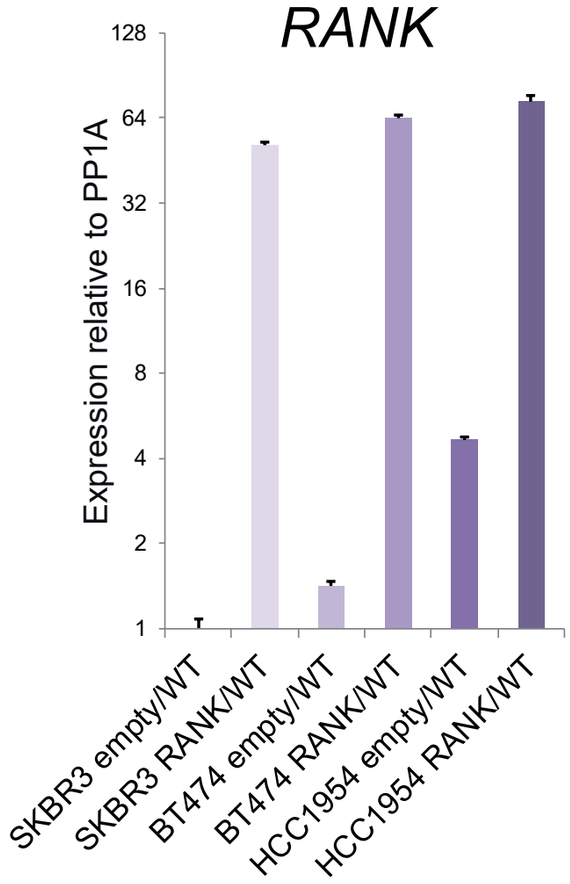

B

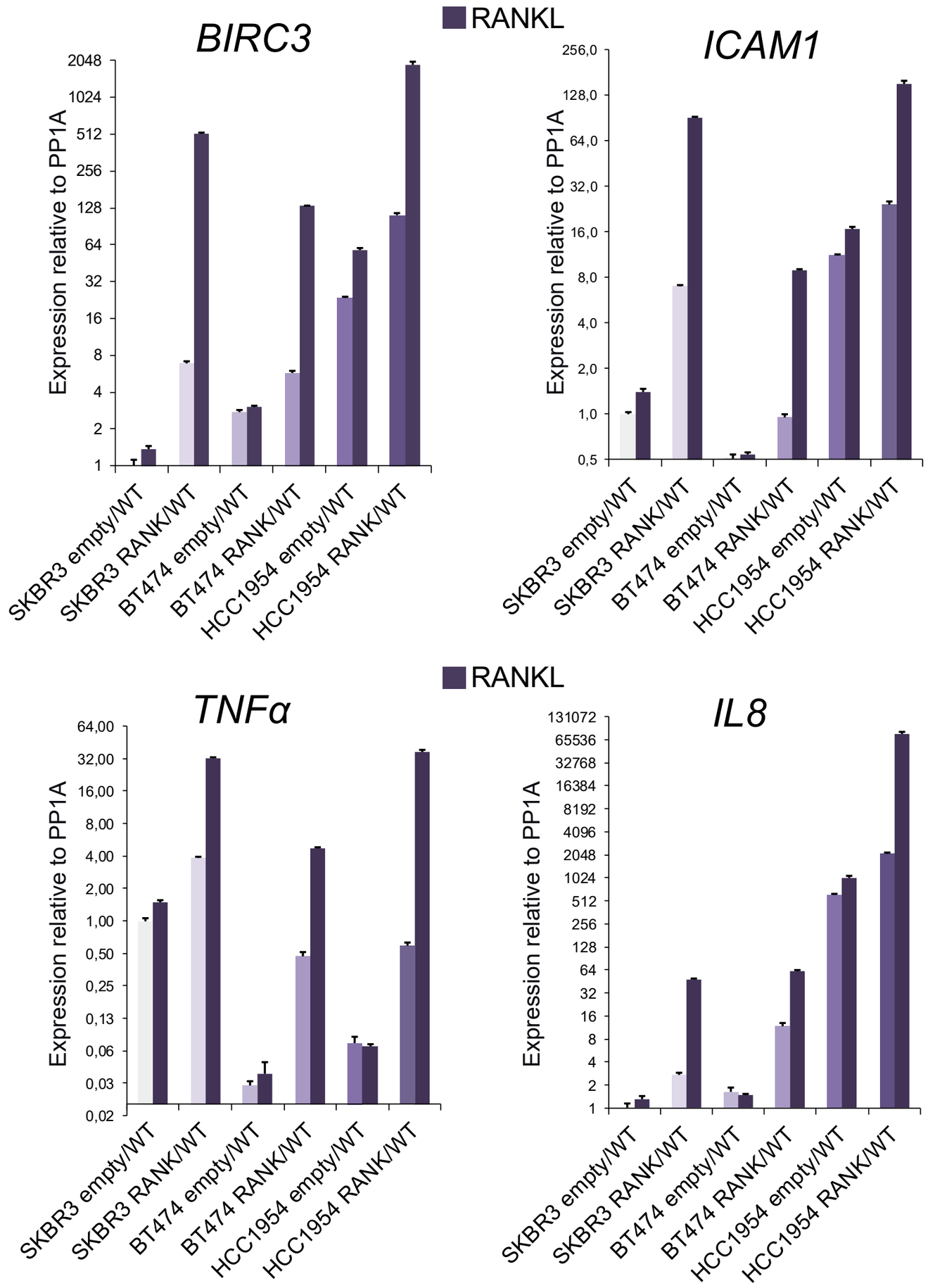

C

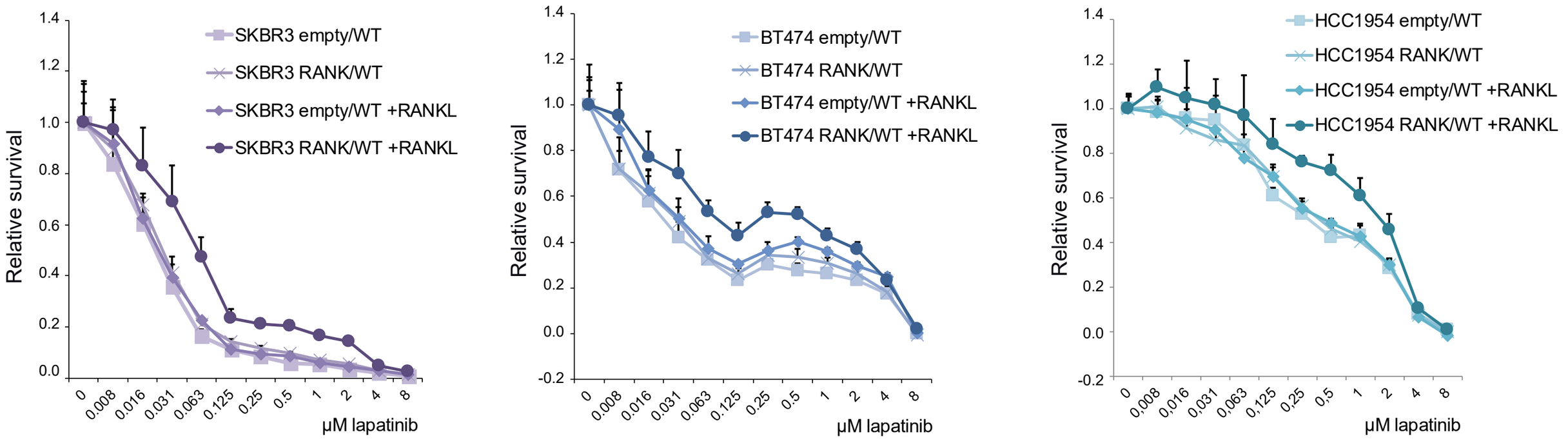

D

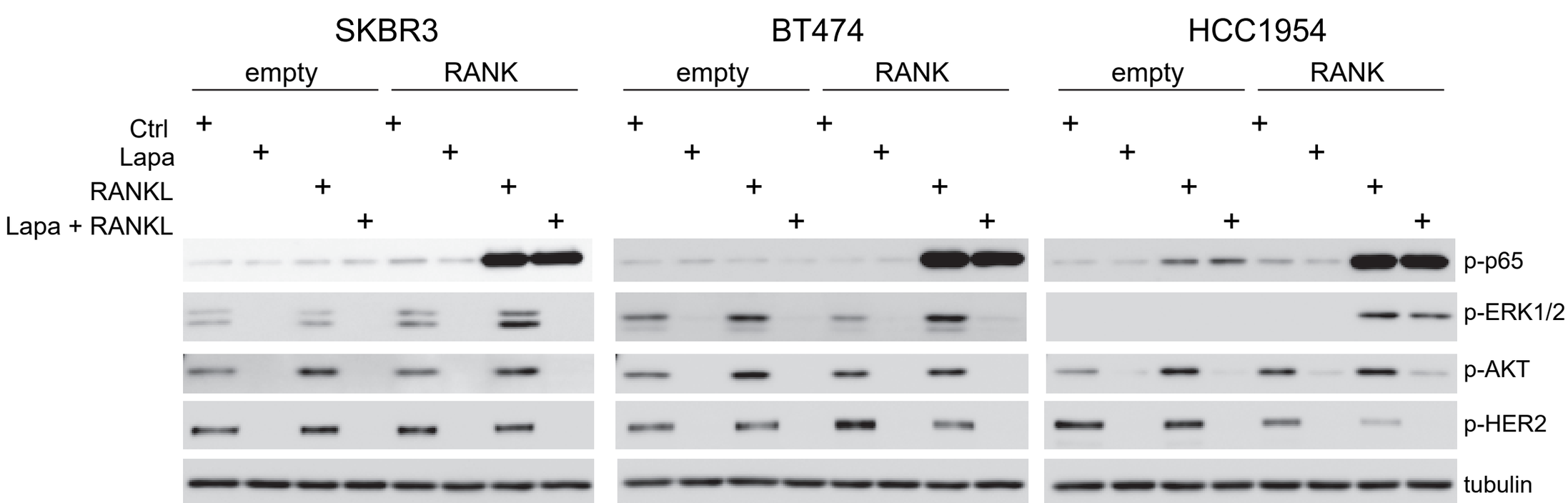

Figure 6

A

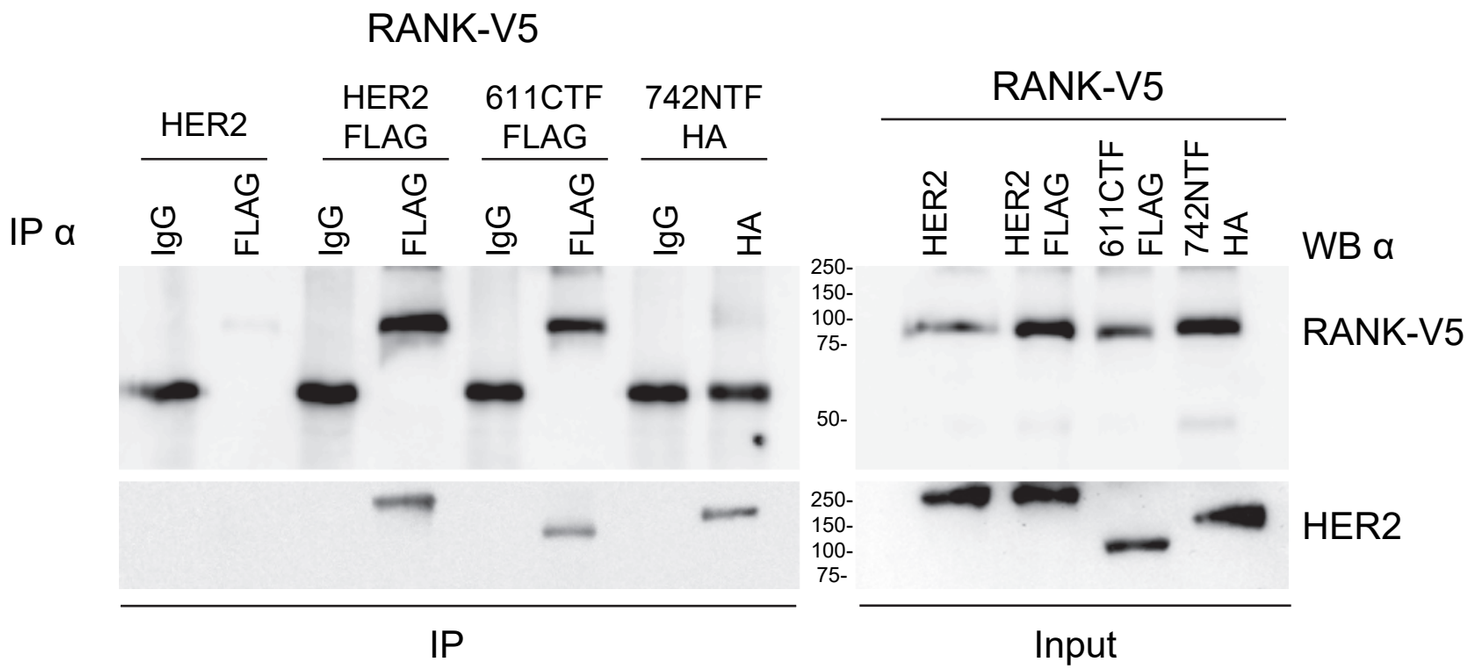
RANK-V5
HER2
HER2 FLAG
611CTF FLAG
742NTF HA
IP α
IgG
FLAG
IgG
FLAG
IgG
FLAG
IgG
HA
250-
150-
100-
75-
50-
250-
150-
100-
75-
IP
RANK-V5
HER2
HER2 FLAG
611CTF FLAG
742NTF HA
WB α
RANK-V5
HER2
Input

B

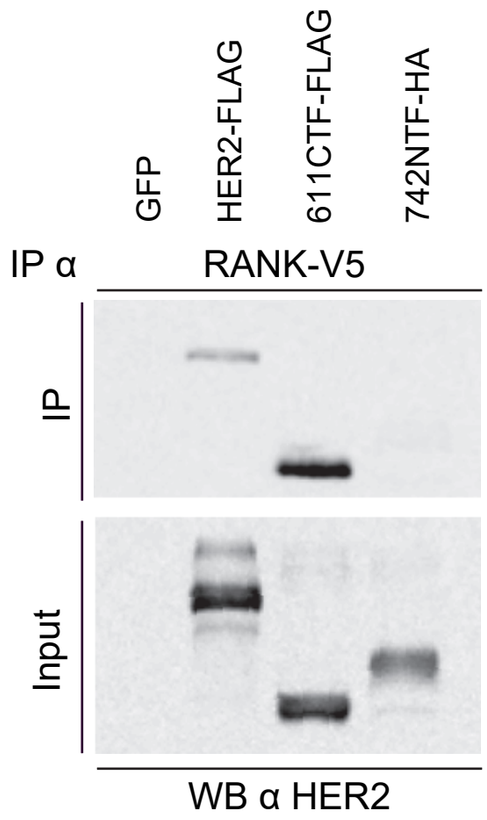
GFP
HER2-FLAG
611CTF-FLAG
742NTF-HA
IP α
RANK-V5
IP
Input
WB α HER2

C

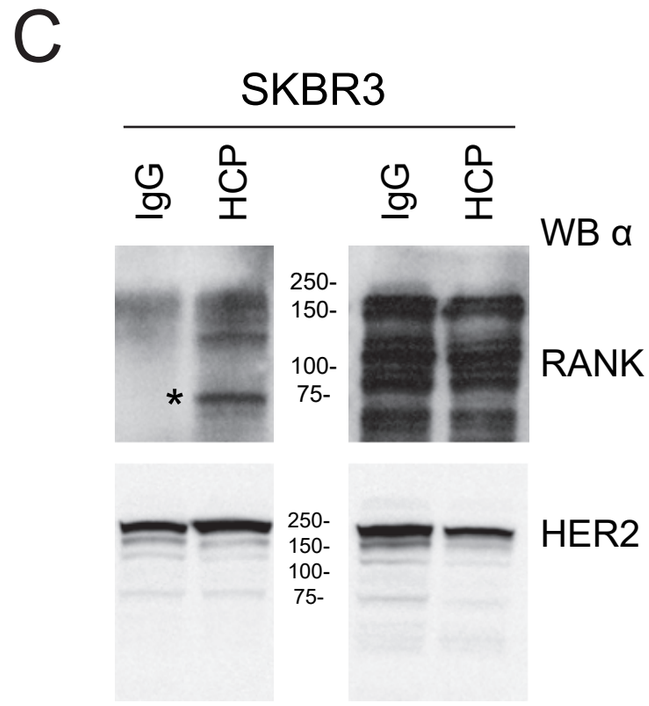
SKBR3
IgG
HCP
IgG
HCP
WB α
250-
150-
100-
75-
*
RANK
250-
150-
100-
75-
HER2

Supplementary figures 1-4 in single pdf